HOMINOID BRAIN ORGANIZATION: HISTOMETRIC AND
MORPHOMETRIC COMPARISONS OF VISUAL BRAIN STRUCTURES

by Alexandra Allison de Sousa

B.A. Anthropology 2000, Arizona State University

A Dissertation submitted to

The Faculty of
The Columbian College of Arts and Sciences
of The George Washington University
in partial fulfillment of the requirements
for the degree of Doctor of Philosophy

August 31, 2008

Dissertation directed by

Chet C. Sherwood
Assistant Professor of Anthropology

UMI Number: 3311323

INFORMATION TO USERS

The quality of this reproduction is dependent upon the quality of the copy submitted. Broken or indistinct print, colored or poor quality illustrations and photographs, print bleed-through, substandard margins, and improper alignment can adversely affect reproduction.

In the unlikely event that the author did not send a complete manuscript and there are missing pages, these will be noted. Also, if unauthorized copyright material had to be removed, a note will indicate the deletion.

The Columbian College of Arts and Sciences of The George Washington University certifies that Alexandra Allison de Sousa has passed the Final Examination for the degree of Doctor of Philosophy as of April 16, 2008. This is the final and approved form of the dissertation.

HOMINOID BRAIN ORGANIZATION: HISTOMETRIC AND MORPHOMETRIC COMPARISONS OF VISUAL BRAIN STRUCTURES

Alexandra Allison de Sousa

Dissertation Research Committee:

Chet C. Sherwood, Assistant Professor of Anthropology, Dissertation Director

Bernard A. Wood, University Professor of Human Origins, Committee Member

Peter W. Lucas, Associate Professor of Anthropology, Committee Member

Dedication

The author wishes to dedicate this work to her grandmothers, Liberdade Lusitana

Nobrega Nunes Moita e Sousa (b. Lubango, Angola, 1917; d. Lisbon, Portugal, 2006)

and June Helyn Beckard Allison Budd (b. Milwaukee, U.S.A., 1925).

Acknowledgements

I wish to acknowledge the following people, without whom this dissertation would not have been possible. First, I would like to thank my dissertation committee, chaired by Brian Richmond: Chet Sherwood, Bernard Wood, Peter Lucas, Patrick Hof, and Ralph Holloway.

At The George Washington University: Chet Sherwood has been the most important source of advice for the duration of my dissertation research, starting long before he joined the faculty at GWU, and has been a constant source of support, particularly in the final months of dissertation preparation. I am grateful to Bernard Wood for his constant support and for promoting my interest in comparative neuroanatomy early on and in every way possible. The CASHP faculty members Brian Richmond, Peter Lucas, Allison Brooks, and Robin Bernstein have all provided important advice and forced me to consider the broader impact of my research. I wish to acknowledge the past and present Hominid Paleobiology postdocs and graduate students who have influenced me through their shared interest in human evolution.

In Düsseldorf and Jülich: Karl Zilles was kind enough to take me into his institute to pursue my dissertation research, and has also been my major source of advice on cortical area parcellation. Axel Schleicher has been a great host, has taught me everything I need to know about GLI, and has provided advice on KS400, AxioVision, MatLab, and ImageJ. Katrin Amunts taught me how to identify cortical areas cytoarchitectonically, and has been fantastic at making the necessary arrangements for me to turn my project ideas into data. Hartmut Mohlberg introduced me to the world of

Abstract of dissertation

HOMINOID BRAIN ORGANIZATION: HISTOMETRIC AND MORPHOMETRIC COMPARISONS OF VISUAL BRAIN STRUCTURES

The visual system is the largest sensory modality in modern humans (*Homo sapiens,* herein referred to simply as "humans") and closely related species, and the size and organization of human visual brain structures have played a central role in discussions of brain evolution. It has been argued that changes in the relative sizes of visual system structures prior to encephalization provide evidence of reorganization in the human lineage. Yet very little is known about the organization of the visual brain structures in the taxa phylogenetically closest to humans – the apes – thus making it difficult to evaluate hypotheses about recent evolutionary changes. Here, visual brain structures -- the lateral geniculate nucleus (LGN), the primary visual cortex (V1), and three extrastriate areas (V2, VP and V5) -- are compared at several anatomical levels in hominoid species. First, the histological organization of hominoid striate and extrastriate cortical areas are compared in terms of cell volume densities and laminar patterns. Second, hominoid visual brain structure volumetric data are used to determine whether the human brain departs from hominoid and other primate patterns of brain organization. V1 volumes are then compared to lunate sulcus position to investigate the reliability of inferences about brain reorganization made on fossil hominin endocasts. Third, the LGN laminar pattern is investigated in catarrhine species. The results indicate that hominoid visual brain structures show evidence of reorganization at multiple anatomical levels. Humans are found to have relatively reduced V1 and LGN volumes. Chimpanzees and

bonobos differ from each other in the size and histological organization of visual areas. Apparent similarities in the visual systems of macaques and humans are reevaluated due to differences between cercopithecoids and hominoids in visual brain structure scaling relationships, and also homoplasy in LGN structure within the catarrhines. The data obtained for this study suggest that interspecific variability in visual system structures can arise independently of global brain and body size scaling relationships.

Table of Contents

List of Figures

List of Tables

xvi

List of Abbreviations

Central nervous system   CNS

Cerebral spinal fluid   CSF

Confidence intervals   CI

Encephalization quotient   EQ

Frontal pole   FP

Generic phylogenetic independent contrasts   G-PIC

Grey level index   GLI

Homo-specific phylogenetic independent contrasts   H-PIC

Koniocellular   K

Lateral geniculate nucleus   LGN

Left occipital right frontal   LORF

Lunate sulcus   LS

Magnocellular   M

Magnetic resonance   MR

Occipital pole   OP

Ordinary least squares   OLS

Parvocellular   P

Principal components analysis   PCA

Phylogenetic independent contrasts   PIC

Reduced major axis   RMA

Region of interest   ROI

Standard error   SE

Primary visual area, Brodmann's area 17   V1

Secondary visual area, Brodmann's area 18   V2

Ventral posterior area   VP

Fifth visual area (also MT - middle temporal area)   V5

Chapter 1. Introduction: The Hominoid Visual System and Brain Reorganization

Differences between modern humans (*Homo sapiens,* herein referred to simply as "humans") and other primates in brain size and organization, as well as in behavior and cognition, have led human evolutionary biologists to stress the distinctiveness of the human brain. The visual system is the largest special sensory modality in humans and closely related species. Visual areas comprise approximately 23% of the human neocortex (Van Essen DC and HA Drury, 1997) and 55% of the macaque neocortex (Felleman DJ and DC Van Essen, 1991). The size and organization of the human visual cortex has played a fundamental role in discussions of brain evolution (e.g., Dart RA, 1925; Falk D, 1980; Holloway RL, 1972; Jerison HJ, 1975). The visual cortex is the most studied and best understood part of the primate cerebral cortex, largely due to extensive research in monkeys.

Physiological and histological investigations have led to the identification of over 25 visual areas in macaques (Felleman DJ and DC Van Essen, 1991; Hof PR and JH Morrison, 1995; Van Essen DC, 2004). The hominoids (humans and apes; see Table 1.1) share with the cercopithecoids (Old World monkeys) a particularly specialized visual system, with well developed stereoscopic vision (a primate synapomorphy), and routine trichromatic color vision (a catarrhine synapomorphy). Recently, functional magnetic

resonance imaging (fMRI) has made it possible to identify visual areas in the human cerebral cortex. In some cases, candidates for homologous areas between the human and monkey brain have been identified (DeYoe EA et al., 1996). In contrast, little is known about the detailed anatomy and physiology of the visual system in the taxa phylogenetically closest to humans, the apes. Only rarely have there been opportunities to conduct physiological studies of ape visual cortices (Vital-Durand F and C Blakemore, 1981).

The aim of the current study is to generate new data about visual brain structures in apes and to investigate brain organization – and reorganization – in the hominin lineage using a phylogenetic perspective.

1.1 Approach to brain evolution

This dissertation focuses on the evolution of the visual system in hominoid species. Hominoid central nervous system (CNS) data are intellectually interesting to anthropology and the neurosciences because they address the basis of complex human behaviors. CNS data also happen to be interesting for the purpose of phylogenetic reconstruction (Johnson JI et al., 1994). The phylogeny of the hominoids has provided an obstacle for taxonomists because skeletal characters and molecular characters have tended to produce conflicting phylogenetic trees. However, non-CNS soft tissue characters were found to be more reliable than hard tissue characters in hominoid phylogenetic reconstruction (Gibbs S et al., 2000). The need to identify new soft tissue characters, including those of the CNS, is made more urgent by the precarious status of hominoid species. In a preliminary review of the published literature on the hominoid

CNS (de Sousa A and B Wood, 2002), one thing was immediately apparent: very little is known about the brains of ape species. In contrast to the 171 non-CNS phylogenetically informative soft tissue characters identified by (Gibbs S et al., 2002), very few are available for the CNS – and this is in spite of the tremendous amount of attention given to neuroscience research compared to the waning interest in comparative anatomy.

Neurobiological researchers were especially active in the comparative neuroanatomy of great apes and humans in the early part of the 20th century (e.g. Bolk L, 1910; Filimonoff IN, 1933; Le Gros Clark WE, 1927; Mauss T, 1911). Around this time and in the decades that followed, ape neurophysiology was also beginning to be investigated (e.g., Beevor CE and V Horsley, 1890; for a review see Jackson WJ et al., 1969; Leyton ASF and CS Sherrington, 1917; Spence KW and JF Fulton, 1936; Woolsey CN et al., 1943), but as neurophysiological techniques became increasingly sophisticated, it became increasingly apparent that apes were not suitable lab animals, for a combination of practical and ethical reasons.

Many of the individuals instrumental in the foundation of paleoanthropology (or, more generally, physical anthropology), for example, Grafton Elliot Smith, Raymond Dart and Wilfrid Le Gros Clark were also neuroscientists (or neurologists). However, paleoanthropology and neuroscience have become well defined fields in and of themselves, each with their own jargon, and communication between these fields has gradually reduced. And yet, clearly, each field needs the other in order to investigate the complexity of the human brain.

Macaques are often used as an experimental stand-in for humans, for ethical and practical reasons. These studies take for granted that macaque brains are very similar to

human brains. Translational research does not seek to investigate the peculiarities of macaque behavior; rather, any species-specific physiological differences are likely to be understated. Over the past 20 or so years, the introduction of noninvasive neuroimaging techniques—such as positron emission tomography (PET), magnetic resonance imaging (MRI), and electroencephalogrammy (EEG) – have expanded neurophysiological experimentation to include humans. This has created a need for studies which directly compare the brains of macaques and the growing data about the brains of humans.

Neurobiology is increasingly brought to bear on human evolutionary studies, as well. The fossil record continues to accumulate, and the recent finds from Dmanisi and Flores further question the old belief that modern human behavior and brain size emerged in a linear fashion (Brown P et al., 2004; Morwood MJ et al., 2004; Vekua A et al., 2002). The 3D imaging of hard tissues using computed tomography (CT) has enabled endocranial studies to be more statistically rigorous, quantitative, and precise. Genetic studies have probably been the most dynamic factor in comparative hominoid neurobiology. With the human genome sequence published and that of the chimpanzees drafted, it is now possible to directly compare genetic sequences related to behavior (Caceres M et al., 2003; Dorus S et al., 2004; Enard W, P Khaitovich et al., 2002; Enard W, M Przeworski et al., 2002; Uddin M, M Goodman et al., 2008; Uddin M, JC Opazo et al., 2008). Meanwhile, evolutionary neuroanatomists have taken full advantage of the available range of noninvasive methods for comparing hominoid variability in cortical area volumes (Semendeferi K et al., 1998, 2001); cortical architecture (Preuss TM et al., 1999), neuronal subtypes (Hof PR et al., 2001; Nimchinsky EA et al., 1999),

behaviorally-based asymmetries (Sherwood CC, E Wahl et al., 2007), and most recently

brain function using noninvasive neuroimaging (Rilling JK et al., 2007).

This dissertation focuses on the visual system. The visual system is the most

"primate" of the special sensory systems of the brain, and a wealth of studies have

investigated visual system structure volumes in primates (e.g., Barton RA, 1998; Bush

EC and JM Allman, 2004; e.g., Joffe TH and RI Dunbar, 1997; Kirk EC, 2006; Stevens

CF, 2001), most of them are based on the Stephan brain collection datasets (in particular,

visual structure data published in Frahm HD et al., 1984; Frahm HD et al., 1982; Stephan

H et al., 1984), and the dissertation of Schulz (1967). The visual system is the best

studied sensory system in neuroscience precisely because it is so important to humans.

The first discovery of a qualitative human autapomorphy of the CNS is the unique

compartmental organization of layer 4A of the primary visual cortex (Preuss TM *et al.*,

1999).

1.2 Methodological advances in brain evolution research

As is often the case when addressing questions of an evolutionary nature, the

questions driving this dissertation invite a variety of methodological approaches. Brain

reorganization is a common thread throughout this dissertation. Smith (1924) speculated

that brain organization preceded encephalization in the hominin lineage, an hypothesis

for which Dart (1925) found evidence in the Taung *Australopithecus africanus* endocast.

In brief, the Taung endocast and its posteriorly-positioned lunate sulcus spurred a

discussion about whether a functional reconfiguration of the cerebral cortex may have

enabled small-brained hominins to engage in humanlike behaviors. This hypothesis of

brain reorganization in early hominins has been expanded in detail by Holloway (1966;

1975). Although Dart's interpretation of the lunate sulcus in Taung has been questioned

(Falk D, 1980), another endocast, Stw 505, has provided clearer evidence for a

posteriorly positioned lunate sulcus in *Au. africanus* (Holloway RL, RJ Clarke et al.,

2004).

Although the current study engages the same hypothesis that originated with

Taung, none of the new data generated in the current dissertation was taken from a fossil

of any kind. In fact, the research in this thesis examined only extant primate species. And

yet, brains of extant primate species are used here to shed light on the changes that

occurred over the past 8-4 million years, since the time of the most recent common

ancestor between *Homo sapiens* and its sister species, *Pan troglodytes* and *Pan paniscus*.

The logic of the comparative anatomical method is that evolutionary associations of traits

are inferred when it is demonstrated that similar ecological variables produce similar

traits in different lineages. Individual taxa cannot be treated independently because they

share traits through common inheritance (Harvey PH and MD Pagel, 1991). Therefore,

in order to understand the evolution of the human brain, it is necessary to consider not

only closely related hominin taxa, but also to consider species in other lineages which

have undergone similar evolutionary trajectories.

Although the specimens here are modern, many of the neuroanatomical methods

used here were in use long before Dart laid his eye on the Taung endocast. Neuroscience

has developed over the past century by focusing on experimental organisms such as birds,

rats, and macaques. In recent decades, it has also been possible to experimentally

6

investigate humans due to modern neuroimaging techniques, particularly functional magnetic resonance imaging (fMRI). Non-human hominoids have rarely been involved in physiological experiments because techniques have not been adapted so as to ethically include them. This is starting to change -- recently, resting state (Rilling JK *et al.*, 2007) and communicative-signaling (Taglialatela JP et al., 2008) brain activation patterns in chimpanzees have been researched using positron emission tomography (PET). But for the most part, hominoid brain investigations have not benefited from the majority of new neurobiological methods, therefore hominoid brain data has been slow to accumulate.

However, this is not to say that this dissertation could have been done in exactly the same way one hundred years ago. The methods of early brain-mappers have been developed into those that have been applied in this dissertation. Over a century ago histologist Franz Nissl developed a stain for what is now known as Nissl substance of the rough endoplasmic reticulum within cell bodies. Most of the sections used in this dissertation, which belong to Karl Zilles' collection of human and nonhuman primate brains, housed at the Cecile and Oskar (C&O) Vogt Institute for Brain Research at Heinrich-Heine-Universität Düsseldorf, Germany, have a particularly high contrast Nissl stain because they have been stained with silver using the Gallyas procedure, modified by Merker (1983). This staining method is well suited for making quantitative observations as well as qualitative observations. Most of the Zilles nonhuman hominoid specimens came from Yerkes and were brought to Düsseldorf through the efforts of Katerina Semendeferi, who was the first researcher to compare cytoarchitecture across all living great ape species.

Cytoarchitectonics is the description and analysis of differences in the neuronal composition of nervous tissue. Observations about regional differences in the cytoarchitecture of the cerebral cortex have resulted in the parcellation (i.e., subdivision) of the cerebral cortex into different cortical areas. Traditionally, cytoarchitectonic studies have been detailed, but mostly qualitative (e.g., Brodmann K, 1909; von Economo C, 1929). Therefore, it had not been possible to objectively compare cortical regions within a brain, or across different brains. This problem was addressed by the introduction of the grey level index (GLI). This GLI method for quantitatively estimating volume fractions of cell bodies was developed by Andreas Wree, Karl Zilles and Axel Schleicher (1982) to describe laminar patterns so efficiently that it can cover entire cortical areas. The procedure for creating GLI data involves creating digitized representations of the cerebral cortex in which neurons are automatically identified and converted into density values. The GLI is structured into profiles which follow the structure of cortical columns, and are calculated to take into account curvature imposed by sulci and gyri. Laminar patterning is determined from a mean of profiles, each of which provides data about differences in neuronal density along a cortical column.

Early parcellations of the cerebral cortex resulted in at most three cortical areas of the occipital lobe. As physiological studies on humans and nonhuman primates have revealed that more areas exist than had been recognized by Brodmann, cytoarchitectonics has developed to better identify actual cortical areas. The observer independent (OI) borders method uses GLI data to parcellate the cerebral cortex into cortical areas.

The earliest and most basic neuroanatomical studies concentrated on the three dimensional structure of the whole brain. With cytoarchitectonics, brains were sectioned

for histological investigation. One disadvantage of histological sectioning is that once a brain is sectioned, the three dimensional structure is lost. Further, a brain can only be sectioned in one plane – in fact, it is not always apparent what is the best way to section a brain, and a debate between Von Economo and Vogt erupted regarding the ideal way of sectioning brains. Recently, MR imaging and software has made it possible to create virtual three dimensional representations of brain structure, and allow for the visualization of a single point on the brain in multiple planes. This is helpful for determining the relationship between histologically-defined structures and external brain structures, as was done in the current study.

Cytoarchitectonic studies have been comparative from the start. Early brain-mappers such as Brodmann, Campbell, and Filimonoff compared humans to other higher primates because they had recognized that apes, and then monkeys, were the animals most closely related to humans. However, the modern phylogenetic perspective is that humans are not only closely related to apes, but in fact are nested in the same clade as apes. The panins (bonobos and chimpanzees) are our closest living relatives, and we are the closest living relative of the panins.

1.3 Major questions addressed in this thesis

This dissertation will address questions about the evolution of the hominoid visual system. These questions fall into three categories: 1) the comparative anatomy of the hominoid visual system, 2) human brain organization, and 3) the contribution of phylogenetic data to translational neuroscience.

The following questions concern comparative anatomy of the hominoid visual system:

Are visual areas V1, V2 and VP present in all hominoid species? Functional areas V1, V2, and VP are known to exist in humans and macaques. Therefore, it is hypothesized that analogues to macaque areas V1, V2, and VP are present and histologically identifiable in all catarrhine species. Microanatomical investigation will demonstrate whether individual species have these areas. If these areas exist, then there should be architecture that is similar to what exists in the literature for humans and macaques. See Chapter 4.

How do hominoid species compare with respect to the histological characteristics of striate area V1 and extrastriate visual areas V2, VP, and V5/MT+? There is evidence that hominoids in contrast to other catarrhines, and humans in contrast to other hominoids, show specializations in the laminar organization of V1. Therefore, it is hypothesized that species may differ in related laminar characteristics of V1 and higher-order areas, which receive input from V1. Individual cortical areas will be described quantitatively in terms of grey level index values and thickness of individual cortical layers. Differences in laminar pattern may be related to species-specific behaviors. Alternatively, differences may be found to correlate with brain, body and visual system variables. See Chapter 4.

How do hominoid species compare in lamination of the lateral geniculate nucleus? The LGN of catarrhines (with the exception of gibbons) has been described as a six-layered structure. Therefore, it is hypothesized that a six-layered LGN is a

sympleisiomorphy among catarrhines. The lamination of the LGN will be investigated in a range of catarrhine species, including several taxa not previously described, and the evolution of the LGN will be reconstructed using information about the phylogeny of the catarrhines. If the six-layered LGN is found to be a primitive characteristic, this might suggest recent changes related to visual information processing in the hylobatid lineage. See Chapter 6.

The following questions deal specifically with human brain organization:

Is human V1 smaller than would be predicted from brain volume? It has been suggested that association areas are expanded in humans, at the expense of V1. Therefore, it is hypothesized that in humans V1 size will be smaller relative to neocortex size than in closely related species. Regression analysis will be used to estimate expected values for all hominoids, against which V1 volumes of humans will be compared. If human V1 volumes are smaller than expected by the regression, this could indicate an expansion in the relative volumes of higher-order cortical areas. See Chapter 5.

How do hominoid visual brain structure volumes relate to volumes of other functional regions? It has been indicated the volumes of visual brain structures LGN and V1 have undergone more reduction in the hominin lineage than have the volumes of other brain components. Across hominoids, some degree of variability exists in the volumes of non-visual brain nuclei and cortical areas to which have been ascribed specific functions. The relative volumes of multisystem structures provide a context for interpreting reduction in visual brain volumes in humans. See Chapter 5.

Is the lunate sulcus a reliable indicator of brain organization in fossil hominins?
The position of the lunate sulcus has been used as an indicator of area V1 volume because it lies anterior to the external V1/V2 cytoarchitectonic border in nonhuman catarrhine brains. Therefore, it is hypothesized that V1 volume can be predicted from the position of the lunate sulcus. V1 volumes will be estimated from histological sections in ape brains and compared to lunate sulcus – occipital pole chord measurements. If the lunate sulcus is found to be a reliable indicator of V1 volume, it may be an indicator of brain organization in fossil endocasts. See Chapter 5.

The following question pertains to the contribution of phylogenetic data to translational neuroscience.

Is the macaque model sufficient for understanding the morphology of the human visual processing system? Macaques are routinely used as stand-ins for humans in studies of the visual system. Visual system data for rarely studied catarrhine species which are equally or more closely related to humans will provide details about potential recent evolution of visual system structures. Such details will shed light on potential similarities, differences, and parallelisms in the visual systems of macaques and humans See Chapters 4 and 6

1.4 Organization of this dissertation

Although all the new data generated in this dissertation pertain to the visual system of hominoids, there are two lines of overarching questioning being addressed

here. First, this dissertation asks: *Do the visual system structures of hominoids relate to species-specific behaviors?* Second, this dissertation asks: *Is there evidence for brain reorganization, i.e., a disproportionate increase in the amount of tissue devoted to higher order versus primary cortical areas, in the human lineage?*

This dissertation comprises seven chapters. All fall under the umbrella of comparative, phylogenetically informed studies, which consider species-specific differences in brain organization, and include newly acquired data about the hominoid visual system. The first chapter is an introduction to the dissertation. The next two chapters provide a review of selected studies relevant to this dissertation. Chapter 2 introduces the catarrhine visual system and cytoarchitectonics, and reviews hominoid physiological and behavioral data relevant to the evolution of the visual system. Chapter 3 reviews paleoneurological methods and the fossil evidence for brain evolution within the human clade.

Chapters 4 through 6 present the new hominoid visual brain structure data obtained by this research program, and each chapter should be read as an independent study, complete with introduction, materials and method, results, and discussion sections. Chapter 4 is a comparative quantitative cytoarchitectural study of the primary visual area V1, and the extrastriate visual areas V2, VP and V5/MT+ in hominoid species, with *Macaca fascicularis* as an outgroup. Its premise is given the evidence for significant differences in hominoid V1 laminar composition, there may also be differences in the extrastriate visual areas which receive inputs from V1. In this chapter, laminar patterns are compared quantitatively for layer widths and layer-wise GLI values. In addition the profile curves of different cortical areas are analyzed using multivariate methods. These

data are explored for evidence of significant scaling relationships with body, brain and visual system variables. Chapter 5 is a comparative volumetric study of visual brain structures V1 and the LGN in hominoids. First, it investigates whether the volume of V1 and LGN are relatively smaller in humans than predicted. Second, it explores the variability in V1 volume among, and within, hominoid species. Third, it addresses the reliability of using the position of the lunate sulcus as determined on magnetic resonance (MR) images for determining relative V1 in hominoid species.

Chapter 7 is a summary of the conclusions of about the organization of visual system structures in hominoid species. This chapter also summarizes the hypotheses to emerge from this thesis and suggests ideas for future research to extend the findings of this dissertation.

Table 1.1. Taxonomy of living and fossil primates discussed in this dissertation.

Taxonomic classification	Extant members
Order Primates ('primates')	primates
Suborder Strepsirrhini ('strepsirrhines')	non-tarsier prosimians
Suborder Haplorrhini ('haplorrhines')	anthropoids and tarsiers
Infraorder Tarsiiformes ('tarsiiformes')	tarsiers
Infraorder Simiiformes ('simiiformes')	simians; anthropoids; monkeys, apes, and humans
Parvorder Platyrrhini ('platyrrhines')	New World monkeys
Parvorder Catarrhini ('catarrhines')	Old World monkeys, apes, and humans
Superfamily Cercopithecoidea ('cercopithecoids')	Old World monkeys
Subfamily Cercopithecinae ('cercopithecines')	cheek-pouch monkeys
Tribe Papionini ('papionins')	
Subtribe Papionina	
Genus *Papio*	hamadryas baboons
Genus *Mandrillus*	drills and mandrills
Genus *Theropithecus*	gelada baboons
Genus *Lophocebus*	arboreal mangabeys
Genus *Cercocebus*	terrestrial mangabeys
Subtribe Macacina	
Genus *Macaca*	macaques
Tribe Cercopithecini ('cercopithecins')	
Genus *Erythrocebus*	patas monkeys
Genus *Chlorocebus*	green monkeys
Genus *Cercopithecus*	guenons
Subfamily Colobinae ('colobines')	leaf-eating monkeys
Tribe Colobini ('colobins')	African colobines
Tribe Presbytini ('presbytins')	Asian colobines
Superfamily Hominoidea ('hominoids')	apes and humans
Family Hylobatidae ('hylobatids')	lesser apes; small apes; gibbons
Genus *Hylobates*	*lar* group
Genus *Bunopithecus*	hoolocks
Genus *Nomascus*	*concolor* group; crested gibbons
Genus *Symphalangus*	siamangs
Family Hominidae ('hominids')	great apes and humans
Subfamily Ponginae ('pongines')	
Genus *Pongo*	orangutans
Subfamily Gorillinae ('gorillines')	
Genus *Gorilla*	gorillas
Subfamily Homininae ('hominines')	
Tribe Panini ('panins')	
Genus *Pan*	chimpanzees and bonobos
Tribe Hominini ('hominins')	
Subtribe Australopithecina ('australopiths')	
Genus *Ardipithecus*	
Genus *Australopithecus*	
Genus *Kenyanthropus*	
Genus *Orrorin*	
Genus *Paranthropus*	
Genus *Sahelanthropus*	
Subtribe Hominina ('hominans')	
Genus *Homo*	humans

Chapter 2. The Catarrhine Visual System

This chapter is devoted to the catarrhine visual system. First, the catarrhine visual system is described. Next, the history of visual cortex parcellation and the methods used to study the catarrhine visual cortex are briefly described. Third, this section briefly reviews the evidence for behavioral, cognitive, and anatomical variation in the visual system of hominoids. Fourth, the reasons neurophysiological studies of the apes are restricted, and the implications of this restriction, are discussed.

2.1 The catarrhine visual system

The following is an overview of the aspects of the catarrhine visual system that are relevant to the topics of this dissertation. For more details, see (Butler AB and W Hodos, 1996; Kaas JH and MF Huerta, 1988; Nolte J, 1998; Rodiek RW, 1988; Yantis S, 2001).

2.1.1 The retinogeniculocortical pathway of the visual system

In catarrhines, the visual system is one of several brain systems in which information passes through and is filtered and sorted by subcortical and cortical structures. Visual information in the form of photons is detected by retina, which is a sensory structure and a component of the CNS. The retina, the inner layer of the eye, is

comprised of three layers of neuronal cell bodies. The deepest region of the retina, outer

nuclear layer, is composed of the receptor neurons which detect visible light. These fall

into two categories, rods and cones, based on differences in morphology and distribution

in the retina. Rods are distributed toward the peripheral part of the retina and contain

rhodopsins, which are highly sensitive to light and have low acuity, and thus are used in

low-light environments. Cones are found in highest density in the central part of the

retina and contain cone opsins, which are less sensitive, have higher acuity, and are used

in color vision and in more brightly lit environments. Photoreceptor neurons synapse on

various categories of neurons in the middle retinal layer, called the inner nuclear layer.

These neurons then transmit information to the ganglion cells, whose cell bodies are in

the ganglion cell layer. Retinal ganglion cells from each eye give rise to afferent axons

which comprise the optic nerves. The two optic nerves partially decussate at the optic

chiasm, in such a way that the fibers of each visual hemi-field end up on the contralateral

side of the brain, i.e., axons of neurons that perceive the left visual field of both left and

right eyes are directed to the right side of the brain. Note that the degree of decussation is

related to binocular and stereoscopic vision, such that primates, which have binocular

vision, half of the fibers decussate, whereas in mammals without binocular vision nearly

all fibers decussate (Allman JM, 2000). After the optic chiasm, these fibers continue as

the optic tracts. Most fibers belong to the retinogeniculocortical pathway, and terminate

directly in the telencephalon, in the lateral geniculate nucleus (LGN) of the dorsal

thalamus (Fig. 2.1 A). The LGN has magnocellular and parvocellular layers, which

receive retinal input from alternating eyes (Fig. 2.1 A). When the parvocellular layers are

further subdivided into leaflets, the leaflets are interdigitated such that a leaflet receiving

retinal input from the ipsilateral eye is adjacent to a leaflet receiving inputs from the contralateral eye. At the level of the lateral geniculate nucleus, visual inputs are processed and modified, and most enter the cerebral cortex through the primary visual area, V1 (Fig. 2.1 B).

In addition, extrageniculocortical visual pathways exist (Butler AB and W Hodos, 1996). In the mesencephalon, the superior colliculus of the rostral tectum receives direct retinal inputs. The superior colliculus has a dual role in vision: it participates in transforming visual inputs into saccadic eye movements and eye-head movements and it also relays visual inputs to the pulvinar of the caudal thalamus, which is in turn an afferent of visual inputs to striate and extrastriate visual cortical areas (Kaas JH and MF Huerta, 1988). In the diencephalon, the suprachiasmatic nucleus of the hypothalamus of receives a direct projection of retinal fibers which is involved in the phasic timing of circadian rhythms to diurnal light. The networking of visual data in the brain is extremely complex and not fully understood. The retinogeniculocortical pathway is the focus of this dissertation because this is the pathway mainly responsible for conscious visual perception.

2.1.2 Visual areas

The visual cortex is the portion of the cerebral cortex concerned entirely or mainly with processing visual information. Visual areas are involved in segregating and analyzing the features (e.g. color, orientation) of visual images. The visual cortex can be further subdivided, or parcellated, into several individual visual areas. Visual areas are distinguished when reliable differences can be demonstrated in one or more of the

following criteria: retinotopy, function, histology, and connections (Felleman DJ and DC Van Essen, 1991; Kaas JH, 1997; Van Essen DC, 1985). Some visual areas are recognized in all parcellation schemes, while others remain controversial. Areas V1 (primary visual area), V2 (secondary visual area) and MT (medial temporal area) occur in all primates and are the least contested visual areas (Kaas JH, 1993; Rosa MG and R Tweedale, 2005). These are the only visual areas that have been fully mapped in all primates and have a complete retinotopic representation of the visual hemifield (Van Essen DC, 1985). In addition to these, many other visual areas occur in primates which are less poorly defined in terms of function, location, and homology across species. Also, areas that are disputed because they do not comprise a complete retinotopic representation of the contralateral visual hemifield are termed "improbable areas" (Kaas JH, 1993; Zeki S, 2003), and it has been argued that the best known of these, VP, should be considered part of V3 (Lyon DC and JH Kaas, 2002). V3A (V3 accessory), on the other hand, is distinct from its neighbor, V3, and fits all the criteria for an independent visual area (Tootell RB et al., 1997). However, as mentioned below, human and macaque analogues of V3 and V3A show physiological differences.

2.1.3 Visual perception

As visual inputs travel from the retina to the LGN to V1 and to extrastriate cortex, there are changes in the receptive field properties of neurons. The classical receptive field of a neuron is the region of space in which the occurrence of a stimulus will evoke action potentials. Consider a neurophysiologist monitoring the activity of a single optic nerve fiber, that is, the axon of a single retinal ganglion cell, in a macaque. A bright

wand is waved in front of the macaque's visual field. The neuron in question will respond when the wand is in the spatial receptive field of that neuron. In the visual system, receptive fields are volumes in visual space. Each photoreceptor (rod or cone) neuron has a cone-shaped visual field volume corresponding to the region of space in which photons entering the eye will alter the firing of that cell. This region of space is normally quantified in terms of degrees of visual angle. As information travels to other neurons, the spatial receptive field of a neuron depends on its afferent inputs. The receptive field of a retinal ganglion cell subsumes the fields of all of the photoreceptor neurons connected to it through synapses with neurons in the inner nuclear layer. In general, visual inputs pass through a hierarchy of structures, such that as information travels from the retina to the LGN to V1 and then to extrastriate cortex, the receptive field size of individual neurons increases. Within the cerebral cortex, structures early in the hierarchy are sometimes termed "lower order" or "early" and those later in the hierarchy are termed "higher order" or "late". However, neuroscience investigations are increasingly demonstrating that there exists a complexity of inputs with reentrant feedback from higher order to lower order structures.

Further, retinal ganglion cells are categorized as either on-center (ON) and off-center (OFF). For each cell the receptive field is comprised of a central circle, called the "center" and the area around the circle, called the "surround". An ON cell fires rapidly when light appears at the center of its receptive field, but the cell's response is inhibited when light is shone in the surround region of its receptive field. An OFF cells fires rapidly when light is shone in the surround, and the cell's response is inhibited when light is shown in the center. As visual information ascends the hierarchy, neurons

preferentially respond to increasingly complex stimuli. For example, in V1 neurons exist which respond best to bars in a particular location or orientation (Hubel DH and TN Wiesel, 1968). In area V4, many neurons are tuned for contours, i.e., angles and curves (Pasupathy A and CE Connor, 2002). In area TE, the final exclusively visual area a large proportion of neurons respond exclusively to faces (Perrett DI et al., 1985).

2.1.4 Parallel pathways of the visual system: magnocellular, parvocellular, and koniocellular parallel pathways

Two systems, called the magnocellular (M) and parvocellular (P) pathways, are involved in processing visual sensory cues (Livingstone M and D Hubel, 1988). The M pathway carries high-contrast visual information, including information about motion. The P pathway carries information about color and fine structure. Each pathway is comprised of a distinct group of nerve fibers originating from retinal ganglion cells and terminating in the lateral geniculate nucleus (LGN) of the thalamus. The M pathway originates in the large, sensitive parasol ganglion cells of the retina, which primarily receives inputs from rods, and which synapse in the magnocellular (i.e., large-celled) layers of the LGN, and then project to layer 4Cα of cortical area V1. The P pathway originates in the small, numerous midget ganglion cells of the retina, which primarily get inputs from cones (see below), and which synapse on the parvocellular (i.e. small-celled) layers of the LGN, which then project to layer 4Cβ of V1 (Leventhal AG et al., 1981; Rodiek RW, 1988).

M and P pathway organization is maintained in V1 and its primary target, V2, as the P-I (P interblob), P-B (P blob), and M streams (DeYoe EA and DC Van Essen, 1988).

Early visual areas V1 and V2 have feed-forward projections to higher visual areas, in which visual streams and related functions become more segregated. Areas V3 (Felleman DJ and DC Van Essen, 1987), V3A (Tootell RB *et al.*, 1997), and MT (Albright TD et al., 1984) are involved in motion detection, and are associated with the M stream (Deyoe EA et al., 1990). Area V4, dubbed the "color center" (Lueck CJ et al., 1989; McKeefry DJ and S Zeki, 1997; Zeki SM, 2004), is associated with the P-B and P-I streams (DeYoe EA et al., 1994; Van Essen DC et al., 1992).

It was originally suggested (Livingstone M and D Hubel, 1988) that the M and P pathway divisions correspond to two previously described divisions of the visual association areas: the dorsal and ventral streams. The ventral stream (the "what" pathway) is involved in object identification and terminates in areas of the inferior temporal cortex, whereas the dorsal stream (the "where" pathway) is involved in the spatial localization of objects (and in action) and terminates in posterior parietal cortex (Gattass R et al., 1990; Goodale MA and AD Milner, 1992; Ungerleider LG and M Mishkin, 1982). The M pathway predominates the input to MT, which itself provides major inputs to inferior temporal cortex, and the P pathway predominates the inputs to V4, which itself provides major inputs to posterior parietal cortex. However, the relationship between the M and P pathways and the dorsal and ventral stream is not precise, as V4 receives strong M and P inputs (Ferrera VP et al., 1994).

It is increasingly clear that visual information is not simply divided into M and P pathways. Recently, data have begun to accumulate about the koniocellular (i.e. very small-celled) neurons in macaques, which are distinguished from LGN neurons of the M and P pathways on the basis of positive immunohistochemical staining for the alpha

subunit of calmodulin-dependant protein kinase 2 (αCAMKII; (Hendry SH and T

Yoshioka, 1994; Yoshioka T and SH Hendry, 1995); the calcium binding protein

calbindin (Goodchild AK and PR Martin, 1998; Jones EG and SH Hendry, 1989) and the

gamma subunit of protein kinase C (Fukuda K et al., 1994). In fact, the koniocellular

neurons in the LGN have been known for quite some time to exist in anthropoids

(Chacko L, 1948; 1954; 1955; 1955; 1949; e.g., Le Gros Clark WE, 1941; 1941;

Solnitzky O and P Harman, 1943), and these neurons have been referred to as

"intercalated layers" or "interlaminar cells". In addition, a third category of LGN

lamination, called the koniocellular layers, had been described as well-formed layers in

other primate groups (lorises and bushbabies; see Kaas *et al.* (1978) for a review) and

these are presumably homologous the koniocellular layers in catarrhines (Hendry SH and

RC Reid, 2000). K cells are distributed in several layers in the LGN, one located ventral

to each M and P layer, plus neurons with the K neurochemical signature are distributed

within the M and P layers (Hendry SH and RC Reid, 2000; Hendry SH and T Yoshioka,

1994; Yoshioka T and SH Hendry, 1995). In macaques, koniocellular LGN axons

originating from ventral LGN layers K1 and K2 terminate in V1 layers 1 and 3A , and

those originating from dorsal LGN layers K3-K6 terminate in layer 3Bα (Casagrande VA

et al., 2007).

 Other pathways in addition to the M, P and K pathways also exist. At the level of

the retina, at least ten classes of ganglion cells have been distinguished (Dacey DM et al.,

2003). Recently it has been shown that there are direct inputs from the LGN to

extrastriate visual areas, which do not match criteria for inclusion in M, P or K pathways

(Sincich LC et al., 2004).

2.1.5 Color vision channels

Photoreceptor neurons of the retina contain photoreceptor proteins called opsins, which contain photopigments. Each type of photopigment reacts only with light in a specific wavelength range of the spectrum. In catarrhines, cone opsins, and the cones in which they occur, fall into three categories according to the wavelength at which light absorption is highest: short (S, ca. 430nm), middle (M, ca. 530 nm), and long (L, ca. 560 nm) (Bowmaker JK et al., 1991; Jacobs GH and JF Deegan, 1999).

Catarrhine species, all of which are routinely trichromatic, possess two subsystems in which color information is processed. The ancient subsystem, which also exists in dichromats, is primarily responsible for differentiating "blue" outputs of S cones from "yellow" outputs of the M and L (M/L) cones. In this subsystem, small bistratified retinal ganglion cells with large receptive fields draw outputs from S cones and M/L cones, and theses outputs are carried to the koniocellular laminae of the LGN (Regan BC et al., 2001). The recent subsystem exits only in trichromats, and is primarily responsible for differentiating green outputs of M cones from red outputs of the L cones. In this system midget ganglion cells with small receptive fields carry outputs of M and L cones to the parvocellular laminae of the LGN (Regan BC *et al.*, 2001).

Although most mammals are dichromatic, catarrhines are routinely trichromatic, that is, both males and females are usually trichromatic. The genes which code for the S opsin is located on an autosome, chromosome 7 in humans (Nathans J et al., 1986). In catarrhines, the genes coding for the M and L opsins are located on two adjacent X-chromosome loci. In most platyrrhines, a single M/L locus on the X chromosome results

in trichromacy in heterozygous females , and dichromacy in males – although the nocturnal owl monkey (*Aotus*) is monochromatic (Jacobs GH et al., 1993) one group of platyrrhines, the howler monkeys (*Alouatta*), have multiple X chromosome pigment loci and exhibit routine trichromacy (Jacobs GH, M Neitz et al., 1996). In addition, lemurs may also be trichromatic, although the mechanism for color vision is distinct from that of anthropoids and seems to involve a combination of signals from rods and cones (Jacobs GH and JF Deegan, 1993).

2.2 Parcellation of the visual cortex

Originally, it was thought that the cerebral cortex was a uniform sheet of tissue. However, the cerebral cortex is now known to be comprised of discreet cortical areas, the existence of which is supported by convergent anatomical and physiological evidence. The earliest brain maps were based on either cyto- or myelo-architectonics alone. In fact the first cortical area ever discovered was the primary visual cortical area, which on an unstained brain stood out from adjacent cortex due to a white stripe of myelinated fibers corresponding to layer 4b – Gennari's stripe, from which the "striate" cortex received its name. Further investigation of the cerebral cortex has led to the naming of numerous architectonically defined cortical areas.

Visual areas were originally distinguished solely on the basis of histological evidence, particularly cytoarchitectonics. Criteria for cytoarchitectural parcellations include: 1) thickness of cortex, 2) thickness of individual cortical layers, 3) number of layers, 4) staining intensity of neurons or of ground substance, 5) vertical or radial

arrangement of neurons, 6) the packing density of neuronal cell bodies, 7) neuronal cell

body size 8) the presence of special cell types, and 9) peculiarities unique to a specific

cortical regions (Lashley KS and G Clark, 1946; Zilles K et al., 2002). Usually, only the

cytoarchitectonic parcellation of Brodmann (1909), and occasionally that of Von

Economo (1929), are referenced in the neurosciences. Brodmann identified three visual

areas – 17, 18 and 19 – in the human occipital lobe on the basis of cytoarchitecture.

These roughly correspond to areas OC, OB and OA, respectively, in the terminology of

Von Economo. Von Economo also mentions some subregions, but does not give much

indication about the borders between them (von Economo C, 1929). It had long been the

goal to ascribe function to structure, and early brain-mappers such as Brodmann and the

Vogts saw the purpose of their work to be "the development of a comparative organology

of the cerebral surface, based upon anatomic criteria"(Brodmann K, 1925). However,

recent comparisons of early cytoarchitectonic maps to functional studies indicate that

these tripartite divisions of the human occipital lobe are oversimplifications.

In contrast, physiological data are used to distinguish over 25 distinct visual areas

in macaques (Felleman DJ and DC Van Essen, 1991; Van Essen DC, 2004), many of

which are outside the occipital lobe and are not included within the extent of areas 17, 18

and 19. In response, a new nomenclature has arisen to describe these functionally-

relevant monkey visual areas (this terminology has also become accepted in human

neuroimaging studies; (e.g., DeYoe EA *et al.*, 1996; McKeefry DJ and S Zeki, 1997;

Sereno MI et al., 1995; e.g., Tootell RB *et al.*, 1997; Vanduffel W et al., 2001).

Recently, neuroimaging has confirmed that humans have more visual areas than

classical cytoarchitecture suggests. De Yoe et al. (1996) demonstrated that on the basis

of physiological data, area 19 can be subdivided in humans, as it is in macaques. In addition, human homologues have been found for several visual areas located outside of the occipital lobe (Van Essen DC, 2004).

Of the human cytoarchitectonic areas, only Brodmann area 17 has been shown to be directly identical to a functional area (V1) on the basis of a high field MRI study which permitted histological identification and functional imaging (Bridge H et al., 2005). Area 17 also happens to be the easiest visual area to identify on histological sections, as its layer 4 is divided into three sublayers, of which 4B corresponds to the macroscopically visible stripe of Gennari.

Cytoarchitectonic-based parcellations of the cerebral cortex have been criticized for being incongruent with each other, even within a species (Lashley KS and G Clark, 1946). Different authors have divided the human brain into different numbers of cortical regions – ranging from just four main types described by Bailey and von Bonin (1951) to over 150 fields identified by the Vogts (Gerhardt E, 1940; Riegele L, 1931). Several variables have driven to this, including the use of different types of staining, differences in cytoarchitectonic criteria, and insufficient consideration of intraspecific variability. It has been argued that many of the criteria used in parcellating cortex many have nothing to do with function. For example, the gyrification of the cortex itself leads the changes in cortical thickness, laminar density, and columnarity (von Economo C, 1929).

It has been stated that cytoarchitectonic parcellations depend largely on the intuition of the observer, that the basis of differentiation cortical areas it is not always obvious, and that individual estimates of cell size and density were not confirmed by actual measurements (Lashley KS and G Clark, 1946). This problem has recently been

addressed by the observer-independent (OI) method of cortical parcellation (Schleicher A et al., 1999). The OI method requires the cerebral cortex to be photographed and converted into grey level images, which provide quantitative data about variation in neuronal volume density. These data are used to estimate laminar pattern across vertical cortical columns, and these patterns are compared for statistically significant differences. Abrupt changes in laminar pattern, which in theory correspond to cortical area borders, are in this way justified on the basis of quantitative data (Schleicher A *et al.*, 1999).

Cytoarchitectonic parcellations are mainly based on Nissl stained material, and the input is limited to the variability visible in the total population of cell bodies. The use of different staining methods and neuronal markers may provide better, or at least complementary, information about cortical area patterns and borders. Braak (1977) subdivided the human occipital lobe into ten different areas on the basis of pigment architecture, which reveals additional details about laminar pattern that are not visible in adjacent Nissl stained sections. Also, extrastriate cortex heterogeneity has been suggested on the basis of the patterns of termination of axons passing through the corpus callosum. This method involves visualizing callosal axons that have degenerated – either due to unilateral occipital infarctions, or, in the case of experimental animals, transection of the posterior corpus callosum – prior to death. In rhesus monkeys, a direct comparison between callosal axon termination pattern and physiological organization has demonstrated that callosal projections characterize boundaries between V1 and V2, V3 and V3A, V3 and V4, and the anterior border of VP (Van Essen DC et al., 1982; Van Essen DC and SM Zeki, 1978). Using a combination of callosal afferent organization and myeloarchitecture, Clarke and Miklossy (1990) have proposed functional human

analogues to macaque areas V1, V2, V3d, VP, V4 and MT. Cytochrome oxidase (CO) is an endogenous mitochondrial enzyme for which postmortem brain tissue is reacted to detect metabolically highly active zones. In two species of Old World monkeys (*Cercopithecus aethiops* and *Macaca mulatta*) and humans, CO histochemistry reveals regional distinctions for several extrastriate visual areas including V1, V2, MT and possibly V3 (Tootell RB and JB Taylor, 1995). Autoradiographic labeling of multiple transmitter receptors in humans and macaques had revealed regional and laminar cortical patterns that are consistent with known myelo- and cytoarchitectonic borders, and additionally delineate regions that are not detectable using cytoarchitecture alone (Zilles K and N Palomero-Gallagher, 2001; Zilles K et al., 1995; Zilles K *et al.*, 2002).

Immunohistochemical techniques may offer the most thorough and readily applicable histological method for parcellating the visual cortex. Immunohistochemistry localizes tissue constituents *in situ* by means of a specific antigen-antibody interaction, using a labeled antibody. This allows visual areas to be identified and defined in terms of laminar patterns of neuronal populations containing a specific protein. In addition, immunohistochemical markers reveal differences between taxonomic groups (Hof PR, 2000; Sherwood CC, MA Raghanti et al., 2007). SMI-32 is an antibody marker that reacts with non-phosphorylated epitopes on neurofilament H (High molecular weight neurofilament; Sternberger and Sternberger 1983). Neurofilament proteins are assembled into neurofilaments, which are the main cytoskeletal components of axons and dendrites (Lacoste-Royal G et al., 1990). In crab-eating macaques (*Macaca fascicularis*), non-phosphorylated neurofilament protein (NPNFP) staining with the SMI-32 antibody has been used to identify twenty-eight visual areas (Hof PR and JH Morrison, 1995). SMI-32

29

primarily visualizes neuronal cell bodies and dendrites of a subset of pyramidal neurons which are defined by large soma size and thick, heavily myelinated axons. Certain SMI32-immunoreactive (SMI32-ir) neurons in human V1 which in monkeys have long projections from lower to higher cortical areas (Hof PR et al., 1996), are reduced in number in Alzheimer's disease cases – possibly related to visual deficiencies observed in Alzheimer's patients (Hof PR and JH Morrison, 1990). A comparison of diverse cortical regions, including V1 and area 4, demonstrates that, overall, hominoids have a greater proportion of SMI32-ir pyramidal neurons then do cercopithecoids (Campbell MJ and JH Morrison, 1989; Sherwood CC, RL Holloway, JM Erwin and PR Hof, 2004). NPNFP labeling has been qualitatively investigated in V1 of several anthropoid including humans, some apes, and some cercopithecines (Preuss TM *et al.*, 1999). Also, V1 and V2 interneurons labeled by calcium binding proteins have been quantified in anthropoids, and it has been found that hominoids had relatively fewer calbindin-immunoreactive interneurons than did monkeys (Sherwood CC, MA Raghanti *et al.*, 2007).

In summary, cortical area mapping based on multiple architectural modalities are bound to produce the most objective and robust cortical area parcellations, particularly when direct physiological data is not available.

Two publications map extrastriate cytoarchitectonic areas in great ape species, both of which are based on tripartite parcellations of the occipital lobe. The first is a parcellation of the occipital lobe by Filimonoff (1933), which uses the nomenclature of Brodmann to parcellate the orangutan occipital lobe. The second is a parcellation of the entire chimpanzee cerebral cortex by Bailey *et al.* (1950), which is based on Von Economo's descriptions. These maps provide an overview of the tripartite organization

of the visual cortex in individuals of these species, but alone are not sufficient to reproduce these cytoarchitectonic areas. For example, Filimonoff (1933) left sulci for which he was unable to find homologues in other species unlabeled. Bailey *et al.* acknowledge that "area OA resembles OB so closely, and the transition between the two areas is so gradual, that it is impossible to draw a line between them" (p. 48; 1950). Although they are able to indicate the position of some cortical areas in superficial maps, borders located deep in sulci are not indicated.

2.3 Behavior, cognition, and anatomy

In order to thoroughly understand human brain evolution, it is important to consider that each primate's brain is specifically adapted to the socioecological problems facing its species (Ghazanfar AA and LR Santos, 2004). Hominoid neuroanatomical comparisons should be made in the context of species-specific behaviors.
All catarrhines studied have been reported to have the photopigments necessary for routine trichromatic vision (Deegan JF and GH Jacobs, 2001; Jacobs GH and JF Deegan, 1999); and the genetic sequences consistent with the production of the necessary cones opsins (Deeb SS et al., 1994; Dulai KS et al., 1994; Hunt DM et al., 1995). Even within the catarrhines, differences in color perception may exist, as behavioral and anatomical evidence points to potential differences in color vision at a post-retinal level. Color perception specializations may be seen at the subcortical level in the organization of the LGN, or at the cortical level in the microstructural organization and volume of V4.

Catarrhine species may differ in aspects of color discrimination, too, although studies are somewhat conflicting. Grether (1940) found that humans had better red discrimination than did macaques and chimpanzees (chimps and macaques were similar to each other), although at the low (blue) end of the spectrum, chimpanzees, humans and macaques were all similar. De Valois (1974) found that macaques and humans were similar at the high (red) end of the spectrum, although macaques were slightly more sensitive at lower (low) wavelengths. Harwerth and Smith (1985) found that humans have greatest sensitivity in the high (red) part of the spectrum; whereas macaques have greatest sensitivity in the low (blue) part of the spectrum. The L:M cone ratio is 2:1 in humans whereas it is 1:1 in macaques (Dobkins KR et al., 2000) and is intermediate in chimpanzees (Jacobs GH, KF Deegan et al., 1996).

A psychophysical study has revealed that gibbons having poorer blue discrimination than orangutans (Tigges J, 1963). Hylobatids seem to have lower cone to rod ratios than do macaques (Polyak S, 1957; Rohen J, 1962). In a physiological study, hylobatids had a strikingly low number of color-receptive cells in any visual area, including an extrastriate area potentially homologous with the "color center" V4 (Vital-Durand F and C Blakemore, 1981).

Hylobatids have simpler parvocellular LGN lamination than other catarrhines that have been examine (with the possible exception of orangutans and some colobines, see Chapter 7; Tigges J and M Tigges, 1987). Tracing experiments of retinofugal fibers did not report intercalated cells (i.e., potentially K cells) between LGN lamina in chimpanzees (Tigges J et al., 1977). In contrast the gibbon, in which a layer intercalated

between the two magnocellular layers 1 and 2 is visible without modern techniques (Chacko L, 1955; Tigges J and M Tigges, 1987).

Hominoids (of which humans, chimpanzees and orangutans were studied) differ from cercopithecoid monkeys (of which several cercopithecine species were studied) in that they lack a band of cytochrome oxidase (CO) activity in layer 4A of V1, indicating a loss of P inputs to this layer (Preuss TM *et al.*, 1999). This difference between these hominoids and monkeys may be related to differences in color perception. Recent evidence has suggested that folivorous behavior has maintained routine trichromatic color vision in catarrhines (Dominy NJ and PW Lucas, 2001; Lucas PW et al., 1998; Lucas PW et al., 2003). Gorillas, which were not included in the above study, stand out among hominoids as being primarily folivorous, rather than primarily frugivorous (Clutton-Brock TH and PH Harvey, 1979). Therefore, gorillas may have brain specialization that better suit them for identifying edible foliage.

Some evidence suggests that humans have anatomical specializations related to the detection of motion. Humans possess a unique meshwork arrangement of M pathway fibers in layer 4A of V1 (Preuss TM and GQ Coleman, 2002; Preuss TM *et al.*, 1999). This specialization may give humans increased sensitivity to motion and luminance contrast. If humans are specialized for motion detection, then it is likely that other aspects of their neuroanatomy are also derived for this skill. Specifically, the magnocellular layers of the LGN and cerebral cortical areas V3, V3A, and, especially, MT have important roles in motion detection, so related specializations may be detected in the volumes and microstructural organization of these extrastriate areas. However,

note that Meynert cells, which are involved in motion detection, show a size increase in terrestrial cercopithecines, but not in humans (Sherwood CC, PW Lee et al., 2003).

Cognitive and behavioral studies demonstrate variation in aspects of visual perception, within catarrhines and within hominoids. For example, when shown a compound visual pattern, humans perceive the global form before the local forms, whereas baboons show a local precedence (Fagot J and C Deruelle, 1997). Chimpanzees seem to have either a local precedence or no consistent bias at all (Fagot J et al., 2001). Physiological studies highlight certain cortical areas as participating in the aforementioned cognitive task for some species. Specifically, dorsal inferotemporal cortex (TEd) appears to be involved in the identification of local, but not global, features by crab-eating macaques (Macaca fascicularis; Horel JA, 1994). This is consistent with an fMRI study of humans and anesthetized rhesus monkeys, demonstrating that early visual areas (e.g. V1 and V2) may respond to global rather than simple local features (Kourtzi Z et al., 2003).

Chimpanzees also differ from humans when perceiving the shape of an object based on shading cues (Tomonaga M, 2001). For example, when humans see a shading pattern from light at the top to dark at the bottom, they see a convex shape, whereas if the shading is from dark at the bottom to light at the top, they see a concave shape. Humans can rapidly segregate these perceived convex and concave shapes when the light gradient is shaded vertically. However, when the shading pattern is varied from left to right (that is, horizontal shading), humans are not able to rapidly discern shape. This suggests that the human visual system has a bias for seeing objects as if they were lit from above. Surprisingly, whereas humans can quickly segregate shapes with vertical shading,

chimpanzees rapidly segregate shapes with horizontal rather than vertical shading (ibid).

Physiological studies highlight certain cortical areas as participating in shape-from-shading tasks for humans and monkeys. An fMRI investigation of humans has demonstrated that lower visual areas V1, V2 and V3 are activated during shape from shading tasks (Humphrey GK et al., 1997), but this finding conflicts with previous studies in monkeys suggesting that V4 is involved in related texture segregation tasks (Hanazawa A and H Komatsu, 2001) and thus has drawn skepticism (Connor CE, 2001).

2.4 Dearth of ape data

Most methods used to understand visual cortex organization have not been systematically applied to apes and humans for ethical and practical reasons. Macaques are the animals most closely related to humans upon which invasive methods, such as single-cell recordings and lesioning, have been most regularly applied in order to understand the structure and function of visual cortex. Monkeys are preferred over apes for physiological studies for pragmatic reasons. These include their relatively small overall size, and relative ease of handling. Their brain sizes are also smaller, and there is less gyrification,

Recent advances in neuroimaging are ending the bias towards using monkeys, and physiological studies of the human visual cortex are rapidly growing in number. However, the foremost method used in human physiological studies is fMRI, which has not been successfully applied to apes. Skepticism abounds as to the precision of the information gleaned from fMRI, and it is not clear how best to combine fMRI and

microelectrode findings (Orban GA et al., 2004). Direct physiological comparisons

between human and macaque visual systems are still rare. One approach at direct

comparison has been to repeat human fMRI experiments on monkeys, although the

procedure requires invasive physical restraints (e.g., Vanduffel W *et al.*, 2001).

For the foregoing reasons, many researchers involved in human brain mapping

treat the human brain as if it were an enlarged macaque brain. Humans and macaques are

both anthropoids with many similarities, including diurnality, terrestrial behavior, and

tool-use (Kawamura S, 1959), and species-specific communication using similar neural

substrates (Gil-da-Costa R et al., 2006). Thus, it is easy to equate macaque behavior and

morphology to human behavior and morphology. However, neuroscientists seldom

consider the evolutionary trajectories of the behaviors and morphologies, and the

possibility that they may not always be identical. In fact, much ecological and behavioral

diversity exists in the extant ape species more closely related to humans than are

macaques. There is also much ecological and behavioral variability within the

cercopithecoid species, which share the same last common ancestor with humans that

macaques do. Therefore, it is possible that similar behavior and anatomy shared between

humans and macaques is not homologous, but could have arisen through convergent (i.e.

most likely "parallel") evolution. This possibility is especially tricky when trying to sort

out structure-function relationships, since homoplasy in closely related species may be

due to a complicated interaction of evolutionary and developmental factors.

Anatomical and functional differences between human and macaque visual

systems occur at all levels of the visual system (for a more detailed review, see Preuss

TM and GQ Coleman, 2002). In the retina, the dendritic fields of parasol cells, but not

midget cells, are larger in humans than in macaques (Dacey DM and MR Petersen, 1992). In the LGN, there may be differences in calbindin lamination pattern in humans and macaques (Leuba G and K Saini, 1996; Munkle MC et al., 2000). Humans and macaques differ in the patterns revealed by cytochrome oxidase staining, in the blobs in V1 and the stripes in V2 (Horton JC and MP Stryker, 1993; Tootell RB and JB Taylor, 1995). In humans, extrastriate visual area V3A is more motion selective, whereas V3 is less so. It is the reverse in macaques (Tootell RB *et al.*, 1997; Vanduffel W *et al.*, 2001).

However, at present little is known about how the microanatomy of the visual cortex of apes compares with that of macaques and humans. The current project studies visual system organization in hominoids using the only type of evidence currently available for all extant hominoid species, that is, histology. These data are considered in light of existent information derived from histological evidence, plus physiological evidence which is *not* currently available for apes.
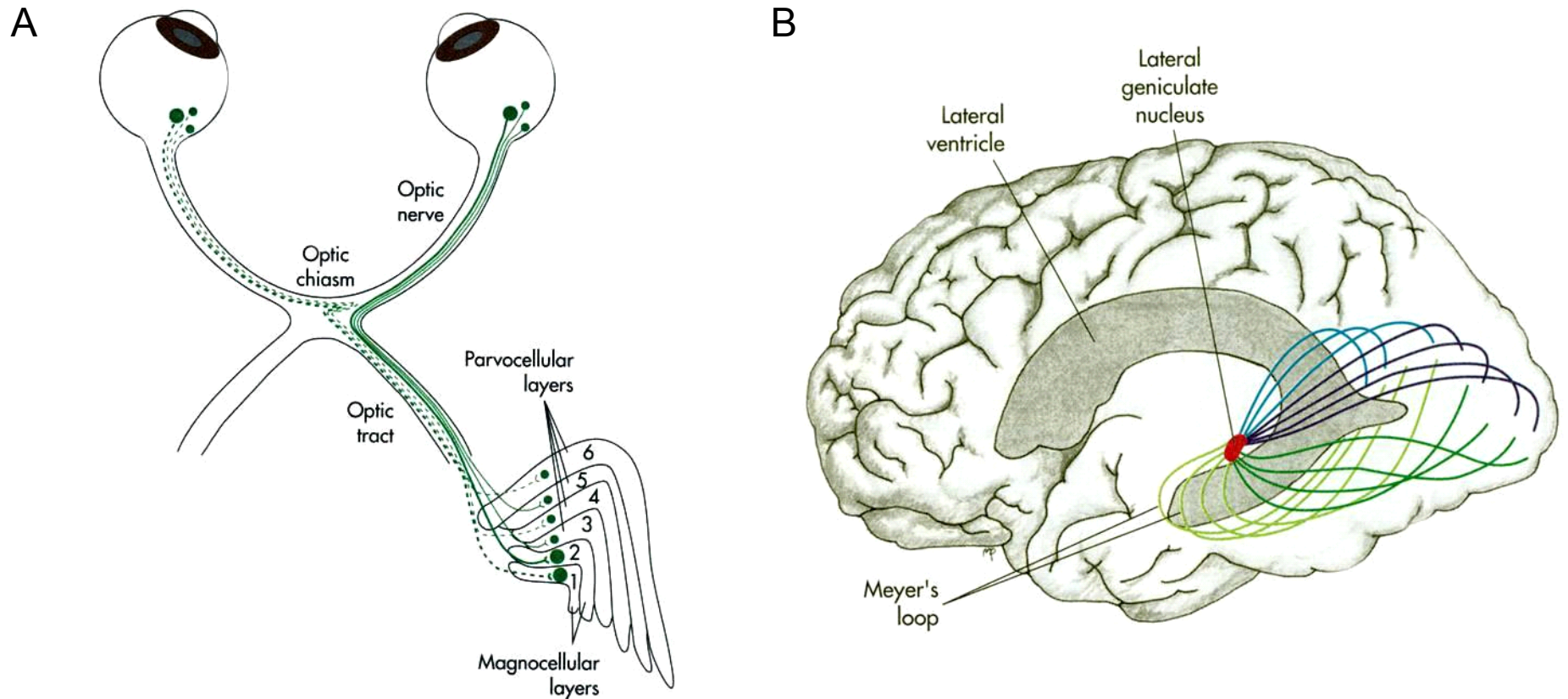
Figure 2.1 Retinogeniculocortical pathways.
Axons originating from retinal ganglion cells synapse in the layers of the LGN (A). The LGN then projects directly to area V1 in the occipital lobe (B). See section 2.1.1 for details.
Reprinted from *The human brain: An introduction to its functional anatomy*, 4th ed., by John Nolte, pp. 418-419, © 1999, Mosby, with permission from Elsevier.

Chapter 3. Hominin Brain Evolution

This chapter focuses on some of the major methodological considerations in the reconstruction of the evolution of the modern human brain. Its scope is the hominin clade, which extends in time from the most recent common ancestor of modern humans, chimpanzees, and bonobos, via the appearance of the first hominins c. 8-4 Ma, to the emergence of anatomically modern humans a little over 190 ka ago. The term "hominin" refers to living modern humans and all extinct species that are more closely related to modern humans than to any other living taxon, and "panin" refers to living chimpanzees and bonobos and all extinct species that are more closely related to chimpanzees and bonobos than to any other living taxon. First, this chapter reviews the ways the fossil record can be used to help reconstruct the central nervous system (CNS) of extinct hominin taxa. Second, trends in the evolution of the hominin CNS are summarized.

3.1 How can fossil evidence be used to reconstruct the evolution of the modern human CNS?

3.1.1 Fossil evidence relevant for reconstructing the size and shape of the brain

The biggest obstacle to understanding the evolution of the modern human CNS is that the CNS is not preserved in the hominin fossil record. However, inferences can be

made about the size and shape of the CNS from natural endocasts, from the fossilized morphology of the neurocranium, the cranial base and the axial skeleton. Endocasts and neurocranial fossils convey information about the size, shape, external convolutional morphology and blood supply of the brain. Cranial base morphology contains information about the brainstem, and the cranial nerves and blood vessels which perforate it. Finally, the neural canal conveys information about the spinal cord which extends in adult modern humans from the atlas (C1) to the first (usually) or second lumbar vertebrae. Across primate species, the cross sectional area of the vertebral canal provides an indication of spinal cord dimensions – particularly in its most rostral aspect, but less so more caudally where a greater proportion of the canal is devoted to spinal nerves (MacLarnon A, 1995).

Although endocasts look remarkably brain-like, an endocast is not a fossil brain, but rather a cast of the neurocranial cavity. A natural endocast is formed during fossilization as the cranial cavity fills with fine sediments that enter through the various foramina and fissures that perforate the floor of the cranial cavity. Similarly, a synthetic endocast is made by stopping these perforations and then lining the inner surface of the endocranial cavity with quick-drying latex. Once dry the thin layer of flexible latex can be peeled off the endocranial surface and removed through the foramen magnum. It is also possible to create a three-dimensional digital cast of the neurocranial cavity, called a "virtual endocast", and this has become the method of choice for investigating delicate and/or fragmentary fossils (e.g., Falk D et al., 2005; Zollikofer CPE et al., 2005). Endocasts potentially preserve details of the convolutional morphology of the surface of the cerebral and cerebellar hemispheres that are imprinted through the three layers of

meninges (from outside in, the dura-, arachnoid- and pia- mater). In addition, endocasts preserve the imprints of blood vessels and skeletal sutures.

Convolutional details are not always well-preserved. The differential imprinting of convolutional detail is influenced by taphonomy, the relative size of the brain, and the effects of ontogeny. In general, natural endocasts produce more details than synthetic endocasts. Falk (1980) proposed two explanations for this: 1) natural endocasts may begin to form before the dura mater has fully disintegrated, so that any details present on it, but absent on the endocranial surface of the inner table of the neurocranium, are preserved, and 2) synthetic endocasts are often produced from crania that have been reconstructed from fragments, and the process of reconstruction can introduce morphological "noise". The relatively small-brained *Australopithecus* endocasts are usually more detailed than endocasts made from crania assigned to larger-brained later *Homo* taxa. It is noteworthy that for various groups of mammals, those with the largest brains *within that group* tend to produce the least detailed endocasts – although this pattern does not hold true for *absolute* brain size across major groups (Radinsky L, 1972). This is related to the fact that endocranial volume increases more rapidly than brain size increases within primates (Martin RD, 1990). The intensity of gyral impressions is also related to ontogeny. In modern humans there are few or no impressions on the endocranial aspect of the cranial vault before one year (Du Boulay G, 1956). Gyral impressions are probably most marked during adolescence, and with increasing age basal markings become more prominent while vault impressions become fainter (Connolly CJ, 1950).

The convolutional details of endocasts are notoriously difficult to interpret (Holloway RL, 1966; Symington J, 1916). A feature may be the impression of a sulcus, or a blood vessel, or a skeletal suture or it may be an artefact, and observers may offer genuinely different interpretations of what the same feature represents (Connolly CJ, 1950; Falk D, 1980). For example, over the past three decades Ralph Holloway and Dean Falk have been providing often conflicting interpretations of the same endocasts. Only a handful of researchers study the details of endocast morphology, and both Falk and Holloway have called on other paleoanthropologists to join the debate (Falk D, 1987; Holloway RL, DC Broadfied et al., 2004).

Not all researchers are convinced that the detailed morphology of endocasts has functional relevance. Many paleoneurologists take it for granted that sulci delimit functional or somatotopic cortical areas (see Radinsky L, 1972, and references therein). However, recently it has become clear that the primate brain exhibits a substantial amount of intraspecific variability in sulcal anatomy and cytoarchitectural boundaries (Geyer S et al., 2001; Rademacher J et al., 2001). Although some cortical areas are always associated with specific sulci (e.g. primary visual cortex in the calcarine sulcus) or on specific gyri (e.g. primary auditory cortex on Heshyl's gyrus), the borders of the cortical areas are rather variable (Amunts K, A Schleicher et al., 2007). There are some cases in which the relationship between sulcal landmarks and functional area borders are maintained, at least within a species (Holloway RL, DC Broadfield and MS Yuan, 2003), but in other cases it varies within species (Sherwood CC, DC Broadfield et al., 2003). It may not be possible to make detailed interpretations of brain function from endocasts alone.

Information about fossil hominin brain evolution is not limited to the hard tissue fossil record. Natural endocasts are a form of trace fossil that record, often in unusual detail, the endocranial morphology of an individual. Archaeologists also claim that artefacts reveal information about the evolution of the hominin CNS. Tools, art and other artefacts found in association with hominin remains provide direct evidence of the capacity of a species for specific behaviors – something that CNS-related fossils cannot reveal.

The combination of paleontological and archaeological evidence provides more insight into the brain function of fossil hominins than either of these two lines of evidence could generate individually.

3.1.2 Data interpretation

In a specimen of an extant taxon, the size and shape of the brain can be estimated from either the brain itself or, indirectly, from cranial measurements. In a fossil specimen, measurements are taken from either an endocast (natural or synthetic) or from a fossil neurocranium. In general, the same measurement methods are used for endocasts and whole brains, and similar methods are applied to extant and fossil neurocrania. However, there are several reasons why data taken from contemporary taxa and data taken from fossil specimens may not be comparable and suggestions have been made to correct for the discrepancies.

First, it is important to appreciate that the volume of an endocast, which is referred to as the endocranial capacity or the endocranial volume, is the volume of the

neurocranial cavity. Endocranial volume includes not only the volume of the brain, but also the space occupied by meninges, cerebral spinal fluid (CSF) and cranial nerves.

All fossils, including endocasts and cranial fossils are imperfect representations of the hard tissues they represent. Problems include incompleteness and plastic deformation. Incomplete fossils require that assumptions are made about the size and shape of the missing parts, and deformation may be difficult to detect when the form of the undeformed brain is unknown. Matrix can fill and widen cracks, expanding the size of the fossil beyond the size of the original bone. Virtual methods have recently been developed to correct for such deformation.

Even well-preserved fossils present sampling problems that affect interspecific comparisons. For example, we do not know the chronological age of individual fossils, yet if the individual is immature it may be necessary to estimate the size of the equivalent adult. However, ontogenetic age is difficult to estimate even in extant animals, let alone in a fossil species for which we will never have a satisfactory reference sample. In addition, sexual dimorphism may account for substantial differences in brain volumes within a species. In hominin species with a sparse fossil record, overrepresentation of a particular sex may give an inaccurate impression of the species' true mean and range of brain size.

3.1.3 Brain size measures and estimates

The brain sizes of fossils can be obtained from a variety of methods that vary in their accuracy and precision. For example, de Miguel and Henneberg (2001) reviewed the brain size estimates for OH5 cited in the literature and found that for this relatively

complete *P. boisei* fossil cranium fifteen different endocranial volume estimates are given

ranging from 500 to 750 cm^3. Holloway (1983) has devised a useful system for indicating

the reliability of endocranial volume measurements which uses a letter code for the

method used and a number code for the reliability of the measurement.

3.1.3.1 Measurements of the volume of a brain or of a solid endocast by water

displacement

The most direct way to determine the volume of a brain or an endocast, natural or

artificial, is by water displacement according to Archimede's principle. For extant species

this is done using postmortem brains, but how well does this method measure brain size?

For postmortem samples one, or more, of the following confounding factors need to be

taken into account: time from death to measurement, time from death to fixation, fixation

method and preparation prior to measurement, whether the leptomeninges and CSF are

included, adequacy of dissection and shrinkage. For example, what Stephan and others

(Stephan H et al., 1988; Stephan H et al., 1970; Stephan H et al., 1981) call "brain

weight" includes meninges, hypophysis and any nerves still attached to the brain (Heiko

Frahm, pers. comm.). Similarly, the largest brain mass datasets for modern humans

(Dekaban AS and D Sadowsky, 1978) and chimpanzees (Herndon JG et al., 1999)

include leptomeninges and CSF in the brain mass estimates. Jerison (1973) estimates

that the effect of including or excluding variables like these can cause measurements to

differ by as much as 20%.

Holloway *et al.* (Holloway RL, DC Broadfied *et al.*, 2004; Holloway RL, RJ

Clarke *et al.*, 2004) found that weighing the water displaced by an endocast was a more

consistent method than measuring its volume. Volumes measured using artificial endocasts may be underestimates of the 'true' volume because endocasts are likely to have undergone shrinkage (Broadfield DC et al., 2001; Gingerich PD and RD Martin, 1981).

3.1.3.2 Measurements of the volume of the endocranial cavity

3.1.3.2.1 Packing methods

Packing methods involve filling the cranial cavity with small particles such as mustard seed, sintered glass beads, or shotgun pellets, and then determining the volume of the packing material. Different types of fillers can produce slightly different endocranial volume estimates (Miller JA, 1991). For fossil crania, packing methods are sometimes preferred over water displacement of a latex endocast because the problem of endocast shrinkage is avoided. However, because of variation in techniques for settling the packing material these methods almost certainly underestimate the 'true' endocranial volume (Gould SJ, 1978, 1996).

3.1.3.2.2 Filling methods

Filling methods are like packing methods, but involve a fluid rather than a solid. Uspenskii (1954) describes a method in which a rubber balloon is put into the cranial cavity and then filled with water. Similar values (mean difference 1.67 cm^3) were obtained with this method and with water displacement, but packing with millet seed resulted in smaller (mean difference 65.4 cm^3) values than those obtained using the balloon method (*ibid.*).

3.1.3.3 Estimating volumes from slices

3.1.3.3.1 Cavalieri's principle

Using Cavalieri's principle, it is possible to produce an unbiased estimate of total

brain volume from measurements of the cross-sectional area of a sample of brain sections

(Gundersen HJ and EB Jensen, 1987; Stephan H *et al.*, 1981). Cavalieri's principle can

be used to determine brain volume from actual and virtual brains. Serial sections of

brains mounted onto slides undergo shrinkage as a result of fixation and embedding, so

volume measurements determined from slide-mounted sections need to be corrected

accordingly. Stephan *et al.* (1981) advised researchers to generate an individual

conversion factor (C_{ind}) for a brain with known mass and known volume,

C_{ind} = volume of fresh brain ÷ serial section volume

In early papers the effect of shrinkage was overlooked. Stephan *et al.* (1981) list

conversion factors for specific types of fixation, ranging from 1.54 - 2.4. Aside from

mismeasurement due to shrinkage, the only disadvantage with using sections as opposed

to water displacement is that the former *estimates* volume, rather than measuring it.

However, what the estimate loses in precision it may gain in accuracy, since imaging

makes it possible to be sure that only brain tissue is included.

In a regular structure such as a cylinder a single section is sufficient for

determining the volume using Cavalieri's principle. Even in a very irregularly shaped

structure (in their example, the suprarenal gland of *Rena temporaria*) 20 sections are

sufficient for estimating a volume (Zilles K et al., 1982). In measuring the volume of a brain of a *Callithrix jacchus* specimen, estimations based on 10 sections had a maximum 2.2 % error, and estimations based on 20 sections had a maximum 1.1 % error.

3.1.3.3.2 In vivo *MRI*

Magnetic resonance imaging (MRI) has recently begun to be applied to comparative samples of living hominoid species in order to obtain volumes of both entire brains and particular brain regions (e.g., Rilling JK and TR Insel, 1999; Semendeferi K and H Damasio, 2000; Sherwood CC, MR Cranfield et al., 2004). Comparison of MRI volumes with volumes obtained by water displacement have established that as few as 5-6 MRI slices per brain are enough to yield reliable estimates of mean brain volume, with a coefficient of error (CE) of ca. 5% (Mayhew TM and DR Olsen, 1991). The CE decreases as the number of slices increases (e.g., for 28 slices the CE <1%).

There are several advantages to using *in vivo* MRI volumes over autopsy brain volumes. *In vivo* MRI brain volumes avoid biases inherent to using autopsy brains − for example, autopsy brain samples over-represent aged individuals. *In vivo* MRI volumes are not affected by changes in brain volume due to the elapsed time between death and measurement or fixation. Peters *et al.* (1998) compared the results of cross-sectional studies in which modern human brain volumes were obtained either *in vivo* by MRI (or NMR) or from autopsy brains. They found large discrepancies between the means of the different samples (even in cases in which the same method was used), but they did not identify the way in which the autopsy and MRI volumes differ.

48

3.1.3.3.3 Post-mortem *MRI*

Peters *et al.* (2000) compared brain volume estimates obtained from MRI and brain volumes from water displacement in autopsy specimens. They found that so long as thin MRI slices (1 – 1.25 mm) were used MRI volumes did not differ significantly from water displacement volumes. However, MRI volumes were found to be overestimates when thicker slices (5 mm) were used.

3.1.3.3.4 CT slices and "virtual endocasts"

A widely applicable and noninvasive way in which to accurately estimate fossil endocranial volumes is by using two-dimensional (2D) computed tomography (CT) slices. It is possible to use these slices to obtain an endocranial volume in two ways which yield similar results: either directly using Cavalieri's principle, or through the construction of "virtual endocasts" (e.g., Conroy GC et al., 1998). Increasingly popular, a three dimensional "virtual endocast" is a 3D model of the fossil constructed from the 2D CT slices (Tobias PV, 2001; Zollikofer CPE, 2002; Zollikofer CPE et al., 1998). For matrix-filled skulls, thresholding to distinguish between local object densities is the method used to separate the walls of the fossil neurocranium from the matrix at their interface (Conroy GC and M Vannier, 1985; Conroy GC et al., 1990; Zollikofer CPE *et al.*, 1998). Fragmentary specimens are completed using mirror-imaged parts from the opposite side (e.g., Conroy GC, D Falk et al., 2000), or scaled parts from another specimen (e.g., Zollikofer CPE *et al.*, 1998). Once the "virtual cranium" is created, it is possible to create a "virtual endocast". If there is uncertainty about the dimensions, several potential endocrania are created to establish a range of endocranial volumes, from

which a most likely endocranial volume can be determined (Conroy GC, GW Weber et al., 2000). The virtual endocast technique has been tested on 10 *H. sapiens* crania whose endocranial volumes were measured using a mustard seed filler, and it was found that the difference between the measured and virtual endocast volumes was around 2% (Conroy GC *et al.*, 1998).

3.1.3.4 Measuring incomplete endocasts

3.1.3.4.1 Partial endocast method

Tobias (1964; 1971) introduced a method which has become known as the "partial endocast method" for estimating endocranial volume. This method involves taking a complete endocast with known endocranial volume, reducing it to the anatomy preserved in the fossil of interest, and then determining what proportion of the complete endocast is represented by the reduced endocast. This provides a conversion factor to estimate complete endocranial volume for the specimen in which there is only a partial endocast. This method was originally used to determine the endocranial capacity of OH 7, the type specimen of *H. habilis* (estimated by the partial endocast method to be 675-680 cm3; Tobias PV, 1964), was one of the factors taken into account when deciding on whether to include the new taxon in the genus *Homo* (Leakey LSB et al., 1964; Tobias PV, 1964; 1969). This spawned a multi-author debate revolving around the reliability and taxonomic implications of the original estimate, in which alternative methods to determine endocranial volumes from partial endocasts were suggested (Holloway RL, 1983; Pilbeam D, 1969; Vaisnys JR et al., 1984; Wolpoff MH, 1981).

3.1.3.4.2 Reconstructed endocast method

Synthetic and natural endocasts are typically reconstructed using plasticene to fill-in missing areas. If only small parts of bilateral structures are missing on one side the necessary reconstruction does not require much guesswork. Holloway (1973; 1975) distinguishes between "minimal plasticene reconstruction" (Method A) and "extensive plasticene reconstruction involving close to half the total endocast" (Method B). Endocast reconstruction should be reevaluated as additional fossils are discovered, and new, improved, methods should be applied to existing endocasts, not just to newly-discovered evidence. Holloway's method involves making one endocast reconstruction based on comparisons with specimens belonging to the same hypodigm, or to members of different fossil hominin hypodigms (e.g., *P. robustus* and *P. boisei*) with brains that are similar in size and shape. Reconstructions made independently by different researchers provide a test of reliability. For example, the differences between the endocranial volumes of Holloway's (914 cm^3) and Broadfield's (921 cm^3) reconstructions of the Sambungmacan 3 calvaria are minimal (Broadfield DC *et al.*, 2001).

3.1.3.5 Extrapolations from ecto- and endocranial linear metrics

Several formulae have been suggested to estimate brain volume from linear dimensions of the endocranial cavity of crania, or endocasts. MacKinnon *et al.* (1956) compared linear measurements of the cranial cavity taken from radiographic images to mustard seed endocranial capacities for 52 modern human crania. They devised the following formula, which predicted endocranial volume with an error of 0.62% (0.87cc in a 1400cc cranium).

$$V = 0.51 \; [½ \; (LHW - LBW)]$$

Holloway (1973) applied this formula to endocasts, but he replaced the value of 0.51 with f, a variable determined for each taxon.

$$V = f \; [½ \; (LHW + LBW)]$$

Where L = endocast length from frontal pole to occipital pole, W is maximum width (usually taken at the level of the superior aspect of the temporal), B is the distance from bregma to basion, and H is the distance from vertex to the deepest portion of the cerebellar lobes.

It is not advisable to calculate endocranial volume from external head or cranial measurements. Simmons (1942) found that crania with similar external perimeter measurements had different internal capacities, and Wickett *et al.* (1994) found that head perimeter measurements were not significantly correlated with total brain size. Bookstein *et al.* (1999) reviewed the factors responsible for the differences between the external and internal cranial form, so the inability of external head dimensions to accurately predict endocranial volume is not surprising. Further, there are particular problems with applying formulae designed for modern humans on fossil hominins. Formulae which have been developed to estimate modern human endocranial volume – such as those of Welcker (1885), Pearson (1926), and Manouvrier (1898) – do not provide accurate estimations of the cranial capacity of fossils (Olivier G and H Tissier, 1975). Olivier and Tissier (1975) have developed formulae specifically designed for "Archanthropians" and

"Paleoanthropians", but the fact that members of the taxon *H. heidelbergensis* fall into both categories suggests that the reliability of this approach is dependant on having a satisfactory taxonomy.

3.1.4 Comparing different types of measurements and estimates

Brain size can be measured as a volume or as a mass (or weight – in most cases these terms are used interchangeably). For consistency we will refer to masses in grams (g) and volumes in cubic centimeters (cm^3).

3.1.4.1 Brain tissue mass from brain mass

Measurements reported as "brain mass" from autopsy brains typically include the "leptomeninges" (i.e., the arachnoid and pia mater) as well as whatever CSF remains in the ventricles (Peters M *et al.*, 1998). Volumes taken from MRI or stained sections measure "brain tissue volume" from which the volume of the meninges and the CSF are excluded (*ibid*.). This is comparable to the "net brain volume" calculated by adding up brain volumes for various brain components (e.g., Stephan H *et al.*, 1981). In modern humans, the meninges and CSF are estimated to contribute an additional 183 g for males and 132 g for females (Peters M *et al.*, 1998). Thus, on average,

brain tissue mass (g) = brain mass (g) – 183 [for male modern humans]

brain tissue mass (g) = brain mass (g) – 132 [for female modern humans]

3.1.4.2 Brain mass from brain volume

For a sample of 78 adult modern human brains, the brain tissue was found to have an average specific mass of 1.032 g/cm^3 (Zilles K, 1972). Thus,

$$\text{brain mass (g)} = \text{brain volume (cm}^3) \times 1.032$$

The specific mass of the brain has also been determined by comparing rodent brain weights with volumes, to give an average specific mass of 1.036 g/cm^3 (Stephan H, 1960). Thus,

$$\text{brain mass (g)} = \text{brain volume (cm}^3) \times 1.036$$

3.1.4.3 Brain volume from endocranial volume

Brain volume and endocranial volume (= cranial capacity) are not identical. Endocranial volume is larger as it also includes meninges, cerebral spinal fluid (CSF), cranial nerves, and the infracranial extracerebral vessels. Few data are available for actual brain volume and endocranial volume from the same specimen because it is difficult to remove the brain from the braincase without causing damage to either. Novel imaging techniques should improve our understanding of this relationship, although at present different techniques are used to visualize soft (MRI) and hard (CT) tissues.

Pickering (1930) found a correlation between nonfixed brain volume as determined by water displacement and endocranial volume measured with mustard seed, in a sample of 29 modern humans, using the following conversion formula ($r^2 = .805$):

$$\text{brain volume} = \text{endocranial volume x .8598}$$

In other words, ca. 14% of the endocranial volume does not represent brain volume.

3.1.4.4 Brain mass from endocranial volume

Count (1947) suggested a value of .876 g/cm^3 for brain mass/endocranial volume, so that

$$\text{endocranial volume (cm}^3\text{)} = \text{brain mass (g) x 1.14}$$
$$\text{brain mass (g)} = \text{endocranial volume (cm}^3\text{)} \div 1.14$$

Ruff *et al.* (1997) suggested an allometric equation to describe the relationship between endocranial volume and brain mass (see Martin RD, 1990). Ruff *et al.* derived brain mass from endocranial volume using a regression based on brain masses from Stephan *et al.* (1970) and cranial capacities from Martin (1990) from 27 primate species ($r^2 = 0.995$),

$$\text{brain mass (g)} = 1.476 \text{ x endocranial volume (cm}^3\text{)}^{.976}$$

This formula describes a relationship between two anatomical structures across an entire order, but it's original purpose was to estimate brain mass in a sample restricted to the genus *Homo*. Although the relationship of endocranial values to brain mass across a range of hominin species is likewise expected to be allometric, note that phylogeny is not controlled for here, and therefore the appropriateness is uncertain.

Jerison (1973) does not recommend converting endocranial volumes into brain volumes or brain masses. Apparently, the specific gravity of the mammalian brain ranges from 0.9-1.1; for example, brain mass in grams is ca. 5% *larger* than endocranial volume in insectivores (Bauchot R and H Stephan, 1967) whereas brain mass in (g) is ca. 3% *smaller* than endocranial volume in a cat (Jerison HJ, 1973).

3.1.5 Indices for estimating and comparing the relative size of brains

Some researchers (e.g., Jerison HJ, 1973; Martin RD, 1990) do not consider absolute brain size to be an appropriate way to compare the mental capacities of different species. Nor is it useful to compare the brain/body ratio, because this ratio decreases with increasing body size. Like many biological variables, brain size has been shown to be related to body size in a nonlinear (i.e., allometric) fashion (Clutton-Brock and Harvey 1979). The relationship of brain size to body size, as analyzed by Snell (1891) was the basis of Dubois' (1897) "index of cephalization", which related brain size to 1) body size and somatic functions and 2) the encephalization of psychic functions. Harry Jerison and Robert Martin have further investigated the relationship between brain size and body

size, and have made contributions to the most widely used measure of relative brain size, the encephalization quotient.

3.1.5.1 Encephalization quotient

The encephalization quotient is a measure which removes allometric effects of body size on brain size. From a plot of log brain mass on log body mass is derived the allometric formula

$$E = kP^{ß}$$

where E is brain size, P is body size, k is the allometric coefficient and ß is the allometric exponent. Different taxonomic groups tend to have a similar value for ß (reflecting a consistent functional relationship), but different values for k (reflecting different grades; Martin RD, 1981).

This is usually expressed as the log-transformed linear equation

$$logE = logk + ß(logP)$$

The key variable ß is typically referred to as "the scaling coefficient".

Jerison (1955) found that the mammal measurements of Count (1947) fit a scaling

coefficient, ß = .67, similar to earlier findings of Snell (1891) and Von Bonin (1937).

Thus he inferred

(Jerison (1961; 1973) a relationship between brain size and body size for all mammals

described by an equation

$$\textbf{brain mass} = \textbf{0.12 x body mass}^{\textbf{2/3}}$$

Jerison developed Dubois' (1897) proposal for an equation to quantify encephalization,

and derived what he referred to as the Encephalization Quotient (EQ).

$$\textbf{EQ} = \textbf{brain mass} /(\textbf{0.12 x body mass}^{\textbf{2/3}})$$

Encephalization occurs when there is a departure from the general relationship between

brain size and body size. Encephalization occurs in mammals and birds, but is rare in

other vertebrates. Encephalization is explained by Jerison's (1973) "additive theory of

brain size": $E = E_v + E_c$, where E is brain size, E_v is brain size determined by body size

and E_c is associated with improved adaptive capabilities. If $E_c=0$, then the brain is of a

size sufficient for somatic maintenance. If one assumes there is a relationship between

brain size and neuron number, and if $E_c>1$, then, it is suggested, the brain has "extra

neurons" designated to deal with extracorporeal pressures. The presence of extra neurons

is referred to as "encephalization".

The fact that brain size does scale to isometrically to body size is not sufficient

reason to believe that the typical brain has "just enough" neurons to maintain basic

somatic function. Jerison's "extra-neuron" hypothesis is appealing when making comparisons between animals that vary greatly in body size, for example, elephants and mice. It has been shown that across mammals, there is a relationship between encephalization and the diversity of behaviors exhibited (Changizi MA, 2003). But the notion that EQ can predict cognitive ability in primates has not been supported by behavioral data. In fact, absolute brain size, and absolute body size predict cognitive ability in primates, whereas EQ and other measures of brain size scaled to body size do not (Deaner RO et al., 2007). Clearly, the brains of all primates are equipped to carry out a range of specialized functions beyond basic somatic requirements. Further, larger brains have more cortical areas which perform higher order and cross-model functions, the existence of which cannot merely be explained as increased somatic maintenance.

3.1.5.2 Scaling coefficients and appropriate taxonomic level

Scaling coefficients are key when determining EQ values, and therefore, when testing hypotheses of encephalization. However, scaling coefficients vary depending on the sample from which the regression line is drawn (Holloway RL and D Post, 1982). Therefore, the use of EQ as a comparative measure should take into account whether the equation from which it is derived includes a sufficiently broad sample, and is calculated at the appropriate taxonomic level.

Scaling coefficients have been the focus of allometric analyses, because they are thought to have functional significance which transcends taxonomic groups. Early studies found a scaling coefficient value of 2/3 (or 0.66) for several sets of mammals (Gould SJ, 1975; Jerison HJ, 1955, 1961; Jerison HJ, 1973; Snell O, 1891) This scaling

coefficient was appealing because a surface area is the square of a linear measurement, and a volume is the cube of a linear measurement, therefore a coefficient of 2/3 suggested that brain volume was a function of body surface area. A later study suggested that a scaling coefficient of ¾ (or 0.75), derived from a broader sample of terrestrial vertebrates, is more appropriate, and was appealing because it is linked brain size to maternal metabolic turnover (Martin RD, 1981). It was based on the latter coefficient, that Ruff *et al.* (1997) derived the equation to generate EQ in hominins

$$EQ = \text{brain mass}/(11.22 \times \text{body mass}^{3/4})$$

A scaling coefficient of approximately ¾ (i.e., 0.78) has been described for a comprehensive sample of primates (Bauchot R and H Stephan, 1969). However, subsets of primates have a range of scaling coefficient values. For example, the scaling coefficient of non-modern human hominoids (i.e., the apes) is much lower (e.g., EQ = 0.58; *ibid.*). Generally, there exists a "taxon-level effect" in which regressions drawn for lower taxonomic groups (i.e., limited to closely related species) tend to have less steep slopes than those drawn for higher taxonomic groups (e.g., the Class Mammalia; Gould SJ, 1975; Pagel MD and PH Harvey, 1989).

The question of which scaling coefficient to use is tied to the question of what is the appropriate taxonomic level at which to draw the regression. Different regression equations result in different EQ estimations, such that for a sample of fossil hominin species, the rank order of the EQ values depends on the taxonomic level at which the regression was drawn (Holloway RL and D Post, 1982). In practice, hominin EQs are

almost always calculated from coefficients drawn from much higher taxonomic group than the focus of the study (e.g., McHenry HM, 1988; Ruff CB *et al.*, 1997; Tobias PV, 1971). Further insight into the evolutionary significance of a taxon-level effect (Pagel MD and PH Harvey, 1989) as well as the demonstration that different vertebrate classes have different scaling coefficients (Van Dongen PAM, 1998) raise potential problems with this practice. Recent methods to control for phylogenetic bias in datasets can alleviate some of these problems in generating prediction equations, as discussed below (Felsenstein J, 1985; Pagel MD, 1992).

It has been suggested that the appropriate taxonomic level for making allometric comparisons depends on the hypothesis being tested (Stephan H *et al.*, 1988). In the case of hominin paleoneurology, the outgroup for comparison tends to range from the hominin sister taxon -- the panins, to a paraphyletic group -- the great apes. There are also practical considerations based on statistical significance; a regression cannot be drawn from a single species, and in order to obtain a regression line which is statistically significant, in some cases it may be necessary to draw the regression from a higher taxonomic group (Schoenemann PT et al., 2005; Sherwood CC, RL Holloway et al., 2005).

Because grade shifts are known to exist in the scaling of brain size to body size, it has become popular to use a method, such as independent contrasts (Felsenstein J, 1985), to correct for this when the sample encompasses a higher taxonomic unit. Independent contrasts analysis uses information about phylogenetic relationships to draw regressions of contrasts, which are calculated from pairs of monophyletic groups (species and clades) joined at nodes. Although independent contrasts analysis has become increasingly

popular for its approach to the problem of phylogenetic non-independence in biological regressions, it is a complex statistical analysis and requires that an ever growing list of assumptions about the phylogenetic relationship be addressed. Most obvious is the assumption that the topology of the phylogeny is accurate, but other considerations include the use of (and accuracy of) branch lengths (Grafen A, 1989; Pagel MD, 1992) and how to deal with polytomies (Garland T, Jr. and R Diaz-Uriarte, 1999; Purvis A and T Garland, Jr., 1993). Therefore, given a primate dataset, it is likely that some of the assumptions about primate taxonomy which figure into an independent contrasts regression will be incorrect, and this imposes error in the regression line. On the other hand, a primate-wide regression which does not correct for phylogeny treats all primate species as equally related to each other in an unrooted, "star" phylogeny, which is certainly not the case. Therefore, recent publications examining brain size scaling relationships tend to include both standard and independent contrasts regressions. Using independent contrasts, the scaling exponent of brain size as a function of body size in mammals is lower, around 0.69 (Harvey PH and MD Pagel, 1991), but it has been claimed that this is in fact vulnerable to sampling and that an exponent of 0.75 can still supported (Martin RD et al., 2005).

3.1.5.3 Other standards for brain size comparison

Although brain size is most often considered in relation to body mass, other standards for brain size comparison have been used. Some authors suggest that the scaling relationship between brain mass and body mass is a surrogate measure for some underlying variable e.g., (Harvey PH and JR Krebs, 1990). CNS or CNS-related

62

standards of comparison are sometimes preferred because they vary less intraspecifically, and measure brain versus nervous system information flow. All standards have advantages and disadvantages.

Krompecher and Lipak (1966) were the first to suggest scaling brain size against the mass of another CNS structure (the spinal cord), and subsequently Passingham (1975) scaled brain mass to a CNS-related structure (the foramen magnum). The latter method has the advantage that it uses a hard-tissue structure that is occasionally preserved in the hominin fossil record. The absolute size of a CNS structure other than the brain gives an approximation of total neuronal input and output to the brain. In fact, an index of brain size to non-brain CNS size provides an estimate of Jerison's (1973) "extra neurons". On the other hand, it has been suggested that body mass is better for use in scaling relationships precisely because, unlike the CNS or CNS-related structures, it is independent of brain mass (Stephan H *et al.*, 1988). Radinsky (1967) suggested that foramen magnum area was a good estimate of body size, though less variable within a species than is body mass. However, others have suggested that foramen magnum area is linked more closely with brain size rather than with overall body size (Gould SJ, 1975; Jerison HJ, 1973; Martin RD, 1981). In fact, the relationship of the size of a given CNS or CNS-related structure to body mass is variable. For example, the relationship between body size and foramen magnum/medulla size may be strongly influenced by specializations such as adaptation to water (Stephan H and F Dieterlen, 1982; Stephan H and HJ Kuhn, 1982).

Finally, it has been suggested that CNS structures make better standards because they vary less within a species than body mass (Radinsky L, 1967). One reason that body

mass varies so much is that it comprises several components, including muscle mass and adipose tissue which are themselves variable (Pitts G and T Bullard, 1968). Muscle tissue, which is well innervated, and other components of fat-free mass scale more closely to CNS mass than does the mass of the less well innervated adipose tissue (Schoenemann PT, 2004). This finding has implications for certain questions about the scaling of brain size to body size. For example, the difference between male and female brain mass, might be partially explained by the fact that male body mass is proportionately more muscle (Ankney C, 1992; Gould SJ, 1996; Manouvrier L, 1903). Along these lines, when scaled to fat-free mass, it has been suggested that the very muscular Neanderthals would have much smaller relative brain size than would modern humans (Schoenemann PT, 2004).

3.1.6 Measures of brain organization

In understanding the complexity of the modern human brain, it is possible that overall brain size may be less informative than brain organization (Holloway, 1966). Discussions of brain organization have been based on studies of scaling relationships between brain size and brain component size, between brain size and neuron density, and between other neurobiological variables -- some of which are discussed below.

3.1.6.1 Scaling brain component sizes to brain size

Allometric scaling relationships between overall brain size and the size of various types of brain components have been used to investigate aspects of brain organization. For a behavioral specialization involving a particular sensory or motor system,

corresponding changes are thought to exist in the anatomy of that system within the brain. It is generally accepted that the most obvious species-specific behaviors correspond to neurological specializations. By the same logic, differences in the size of a brain structure might be taken as evidence of functional specialization, particularly in poorly known fossil species.

There is some evidence that the volumes of brain structures are developmentally constrained, and that overall brain volume accounts for much of the variation observed in brain structure volumes (Finlay BL and RB Darlington, 1995; Finlay BL et al., 2001), although this is debated (Barton RA and PH Harvey, 2000; comments in Finlay BL *et al.*, 2001). Similarly, it is possible for brain regions to be maintained in the absence or near absence of corresponding function. For example, the retino-geniculate pathway and visual cortex are maintained in the visually-poor platypus and star-nosed mole, and even in blind mole rats – and the involvement of pleiotropic genes have been suggested as the source of such conservation of structure (Krubitzer L, 1995). On the other hand, if brain organization is highly constrained, this would suggest that any departures from the "predicted" pattern of brain organization are likely to be functionally significant.

In regards to scaling brain component size to brain size, there are several "usual" points of contention. First, certain brain components are indicated as not being functionally meaningful units, as is often the case when scaling entire lobes of the brain encompassing multiple functional regions. Second, some components are delimited by unreliable sulcal landmarks. Third, in cases where a large part of a structure is regressed against a whole, autocorrelation is a potential source of error (Deacon T, 1990), a problem addressed by subtracting the size of the part from the size of the whole. Fourth,

the issues of choosing the appropriate taxonomic level for comparison, and, potentially, the need to correct for taxonomy, apply to these scaling relationships.

Finally, the relevance of the types of brain components used has been a source of confusion, and thus may warrant some attention. The term brain component is, by intention, rather loosely defined here as "any distinct part of the brain", because there have been investigations of brain size scaling relationships for components as specific as the trigeminal nucleus, to components as encompassing as the neocortex (grey and white matter included). Usually the larger, more encompassing brain components are easy to define, and can often be estimated solely on the basis of gross anatomy, and some, like the cerebellum, can even be identified on fossil endocasts; however, they are functionally vague. For this reason, the relative volumes of these structures are most likely to be informative for comparisons at higher taxonomic levels, but are rarely informative for understanding the fine details of brain organization among modern humans and closely related species. Thus, there is a growing amount of data on the volumes of nuclei and cortical areas in modern humans and closely related species (e.g., Frahm HD et al., 1998; Schenker NM, 2007; Semendeferi K *et al.*, 1998, 2001; Sherwood CC, PR Hof et al., 2005). Conroy and Smith's (2007) recent attempt to describe the brain organization of fossil hominin species on the basis of some of Stephan *et al.*'s (1981) brain component volumes overlooks the crux of the discussion about hominin brain reorganization. In essence, "brain reorganization" in hominins refers to more fine-tuned changes in brain anatomy, such as changes in the lamination, function, and size of regions of cerebral cortex or of brain nuclei, as well as changes in the occurrence, function, size and frequency of particular cell types. Also, for a given cortical area, grey matter volumes

are more precise than white matter volumes because the cortex is defined according to architectonic criteria of the grey matter, whereas the limits of the corresponding white matter are approximated from the extent of the grey matter (but note that advances are being made in the imaging of white matter). Thus, primary visual *cortex* is an exceptionally well defined brain region both in terms of function and anatomy; however primary visual cortex *white matter* can only be roughly estimated, particularly in modern humans.

3.1.6.2 Proportional volumes of different cerebral cortex types

Scaling brain size to other appropriate parts of the CNS gives a direct indication of the size of the brain in relation to the amount of input and output. Hebb (1949) advocated replacing brain/body size comparisons with an A/S (association cortex/primary sensory cortex) ratio, since the primary sensory areas are related to input from an animal's surroundings, whereas association areas are involved in higher level cognitive processing. Similarly, Shariff (1953) compared the cerebral cortices of several species in terms of the volumes of eulaminate cortex (association cortex), koniocortex (primary sensory cortex), and agranular cortex (primary motor cortex). Such methods are advocated by Holloway who discusses in detail the problems associated with basing intelligence on brain/body size relationships (Holloway RL, 1968; Holloway RL, 1979; Holloway RL and D Post, 1982).

3.1.6.3 Neuron density

Patterned, species-level differences in neuronal cell density have long been recognized to exist (Nissl F, 1898). Such a finding has implications for hominin brain size comparisons.

As mentioned above, the theoretical framework behind EQ includes the assumption that brain size is a proxy for total neuron number. Therefore, in order to support its usage, it needs to be demonstrated that brain size and neuronal density are correlated, and that this relationship is not disrupted by species-specific differences in brain organization. Several studies have demonstrated that, across a range of mammalian species, there is a negative allometric relationship between brain size and neuron density in the neocortex, which follows a -1/3 power law (Haug H, 1987; Nissl F, 1898; Prothero J, 1997; Tower DB, 1954). However, the early studies upon which the -1/3 power law is based are somewhat inconsistent due to technical factors including the failure to account for tissue shrinkage; as well as differences between taxonomic groups and cortical areas sampled (Cragg BG, 1967; Sherwood CC et al., 2006).

At a lower taxonomic level, neuron density as a function of brain weight varies across mammalian orders. It has recently been suggested that primates have more neurons per unit tissue in the whole brain than do rodents; also, the scaling relationship between neuron number and brain size in primates is isometric, where as in rodents brain size increases more rapidly than does neuron number (Herculano-Houzel S et al., 2007).

The -1/3 power law was originally based on sampling of particularly, although not exclusively, agranular motor cortex (see Sherwood CC *et al.*, 2006 for more details; Tower DB, 1954). Cragg (1967) pointed out that the primary visual and motor areas show differences in scaling relationships to brain mass. Motor and visual area neuronal

densities are consistent with the -1/3 power law across the range of mammals, and in all species the primary visual cortex is more neuron dense than in the motor cortex. However, in primates (but not non-primates) there is a grade-level shift in the scaling relationship of the visual cortex, such that the number of primary visual cortex neurons is about double what would be expected for a non-primate mammal of similar brain size (Cragg BG, 1967; Rockel AJ et al., 1980). For a single anthropoid sample, it was found that the neuron density of visual areas V1 and V2 scale to brain mass to the -1/3 power (Sherwood CC, MA Raghanti *et al.*, 2007), but that of area 9L does not correlate with brain mass (Sherwood CC *et al.*, 2006). Similarly, it has been found that within hominoids, area 13 and area 4 neuron densities vary independently of brain size (Sherwood CC and PR Hof, 2007).

3.1.7 Major lines of fossil evidence for CNS evolution

The following categories are the major lines of evidence that can be used to infer CNS evolution from the hominin fossil record. Their comparative contexts are data from extant primates from the endocranium and brain, and from the vertebral column and spinal cord. There is a dearth of data about the CNS of extant hominoids, so most inferences should be treated as preliminary. The extant hominoid data tend to be based on very small samples (e.g., one or two individuals per species, and often the same individuals are used in several studies), and, with respect to the cerebral cortex, rely on gross morphological landmarks as proxies for functional regions.

3.1.7.1 Absolute and relative brain size

Sample mean encephalization quotients (EQs) are calculated using Ruff *et al.*'s (1997) formula, which is based on Martin (1981), and using Ruff *et al.*'s (1997) calculation for estimating brain mass from endocranial volume, based on Martin (1990). For comparison, EQs were also calculated from the equations for "homocentric" and "pongid" (i.e., great ape) brain mass/body mass scaling relationships (Bauchot R and H Stephan, 1969; Holloway RL and D Post, 1982) as follows, given brain mass and body mass in grams (g):

$$\textbf{pongid EQ = brain mass / (.6216 x body mass}^{0.58152}\textbf{)}$$

$$\textbf{homocentric EQ = brain mass / (1 x body mass}^{0.64906}\textbf{)}$$

Only the results of the more conventional Ruff/Martin equation are discussed in the text. A list of endocranial volumes used here is available from the author upon request; mean body mass estimates are from Skinner and Wood (2006).

3.1.7.2 Left occipital right frontal (LORF) petalia

A petalia is a protrusion of one cerebral hemisphere relative to the other. The left occipital right frontal (LORF) petalia is an asymmetrical pattern in which there is a wider and more posteriorly protruding left occipital pole, and a wider right frontal lobe. The LORF petalia is typical of modern humans, and is statistically related to right-handedness – i.e., left-handed and ambidextrous people are more likely to be symmetrical or have the

opposite pattern (Le May M, 1976). It is not clear whether apes exhibit modern

humanlike petalias.   Le May and others (1976; 1982), found that petalias are also

common in great apes. However, Holloway and de Lacoste-Lareymondie (1982) found

them to be less frequent in apes than in modern humans and rarely involved both the

frontal and the occipital lobes, but noted a high incidence of left occipital petalias in

gorillas. In a more recent MR study, however, Hopkins and Marino (2000) found that

great apes display modern humanlike right-frontal and left-occipital petalias.

3.1.7.3 Orbital surface of frontal lobe

The orbital surface of the frontal lobe is blunt and expanded in modern humans.

In contrast, it is beaked and pointed in the African apes. This region corresponds to

cytoarchitectural area 10, which is involved in planning future actions, abstract thinking,

and undertaking initiatives (Semendeferi K *et al.*, 2001). A regression of nonmodern

human primate area 10 volumes against brain volumes in a sample of 1 individual per

species shows that modern humans have a larger than expected area 10 volume – but the

residual (6%) is less striking than for other regions (Holloway RL, 2002).

3.1.7.4 Fronto-orbital sulcus

The fronto-orbital (orbitofrontal) sulcus typically incises the orbitolateral border

of the frontal lobe of African apes, but is rarely present on modern human brains (Falk D,

1980). Due to the opercular expansion of the frontal lobe in modern humans, this sulcus

has probably been shifted so far posteriorly that it now comprises the anterior limiting

sulcus of the insula, giving modern human brains a distinctly shaped lateral edge of the

frontal lobe (Connolly CJ, 1950). The modern human frontal lobe (Semendeferi K and H Damasio, 2000; Semendeferi K et al., 1997) and its cortex (Semendeferi K et al., 2002) have volumes expected for an ape of similar brain size. It has been suggested that the modern human prefrontal cortex is larger than expected for a primate with a similar sized brain (Deacon TW, 1997), supported by the finding of increased gyrification in this region (Rilling JK and TR Insel, 1999), Further, it has been suggested that it has a higher than expected white matter-to-gray matter ratio (Schoenemann PT *et al.*, 2005). Note, however, that many of these inferences about prefrontal cortex expansion in modern humans are not reliable (Semendeferi K *et al.*, 2002; Sherwood CC, RL Holloway *et al.*, 2005) and that even if the frontal lobe did not become relatively larger, it is possible that the prefrontal cortex became proportionally larger within it.

3.1.7.5 Broca's cap region

Broca's cap, as seen on endocasts, represents portions of Brodmann's areas 47 and 45 (Broadfield DC *et al.*, 2001). Broca's cap overlaps (but does not exactly correspond to) Broca's language area. Broca's area corresponds to Brodmann's cytoarchitectural areas 45 and 44, (respectively, pars triangularis and pars opercularis of the inferior frontal gyrus; Aboitiz F and R Garcia, 1997). In the majority of modern humans, the left hemisphere is dominant for language, and area 44 (but not area 45) on the left hemisphere is asymmetrically enlarged in comparison to the contralateral area 44 (Amunts K et al., 1999). Although an enlarged Broca's cap is a characteristic of modern humans, it does occur, albeit more rarely, in apes (Holloway RL, 1996). Questions persist about whether the African ape Broca's area homologue exhibits modern

humanlike asymmetry (Cantalupo C and WD Hopkins, 2001; Holloway RL, 1996; Sherwood CC, DC Broadfield *et al.*, 2003). A recent study of minicolumn size in Brodmann's areas 44 and 45 has indicated that nonmodern human hominoid species lack a species-level pattern of asymmetries like that seen in modern humans (Schenker NM et al., in press). Investigators draw attention to modern humanlike Broca's cap asymmetry in fossil hominin endocasts, in particular to those specimens in which the left side is larger than its homologue on the right. They also describe overall size and convolutional detail – particularly in fossils where only one hemisphere is present. Because an asymmetry in which the left Broca's area is larger than the right (L>R) is related to right-handedness and is a characteristic of most modern humans, attention is drawn to cases in which Broca's area L>R asymmetries are found along with LORF L>R asymmetries.

3.1.7.6 Temporal poles

Falk (2005; 2000) described modern human endocasts as having temporal poles which are extended in the anterior and lateral directions, whereas African apes have rounded temporal poles. More generally, modern human temporal lobes are larger in total volume, white matter volume, and surface area than predicted for an ape of similar brain size (Rilling JK and RA Seligman, 2002). In modern humans, the anterior lateral temporal pole, particularly in the left hemisphere, is involved in face recognition and naming (Damasio H et al., 1996; Grabowski TJ et al., 2001). The corresponding monkey area, TG, also functions in visual learning and recognition (Horel JA et al., 1984; Nakamura K and K Kubota, 1995).

3.1.7.7 Lunate sulcus

3.1.7.7.1 Primary visual cortex reduction

The lunate sulcus is within the secondary visual area, close to the anterior border of the primary visual cortex. Modern humans have a more posteriorly-located lunate sulcus than do the great apes. A regression of striate cortex volumes against mean brain volumes from small samples of diverse primate species suggests that modern humans have substantially less (-121%) primary visual cortex than expected for a nonmodern human primate of similar brain size (Holloway RL, 1992). Although chimpanzees typically have a relatively larger primary visual cortex than do modern humans, a minority of chimpanzees show repositioning of the lunate sulcus to a more modern humanlike posterior position (Holloway RL, DC Broadfield and MS Yuan, 2003). Holloway *et al.* (2003) use this point to argue that the hypothetical panin-hominin common ancestor must also have had within its population individuals with reduced primary visual cortices, so one would expect this condition in early hominins such as *Au. afarensis*. The lunate sulcus may be unique among the cortical sulci visible on endocasts in that it may provide information about the proportion of cortex allocated to distinct functional categories, and provides an estimate of the aforementioned ratio of association to sensory cortex (Holloway RL, 1966; Holloway RL, 1968).

3.1.7.7.2 Parietal lobe expansion

The posterior location of the lunate sulcus in modern humans is associated with relative reduction of the primary visual cortex and relative expansion of the posterior parietal association cortex. The posterior parietal lobe is concerned with several aspects

74

of sensory processing and sensorimotor integration (Hyvarinen J, 1981; Lynch JC, 1980).

The superior parietal lobule subcomponent is involved in visuomotor tasks, including

finger movements (Shibata T and AA Ioannides, 2001) and visual attention (Yantis S et

al., 2002). The superior parietal lobule (Brodmann's area 7) functions in spatial

cognition and demonstrates differential activation during an Oldowan tool-making task

(Stout D et al., 2000). The inferior parietal lobule subcomponent is involved in language

and calculation abilities, and it is greatly expanded in modern humans compared to

monkeys (Simon O et al., 2002). Derived modern human behaviors involving the

posterior parietal lobe include enhanced social behavior including communication, tool

making, and tool use (Holloway RL, DC Broadfied *et al.*, 2004). Bruner *et al.* (2003)

suggest that the unique globular shape of the neurocranium of *H. sapiens* is related to an

additional expansion of the parietal lobe in modern humans. Bruner (2004) associates the

manufacture of more sophisticated tools and refined language ability with this difference.

3.1.7.8 Posterior cranial fossa size and shape

A cerebellar quotient (CQ= actual/predicted value) was obtained when recent

modern human cerebellar volume (determined from posterior cranial fossa volume) was

regressed against brain volume (determined from endocranial capacity) minus cerebellar

volume (Weaver AGH, 2001, 2005). Extant hominoid brain data suggest that the modern

human cerebellum is smaller than would be expected for an ape of similar brain size

(Rilling JK and TR Insel, 1998; Semendeferi K and H Damasio, 2000). The difference

between modern human and great ape relative cerebellar volumes is statistically

significant, although less dramatic when considered along with the range of inferred

relative cerebellar volumes found within the hominin fossil record (Weaver AGH, 2005). The cerebellum of modern humans is relatively larger than in some earlier hominins, perhaps because its size is linked to the complexity of cognitive functions (Weaver AGH, 2005).

3.1.7.9 Thoracic vertebral canal size and shape

Differences in thoracic vertebral canal size between modern humans and nonmodern human primates have been related to unique aspects of breathing in modern human speech (MacLarnon A, 1993). The thoracic part of the vertebral canal and the spinal cord segments which it encases (in modern humans, ca. T2-S2) are enlarged in modern humans relative to nonmodern human primates. It is inferred that this difference is due to an increase in the size of the anterior horns of the spinal cord and of nerves stemming from the segments which innervate the mid or lower trunk region. Some of these nerves innervate intercostal muscles and a set of abdominal muscles which are responsible for the fine control of breathing in modern human speech (Campbell EJM, 1968; Campbell EJM, 1974; Gould WJ and H Okamura, 1974). Modern human speech involves long, punctuated, and modulated utterances (Campbell EJM, 1968; Draper MH et al., 1959; Hixon TJ and G Weismer, 1995), which require respiratory control mechanisms far beyond those necessary for nonmodern human primate vocalizations. For example, it appears that in modern human speech the exhalatory portion of the breathing cycle is extended (Borden GJ and KS Harris, 1984), in contrast to primate vocalizations, which drop in pitch during their duration (MacLarnon AM and GP Hewitt, 1999, 2004). MacLarnon and Hewitt (1999) explore several hypotheses for increased thoracic vertebral

canal size in modern humans – including postural control for bipedalism, endurance running, and parturition – but find that none are fully congruent with the fossil and neurological evidence.

3.2 Trends in hominin CNS evolution

3.2.1 Primitive brain morphology

In order to determine whether a morphological feature is "primitive" or "derived" within the hominin clade it is necessary to consider the brain morphology of the most recent hypothetical common ancestor of hominins and panins. The principle of parsimony suggests the panin-hominin ancestor possessed all shared derived features of extant modern humans, chimpanzees, and bonobos, but it would lack those features acquired solely along either the panin or the hominin lineages. It is difficult to reconstruct the panin-hominin ancestor with certainty with respect to well-represented regions of the hard tissue fossil record, and it is particularly difficult to do so for CNS-related morphology for which the extant and fossil evidence is both sparser and more difficult to interpret. For simplicity, we will assume that the panin brain is equivalent morphologically to the primitive hominin brain. At present, there is no significant evidence for derived panin brain morphology which is not also shared with modern humans. However, it is actually very difficult to include much about panin brain morphology because only a few chimpanzee, and even fewer bonobo, specimens have been studied, and future hominoid comparative neuroanatomical studies will potentially bring to light panin CNS autapomorphies related to species-specific behaviors.

3.2.2 Derived brain morphology

3.2.2.1 Earliest appearance of derived modern human morphology

The data suggest that while fully modern human brain morphology only occurs in recent modern humans, some aspects of modern human brain morphology are present in earlier forms (see Table 3.1).

The aspect of modern human brain morphology which may have appeared earliest is the reduction of the primary visual cortex, as evidenced by the position of the lunate sulcus. A posterior lunate sulcus has been reported for some *Au. afarensis* specimens, and it is variable within the taxon. Given the small sample it is difficult to tell whether the *Au. afarensis* brain really is derived in the direction of the modern human brain, or whether it expresses variability similar to that seen in chimpanzees. In contrast, several aspects of endocast anatomy derived in the direction of modern humanlike brain reorganization in *Au. africanus,* which has better evidence for a reduced primary visual cortex. In addition, *Au. africanus* shows evidence of: 1) a somewhat expanded, blunt orbitofrontal cortex, 2) anteriorly-expanded, laterally pointed temporal poles, 3) an incipient LORF petalial pattern, and 4) a modern humanlike Broca's cap region. Although these features are not as pronounced as in modern humans, they can be interpreted as being derived in the direction of modern humans. The LORF petalial pattern and Broca's cap region become even more modern in *H. rudolfensis*, the earliest taxon for which there is strong evidence for modern humanlike brain organization (there are insufficient data for the other three aforementioned features until later *Homo*). In addition, *H. rudolfensis* is the earliest taxon not to have an orbitofrontal sulcus (but the

evidence is based on very little endocranial morphology). Interestingly, there is no good

evidence for a modern humanlike LORF petalial pattern and a Broca's cap region in *H.*

habilis; Indeed there is evidence of an African ape-like orbitofrontal sulcus. Where data

exist, *H. erectus* and *H. ergaster* endocasts tend to share the modern humanlike features

that are found in *H. rudolfensis*. *H. neanderthalensis* is the earliest taxon known to have

an expanded thoracic vertebral canal. Globular brain shape due to parietal lobe

expansion has been proposed as an autapomorphy of modern humans (Bruner E *et al.*,

2003). An increase in relative cerebellum size from fossil to recent anatomically modern

humans might be a final refinement within this species.

3.2.2.2 Earliest appearance of increase in absolute and relative brain size

Modern human mean brain mass for adults 21-39 years old is 1450 g for males,

and 1290 g for females (Fig. 4; Table 4) (Dekaban AS and D Sadowsky, 1978). The

chimpanzee mean brain weight for adolescent and young adult individuals (7-30 years) is

406 g for males and 368 g for females (Herndon JG *et al.*, 1999). In both species,

average brain mass decreases in older individuals – for example, Dekaban and Sadowsky

(1978) report a 7.4% decrease (~ 100 g) in modern human brain mass between 20-30

years and 70-80 years. In fact, the mean endocranial volumes from a more typical

modern human autopsy data set (average age = 65) are substantially different (male=1308

g, female=1179 g; Zilles K, 1972). Sex is also an important consideration in brain size

comparisons because male and female samples of hominoid taxa have significantly

different brain sizes. It is not possible to know the sex of fossil specimens, and statistical

methods of sexing are not possible for the small early hominin cranial samples.

Therefore, fossil taxa are not assigned to sex, but are compared as whole taxon samples to samples of both sexes of extant taxa.

Previously, absolute brain size has been used to determine a cerebral rubicon criterion for inclusion in the genus *Hom*o, variably set between 600 and 800 cm^3 (Leakey LSB *et al.*, 1964). Until recently, absolute brain size was thought to lack biological significance, since it does not give an indication of degree of encephalization, or the number of "extra neurons" (Jerison HJ, 1973; Martin RD, 1990). However, the relevance of EQ is also problematic, in particular because it does not appear to predict cognitive ability in primates (Deaner RO *et al.*, 2007). Also, note that aspects of brain morphology such as brain component volumes and degree of gyrification scale to absolute brain size (Semendeferi K and H Damasio, 2000; Semendeferi K *et al.*, 2002; Weaver AGH, 2005; Zilles K et al., 1989; Zilles K et al., 1988), an important consideration when making comparisons between the morphology of fossil endocasts.

The smallest adult hominin brain belongs to the single cranial specimen of *Sahelanthropus*, the earliest possible hominin, and its endocranial volume falls slightly below the female chimpanzee mean. Single specimens of *P. aethiopicus*, *Au. garhi* and *H. floresiensis* plot around the male chimpanzee mean. The *Au. afarensis* sample is not significantly different from the combined sex sample of chimpanzees ($p = .093$), nor from the male chimpanzee sample ($p = .456$), although it is significantly larger than the female chimpanzee sample ($p = .011$) (all statistical comparisons are derived from a Kruskal-Wallis test of significance). The *Au. africanus* sample is significantly different from the combined sex sample ($p < .001$), and the male ($p = .001$) and female ($p < .001$) subsamples of chimpanzees. However, this does not suggest that the brain size of *Au.*

africanus is significantly increased relative to chimpanzees and that of *Au. afarensis* is not – these two groups do not differ significantly from each other (*p* = .385). Although the *Au. africanus* mean value (455 g) is only slightly larger than that for *Au. afarensis* (442 g), the range for *Au. africanus* is much smaller than that for *Au. afarensis* (but see Reno *et al*. [(2005)] for an alternative interpretation that suggests only modest levels of sexual dimorphism in *Au. afarensis*). In addition, *Au. afarensis* attains higher individual brain mass estimates than *Au. africanus*.

Early hominin fossil crania for which endocranial volume and body mass have been reliably estimated are rare, making it impossible to do comparative statistical tests of encephalization quotients. However, given that early fossil hominins (e.g., *Australopithecus* and *Paranthropus*) have smaller estimated body masses than chimpanzees (mean body mass = 58 kg for males, 43 kg for females; (Herndon JG *et al.*, 1999), any significant increase in relation to chimpanzee brain volume can be assumed to be an increase in both absolute and relative brain size (Table 4). Thus, the increase from the brain size of a chimpanzee-like hypothetical common ancestor to brains the size of those belonging to *Au. afarensis* and *Au. africanus* is evidence of an increase in relative brain size. This finding is further evidenced by the EQ values of *Au. afarensis* (2.5) and *Au. africanus* (2.8) which are well above those for chimpanzees (male EQ = 1.7; female EQ = 1.9), overlapping with those of *Paranthropus* (*P. boisei* EQ = 2.5; *P. robustus* EQ = 3.1), and approximating that of *H. ergaster* (2.8).

By the time of the appearance of *H. rudolfensis* and *H. habilis*, both absolute and relative brain size have clearly departed from the *Pan*-like condition. *H. habilis* is the smallest brained hominin for which all the specimen values fall outside of two standard

deviations of the male chimpanzee mean. *H. habilis* and *H. rudolfensis* are significantly

different in brain mass ($p = 0.02$) , and the entire range of *H. rudolfensis* values plot

above the range of *H. habilis* values. However, when the brain mass data are seen in the

light of body mass data, *H. habilis* (EQ = 3.7) is more encephalized than *H. rudolfensis*

(EQ = 3.2). Relative brain mass in both *H. habilis* and *H. rudolfensis* is greater than that

in *Australopithecus* and *Paranthropus,* and it approaches the values for *H. erectus* (EQ =

3.9).

In summary, encephalization in the hominin lineage may have begun as early as

Au. afarensis and it was more evident in *Au. africanus* (in parallel to the encephalization

of *Paranthropus*, see section 4.3) and had definitely occurred by the time of the

appearance of *H. habilis* and *H. rudolfensis*.

3.2.2.3 Appearance of derived modern human CNS morphology in relation to brain size

Although there are hints of a trend toward a modern humanlike relative brain size

and brain morphology in *Au. afarensis*, there is a lot of variability in the size and

morphology of this taxon. Given small samples, one cannot be certain whether this

variation is different from the variation seen in chimpanzees. Further, the functional and

adaptive significance of these features in the early taxa is questionable. Modern

humanlike endocranial anatomy in *Au. afarensis* might be a pre-adaptation which only

acquires its modern functions in *Au. africanus*, *H. rudolfensis,* or in even later hominins.

Most aspects of modern humanlike endocast morphology make an appearance in

Au. africanus, but they do not yet show the fully modern form. The reason for their

occurrence in this taxon is uncertain, but may be influenced by brain size increase, and it

is quite possibly related to exceptional preservation of brain morphology in *Au. africanus*. The appearance of several aspects of modern brain morphology in *Au. africanus* complement the fact that this taxon is the first to have a brain size significantly different from chimpanzees. However, as a whole the *Au. africanus* brain still differs considerably from the modern human brain, and any similarities are not considered sufficient to suggest a modern humanlike cognitive capacity or behavior for *Au. africanus*.

In contrast, the more modern-modern humanlike brain morphology of *H. rudolfensis* is generally taken as evidence of more modern humanlike cognitive capacities. Most notably, these features are suggestive of language ability and right-handedness – coincident with the first stone tools which apparently were made by right-handed hominins. This is associated with the earliest brain masses outside of what is expected for a chimpanzee, and an EQ value higher than that of earlier taxa. However, *H. habilis* has a higher EQ than *H. rudolfensis*, and this later appearing hominin also has brain mass values outside of what is expected for a chimpanzee. As yet, it is not possible to tell whether the more modern humanlike brain morphology of *H. rudolfensis*, compared to *H. habilis* is, or is not, size-related.

3.2.3 Brain evolution in non-*Homo* hominin lineages

The *P. boisei* mean value (483 g) for estimated brain mass is larger than the value for *P. aethiopicus* (407 g) and somewhat larger than the means for *Au. africanus* (455 g) and *Au. afarensis* (442 g). Further, the majority of the *P. boisei* specimens fall outside of two standard deviations of the male chimpanzee mean. Therefore, it is inferred that *P. boisei* has increased its absolute brain size relative to the primitive condition. The *P.*

boisei sample mean is not significantly different (*p* = .357) from that of the later occurring *P. robustus* sample, even though the latter attains a much higher maximum value (638 g) and has a much higher mean (565 g). *P. boisei* and *P. robustus* have EQs that are higher than those for male and female chimpanzees. However, the *P. boisei* EQ is smaller than the *Au. africanus* and it is similar to the *Au. afarensis* value. Given the lack of postcranial evidence, one cannot be certain that EQ has increased from *P. aethiopicus* to later *Paranthropus* taxa. These data are, however, consistent with the suggestion of a temporal trend for brain size increase within the *Paranthropus* lineage (Elton S et al., 2001).

There is little evidence suggesting modern humanlike reorganization of the *Paranthropus* brain. In particular, slight LORF petalial patterns are found in *P. aethiopicus* and *P. boisei*, and a posteriorly-positioned lunate sulcus has been identified in *P. boisei*. The evidence does not suggest that the *Paranthropus* brain becomes increasingly modern humanlike over time, as is the case for *Homo*. Further, *Paranthropus* retains an ape-like beak-shaped orbital surface of frontal lobe and rounded temporal poles, differentiating it from *Au. afarensis* and *H. sapiens*. The modern humanlike endocranial features seen in *Paranthropus* most likely reflect a shared ancestry with the modern human lineage. Similarly, brain size increase in *Paranthropus* is probably the continuation of a trend beginning in a common ancestor of *Paranthropus* and modern humans.

There is presumed to be a decrease in absolute and relative brain size in *H. floresiensis* (Brown P *et al.*, 2004), but this trend may also apply to other fossil hominin taxa. *H. floresiensis* had a very small brain (414 g), with an EQ (3.0) much lower than

that of its presumed closest fossil relative, *H. erectus*. Interestingly, its EQ is higher than the one listed here for *H. ergaster* (2.8 – includes Dmanisi) and only slightly lower than the EQ for African *H. ergaster* (3.1). Body mass estimates obtained from Dmanisi postcranial remains will refine the *H. ergaster* EQ. Given that *H. ergaster* is thought to have expanded in range outside of Africa, evidence from the relative brain size alone suggest that it rather than *H. erectus* may be the sister-taxon of *H. floresiensis*. If so, this would indicate that EQ did not actually decrease in *H. floresiensis* – solving one of the major puzzles of this taxon (Brown P *et al.*, 2004). It is noted that *H. floresiensis* possesses much morphology that is derived from the primitive ape-like condition. Several of these features are thought to be found in the most recent *H. floresiensis*-modern human common ancestor (which may also be the most recent *H. erectus*-modern human common ancestor).

Brain size increase and the appearance of some aspects of modern humanlike brain morphology occur in at least two hominin lineages. Both *Paranthropus* and *Homo* have absolutely and relatively significantly larger brains than *Australopithecus*. However, only in *Homo* does brain size increase occur in parallel with the acquisition of modern humanlike brain morphology. Interestingly, *H. floresiensis* provides striking evidence that even within *Homo* estimated brain mass and inferred brain morphology can become disassociated.

Table 3.1. Aspects of endocranial morphology and/or inferred CNS morphology

Taxon	First Appearance Datum (mya)	Mean endocranial vol. (cm3)	EQ	L.O.R.F. petalial pattern [a]	Fronto-orbital sulcus [b]	Orbital surface of the frontal lobe [c]	Broca's cap region [d]	Neurocranial globularity [e]	Temporal pole morphology [f]	Lunate sulcus position [g]	Relative size of cerebellum (CQ) [h]	Thoracic vertebral canal [i]
Pan troglodytes (M)			1.6									
Pan troglodytes (F)			1.9	P	P	P	P	P	P	P	1.2	P
Recent *H. sapiens* (M)			5.1									
Recent *H. sapiens* (F)			5.4	M	M	M	M	M	M	M	1	M
S. tchadensis	7	365		--	--	--	--	--	--	--	--	--
Orrorin tugenensis	6			--	--	--	--	--	--	--	--	--
Ar. kadabba	5.8			--	--	--	--	--	--	--	--	--
Ar. ramidus	4.5			--	--	--	--	--	--	--	--	--
Au. anamensis	4.2			--	--	--	--	--	--	--	--	--
Au. afarensis	3.9	446	2.5	I	--	--	P	--	--	P/M	--	P
Kenyanthropus platyops	3.5			--	--	--	--	--	--	--	--	--
Au. bahrelghazali	3.5			--	--	--	--	--	--	--	--	--
Au. africanus	3	460	2.8	m	P	m	m	--	m	M	0.8	P
Au. garhi	2.5	450		--	--	--	--	--	--	--	--	--
P. aethiopicus	2.5	410		m	--	P	--	--	P	--	--	--
P. boisei s.s.	2.3	488	2.5	m	--	P	--	--	P	M	1	--
P. robustus	2	533	3.1	I	--	P	--	--	P	M	--	--
H. habilis s.s.	2.4	609	3.7	P	P	--	I	--	--	--	1	--
H. rudolfensis	1.8	776	3.2	M	M	--	M	--	--	--	0.9	--
H. ergaster	1.9	763	2.8	M	--	--	I	--	--	--	0.9	P
H. erectus s.s.	1.8	991	3.9	M	--	--	M	P	--	M	0.9	--
H. antecessor	0.7			--	--	--	--	--	--	--	--	--
H. heidelbergensis	0.6	1242	4.2	M	--	--	M	P	--	M	0.8	--
H. neanderthalensis	0.2	1404	4.7	M	--	--	M	P	--	M	0.7	M
H. sapiens s.s.	0.19	1463	5.3	M	--	--	M	M	--	M	0.7	M
H. floresiensis	0.09	417	3.1	M	M	M	I	--		M	--	--

Notes: "--" No relevant evidence; "I" -- Insufficient evidence; "M" -- Modern human-like morphology either described or inferred; "m" -- incipient modern human morphology either described or inferred; "P" *Pan*-like morphology either described or inferred.

Pan-like (P) and Modern human-like (M) morphology as follows. Please refer to text (pp.) for a more detailed explanation. a. Left occipital right frontal petalial pattern (P) infrequent, rarely involves both frontal and occipital lobes; (M) usual. b. Fronto-orbital sulcus (P) present; (M) absent. c. Orbitofrontal region (P) beak-shaped; (M) blunt and expanded. d. Asymmetrical Broca's area (P) not asymmetrically enlarged; (M) L>R asymmetry. e. Endocast shape (P) "archaic"; (M) globular, suggests expanded parietal. f. Temporal pole morphology (P) rounded; (M) expanded in anterior and lateral directions. g. Lunate sulcus position (P) anterior (some variability); (M) more posterior. h. Taxon mean EQ values, calculated from specimen CQ values (LSR-05 in Weaver, 2001). i. Thoracic vertebral canal cross sectional area (P) size expected for a primate of similar body mass; (M) larger than expected for a primate of similar body mass.

Table 3.2. Absolute and relative brain size values for fossil and extant panin and hominin taxa.

Taxon[a]	FAD (mya)	number in sample	mean endocranial vol., cm³	minimun endocranial vol., cm³	maximum endocranial vol., cm³	mean brain mass, g[b]	minimum brain mass, g	maximum brain mass, g	brain mass SD	mean body mass, kg	EQ[c]	pongid EQ[d]	homocentric EQ[d]
Pan troglodytes (M)		17				406	347	530	39	58	1.65	1.11	0.33
Pan troglodytes (F)		17				368	308	458	37	43	1.88	1.20	0.36
recent *H. sapiens* (M)		351				1450	1343	1526	20	70	5.10	3.54	1.04
recent *H. sapiens* (F)		201				1290	1239	1366	30	57	5.35	3.57	1.06
S. tchadensis	7	1	365			363							
Au. afarensis	3.9	5	446	387	550	442	385	542	69	38	2.50	1.55	0.47
Au. afarensis (M?)		2	521	492	550	514	486	542	40	45	2.56	1.64	0.49
Au. afarensis (F?)		3	396	387	400	393	385	397	7	29	2.69	1.60	0.50
Au. africanus	3	9	460	428	515	455	424	508	33	34	2.78	1.70	0.52
Au. garhi	2.5	1	450			446							
P. aethiopicus	2.5	1	410			407							
P. boisei	2.3	10	488	400	545	483	397	537	43	41	2.54	1.61	0.49
P. robustus	2	4	533	450	650	525	446	638	82	36	3.07	1.89	0.58
H. habilis	2.4	6	609	509	687	599	503	674	60	33	3.72	2.26	0.70
H. rudolfensis	1.8	3	776	750	825	758	734	805	41	55	3.21	2.13	0.63
H. ergaster	1.9	6	763	600	900	746	590	877	111	64	2.81	1.92	0.56
H. ergaster (Africa)		3	851	804	900	830	785	877	46	64	3.12	2.14	0.63
H. ergaster (Dmanisi)		3	675	600	775	662	590	758	86				
H. erectus	1.8	36	991	727	1260	963	712	1218	134	58	3.94	2.64	0.78
H. antecessor	0.7	1	1000			972							
H. heidelbergensis	0.6	21	1242	880	1450	1200	858	1397	131	71	4.21	2.93	0.86
H. neanderthalensis	0.2	27	1404	1172	1740	1353	1135	1669	153	72	4.67	3.25	0.95
H. sapiens	0.19	79	1463	1090	1880	1408	1057	1799	124	64	5.30	3.62	1.07
H. floresiensis	0.09	1	417			414				26	3.10	1.80	0.56

Notes:
a. Sources as follows: Chimpanzee brain and body mass data for individuals 7-30 yrs., from Herndon *et al.* (1999). Recent modern human brain and body mass data for adults 21-39 yrs., (except min. and max. brain mass, which are for 20-30 yrs.) from Dekaban and Sadowsky (1978). In both datasets, "brain mass" is taken from fresh autopsy specimens and includes brain tissue as well as leptomeninges and CSF. Fossil hominin endocranial volume raw data and sources available from the author, by request.
b. Fossil endocranial volumes were converted into brain masses after Ruff et al.'s (1997).
c. EQ values after Martin (1981) and Ruff *et al.* (1997). Extant taxon EQ values are means of individual EQ values. Fossil taxon sample mean EQ values are obtained from each taxon's mean brain mass and mean body mass estimates. EQ values obtained by either method are very similar and have been used interchangeably (e.g., Ruff *et*
d. Homocentric and Pongid EQ values after Bauchot and Stephan (1969) and Holloway and Post (1972)

Fig. 3.1. Fossil hominin brain size.
Chimpanzee and recent modern human male and female brain mass means are plotted, with dashed lines showing ranges within two standard deviations. Fossil hominin brain mass individual specimen values are plotted with Y-axis bars showing range within two standard deviations from the mean. For more information, see Table 3.2.

Chapter 4. Comparative Cytoarchitectural Analyses of Striate and Extrastriate Areas in Hominoids

4.1 Introduction

The visual cortex is the largest special sensory modality representation in the neocortex of humans and closely related species. Visual areas (i.e., cortical areas devoted entirely or mainly to vision) comprise ca. 23% of the adult modern human neocortex (Van Essen DC and HA Drury, 1997) and ca. 55% of the macaque neocortex (Felleman DJ and DC Van Essen, 1991). The size and organization of the human visual cortex has played a fundamental role in discussions of brain evolution (e.g., Dart RA, 1925; Falk D, 1980; Holloway RL, 1972; Holloway RL, DC Broadfield, MS Yuan et al., 2003; Jerison HJ, 1975).

The visual cortex is the most studied and best understood part of the primate cerebral cortex, largely due to extensive research in monkeys. Physiological and histological investigations have lead to the identification of over 25 visual areas in macaques (Felleman DJ and DC Van Essen, 1991; Van Essen DC, 2004). Apes and humans share with Old World monkeys a particularly specialized visual system, with well developed stereoscopic vision (a primate synapomorphy), and routine trichromatic color vision (a catarrhine synapomorphy). Recently, functional magnetic resonance

imaging (fMRI) has made it possible to map and identify visual areas in the human cerebral cortex, and in some cases, candidates for homologous areas between the human and monkey brain have been identified (DeYoe EA *et al.*, 1996).

In contrast, little is known about the detailed anatomy and physiology of the visual areas in the taxa phylogenetically closest to humans – the apes. Only rarely have there been opportunities to conduct physiological studies of ape visual cortices (e.g., Tigges J and M Tigges, 1979; Vital-Durand F and C Blakemore, 1981). The focus of the current study is to improve the representation of apes in cytoarchitectural datasets, which, in combination with independent molecular evidence about their relationships, will make it possible to generate hypotheses about the evolution of the higher primate visual cortex.

In addition, this study explores the possibility of scaling relationships between neuronal volume density (indicated by the grey level index, GLI) and several brain, body and visual system variables. GLI is highly correlated with neuronal volume density (Wree A *et al.*, 1982) a component of which is neuronal numerical density. Several studies have demonstrated that, across a range of mammalian species, there is a negative allometric relationship between brain size and neuron density in the neocortex, which follows a -1/3 power law (Haug H, 1987; Prothero J, 1997; Tower DB, 1954). In primates (but not non-primates) there is a grade-level shift in the scaling relationship of the visual cortex, such that the number of primary visual cortex neurons is about double what would be expected for a non-primate mammal of similar brain size (Cragg BG, 1967; Rockel AJ *et al.*, 1980). Thus far, no scaling relationships have been found between cortical area GLI values and brain size. However, GLI scaling relationships have only been explored in hominoids in areas 10, 13, and 4, and in these areas neuron

numerical density likewise does not scale to brain weight, although it is possible that the hominoid sample is not large enough to exhibit such scaling relationships (Sherwood CC and PR Hof, 2007). However, scaling relationships seem to differ between cortical areas. For a single anthropoid sample, it was found that the neuron density of visual areas V1 and V2 scaled to brain mass to the -1/3 power (Sherwood CC, MA Raghanti *et al.*, 2007), but that of area 9L did not correlate with brain mass (Sherwood CC *et al.*, 2006 suppl.). It has been speculated that departures from brain size scaling trends may reflect differences in the organization of neuronal connections related to specific functions (Sherwood CC and PR Hof, 2007). Therefore, in the current study, the possibility that visual area GLI values vary according to functionally related visual system structures is explored.

4.2 Materials and methods

4.2.1 Specimens and tissue preparation

The sample for comparative cytoarchitectural analysis comprised a total of nine brains representing seven catarrhine species (one each of *Macaca fascicularis*, *Hylobates lar*, *Pongo pygmaeus*, *Gorilla gorilla*, and *Pan paniscus*, and two each of *Pan troglodytes* and *Homo sapiens*).

Included were sections from the left hemispheres of adult specimens. The age and sex distribution is shown (Table 4.1). All specimens were included in the studies of cortical areas V1, V2, and VP (V3v). Only one human (HS5) and one chimpanzee (PTD) were used for V5 studies. Specimens in the study belong to the Zilles comparative

neuroanatomy collections at C&O Vogt Institute of Brain Research in Düsseldorf, Germany. The macaque was provided by Hans-Jürgen Bidmon, and is also at the C&O Vogt Institute.

The human and nonhuman hominoid brains from the Zilles collection were immersion fixed with either 4% formaldehyde or Bodians's solution (a mixture of formalin, glacial acetic acid, and ethanol), within a post mortem interval of <36 hours after death for the human brains and <12 hours after death for the nonhuman hominoid brains, embedded in paraffin and serially-sectioned along the coronal plane at a thickness of 20μm. Sections used in this analysis were stained for Nissl substance (cell bodies) using silver according to the technique described by Merker (1983), based on Gallyas' procedure. Merker stain is ideal for quantitative cytoarchitectural analysis due to high staining intensity and contrast. Although Merker stains for Nissl substance, it has been found that due to differences in the intensity and cytoarchitecture that is stained, GLI profiles are not comparable between different types of Nissl stains (i.e., cresyl violet versus silver Merker, K. Amunts, personal communication), therefore only sections stained according with this method were used. The macaque brain was perfusion fixed with 4% formaldehyde in phosphate buffer, embedded in paraffin and serially-sectioned along a coronal plane at 20 μm, and Merker stained for Nissl.

4.2.2 Identification and sampling of cortical areas V1, V2, VP, and V5

All cortical regions were identified on the basis of cytoarchitectonic criteria rather than sulcal and gyral landmarks. This is primarily because sulci and gyri are not reliable indicators for the location of cortical areas, especially higher-order cortical areas

92

(Scheperjans F et al., 2008). Further, catarrhine species vary significantly in the sulcal patterns of their occipital lobes. For example, an intact lunate sulcus occurs in nonhuman catarrhines, but is not typical in humans (Allen JS et al., 2006). To a lesser degree, even the similarly-sized brains of great ape species vary somewhat in the appearance of sulci and gyri. For example, several publications have described the sulcal patterns of African ape occipital lobes, and a comparison of these demonstrates that sulci are not consistently apparent even within species, e.g., in gorillas (Connolly CJ, 1933; Le Gros Clark WE, 1927; Noback CR and L Gross, 1959) and chimpanzees (Bailey P *et al.*, 1950; Walker AE and JF Fulton, 1936). Therefore, it is impossible to determine the homology of most sulci without consideration of cortical cytoarchitecture. However, approximation to sulcal and gyral landmarks was considered as an additional criterion to select samples from within cortical regions (see Table 4.3), to increase the likelihood that the areas were in fact homologous, and that similar representation of the visual field were being sampled.

The cortical area V1 was distinguished from adjacent cortical areas by the presence of the stripe of Gennari. Although it was possible to identify the entire extent of V1, this area was not sampled in full because it spans regions for which the laminar pattern is obscured by plane of sectioning. Only external and/or lateral parts of V1, away from the calcarine sulcus and towards the occipital pole, were included in the analysis. From this region, ROIs were selected from three different parts of the cortical ribbon and the results averaged. Three regions were chosen on the basis of: 1) relatively few artifacts, so that the GLI gives an accurate representation of laminar pattern and 2) low

93

gyrification, such that laminar widths and densities are constant within the sample, and thus are more "typical" of the region.

Qualitative cytoarchitectonic criteria were used to determine the location of cortical areas V2 and VP (also known as V3 ventral or V3v) on all specimens (Table 4.2). Due to difficulties in distinguishing the precise borders between extrastriate areas (see Chapter 2), only portions of these cortical areas were sampled, and several steps were taken to ensure that the sampled regions were homologous across species, and that adjacent areas were not included. The ventral portion of areas V2 and VP were investigated, because in humans, cytoarchitectonic differences are more obvious between ventral V2 and ventral V3 (i.e., VP), than between dorsal V2 and dorsal V3 (also known as V3d; Clarke S and J Miklossy, 1990; Zilles K and S Clarke, 1997). In the nonhuman primates, V2 and VP were sampled at a dorso-ventral position near the anterior limit of the external portion of V1 (delimited by the lunate sulcus); at this location it is easiest to identify homologous ventro-occipital sulci because the extent of V2 and VP are both relatively large and are the easiest to distinguish. Problematic border regions were avoided, and both areas were sampled close to their medial borders (i.e. V2 towards the V2/V1 border and VP towards the V2/VP border). In the humans, it was not possible to apply an identical sampling strategy as in the nonhuman primates because they lacked the lunate sulcus. V2 and VP had been previously mapped on the two human specimens using the observer independent method (Amunts K, E Armstrong et al., 2007; Amunts K et al., 2000; Rottschy C et al., 2007). As in the nonhuman primates, a continuous, cytoarchitectonically homogenous, relatively straight portion from within each cortical area was selected.

For comparison, area V5/MT+ (hereinto referred to as V5) was included for one of the humans and one of the chimpanzees. V5 is particularly difficult to identify on ape Nissl stained material and was not cytoarchitectonically localized specifically as part of the current study. However, because due to previous studies, the borders of V5 were available for two of the brain specimens partaking in this study, they were also scanned and processed for V5 GLI data using the parameters described below. In the chimpanzee, the extent of V5 (referred to as primate area MT) had been determined on the basis of adjacent myelin stained sections and was within the depth of the superior temporal sulcus (Frahm HD *et al.*, 1998). In the human, the V5 (referred to as hOc5, the cytoarchitectonic correlate of V5/MT+) cytoarchitectonic borders had been determined using the observer independent method and it was located in the upper bank of the inferior occipital sulcus (Malikovic A et al., 2007).

4.2.3 Laminar boundaries

Cortical layers were distinguished for the purpose of obtaining relative layer width patterns and layerwise GLIs (see below). The procedure for obtaining laminar boundaries is described here.

4.2.3.1 V1

Area V1 laminar nomenclature is based on Lund (1973). In addition, criteria were taken from several publications which describe the cytoarchitecture of V1 layers in catarrhines (Amunts K *et al.*, 2000; Bailey P *et al.*, 1950; Hof PR and JH Morrison, 1995;

Hof PR et al., 2000; Lund JS, 1973; Peters A and C Sethares, 1991, 1991; Preuss TM and GQ Coleman, 2002; Sherwood CC, PW Lee *et al.*, 2003; Sherwood CC, MA Raghanti *et al.*, 2007; Tigges M et al., 1981; von Economo C, 1929). Laminar patterns were similar across species, however, due to some variability, the criteria found to be the most consistent across species and useful for determining borders were emphasized over other criteria. A full list of criteria can be seen in Table 4.4 , but the most significant criteria are highlighted here. For V1, layers II/III, IVA, IVB, IVCα, IVCβ, V, and VI were identified. Narrow, sparse layer I was excluded. Layer II was distinguished from layer I by an abrupt increase in neuron number. Layer II merges gradually with the upper part of layer III. Although an attempt was made to identify the border between layers II and III, this could not be done systematically since the upper part of layer III is difficult to distinguish from the lower part of layer II, so II and III were merged as II/III. Layer IVA is dense and packed with small cells. Layer IVB is very sparse and includes multipolar Meynert-Cajal cells and pyramidal bodies. Layer IVCα is more cell dense and packed with small granule cells. Layer IVCβ was distinguished from layer IVCα only in being denser. Layer V is sparser than adjacent layers. Layer VI is distinguished from layer V by an increase in density, although the density decreases in the lower part of layer VI. Meynert cells occur in the border region of layer V and layer VI, but they in themselves cannot indicate the precise border since they span the two layers.

4.2.3.2 Extrastriate areas V2, VP and V5

Extrastriate laminar nomenclature is based on Lund (1981). Laminar criteria were taken from several publications which describe the cytoarchitecture of extrastriate areas

in chimpanzees (Bailey P *et al.*, 1950), humans (Amunts K *et al.*, 2000; Rottschy C *et al.*, 2007; von Economo C, 1929) and macaques (Lund JS *et al.*, 1981; Valverde F, 1978). Although extrastriate areas can be differentiated from each other on the basis of cytoarchitectonic criteria, major criteria for differentiating laminae are consistent across extrastriate areas V2, VP and V5. For V2, VP and V5, layers II, III, IV, V, and VI were identified. For V2 and VP, it was also possible to further subdivide layer III into components IIIA and IIIB. In statistical comparisons across cortical areas, the sublaminae are merged. A full list of criteria can be seen in Table 4.5, and the most significant criteria are highlighted here. Layer II is quite dense, packed with small cells, with a sharp border with layer I and also clearly denser than layer III. Layer IIIA is more columnar than II, less dense, and with larger cells. Layer IIIB is most readily distinguished from layer IIIA by the presence of large pyramidal cells. Layer IV is extremely dense and distinguished from adjacent layers by the presence of small granule cells. Layer V is relatively sparse. Layer VI is denser than layer V (although the transition is often gradual), lacks very large pyramidal cells, and contains fusiform cell bodies; layer VI cell density decreases in its lower part.

4.2.4 Grey Level Index Acquisition

Grey Level Index (GLI) values were obtained to quantify laminar organization of areas V1, V2, VP, and V5. The GLI encompasses the density of Nissl stained cell bodies and their sizes per unit volume of cerebral cortex. GLI values measure the proportion of neuronal cell nuclei, glial cell nuclei, and endothelial cell nuclei versus neuropil. As the volume fraction of glial and endothelial cells is small and does not vary significantly

97

across cortical layers, the GLI is an estimate of neuronal volume density (Wree A *et al.*, 1982). Differential shrinkage of cell bodies versus neuropil may occur, although it is expected to be lower than 9% (Kretschmann HJ et al., 1982). The steps involved in obtaining GLI values for a region of interest are described here.

4.2.4.1 Obtaining a grey level image

First high resolution images of Nissl stained sections were obtained. For each specimen, five adjacent sections equally spaced 300-400 microns apart were quantified per cortical area. A rectangular image of the region of interest (ROI) was obtained using an image analysis system (KS 400; Zeiss, Oberkochen, Germany). This was done by an automatic scanning technique. The ROI is viewed one image frame at a time through a light microscope (Zeiss Planapo) at 10 X 1.25, and photographed using a digital camera (AxioCam MRm, Zeiss, Germany). A motorized stage controlled by KS400 software is used to move between image frames. Thus, the ROI is actually a mosaic of several adjacent rectangular image frames, each an 8-bit greyscale image 713 x 537 μm in size and 1376 x 1036 pixels in spatial resolution (i.e., each pixel was 0.518 μm in length).

Note that the GLI values reported here are not directly comparable to previous reports of cortical area GLI values (Amunts K, E Armstrong *et al.*, 2007; e.g., Semendeferi K *et al.*, 1998; Semendeferi K *et al.*, 2001; Sherwood CC, RL Holloway, JM Erwin, A Schleicher et al., 2004) due to differences in staining, magnification, and/or segmentation of cell bodies. Although a magnification of 4x1.26 is routine and sufficient for producing GLI images in most cases, it was found that the densest layers of more cell dense nonhuman primate brains -- e.g., V2 granular layer 4, perhaps the densest layer in

the cerebral cortex (von Economo C, 1929) -- required a higher magnification in order to ensure accurate discrimination of neurons during image acquisition. Further, the procedure for segmenting cell bodies from neuropil was adjusted so as to be optimized for this higher magnification. Although a smaller field of view results in lower, more precise, and more accurate GLI values (Wree A *et al.*, 1982), the effect of the adjusted segmentation overcompensates for this effect through the identification of smaller points than in previous studies, therefore the human GLI values reported here are about twice as high as those reported by Amunts et al. (2007).

Next, each image frame was converted to binary values using adaptive thresholding, and further subdivided into a grid of 81x61 measuring fields (17x17 pixels per square, comprised of 16 pixels which are measuring field and 1 pixel which is border) (Fig. 4.1). This sampling procedure resulted in a measuring field size 8.3 x 8.3 microns. For each measuring field, a GLI value was obtained, and these were combined in a composite data matrix called the GLI image.

4.2.4.2 Obtaining GLI profiles

GLI profiles were extracted from a GLI images as follows. On a GLI image, two contour lines were manually traced at the borders between cortical layers I and II, and between cortical layer VI and the white matter (Fig. 4.2). Attempts to develop an automated method resulted in inaccuracies (A. Schleicher, personal communication), therefore this step required very careful observation of cortical layer limits. GLI profiles represent variation in cell volume density in different cortical layers. Profiles were extracted using a MatLab v. 7.1 (2005, The MathWorks, Inc., Natick, MA, USA) based

routine, by calculating equally spaced profile lines (transverses) perpendicular to the two contours and parallel to the cortical columns (Jones SE et al., 2000). Transverses were calculated to be curved, to best represent the actual shape of cortical columns. Cortical thickness is not constant, so each profile is standardized to encompass 101 values corresponding to cortical depth, ranging from 0% (border between layer 1 and layer 2) to 100% (border between layer 6 and white matter), which is achieved by resampling for linear interpolation.

GLI profiles were quantitatively represented by a set of 10 feature vectors describing the shape of the curve, based on its central moments (Amunts K et al., 1997). These data formed the basis of all the subsequent multivariate analyses.

4.2.5 Layerwise GLI values

For each area, the mean GLI profile for each cortical layer is calculated by subdividing the mean GLI profiles into segments corresponding to cortical layers and sublayers (except layer 1). For each ROI, the maxima and minima of the mean GLI profile were matched to cytoarchitecturally identified layer divisions (Fig. 4.2 C). This was achieved by fitting a translucent mean profile graph over 10x1.25 magnification histological image of representative portions of cortex, and the breakpoints between lamina were recorded.

Because mean GLI values have been found to vary among species (Armstrong E et al., 1986; Semendeferi K *et al.*, 1998; 2001; Sherwood CC, RL Holloway, JM Erwin, A Schleicher *et al.*, 2004; Zilles K and G Rehkämper, 1988), normalized GLI values, in

which the value for a particular layer was divided by the mean for that cortical area, were

calculated for comparative purposes.

Normalized GLI = Layerwise GLI / Mean GLI

In order to better visualize the relationship between normalized GLI and laminar

patter, adjusted layerwise GLI values were calculated. Adjusted GLIs were calculated

using the formula:

Adjusted GLI = Normalized GLI – 1

4.2.6 Comparative statistical methods

4.2.6.1 Brain, body, and visual system variables

Bivariate and multivariate statistical methods were used to examine possible

scaling relationships between V1, V2 and VP mean GLI and two sets of macroanatomical

variables: brain and body size variables, and visual system variables (Table 4.1). First

correlations between V1, V2 and VP mean GLI and the brain, body and visual system

variables were examined, and these were then followed up by regression analyses to

determine the slope of the scaling relationships (see 4.2.6.1.3).

The selection of the four brain and body size variables was based on Sherwood *et*

al. (2004) and included brain mass (BRAIN), body mass (BODY), encephalization

quotient (EQ), and neocortex volume (NEOCORTEX). Because it is possible that

scaling relationships could occur at the level of sensory modality, correlations were also

conducted to include four visual system variables: left LGN volume (LGN), left V1

volume (V1 VOL), half surface of eye area (EYE), and optic nerve cross sectional area (OPTIC NERVE).

In most cases these data were available for the individual specimens (see Chapter 5), but where not available, species means were used from the literature (Stephan H *et al.*, 1981). Neocortex volumes were provided by Carol MacLeod. Encephalization quotients (EQs) were calculated using Ruff *et al.*'s (1997) formula, which is based on Martin (1981), using the formula:

$$EQ = \textbf{brain mass}/(\textbf{11.22 x body mass}^{3/4})$$

Prior to statistical analyses, each of the brain, body and visual system variables was transformed to match the dimensions of the GLI data to which it was being compared (Sherwood *et al.*, 2005). GLI was compared to the cubic root of the volume measurements V1, LGN, NEO and BRAIN, and the mass measurement BODY (a proxy for body volume). GLI was compared to the square root of the area measurements OPTIC NERVE and EYE. EQ was not transformed since it is a residual value. Next, the GLI values and the brain, body, and visual variables were $\log_{10}$ transformed, as this has been found to be appropriate in similar analyses (Sherwood CC, PR Hof *et al.*, 2005).

Simultaneous correlations were done for three cortical areas, V1, V2 and VP, tripling the probability of false positives, so in order to obtain significance at alpha level 0.05 only p values of 0.05/3 = 0.0167 were considered to be statistically significant.

4.2.6.1.1 Relative layer width patterns

A change in one relative layer width automatically results in a change in at least one other relative layer width, therefore the group of layer widths are analyzed as part of a "relative layer width pattern". Because relative layer width pattern is an aspect of laminar pattern which might predict the macroanatomical variables (as dependent variables), the proportional widths of all layers were considered simultaneously in stepwise linear regression models of layer widths (as independent variables).

4.2.6.1.2 Normalized GLI patterns

Like relative laminar width, normalized GLI values describe an aspect of laminar pattern per cortical area. For this reason, identical statistical analyses were performed to investigate possible scaling relationships between "normalized GI patterns" and the macroanatomical variables.

4.2.6.1.3 Mean GLI values

First nonparametric correlation analyses (Spearman's rho) were performed to investigate the relationships between mean cortical area GLI and the sets of brain and body size and visual system variables. After correlations were determined, each brain, body and visual system variable that was significantly correlated with the mean GLI for V1, V2 or VP was treated as the independent variable in regressions in which mean GLI was the dependent variable. Slopes were calculated in SMATR (Warton DI et al., 2006) from reduced major axis (RMA) regressions, which assumes that the error variance of the X and Y variates is equal.

Because the variables had been put into the same dimension and then log transformed (see 4.2.6.1), the slope of the linear regressions correspond to scaling coefficients. Therefore, an isometric relationship would be represented by slope of one, a positive allometric scaling relationship would be represented by a slope of greater than one, and a negative allometric scaling relationship would be represented by a slope of less than one.

4.2.6.2 Mean GLI profiles

Multivariate methods were used to analyze mean cortical GLI profiles. Mean cortical profiles were analyzed for each specimen rather than averaged between members of the same species because including multiple specimens tends to blur profiles data (Schleicher A et al., 2000). Euclidean distances were calculated to summarize cytoarchitectural distances within and between species, per cortical areas. Euclidean distances were also used to compare distances within cortical areas to distances between cortical areas for the entire group of specimens. Principal components analysis (PCA) was used to explore the contribution of different GLI feature vectors to phylogenetic differences in profile shape. Finally, discriminant function analysis was used to determine whether GLI profile data could be used to assign a pattern to each cortical area, across the range of species.

4.3 Results

4.3.1 Cytoarchitecture of V1, V2, VP and V5

Using the cytoarchitectural criteria described above, it was possible to locate areas V1, V2, and V3 in each of the species studied (Figs 4.3 through 4.5). The cytoarchitecture of area V5 in humans and chimpanzees, as located in previous studies, is also shown (Fig. 4.6).

4.3.2 Relative laminar width patterns

The layer width values for each specimen are given in Table 4.6, and species mean relative cortical layer widths are shown for areas V1, V2, VP and V5 in Fig. 4.7. In general, cortical layer widths were found to be quite similar across species, in all the cortical areas. The variation that exists in layer width patterning does not seem to reflect taxonomic relationships. This is in agreement with a previous study (Zilles K and G Rehkämper, 1988) which did not identify much variation in V1 layer widths in a smaller hominoid sample.

Relative layer width patterns were able to predict several visual system variables, statistically significant at alpha .05 after correction for multiple comparisons (increased Type I error, i.e., $p<.0167$). Area V2 relative laminar width pattern was found to predict all four visual system variables: V1VOL (independent variable = V2 layer IIIA width) $F(1,6)=15.706$, $p<.0167$, Adjusted R squared .71; LGN (independent variable = V2 layer IIIA width), $F(1,6)=13.175$, $p<.0167$, Adjusted R squared .67; EYE (independent variable entered in model 1 = V2 layer III width) $F(1,5)=33.069$, $p=.005$, Adjusted R squared .865, (independent variable entered in model 2 = V2 layer V width) $F(2,5)=67.644$, $p=.003$, Adjusted R squared .964; OPTIC NERVE (independent variable = V2 layer IIIA width) $F(1,5)=23.167$, $p<.01$, Adjusted R squared .816. Area VP relative laminar width

pattern was found to have correlations with two visual system variables. LGN (independent variable = VP layer II width), $F(1,6)=25.480$, $p<.0167$, Adjusted R squared .803; and EYE (independent variable = VP layer II width), $F(1,5)=22.924$, $p<.01$, Adjusted R squared .814. Surprisingly, Area V1 relative laminar width pattern did not correlate with any visual system variables, even though V1 is earlier in geniculocalcarine pathways than are V2 and VP. No relative laminar width patterns were found to correlate with any brain or body size variables.

4.3.3 Grey level index

Species mean cortical GLI values (Fig. 4.8) and layerwise GLI values (Fig. 4.9 A, B and C) are shown for areas V1, V2, VP and V5. Mean and layerwise GLI values for individual specimens are given in Table 4.7.

For all visual areas studied, species mean GLI values generally decrease with increased phylogenetic proximity to *Homo*, with some notable exceptions. In V1, V2, VP and V5, humans have the lowest mean GLI value, which corresponds to the finding that humans have the lowest neuronal density in striate and extrastriate cortical areas among anthropoid primates (Sherwood CC, MA Raghanti *et al.*, 2007). In V1, *Macaca fascicularis* had the highest mean GLI values, although in V2 and VP, the mean GLI values are higher in *Hylobates lar*. *Pan troglodytes* GLI values diverge from the phylogenetic trend in that they are consistently high, in areas V1, V2, VP and V5, and in both individuals (Fig. 4.3). The high GLI values of *Pan troglodytes* contrast with the much lower values of *Pan paniscus*.

Correlation analysis was performed on mean V1, V2 and VP GLI values and several brain and body and visual structure size variables. Mean V1 GLI values were found to be negatively correlated with three visual system structures: OPTIC NERVE ($r = -1$, $p < 0.0001$), LGN ($r = -0.93$, $p = 0.0025$) and V1 VOL ($r = -0.96$, $p = 0.0004$), and with the volume of the brain structure NEOCORTEX($r = -0.94$, $p = 0.0048$). Mean V2 GLI values were negatively correlated with OPTIC NERVE ($r = -0.94$, $p = .0048$) and V1 VOL($r = -0.89$, $p = 0.0069$). Mean VP GLI values were also negatively correlated with OPTIC NERVE ($r = -0.94$, $p = 0.0048$) and V1 VOL ($r = -0.89$, $p = 0.0068$). No other correlations were found to be statistically significant.

These correlations were followed up by regression analyses to determine the slopes of the scaling relationships (Table 4.8 and Fig. 4.10). Reduced major axis (RMA) regressions were calculated because they assume equal error variance for *X* and *Y* axis variates. All scaling relationships were found to be negatively allometric (i.e., with a slope of less than one) that is, GLI decreases at a slower rate than changes in the size of the macrostructures. Thus for example, as V1 volume increases, V1 GLI decreases, but at a slower rate. Also, as the sizes of the neocortex, the LGN and the optic nerve increase, V1 GLI decreases, but does not keep pace with the changes in macrostructure size. As the size of V1 and optic nerve increase, V2 and V3 GLI decrease at a slower rate.

4.3.4 Normalized and adjusted layerwise GLI

Species mean normalized layerwise GLI patterns are shown for each area (Fig. 4.9B). These values demonstrate when the magnitude of the mean GLI per specimen is

taken into account, the relationship of layerwise GLI to the mean cortical GLI is fairly

constant across species.

In order to better visualize the relationship between normalized GLI and laminar

patter, adjusted layerwise GLI values are shown (Fig. 4.9C). In general, cortical layers

described as being dense or having very large cells correspond to positive values,

whereas layers which are cell poor and heavily myelinated have negative values

(compare with laminar descriptions in Tables 4.4 - 4.5). In V1 (Fig. 4.9C A), cell dense

layers II/III, IVA, IVCA, IVCB and VI have positive values in most species, and the

more sparse layers IVB and V have negative values in all species. In V2 (Fig. 4.9C B),

the cell dense granular layer IV had positive adjusted layerwise GLI values in all species,

as did IIIB, which is distinguished from upper layer 3 by the presence of large pyramidal

neurons. Layers II and IIIA also had positive adjusted layerwise GLI values in most

species. Layers V and VI had negative adjusted layerwise GLI values in all species.

Layer V is described as being sparser than layer VI. However, layer VI has lower GLI

values, apparently because the part near the border with the white matter is consistently

sparse. This is illustrated in the profile curves, in which layer 6 is represented by a

narrow peak and reduces to much lower GLI values near the border with the white

matter. The residual pattern of VP (Fig. 4.9C C) is similar to that of V2. Again, layer IV

has positive GLI values in all species; IIIB has positive values in all species except

Macaca fascicularis. Layer II has positive values in all species. Layer IIIA has positive

and negative values of low magnitude in all species. As in V2, layers V and VOI have

the adjusted layerwise GLI values of highest negative magnitude, although layer V

adjusted layerwise GLI values in *Macaca fascicularis* is of very low positive magnitude.

In V5 (Fig. 4.9C D), the direction of the adjusted layerwise GLI values is identical in the single human and single chimpanzee specimens, although the magnitudes vary. Layers II and IV are positive, and layers II V and VI are negative.

Normalized layerwise GLI patterns were able to predict several brain, body, and visual system variables, statistically significant at alpha .05 after correction for multiple comparisons (i.e., $p<.0167$). V1 layerwise GLI pattern predicted one visual system variable, V1 VOL (independent variable = V1 layer IVCα normalized GLI) $F(2,6)=20.852$, $p=.008$, Adjusted R Squared =.869. V1 normalized layerwise GLI pattern predicted EQ (independent variable = V1 layer IVCα normalized GLI), $F(1,6)=65.308$, $p<.001$, Adjusted R squared =.915.

VP normalized layerwise GLI pattern predicted all four visual system variables: V1 VOL (independent variable = VP layer V normalized GLI) $F(1,6)=14.961$, $p<.0167$, Adjusted R squared=.699; LGN VOL (independent variable = VP layer V normalized GLI) $F(1,6)=40.849$, $p<.01$, Adjusted R squared = .869; EYE (independent variable = VP layer V normalized GLI) $F(1,5)=79.669$, $p<.01$, Adjusted R squared = .94; OPTIC NERVE (independent variable = VP layer V normalized GLI) $F(1,5)=16.403$, $p<.0167$, Adjusted R squared = .755. VP normalized layerwise GLI pattern also predicted NEOCORTEX (independent variable = V1 layer IIIB normalized GLI) $F(1,5)=22.074$, $p<.009$, Adjusted R squared = .808. V2 normalized layerwise GLI pattern did not predict brain any body size variables, nor did it predict any visual system variables.

4.3.5 GLI profile analysis

Mean GLI profiles were calculated for each specimen to represent the laminar patterns of areas V1, V2, VP and V5 (Figs. 4.11-4.14). Species mean GLI profiles were not calculated since individual differences smooth the profile curves (Schleicher *et al.*, 2000). GLI profiles were characterized quantitatively by conversion into ten feature vectors based on the central moments of the mean GLI curve (Table 4.9). The features are the mean GLI (meany.o), the mean cortical depth (meanx.o), the standard deviation (sd.o), the skewness (skew.o), the kurtosis (kurt.o) and the same parameters for the first derivative of each mean profile (meany.d, meanx.d, sd.d, skew.d, kurt.d); for more details see Amunts et al, 2003. These data were then Z transformed to assign equal weights to each variable in the subsequent statistical analyses.

Multidimensional scaling was performed to compute distances from four multivariate datasets of the ten feature vectors as a data reduction technique. Identical procedures were followed for the following datasets: V1, V2, VP, and all areas. For each of the areas V1, V2, and VP, the mean Euclidean distances between species exceeded the distance within species (Fig. 4.15). The Euclidean distance model plot (Fig. 4.16) demonstrates how well groups can be differentiated based on Euclidean distance data. In some cases, clusters differentiate cortical areas; in other cases, they differentiate species. For example, an area V1 cluster is differentiated mainly on the basis of Dimension 1 (X axis). Also, human extrastriate areas form a cluster in the negative Dimension 1, negative Dimension 2 quadrant of the graph.

Because this indicates that in some cases interspecific (or inter-individual) differences eclipse differences in cortical pattern (Table 4.10 A), Euclidean distances between areas per specimen were averaged to determine the mean distances between

110

different cortical areas (Table 4.10 B). Area V1, which has the most distinct laminar pattern, had the greatest mean distances from the other three areas. Interestingly, Euclidean distances correspond to topographical distances along the visual processing hierarchy. V1 is closest to V2, next to VP, and farthest from V5. The smallest mean distance between areas was between the adjacent extrastriate areas V2 and VP. Also, V5 is closer to VP than to any other area.

A stepwise discriminant analysis was performed to determine whether assignment to cortical areas V1, V2, VP and V5 could be predicted on the basis of GLI profile data alone. All ten feature vectors were entered, but only three of these variables were included in the reduced model: skew.d, sd.d, and kurt.o. The classification (Table 4.11) resulted in 100% accurate predicted group membership to V1. The results for extrastriate areas were less accurate. Those assigned to V2 included 55.6% of V2, plus 11.1% of VP. Those predicted to be VP included 66.7% of VP, plus 22.2% of V2. Those predicted to be V5 included 100% of V5, 22.2% of V2, and 22.2% of VP. Although GLI feature vector data are not sufficient for assigning cortical areas across the range of taxa, it is interesting to note that cortical area classification into striate versus extrastriate cortex can be accomplished across taxonomic groups on the basis of only three features.

A principal components analysis was conducted to summarize the variance and to explore the contributions of the different feature vectors to differentiating cortical areas. The first three components had eigenvalues above 1, and combined explained 83.3% of the variance. The contributions of each of the feature vectors to the first three components are shown (Table 4.12). Although V1 values cluster on Factor 1, none of the first three factors was alone able to totally separate any of the cortical areas. For factor 1,

the greatest positive loading was meanx.d, followed by meany.o, meanx.o, sd.d, and sd.o.

The greatest negative loading was skew.d, followed by kurt.o, meany.d, skew.o, and

kurt.d. A plot of the strongest positive and negative loadings separates V1 from the

extrastriate areas, and most of the V2 and VP values fit into two separate clusters (Fig.

4.17).

4.4 Discussion

4.4.1 Correlations and scaling relationships

Overall, there is a pattern of striate and extrastriate cortex GLI values scaling to

visual system variables, particularly V1 volume and optic nerve cross sectional area, and

not significantly correlating with brain and body variables. The only statistically

significant correlation between any of the brain or body size variables and mean GLI is

the correlation of V1 GLI to neocortex size. In fact, because the neocortex is around 23-

55% all, or mostly, visual in function, it might be considered yet another visual system

variable of which V1 GLI is a function. In contrast, aside from neocortex, there were

seven instances of significant correlations between visual area GLI values and visual

system variables. Therefore, as discussed below, there may be a general pattern of

scaling between cytoarchitectonic and gross-level anatomical variables within the visual

system.

The finding that cortical GLI values do not significantly correlate with any brain

or body size variables is congruent with previous studies. In a similar study of motor

cortex area 4 in a sample of catarrhines, Sherwood *et al*. (2004) found that layerwise GLI values did not correlate with any brain or body size variable. Similarly, Sherwood and Hof (2007) did not find any correlations between area 10 and area 13 GLI and brain volume across a series of catarrhines.

Of particular interest is how the relationship between GLI values and other variables correspond to previous findings about the scaling of neuron density. Several studies have demonstrated that, across a range of mammalian species, there is a negative allometric relationship between brain size and neuron density in the neocortex, which follows a -1/3 power law (Haug H, 1987; Nissl F, 1898; Prothero J, 1997; Tower DB, 1954). Based on the idea that cortical areas maintain a similar amount of influence over one another regardless of brain size, a model has been proposed, based on two assumptions (Changizi MA, 2001). First, as the volume of grey matter increases, the number of cortical areas increases. Second, neocortical areas are connected to a certain percentage of the total number of neocortical areas, and for each area-to-area connections a certain percentage of the number of neurons which are interconnected is maintained.

It is important to note that although high neuronal density can result in high GLI values, GLI values are not direct indications of neuron number or density. GLI values indicate the volume fraction of cortical tissue occupied by stained cell bodies and can be taken as estimates of neuronal volume density, since glial and endothelial contribute only little to these values (Wree A *et al.*, 1982). Whereas neuronal density increases with neuron number, GLI can increase with neuron size and/or neuron number. Therefore, in relatively homogenous regions, like V2 layer IV, an increase in GLI values could indicate

113

increased cell density. However increased GLI values in V2 layer IIIb could be due to an increase in the size of giant pyramidal neurons.

For visual areas V1 and V2, neuron density has been found to scale with negative allometry against brain weight across higher taxonomic levels, however, this relationship does not apply to closely related species (Sherwood CC, MA Raghanti *et al.*, 2007). It is probable that the same pattern applies to GLI values: GLI values do differ significantly between cercopithecoids and hominoids in area 4 (Sherwood CC, RL Holloway, JM Erwin, A Schleicher *et al.*, 2004). In the current study, which included a taxonomically narrow sample, it was found that V1, V2 and VP mean GLI values did not correlate with any brain or body size variable. This, together with the GLI data discussed in Sherwood and Hof (2007), implies that within lower taxonomic groups, cell volume density is not constrained by brain or body size alone.

The sample here is taxonomically limited, and across higher taxonomic groups GLI is more likely to scale to brain size. For example, in the current dataset if only the macaque, a single great ape species, and humans were considered, one would observe a negative allometric relationship between GLI and brain size, and also between GLI and phylogenetic proximity to humans. However, interestingly, GLI values can be predicted by some visual system gross anatomical variables. This suggests that the total amount of input as well as details of interneuronal connections of a specific sensory modality, the visual system, may be the primary determinant of GLI values in visual areas. However, interestingly, the more fine tuned differences between hominoid species in visual area cell volume density seem to be better explained by gross level size differences specific to the visual system.

In the current study, several visual system cytoarchitectonic variables scale against gross-level visual system variables. The gross level visual system variables roughly indicate the amount of input to the visual cortical areas. Therefore, within this group of taxa, the total amount of visual input seems to influence different aspects of cytoarchitectural organization.

The clearest example of such a relationship is the negative allometric scaling relationship of GLI as a function of volume within the area V1. That is, within V1, an increase in GLI value corresponds to a decrease in volume fraction cell bodies, and, thus, an increase in volume fraction neuropil. Cortical areas V2 and VP (V3v) also show the pattern of having GLI values negatively scale against V1 volume. This could be due to the fact that V1 serves as the primary source of visual inputs to extrastriate areas, and/or because these early extrastriate areas are, like V1, dependent on visual structures for input. In the case of V2, it is possible that this is a direct extrapolation of the scenario for V1, since V2 is the primary recipient of V1 inputs (Kuypers HG et al., 1965; Lund JS and T Yoshioka, 1991; Van Essen DC et al., 1986). Note that although it has been argued that in macaques VP (in contrast to V3d) is not a target of V1 inputs (Felleman DJ et al., 1997; Felleman DJ and DC Van Essen, 1991), it has been pointed out that V2 projects symmetrically to V3d and VP (Gattass R et al., 1997), therefore VP is certainly indirectly impacted by V1.

Interestingly, among visual cortex GLI values, only V1 GLI scales significantly against the LGN volume. Perhaps this is because V1 is the first cortical recipient of most LGN projections in the geniculocalcarine pathway. However, although LGN is normally thought to serve as a "relay" for visual information that then goes to V1, in fact, V1 is not

in fact the sole cortical recipient of LGN inputs. A direct projection from LGN to V5 has been identified (Sincich LC *et al.*, 2004), and additional direct connections between the LGN and extrastriate areas could exist.

Given the model of Changizi (2001) for explaining neuronal density, what might explain the observation that visual cortex GLI values scale with negative allometry to visual system structures? It is only possible to speculate given the data given here, but a similar model, at the level of the visual system, might explain these negative allometric relationships.

There does seem to be a relationship between GLI pattern and neuronal density across higher taxonomic orders. The finding that *Macaca fascicularis* has a higher V1 GLI value is consistent with the high neuronal density of striate cortex in cercopithecoids compared to hominoids (Sherwood CC, RL Holloway, JM Erwin, A Schleicher *et al.*, 2004). In V2 and VP, *Hylobates lar* had slightly lower mean GLI values than *Macaca fascicularis*, which is surprising since cercopithecoids have also been found to have higher neuronal density than hominoids in extrastriate cortical area V2 (Sherwood CC, MA Raghanti *et al.*, 2007). However, only one cercopithecoid individual was examined here, and the degree of overlap seems quite reasonable.

It is interesting to note that the species which most clearly diverges from the trend of decrease in GLI coincident with increased distance with *Homo sapiens* is *Pan troglodytes*. *Pan troglodytes* has also been found to have a high V1 neuronal density for a great ape (Sherwood CC, MA Raghanti *et al.*, 2007). In contrast, *Pan paniscus*, the sister species of *Pan troglodytes*, has the lowest nonhuman GLI values for areas V1, V2 and VP, and is the only nonhuman to have GLI values within the human range. The

intrageneric differences reported here between *Pan troglodytes* and *Pan paniscus* are interesting in combination with the observation that the two panin species also differ in regards to V1 volume (see Chapter 5 for a discussion). Similarly, intrageneric variation in the layout of visual cortical areas has been indicated for closely related species of macaques, which show variable morphology of the prelunate gyrus, in which V4 is positioned (Van Der Gucht E et al., 2006).

4.4.2 Comparisons of cortical areas

Multivariate analyses demonstrated how GLI profile data can be used to compare cortical areas to each other in a multi-species sample. Area V1 was found to be most distinct cortical area in terms of its cortical profile, not surprising given its distinct laminar pattern. On the basis of just three feature vectors, it was possible to distinguish V1 from the extrastriate areas. Distinctions between extrastriate areas were found to be much more subtle. Visual area GLI profiles are more similar among members of the same species then among members of different species, as is the case with motor cortex (Sherwood CC, RL Holloway, JM Erwin, A Schleicher *et al.*, 2004). Finally, similarities between homologous extrastriate areas seem to be blurred by species-specific and inter-individual differences in cortical lamination. However, as demonstrated in Fig. 4.13D, some aspects of GLI profiles show potential for correctly sorting extrastriate areas into groups within the multi-specific sample.

Overall, the analyses show that in terms of cytoarchitecture, V1 is more phylogenetically invariant than are the extrastriate areas. Because species–level extrastriate cortex cytoarchitectural differences might be based in the subtle differences

of species-specific developmental trajectories, it is interesting to consider this observation in terms of the development of visual cortical areas. In enucleated fetal macaques, the region of cortex normally fated to become V1 develops cytoarchitectural characteristics of V2 (Dehay C et al., 1996; Rakic P et al., 1991). Because of this, it has been said that V2 cytoarchitecture is the default cytoarchitectural pattern of the occipital cortex (Dehay C *et al.*, 1996). The implications are twofold. First, there is a very specific relationship between V1 cytoarchitecture and specific retinogeniculo inputs. The relative standardization of V1 cytoarchitectural pattern in the range of species studied here indicates that this relationship is conserved across species. Second, because V2-like cytoarchitecture occurs by default, then the differences between V2 and VP cytoarchitecture, such as increased columnarity in VP, and a denser layer IV in V2, are probably due to differences in the development of interneuronal connections. Note that V1 has firm cytoarchitectonic criteria which apply to the full extent of the area and has clear borders with adjacent areas. Extrastriate area borders are so subtle that they were not defined in the present study, and although criteria are used to distinguish extrastriate areas from each other, their occurrence is not uniform even within an individual. Therefore, the variability observed here in extrastriate areas most likely reflects the complexity of neuronal networks which are involved in the development of their cytoarchitectural patterns.

4.5 Conclusions

The volume fraction of cell bodies, indicated by GLI, provides information about the uniformity of cortical neuronal organization across closely related species, but also provides information about organizational differences among species. In this study, it was found that the laminar pattern of V1 is distinct from that of extrastriate areas in hominoids, and also in a cercopithecoid species. However, the organization of extrastriate areas V2, VP and V5 are much less uniform, and in general interspecific and interindividual differences in laminar organization overshadow distinctions between these cortical areas.

In addition, it was found that although there is as of yet no evidence of cortical area GLI values scaling to brain or body size, visual area GLI values seem to be influenced by visual system organization and/or the total amount of visual input within this limited sample of hominoids plus one cercopithecoid. This has implications for the nature of brain organization. It is generally thought that neuronal numerical density is constrained by brain size, and this does seem to be the case for higher taxa. However, the results here suggest that brain size is not sufficient for predicting differences in cortical area microanatomical organization among closely related species. Rather, the implication is that species specific differences in aspects of histological organization, such as the density of neuronal connections, evolve as a part of functionally specific brain systems, and not as a function of overall brain size.

Table 4.1. Samples used in analyses of V1, V2, VP and V5

Species	code	archive number	sex	age (yrs)	body mass (kg)	brain mass (g)	EQ[e]	neocortex volume (cm³)	left V1 vol (mm³)	left LGN vol (mm³)	optic nerve cross sectional area (mm²)[f]	surface area (mm²)[f]
Gorilla gorilla	ggy	YN82-140	F	20	84.70	376.0	1.20	254.31	4043.62	150.06	17.60	1774
Hylobates lar	hld	Disco	F	22	6.80	120.0	2.54	77.05	2292.40	89.67	12.70	1299
Homo sapiens [a, b]	hs5	54491	F	79	62.53	1350.0	5.41	974.00	7586.59	185.63	22.80	1855
Homo sapiens [a, b]	hs6	6895	F	79	62.53	1110.0	4.45	974.00	7012.82	156.40	22.80	1855
Macaca fascicularis	mf2	ma22	M	3	2.90	57.6	2.31		1356.67	45.94	8.36	985
Pongo pygmaeus	ouy	YN 85-38	M	16.5	58.00	369.0	1.56	268.51	3504.17	92.08	16.10	1282
Pan paniscus [c]	ppz	Zahlia	F	11	33.20	324.0	2.09	278.97	5686.65	130.37		
Pan troglodytes	ptb	Bathsheba	F	24	80.00	359.5	1.20	262.77	4704.87	168.22	16.00	1446
Pan troglodytes [d]	ptd	1548	NA	NA	50.57	386.9	1.82	198.35	2799.11	85.89	16.00	1446

a. Used same sex species mean value for body weight (Zilles 1972)

b. Used combined sex mean human neocortex value (n=8) based on unpublished data provided by Carol MacLeod

c. Used same sex species mean value for body weight (Jungers and Susman 1984)

d. Used combined sex species mean values for brain and body weight (Herndon et al. 1999.)

e. Encephalization quotient (EQ) after Martin (1981) and Ruff et al. (1997)

f. Species mean data from Stephan and Frahm 1981

Table 4.2. Criteria for distinguishing cortical areas V2 and VP (V3v)[a]

V2	VP (V3v)
2 higher density	
deep 3 has particularly large pyramidals (size increases from upper to lower part of layer)	
3 is much more dense than 5	
3 denser	
3 thinner	
4 denser	
denser 4 has well defined border with sparser 5	
diff btwn cell packing density btwn 5 and 6 more obvious	
6 denser	
6 thinner	
border between 6 and white matter more pronounced	
	more columnar (esp layers 3,5)
	cortex thicker (esp. 3)

a. Sources: Economo 1929, Filimonoff 1932, Bailey et al. 1950, Zilles and Clarke 1997, Amunts et al. 2000, Rottschy et al. 2007

Table 4.3 Location of areas V2 and VP in each specimen relative to sulcal and gyral landmarks

Species	Indiv.	V2[a]	VP[b]
Macaca fascicularis	MF2	medial to collateral sulcus	occipitotemporal sulcus, and medial to occipitotemporal sulcus
Hylobates lar	HLD	collateral sulcus, and medial and lateral to collateral sulcus	lateral bank occipitotemporal sulcus, and lateral to occipitotemporal sulcus
Pongo pygmaeus	OUY	collateral sulcus	medial bank occipitotemporal sulcus and medial to occipitotemporal sulcus
Gorilla gorilla	GGY	medial bank collateral sulcus, and medial to collateral sulcus	medial bank occipital temporal sulcus through lateral bank collateral sulcus
Pan paniscus	PPZ	medial bank collateral sulcus, and medial to collateral sulcus	occiptotemporal sulcus, and medial and lateral to occipitotemporal sulcus
Pan troglodytes	PTB	medial bank collateral sulcus, and medial to collateral sulcus	between occipitotemporal sulcus and collateral sulcus, and lateral bank collateral sulcus
Pan troglodytes	PTD	medial bank collateral sulcus, and medial to collateral sulcus	between occipitotemporal sulcus and collateral sulcus, and lateral bank collateral sulcus
Homo sapiens	HS5	medial bank collateral sulcus	medial bank occipitotemporal sulcus
Homo sapiens	HS6	collateral sulcus, and lateral to collateral sulcus	medial bank occipitotemporal sulcus, and medial to occipitotemporal sulcus

Notes:
a. roughly in the region of the collateral sulcus, or medial to it
b. roughly in the region of the occipittemporal sulcus, or just medial to occipitotemporal sulcus

Table 4.4. Layers of the striate cortex

Layer	Description	Source[a]
I	narrow, sparse; neurons with sparse or smooth dendrites, somata near layer 2 border	L
II	upper border: abrupt decrease in neuron number.	L
	no pyramidal cell somata	L
III	merges gradually with 2: differs from 2 only in having fewer stellate neurons and having more projections of neurons from lower laminae	L
	deep 3 (3B) pyramidal cells set it apart from IVa	
IVa	lacks pyramidal cells of 3B	
	also set apart from 3 because denser, and packed with granule cells	
	narrow	L
	border with 3 often not distinct because deep layer 3 may appear only slightly less dense than layer 4A	PC
	more densely packed with small cells than 4B	PC
	lacks prominent Meynert-Cajal cells[b]	PC
	clear border with 4B.	PC
	especially indistinct - and perhaps absent - in humans	PC
IVb	less densely packed than 4A	PS
	solitary Meynert-Cajal cells (rarely form bands)	H
	has pyramidal bodies, which are lacking in 4C	L
IVCα	no pyramidals	L
	less cell dense than 4Cβ	PC
	loosely packed bubble-like granule cellls	
IVCβ	no pyramidals	L
	more cell dense than 4Cα	PC
	densely packed bubble-like granule cellls	
V	Meynert cells[c] at border of 5 and 6	H
VI	pyramidal neurons, neurons with smooth or beaded dendrites, stellate neurons.	L
	Meynert cells at border of 5 and 6	H
	Meynert cells mostly within 6	S

Notes:
a. Sources: Hof et al. 2000 (H); Lund 1973 (L), Peters and Sethares 1991 (PS), Preuss and Coleman 2003 (PC); Sherwood et al 2003 (S)
b. Meynert cells:
    - Morphology: triangular, frequently squat shape (more wide than tall), very large soma size, acentric nucleus
    Location: isolated, or in small groups of up to five neurons. Small clusters frequently observed in the calcarine cortex, whereas they tended to be more
    - isolated in the opercular region.
    - NOTE: there also exists a different type of larger pyramidal throughout layers V and VI, but it is taller than wide (Tigges et al. 1981)
    - Description: Meynert (1867); Ramon y Cajal (1899); Tigges et al. (1981).
c. Meynert-Cajal cells (aka "layer IVB cells", "outer Meynert cells", "Meynert-Cajal cells"):
    - Morphology: large, multipolar neurons
    Location: distributed in a band occupying most of layer IVB, occurred in large clusters up to several millimeters in length. Clusters more conspicuous in
    - the opercular part of area V1 (particularly the foveal representation) than in the calcarine cortex
    - Description: Meynert (1872); Valverde (1985); Peters and Sethares (1991)

Table 4.5. Layers of the extrastriate cortex

Layer	Description	Source[a]
I	almost cell free	V
	thin layer	E
II	upper border unusually sharp and regular	B
	dense	V
	small granule and triangular cells	E
	scatterd, small, mostly pyramidal	B
	lower limit marked by slight fall-off in cell density	V
III (A&B)	uniformly populated with medium cell bodies	V
	cells arranged in columns, pyramidal cells show gradual size decrease	B
IIIA	slightly less dense than II	B
IIIB	fewer neurons than layer 4	L
	pronounced clusters of large triangular pyamidals	V
	cells frequently collected in radiating short columns of IIIb middle sized cells, with bases in 3B pyramidals, and sprout into small cells of IIIa and II	E
IV	perhaps the densest layer of the entire cerebrum, looks like dark stripe	E
	darkly stained, round or oval, relatively large granule cells	E
	strikingly coarse columnarization	B
	occasionally larger cells	L
V	sparse: the lighest layer	V
	narrow	E
	medium and large cell bodies	V
	most cells even smaller than layer IV cells	E
	contains round to oval, small and medium perikarya	V
	also contains some scattered giant triangular cell bodies	V
	boundary btwn IV and V not uniform, as clusters of small cells "invade" layer V	V
VI	small to medium pyramidals	L
	VI distinguished from V by fusiform cell bodies	B
	cells mostly triangular, only a few fusiform	E
	clearly distinguished from V by higher cell density	V
	lower part: lighter, sparser, less structured, more fusiform cells	E
	VIb is very narrow, distinctly defined from white matter	E
	dense, narrow band	E

a. Sources: B: Bailey et al (1950; OB, chimpanzee); E: Economo (1929; OB, human); V: Valverde (1978; area 18, *Macaca*); L: Lund et al 1981 (*Macaca*)

Table 4.6. Relative layer widths for areas V1, V2, VP, and V5 (individual data)[a]

Species	code	V1								V2					
		II/III	IVA	IVB	IVCα	IVCβ	V	VI		II	IIIA	IIIB	IV	V	VI
Macaca fascicularis	mf2	28	8	12	9	8	13	22		14	17	11	17	18	23
Hylobaytes lar	hld	31	7	14	10	10	12	15		10	19	13	17	21	20
Pongo pygmaeus	ouy	32	8	14	10	9	11	17		11	21	19	17	15	17
Gorilla gorilla	ggy	31	8	15	10	11	12	13		10	24	16	18	16	16
Pan paniscus	ppz	32	8	14	10	10	11	14		11	25	11	16	17	20
Pan troglodytes	ptb	28	8	15	10	10	13	15		11	16	13	15	21	25
Pan troglodytes	ptd	31	8	15	10	9	11	16		11	25	14	15	16	20
Homo sapiens	hs5	30	7	15	10	10	10	18		12	22	13	15	19	19
Homo sapiens	hs6	31	8	15	10	9	10	17		10	26	11	15	19	17

Species	code	VP						V5				
		II	IIIA	IIIB	IV	V	VI	II	III	IV	V	VI
Macaca fascicularis	mf2	16	20	11	20	19	14					
Hylobaytes lar	hld	12	20	12	15	18	22					
Pongo pygmaeus	ouy	13	23	15	17	15	17					
Gorilla gorilla	ggy	10	22	12	18	18	20					
Pan paniscus	ppz	12	21	12	16	21	19					
Pan troglodytes	ptb	13	15	11	17	25	19					
Pan troglodytes	ptd	12	21	12	16	20	20	11	34	14	22	19
Homo sapiens	hs5	11	21	15	14	19	21					
Homo sapiens	hs6	11	26	13	12	21	17	15	42	12	16	16

Notes:

a. Layer width values are given as a percent (%) of the total width of the cortex spanning from the border of layers I and II to the border between layer VI and the white matter.

Table 4.7. Mean and layerwise GLI for areas V1, V2, VP, and V5 (individual data)

Species	Code	V1 mean	II/III	IVA	IVB	IVCα	IVCβ	V	VI	V2 mean	II	IIIA	IIIB	IV	V	VI
Macaca fascicularis	mf2	14.56	14.76	15.20	13.79	14.79	15.86	13.65	14.52	13.47	14.14	13.68	14.06	14.08	12.88	12.55
Hylobaytes lar	hld	14.15	14.37	14.12	13.16	14.18	14.63	13.56	14.67	13.64	14.04	13.73	14.08	14.18	13.27	13.00
Pongo pygmaeus	ouy	13.00	13.18	13.98	11.94	13.22	14.51	11.96	12.76	11.45	11.19	11.14	11.76	12.19	11.52	10.80
Gorilla gorilla	ggy	11.64	11.73	12.64	10.76	11.90	12.73	10.38	11.99	11.27	11.91	11.25	11.50	11.76	10.80	10.50
Pan paniscus	ppz	11.20	11.50	11.93	10.71	11.26	11.95	9.67	11.30	9.24	9.39	9.46	9.77	9.74	8.59	8.55
Pan troglodytes	ptb	13.34	13.51	14.47	13.03	13.78	14.25	11.98	13.02	11.55	12.22	12.02	11.97	12.36	11.41	10.44
Pan troglodytes	ptd	14.50	15.09	14.85	13.88	14.69	14.93	13.44	14.10	12.65	13.28	13.08	13.40	13.11	12.08	11.32
Homo sapiens	hs5	10.48	10.77	10.90	9.76	10.26	11.01	9.25	10.87	10.14	10.91	10.24	10.14	10.27	10.01	9.68
Homo sapiens	hs6	10.14	10.71	10.47	9.46	9.85	10.60	8.93	10.02	8.98	10.07	9.12	9.24	9.22	8.43	8.32

Species	Code	VP mean	II	IIIA	IIIB	IV	V	VI	V5 mean	II	III	IV	V	VI
Macaca fascicularis	mf2	12.88	13.25	12.65	12.64	13.25	12.91	12.39						
Hylobaytes lar	hld	13.33	13.78	13.25	13.93	13.96	13.25	12.42						
Pongo pygmaeus	ouy	11.05	11.27	10.78	11.44	11.75	10.86	10.34						
Gorilla gorilla	ggy	10.94	11.95	10.92	11.39	11.60	10.38	10.05						
Pan paniscus	ppz	9.22	10.00	9.32	9.65	9.65	8.83	8.43						
Pan troglodytes	ptb	11.20	11.78	11.34	11.46	11.92	11.02	10.13						
Pan troglodytes	ptd	12.90	13.87	12.96	13.53	13.58	12.51	11.78	12.46	13.73	12.41	12.69	12.28	11.95
Homo sapiens	hs5	9.69	10.32	9.37	9.78	10.14	9.22	9.72						
Homo sapiens	hs6	9.07	10.22	9.12	9.27	9.20	8.60	8.65	8.91	9.53	8.85	9.24	8.53	8.62

Table 4.8. RMA regressions of V1, V2, VP and V5 GLI values on brain and visual system variables.

Y	X	n	R2	p	Slope	Lower CI	Upper CI	Intercept	Lower CI	Upper CI
GLI_V1	NEOCORTEX	6	0.677	0.044	-0.4734	-0.9761	-0.2296	1.878	1.574	2.181
	V1_VOL	7	0.788	0.008	-0.237	-0.3937	-0.1427	2.348	1.902	2.794
	LGN	7	0.61	0.038	-0.9005	-1.7556	-0.4619	2.116	1.677	2.555
	OPTIC_NERVE	6	0.704	0.037	-0.7864	-1.5788	-0.3917	1.976	1.626	2.327
GLI_V2	V1_VOL	7	0.821	0.005	-0.2719	-0.4344	-0.1702	2.429	1.959	2.898
	OPTIC_NERVE	6	0.777	0.02	-0.7721	-1.4286	-0.4172	1.933	1.634	2.231
GLI_VP	V1_VOL	7	0.783	0.008	-0.2579	-0.4308	-0.1544	2.37	1.878	2.861
	OPTIC_NERVE	6	0.707	0.036	-0.7544	-1.5104	-0.3768	1.911	1.576	2.245

Notes:

Regression were calculated for variables found to be correlated to GLI. These were converted into the same dimension as the GLI data, and then the data were all log transformed.

Table 4.9. Feature vectors for areas V1, V2, V3 and V5 (individual data)

Feature vector	*Gorilla gorilla* GGY	*Hylobates lar* HLD	*Homo sapiens* HS5	*Homo sapiens* HS6	*Macaca fascicularis* MF2	*Pongo pygmaeus* OUY	*Pan paniscus* PPZ	*Pan troglodytes* PTB	*Pan troglodytes* PTD
V1									
meany.o	29.7039	36.0708	26.7499	25.8706	37.2028	33.2226	28.577	34.0683	36.9911
meanx.o	49.7049	49.9138	49.6526	48.7742	49.5406	49.6045	49.2455	49.3057	49.0572
sd.o	29.6188	29.9144	29.8313	29.8223	29.5481	29.4128	29.6683	29.3972	29.6952
skew.o	0.0148	-0.0038	0.0117	0.0397	0.0029	0.0138	0.0338	0.0354	0.0305
kurt.o	-1.1937	-1.2188	-1.2256	-1.221	-1.2041	-1.1966	-1.1977	-1.1822	-1.2063
meany.d	0.1303	0.1015	0.1445	0.1707	0.0871	0.117	0.1386	0.1021	0.0876
meanx.d	53.0599	51.8865	52.6639	52.3403	55.2223	53.0487	52.6076	53.9601	53.7096
sd.d	30.337	30.0915	30.4611	30.2731	30.3695	29.5896	30.6839	30.44	30.6729
skew.d	-0.1131	-0.0707	-0.1305	-0.1079	-0.2259	-0.1411	-0.0805	-0.155	-0.1286
kurt.d	-1.1496	-1.1584	-1.1783	-1.1931	-1.1453	-1.1008	-1.1979	-1.179	-1.1847
V2									
meany.o	28.7506	34.9613	25.8828	22.924	34.5297	29.2373	23.6696	29.457	32.3224
meanx.o	49.0759	49.2222	49.0279	48.3276	48.6868	49.9355	48.7977	48.2812	48.3741
sd.o	29.4411	29.4469	29.6424	29.6285	29.3265	29.1333	29.1814	29.2431	29.2095
skew.o	0.0232	0.0274	0.0262	0.0515	0.0509	-0.0166	0.0516	0.0671	0.0594
kurt.o	-1.1704	-1.1823	-1.1945	-1.183	-1.1722	-1.1627	-1.1595	-1.1581	-1.1608
meany.d	0.1311	0.1077	0.1862	0.2035	0.0974	0.144	0.182	0.137	0.1114
meanx.d	50.6822	50.8798	51.6159	50.6034	49.1307	51.1493	50.7136	50.5809	50.4499
sd.d	30.2231	30.2745	29.4036	29.5396	30.5286	29.831	30.1126	30.0257	30.3242
skew.d	-0.0381	-0.039	-0.0662	-0.0327	0.0293	-0.0494	-0.0419	-0.0317	-0.0529
kurt.d	-1.1754	-1.1724	-1.1126	-1.1368	-1.1606	-1.1313	-1.1614	-1.1638	-1.1691

Feature vector	Gorilla gorilla GGY	Hylobates lar HLD	Homo sapiens HS5	Homo sapiens HS6	Macaca fascicularis MF2	Pongo pygmaeus OUY	Pan paniscus PPZ	Pan troglodytes PTB	Pan troglodytes PTD
V3									
meany.o	28.0302	34.0692	24.6626	23.1112	32.8431	28.2326	23.4731	28.642	32.9548
meanx.o	48.6353	49.09	49.6588	48.6384	49.6643	49.5268	48.476	48.6432	48.591
sd.o	29.3999	29.2978	29.7072	29.7876	29.5315	29.2128	29.3784	29.2404	29.3461
skew.o	0.0443	0.0206	0.0018	0.0407	0.0005	-0.002	0.0522	0.0448	0.0435
kurt.o	-1.1625	-1.1698	-1.1882	-1.1924	-1.1973	-1.1633	-1.1659	-1.1616	-1.1666
meany.d	0.1444	0.1133	0.2001	0.2146	0.1159	0.1618	0.202	0.1555	0.1177
meanx.d	49.5554	50.1577	51.5259	50.2782	49.9612	50.6745	50.6916	50.4933	50.2992
sd.d	29.8099	30.2682	29.3099	29.0635	30.4821	29.5584	29.5727	29.8464	30.2618
skew.d	0.0021	0.0085	-0.058	0.0029	0.0187	-0.0352	-0.0276	-0.0245	-0.0366
kurt.d	-1.1407	-1.1629	-1.1196	-1.1039	-1.1801	-1.1133	-1.1439	-1.1573	-1.181
V5									
meany.o				22.8764					31.8838
meanx.o				49.2374					49.0592
sd.o				29.7365					29.7853
skew.o				0.0176					0.0205
kurt.o				-1.1894					-1.1965
meany.d				0.2348					0.137
meanx.d				51.4899					50.4836
sd.d				28.8672					29.8114
skew.d				-0.0577					-0.0214
kurt.d				-1.076					-1.1456

Table 4.10. Average euclidean distances between cortical areas V1, V2, VP, and V5 based on GLI profile feature vectors.

A. Average distances between cortical areas, only comparisons per specimen[a] — only within same specimen

AREA	V1	V2	VP	V5		mean	SD	no.	conf.	mean distance
V1	0.00					4.34	1.16	9	0.76	btwn V1 and V2
V2	4.34	0.00				4.60	0.62	9	0.41	btwn V1 and VP
VP	4.60	1.91	0.00			4.90	1.12	2	1.55	btwn V1 and V5
V5	4.90	3.92	2.84	0.00		1.91	0.72	9	0.47	btwn V2 and VP
						3.92	0.35	2	0.49	btwn V2 and V5
						2.84	0.61	2	0.84	btwn VP and V5

B. Average distance between cortical areas, comparisons including all specimens[b] — across all specimens

AREA	V1	V2	VP	V5		mean	SD	no.	conf.	mean distance
V1	3.44					4.93	1.09	81	0.24	btwn V1 and V2
V2	4.93	3.60				5.11	1.01	81	0.22	btwn V1 and VP
VP	5.11	3.49	3.67			5.04	1.48	18	0.68	btwn V1 and V5
V5	5.04	4.46	4.02	4.50		3.49	1.33	81	0.29	btwn V2 and VP
						4.46	1.54	18	0.71	btwn V2 and V5
						4.02	1.35	18	0.62	btwn VP and V5

Notes:
a. For example, V2-VP distance average includes distance between HS5-V2 and HS5-VP, PPY-V2 and PPY-VP...
b. For example, V2-VP distance average includes distance between HS5-V2 and HS5-VP, GGY-V2 and HLD-VP…

Table 4.11. Classification of GLI profiles to cortical areas by discriminant function analysis.

	Area	Predicted group membership				
		V1	V2	VP	V5	TOTAL
count	V1	9	0	0	0	9
	V2	0	5	2	2	9
	VP	0	1	6	2	9
	V5	0	0	0	2	2
percent (%)	V1	100.0%	0.0%	0.0%	0.0%	100.0%
	V2	0.0%	55.6%	22.2%	22.2%	100.0%
	VP	0.0%	11.1%	66.7%	22.2%	100.0%
	V5	0.0%	0.0%	0.0%	100.0%	100.0%

Table 4.12. Component matrix of principal component analysis (PCA) of GLI profiles[a]

	Component		
	1 (39.658%)	2 (29.146%)	3 (14.522%)
Zmeany.o	0.673	-0.528	0.297
Zmeanx.o	0.668	0.431	0.524
Zsd.o	0.377	0.602	-0.507
Zskew.o	-0.53	-0.503	-0.611
Zkurt.o	-0.686	-0.483	0.399
Zmeany.d	-0.679	0.654	-0.224
Zmeanx.d	0.787	0.29	-0.204
Zsd.d	0.612	-0.716	-0.156
Zskew.d	-0.747	-0.244	0.209
Zkurt.d	-0.398	0.718	0.374

Notes:

a. 3 components extracted using the principal component analysis extraction method.

Suppl. Table 4.1 Mean GLI correlations, based on species mean data.

			GLI V1 mean	GLI V2 mean	GLI V3 mean
Spearman's rho	BODY	Correlation Coefficient			
		Sig. (2-tailed)			
		N			
	BRAIN	Correlation Coefficient			
		Sig. (2-tailed)			
		N			
	EQ	Correlation Coefficient			
		Sig. (2-tailed)			
		N			
	NEOCORTEX	Correlation Coefficient	**-0.9429**	-0.8857	-0.8857
		Sig. (2-tailed)	**0.0048**	0.01885	0.01885
		N	**6**	6	6
	V1_VOL	Correlation Coefficient	**-0.9643**	**-0.8929**	**-0.8929**
		Sig. (2-tailed)	**0.00045**	**0.00681**	**0.00681**
		N	**7**	**7**	**7**
	LGN	Correlation Coefficient	**-0.9286**	-0.8214	-0.8214
		Sig. (2-tailed)	**0.00252**	0.02345	0.02345
		N	**7**	7	7
	EYE	Correlation Coefficient	-0.8286		
		Sig. (2-tailed)	0.04156		
		N	6		
	OPTIC_NERVE	Correlation Coefficient	**-1**	**-0.9429**	**-0.9429**
		Sig. (2-tailed)	**1E-06**	**0.0048**	**0.0048**
		N	**6**	**6**	**6**

All correlation values shown have p values p<.05. To correct for simulteous comparison of three corticle areas (Bonferonni), only those in bold (p<.0164) are considered significant at alpha .05

Suppl. Table 4.2 Normalized layerwise GLI pattern correlations, based on species mean data.

		V1 GLI pattern	V2 GLI pattern	VP GLI pattern
V1 VOL		**F(1,6)=12.339**		**F(1,6)=14.961**
	p	**0.008**		**0.012**
	adj r sq	**0.869**		**0.699**
LGN				**F(1,6)=40.849**
	p			**0.001**
	adj r sq			**0.869**
EYE		F(1,5)=8.930		**F(1,5)=79.669**
	p	0.04		**0.001**
	adj r sq	0.613		**0.94**
OPTIC NERVE		F(1,5)=8.759		**F(1,5)=16.403**
	p	0.042		**0.015**
	adj r sq	0.608		**0.755**
BODY				
	p			
	adj r sq			
BRAIN		F(1,6)=7.515		
	p	0.041		
	adj r sq	0.521		
EQ		**F(1,6)=65.308**	F(1,6)=11.376	F(1,6)=9.068
	p	**0**	0.02	0.03
	adj r sq	**0.915**	0.634	0.573
NEOCORTEX				**F(1,5)=22.074**
	p			**0.009**
	adj r sq			**0.808**

All correlation values shown have p values p<.05. To correct for simulteous comparison of three corticle areas (Bonferonni), only those in bold (p<.0164) are considered significant at alpha .05

Suppl. Table 4.3 Relative layer width pattern correlations, based on species mean data.

		V1 layer width pattern	V2 layer width pattern	V3 layer width pattern
V1 VOL			**F(1,6)=15.706**	
	p		**0.011**	
	adj r sq		**0.71**	
LGN		F(1,6)=8.663	**F(1,6)=13.175**	**F(1,6)=25.480**
	p	0.032	**0.015**	**0.004**
	adj r sq	0.561	**0.67**	**0.803**
EYE			**F(2,5)=67.644**	**F(1,5)=22.924**
	p		**0.003**	**0.009**
	adj r sq		**0.964**	**0.814**
OPTIC NERVE			**F(1,5)=23.167**	F(1,5)=10.515
	p		**0.009**	0.032
	adj r sq		**0.816**	0.656
BODY				
	p			
	adj r sq			
BRAIN		F(1,6)=7.164		
	p	0.044		
	adj r sq	0.507		
EQ				
	p			
	adj r sq			
NEOCORTEX				
	p			
	adj r sq			

All correlation values shown have p values $p<.05$. To correct for simulteous comparison of three corticle areas (Bonferonni), only those in bold ($p<.0164$) are considered significant at alpha .05
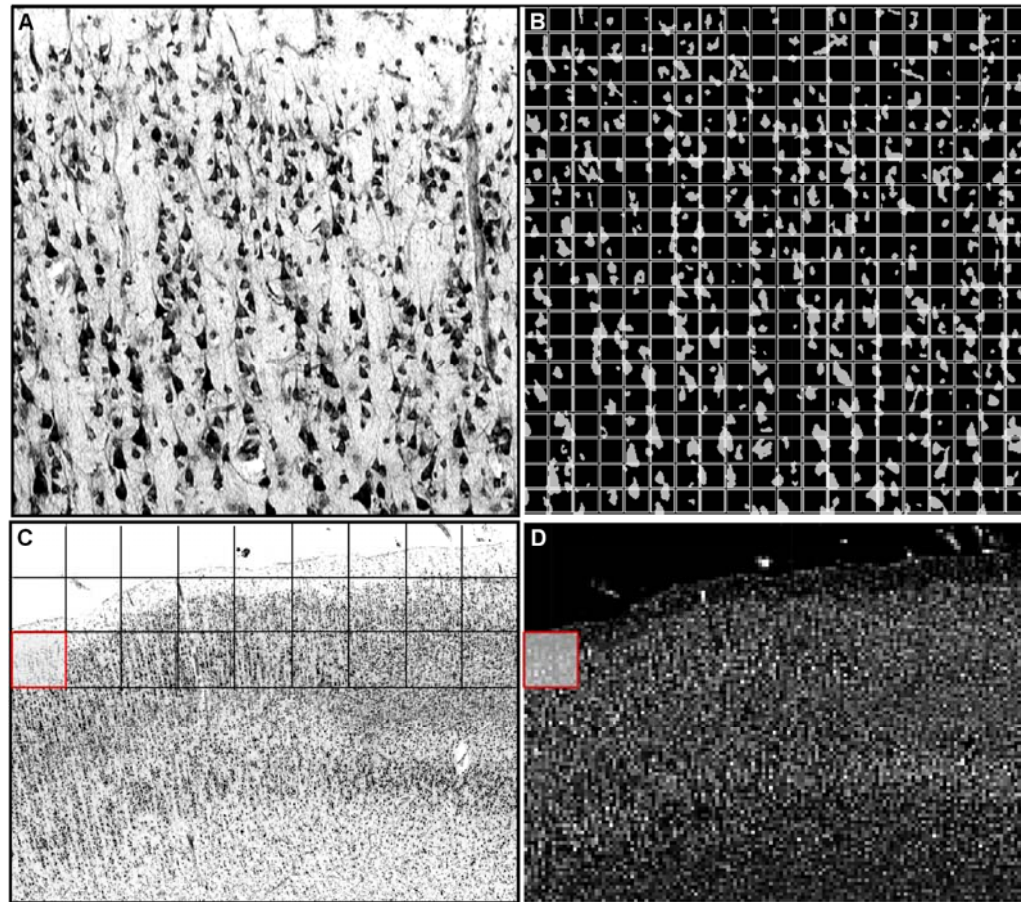
Fig. 4.1. Procedure for converting high-resolution histological images into GLI data.
Each histological image (A) was converted to binary by adaptive thresholding, and was further subdivided into a grid of measuring field (B). A GLI value was obtained for each measuring field. This step is repeated for each of the tiles in the ROI (A), which are combined as a mosaic in GLI images (D).
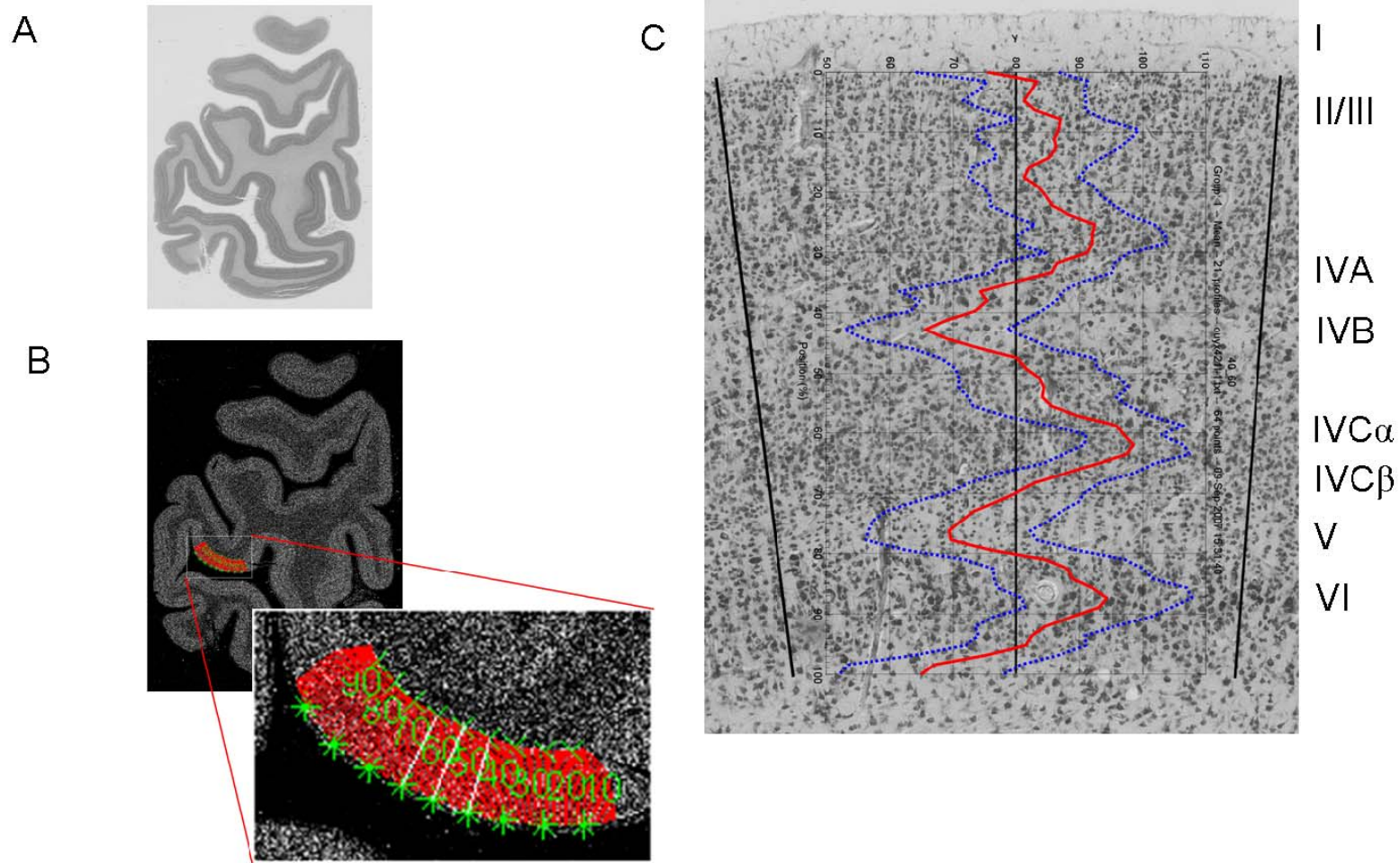
Fig. 4.2. Procedure for obtaining GLI profiles and layerwise GLI values.
On each GLI image (B), the borders between layer 1 and layer 2, and layer 6 and the white matter -- as indicated by images of histological sections (A) -- were traced for each ROI. GLI profile graphs were extracted and superimposed over histological images to determine layer divisions (C).

V1

I
II
III
IVa
IVb
IVCα
IVCβ
V
VI

Macaca fascicularis
Hylobates lar
Pongo pygmaeus
Gorilla gorilla
Pan paniscus
Pan troglodytes
Homo sapiens

200 µm
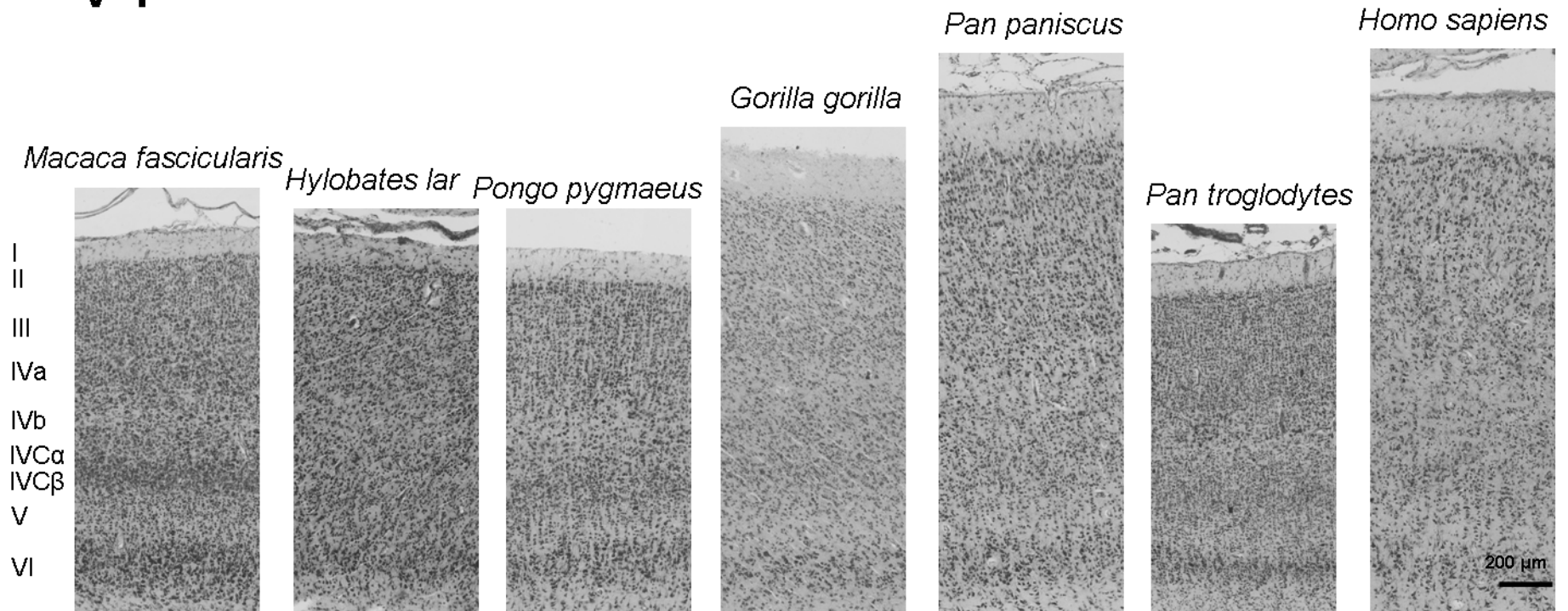
Fig. 4.3. Cytoarchitecture of cortical area V1 in macaques, gibbons, orangutans, gorillas, bonobos, chimpanzees, and humans.

V2

Pan paniscus

Homo sapiens

Hylobates lar

Gorilla gorilla

Pongo pygmaeus

Pan troglodytes

Macaca fascicularis

I
II
IIIA
IIIB
IV
V
VI
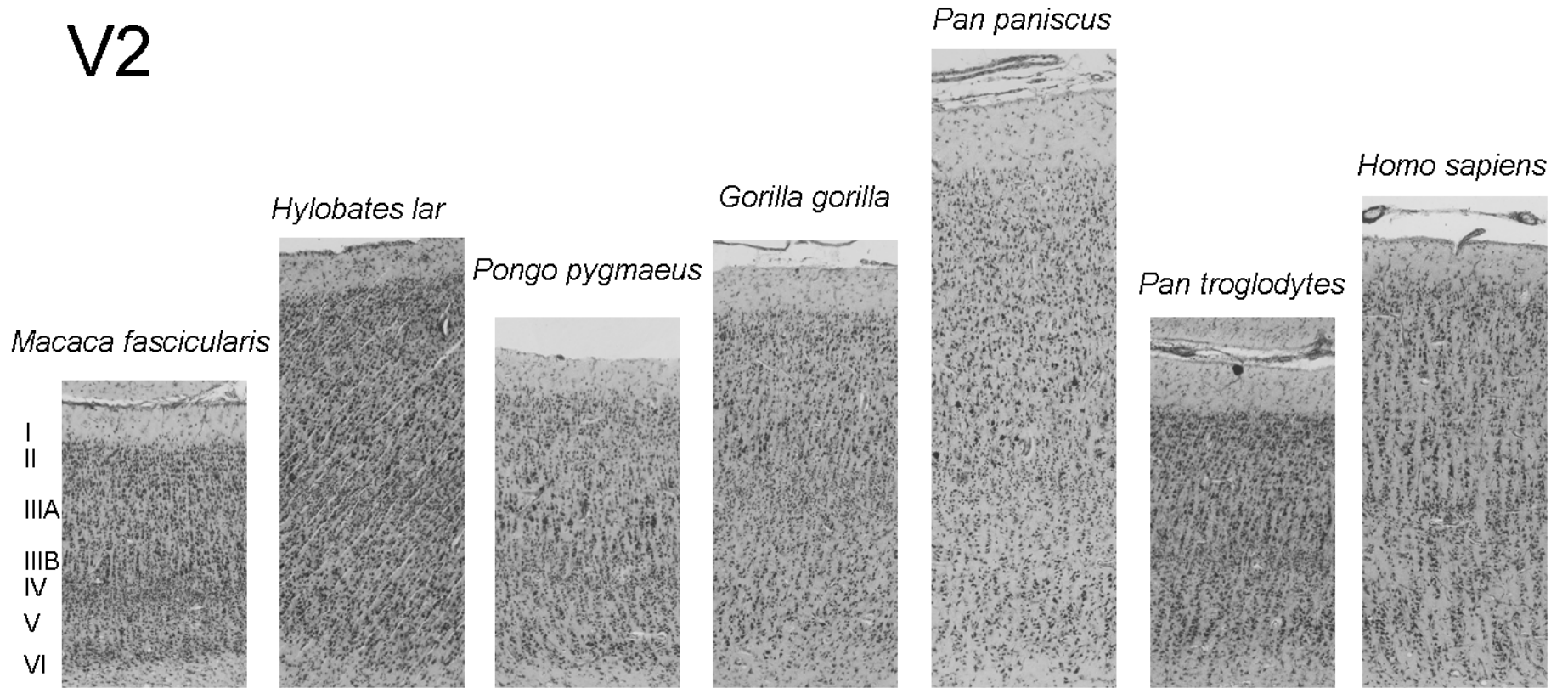
Fig. 4.4. Cytoarchitecture of cortical area V2 in macaques, gibbons, orangutans, gorillas, bonobos, chimpanzees, and humans.

VP
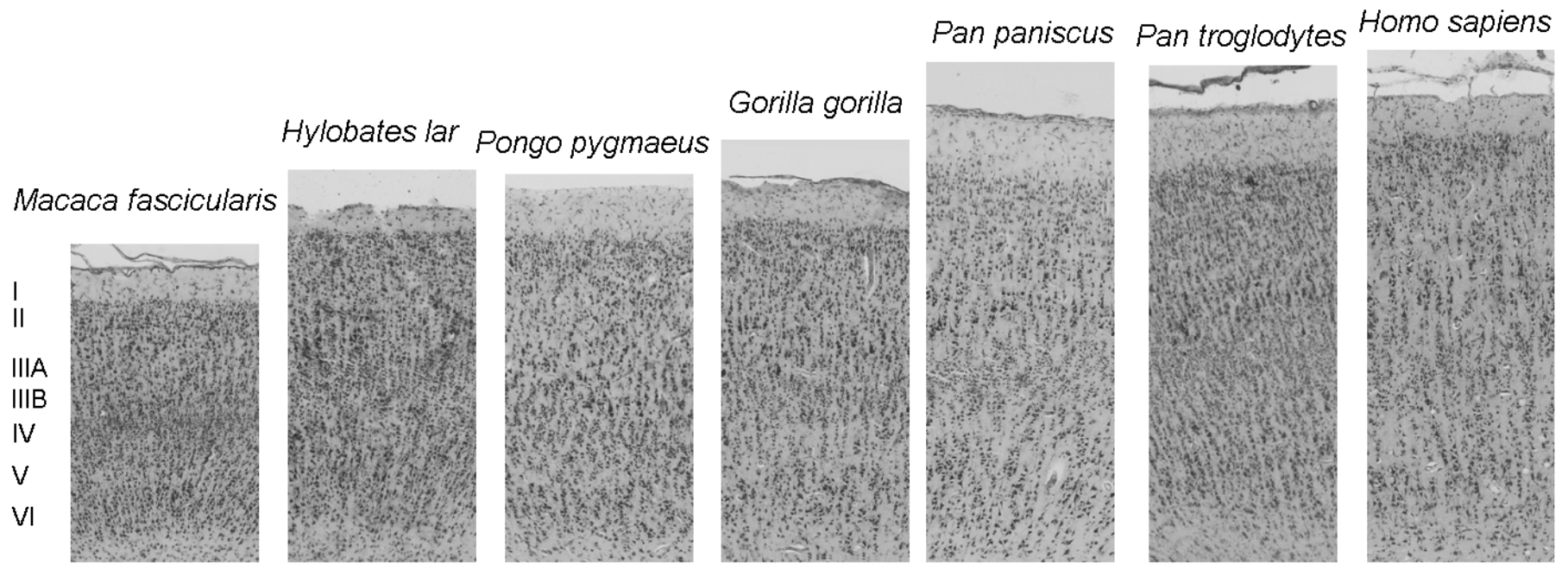
Fig. 4.5. Cytoarchitecture of cortical area VP in macaques, gibbons, orangutans, gorillas, bonobos, chimpanzees, and humans.

V5

Pan troglodytes

Homo sapiens

I
II
III
IV
V
VI
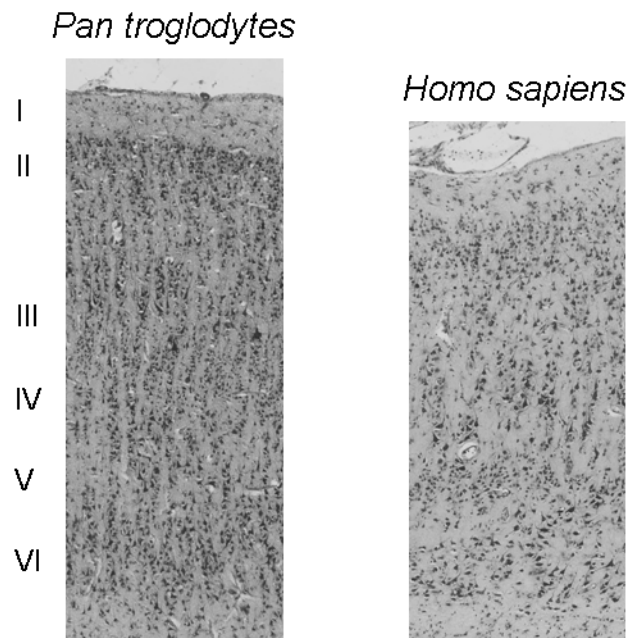
Fig. 4.6. Cytoarchitecture of cortical area V5 in chimpanzees and humans.
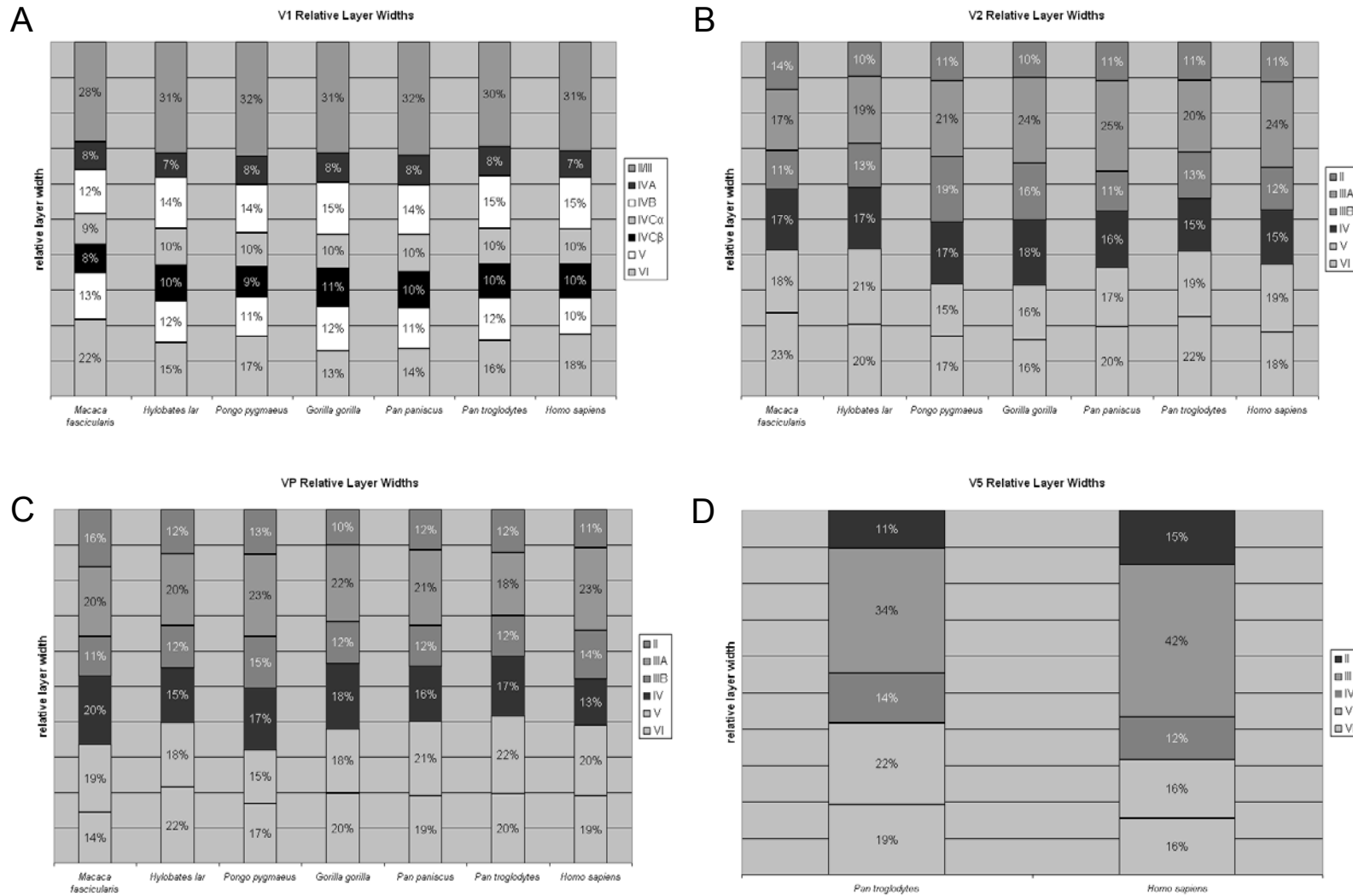
Fig. 4.7. Species mean relative layer widths for areas V1 (A), V2 (B), VP (C), and V5 (D).
Each bar represents the proportion of the total cortical thickness occupied by each layer.
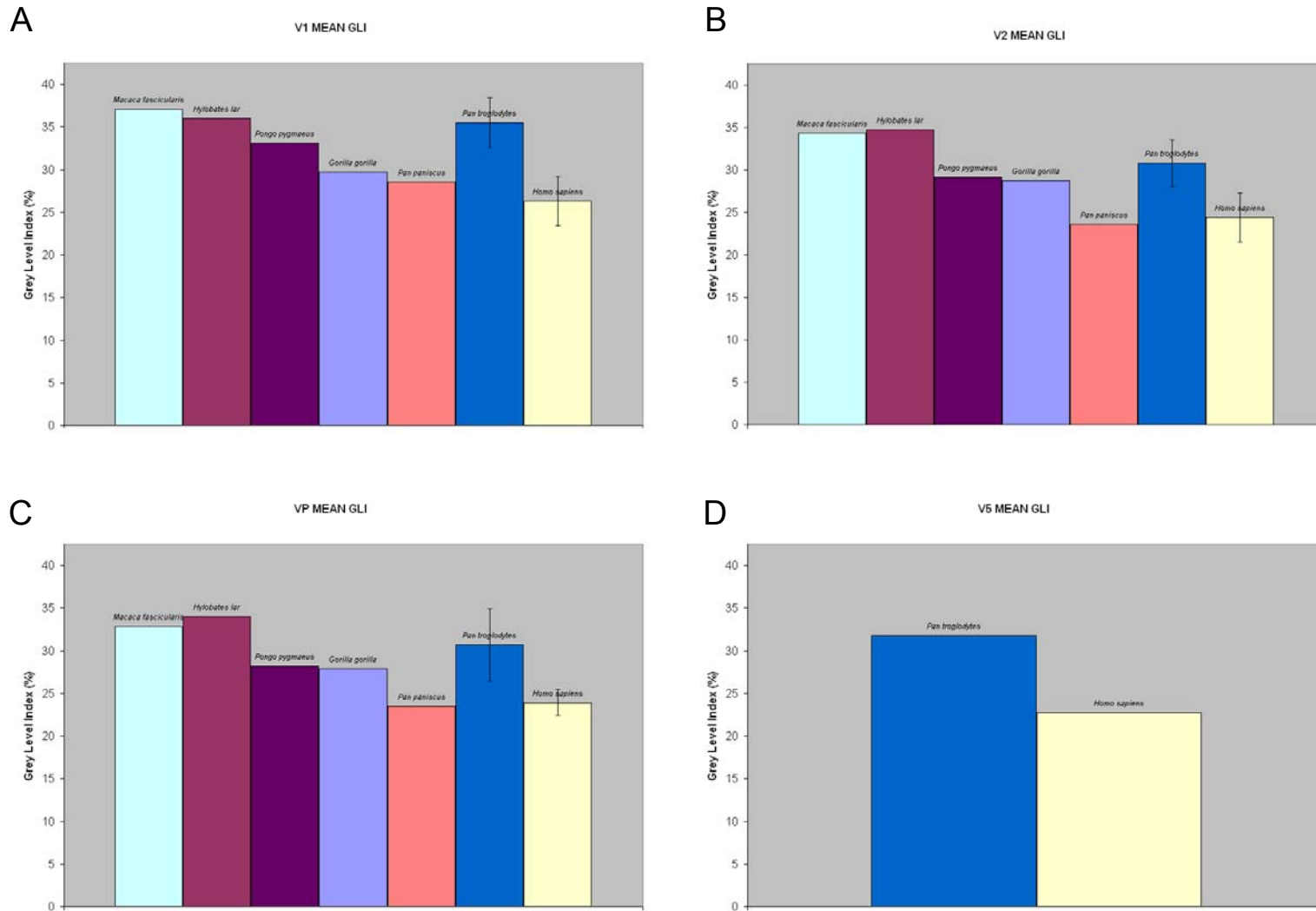
Fig. 4.8. Species mean GLI values for areas V1 (A), V2 (B), VP (C), and V5 (D).
Vertical bars denote 95% confidence intervals.

143
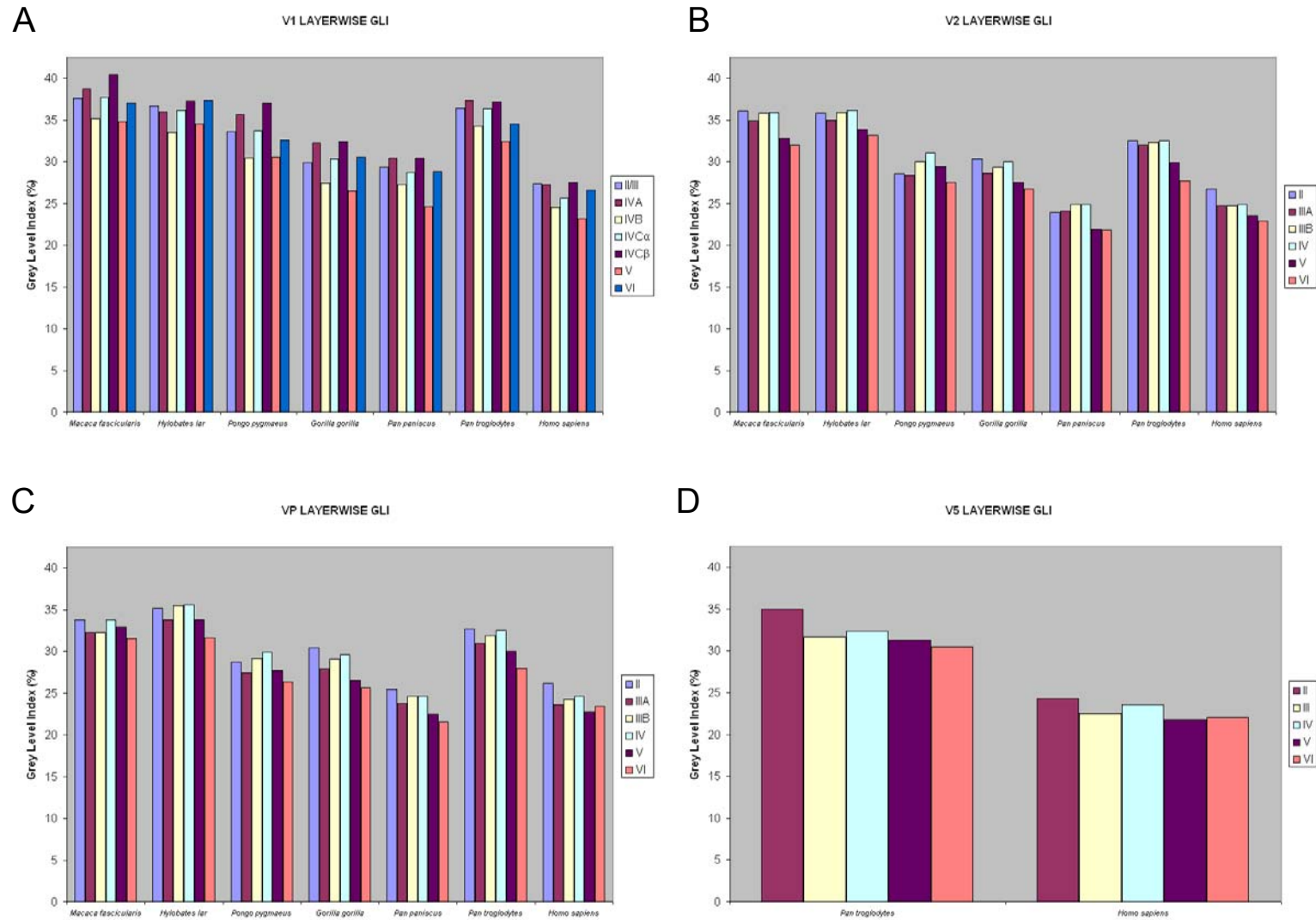
Fig. 4.9A. Species mean layerwise GLI values for areas V1 (A), V2 (B), VP (C), and V5 (D)
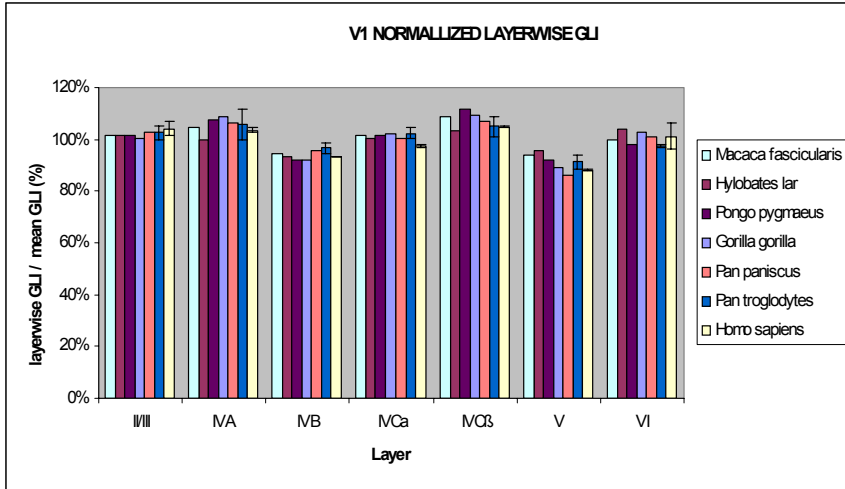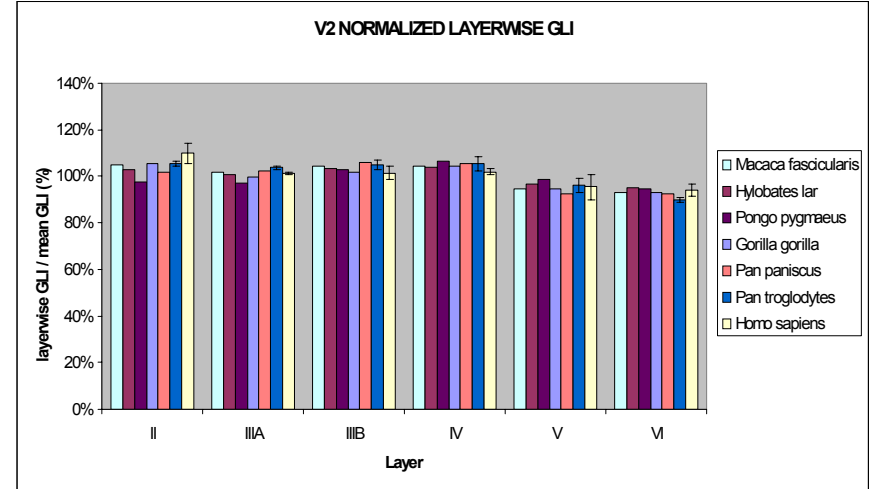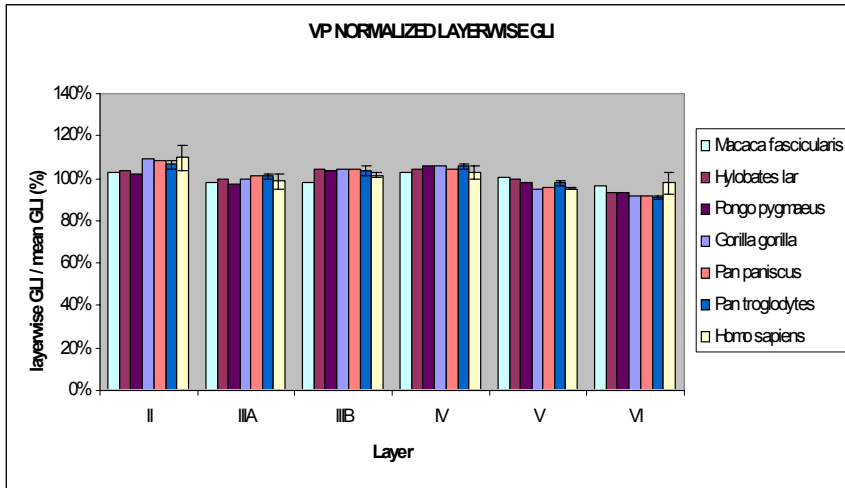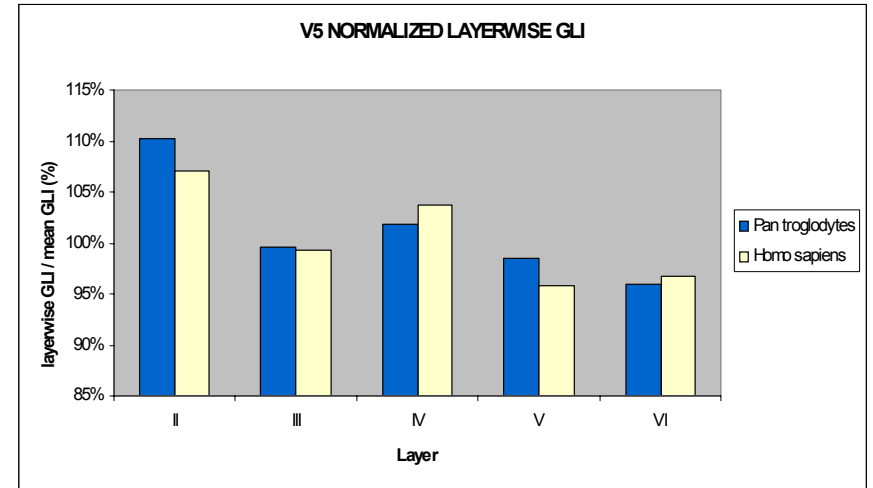
Fig. 4.9B Species mean normalized layerwise GLI values for areas V1 (A), V2 (B), VP (C), and V5 (D)
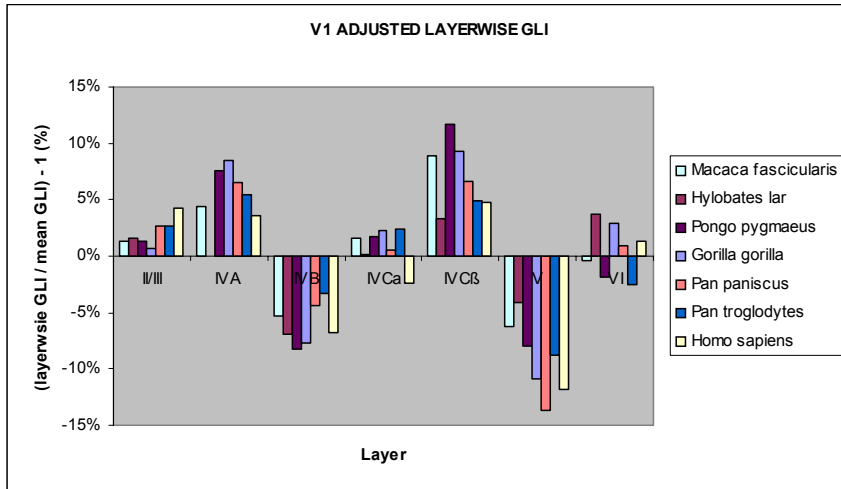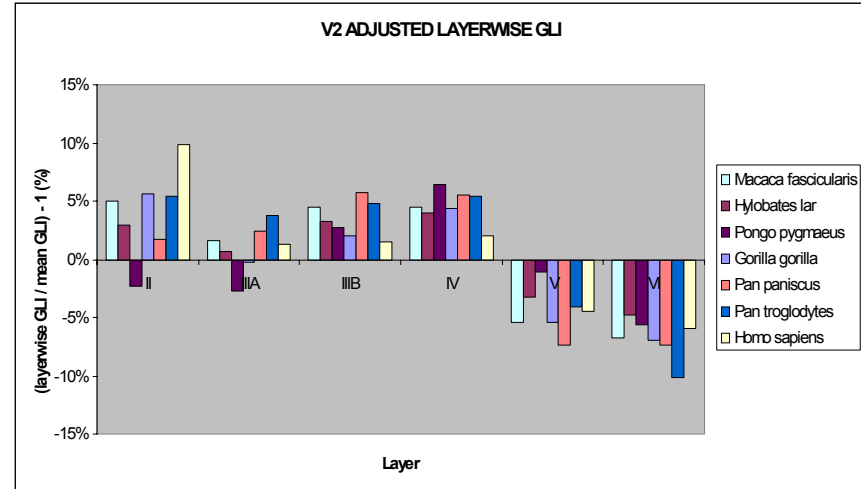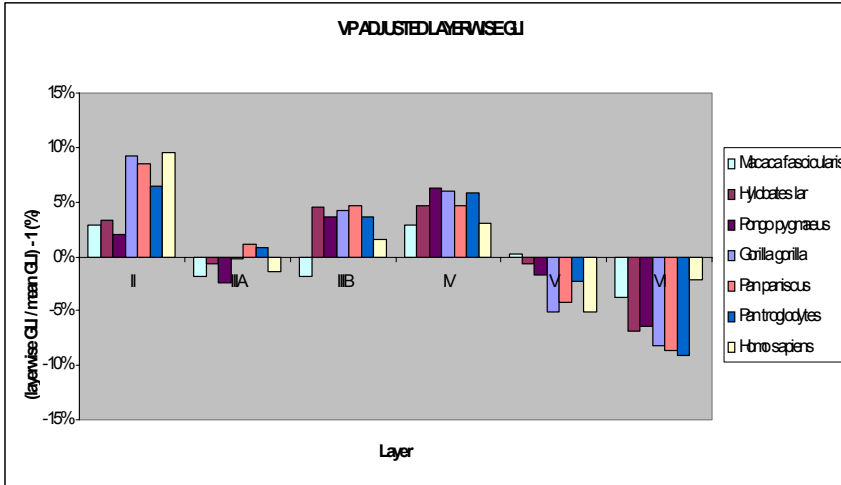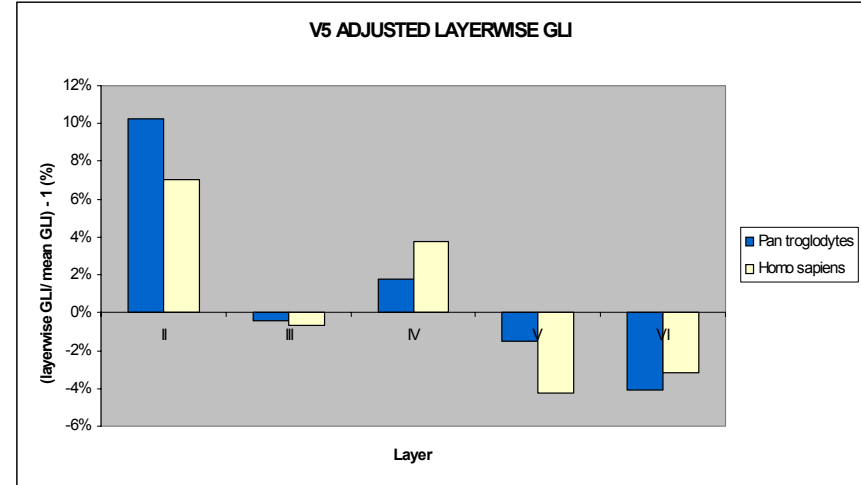
Fig. 4.9C Species mean adjusted layerwise GLI values for areas V1 (A), V2 (B), VP (C), and V5 (D)

146
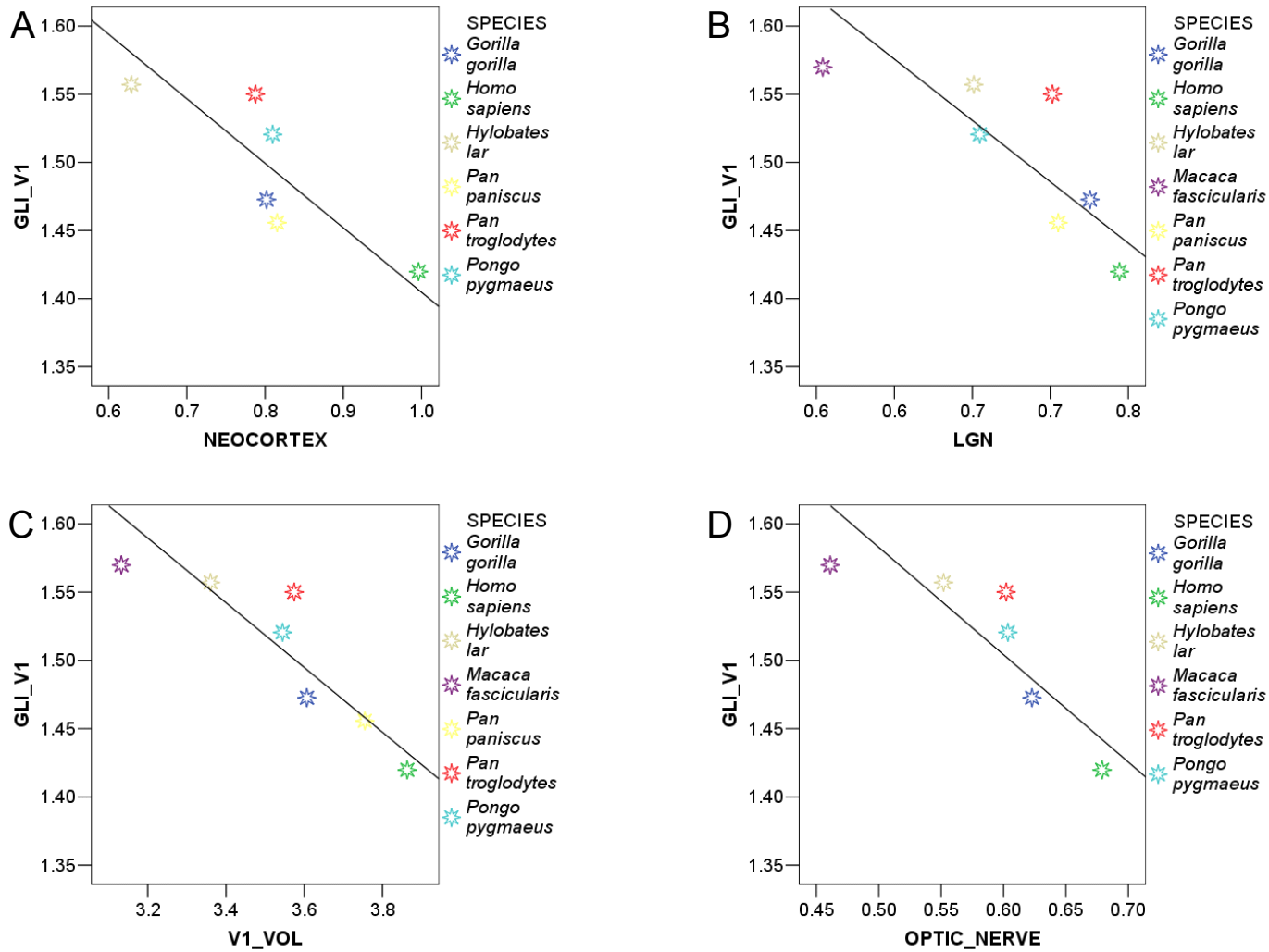
Fig. 4.10 RMA regressions of species mean GLI values on brain and body size variables.
V1 GLI as a function of neocortex volume r² = 0.677, p = 0.044 *y* = -0.4734*x* +1.878 (**A**), LGN volume r² = 0.61, p = 0.038, *y* = -0.9005*x* +2.116 (**B**), V1 volume r² = 0.788, p = 0.008, *y* = -0.237*x* +2.348 (**C**), and optic nerve volume r² = 0.704, p = 0.037, *y* = -0.7864*x* +1.976 (**D**);
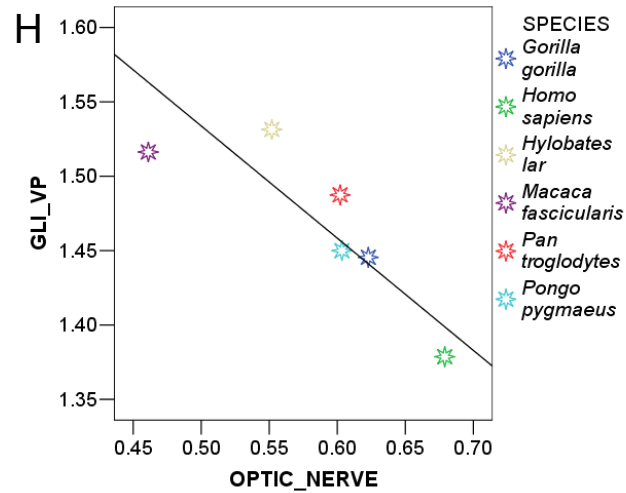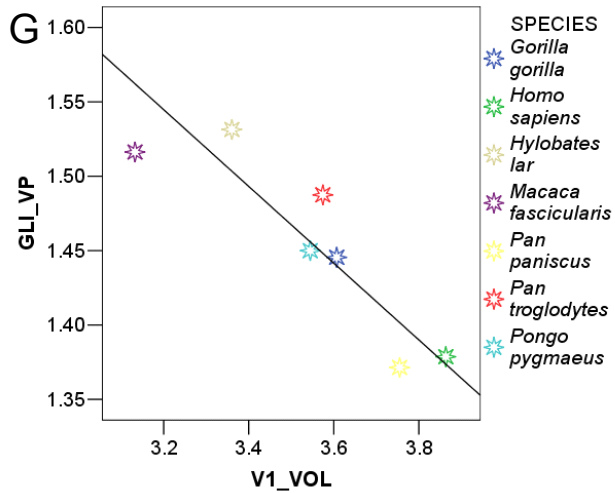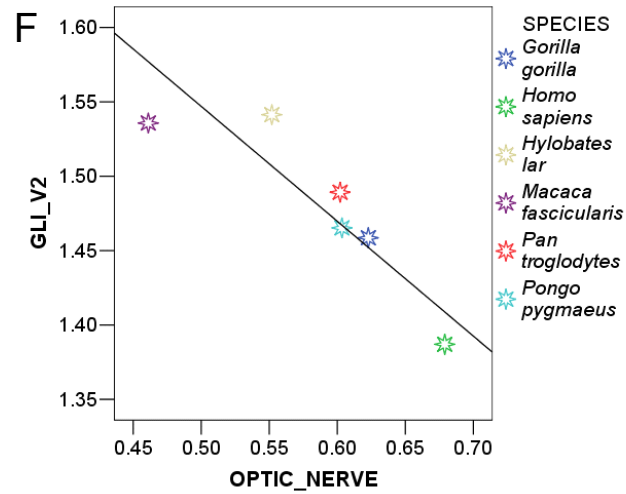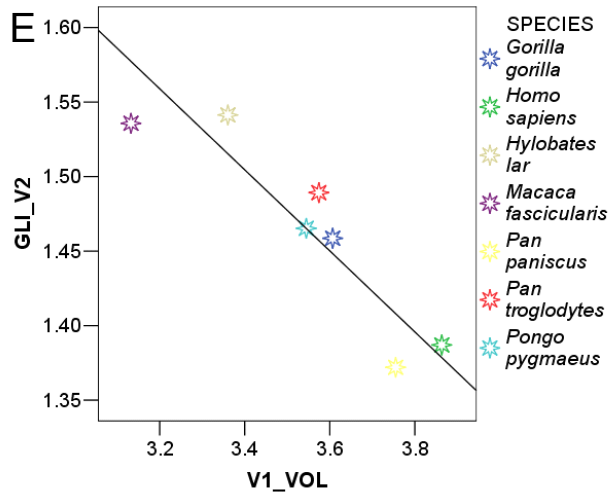
V2 GLI values as a function of V1 volume r^2 = 0.821, p = 0.005, y = -0.2719x +2.429 (**E**); and optic nerve volume r^2 = 0.777, p = 0.02, y = -0.7721x +1.933 (**F**); and VP GLI values as a function of V1 volume r^2 = 0.783, p = 0.008, y = -0.2579x +2.37 (**G**); and optic nerve volume r^2 = 0.707, p = 0.036, y = -0.7544x +1.911 (**H**)

Gorilla gorilla (GGY)
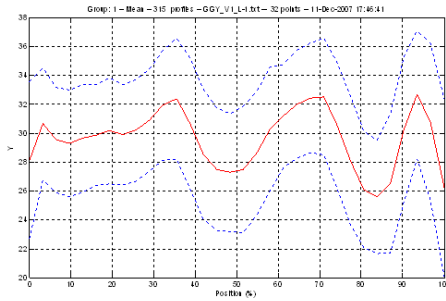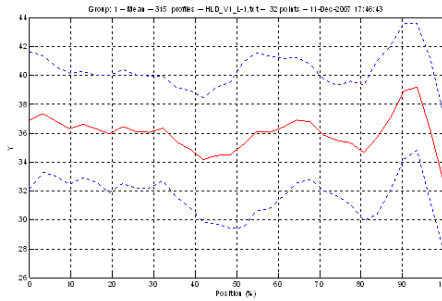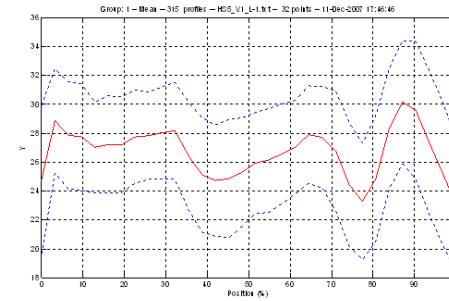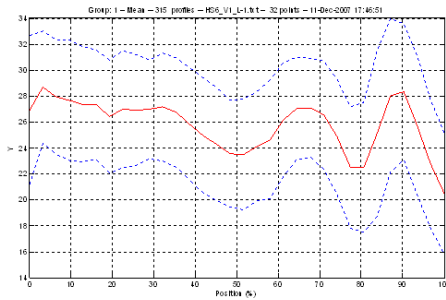
Hylobates lar (HLD)

Homo sapiens (HS5)

Homo sapiens (HS6)

## *Macaca fascicularis* (MF2)
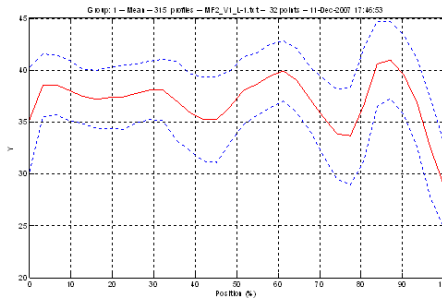
Pongo pygmaeus (OUY)
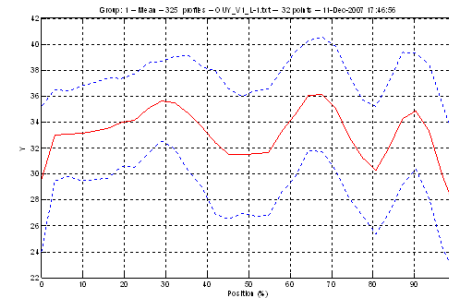
Pan paniscus (PPZ)
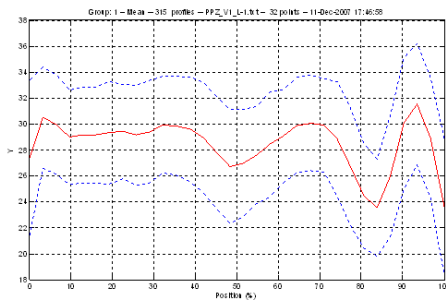
Pan troglodytes (PTB)
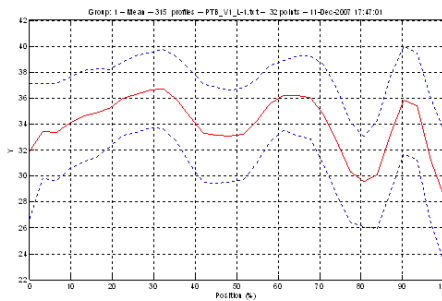
Pan troglodytes (PTD)
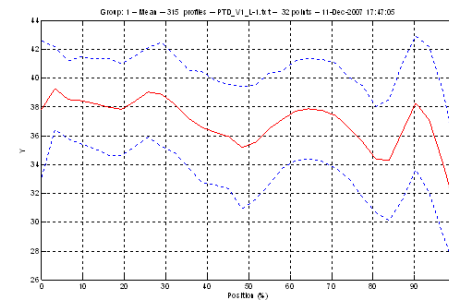
Fig. 4.11. Mean V1 GLI profiles of individual specimens (solid lines) with standard deviation indicated (dotted lines)

149
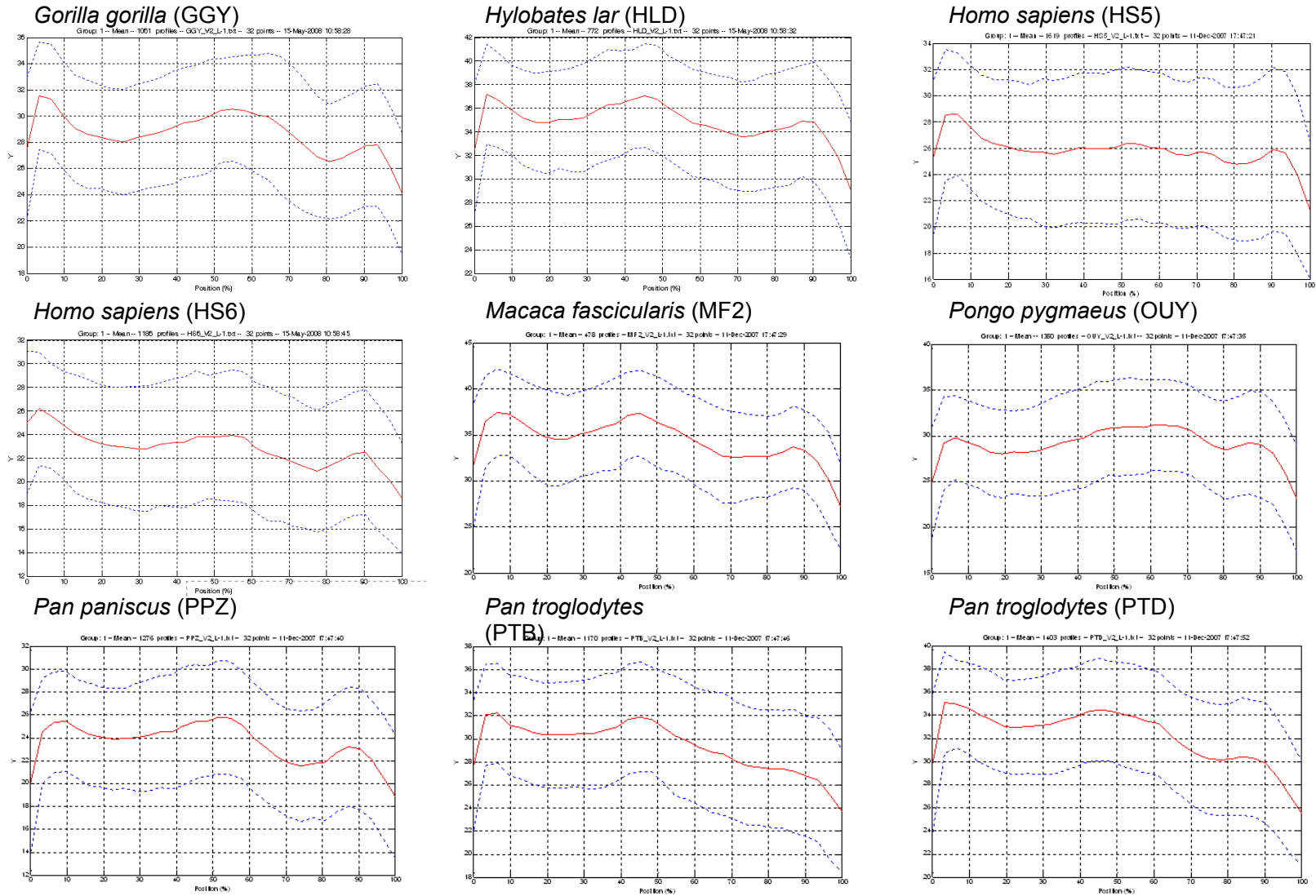
Fig. 4.12. Mean V2 GLI profiles for each individual specimen (solid lines) with standard deviation indicated (dotted lines)
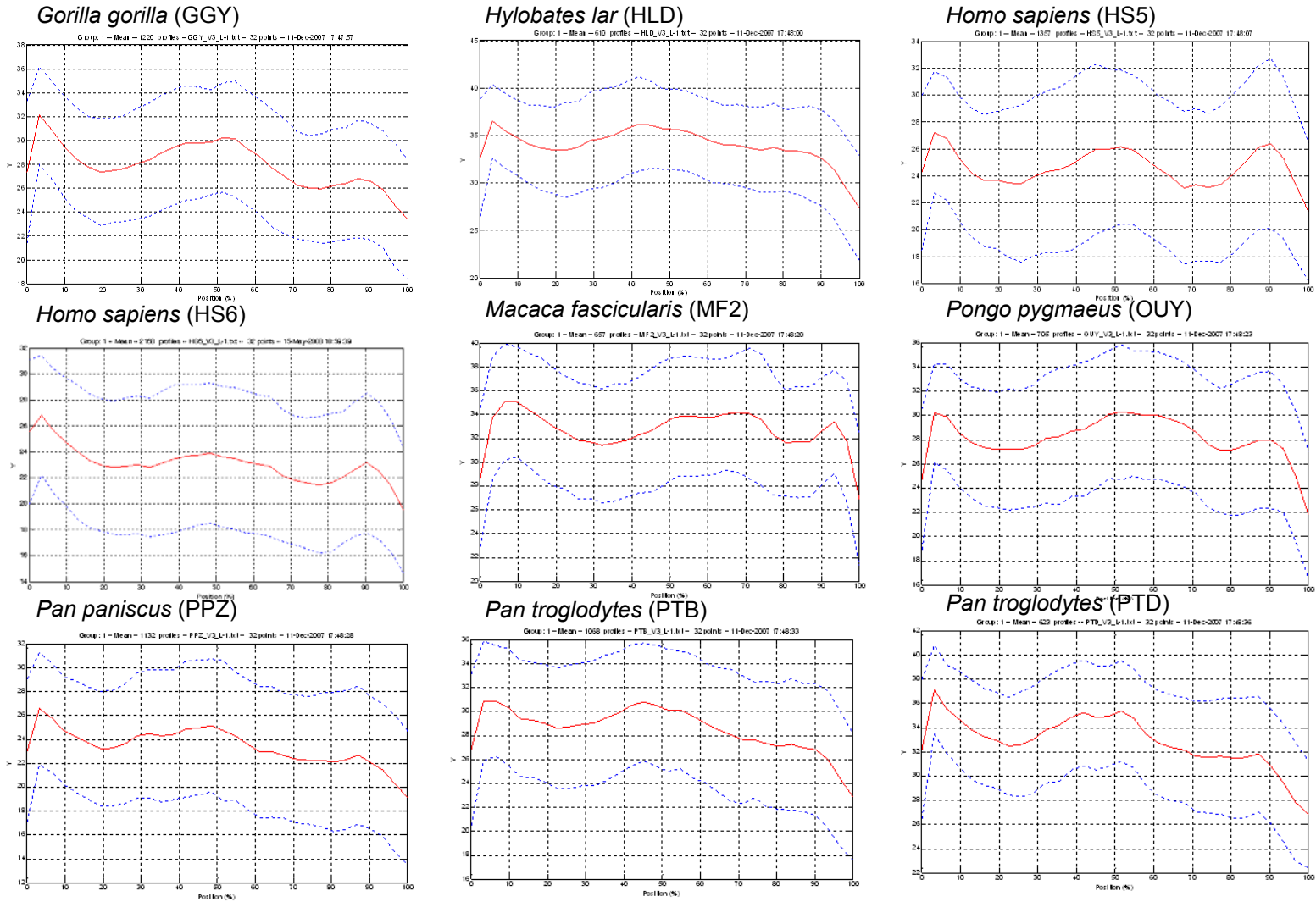
Fig. 4.13 Mean VP GLI profiles of individual specimens (solid lines) with standard deviation indicated (dotted lines)

151
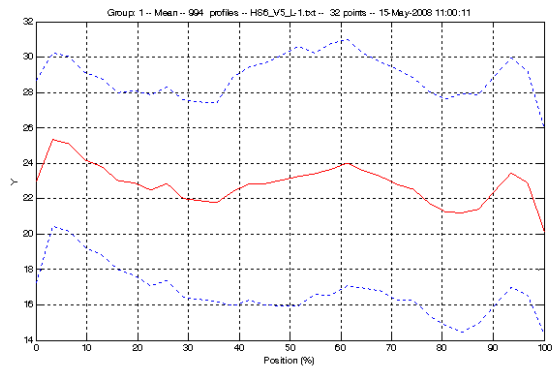
*Homo sapiens* (HS6)   *Pan troglodytes* (PTD)
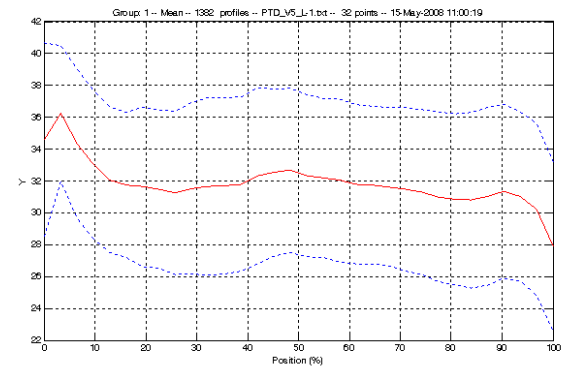
Fig. 4.14 Mean V5 GLI profiles of individual specimens (solid lines) with standard deviation indicated (dotted lines)
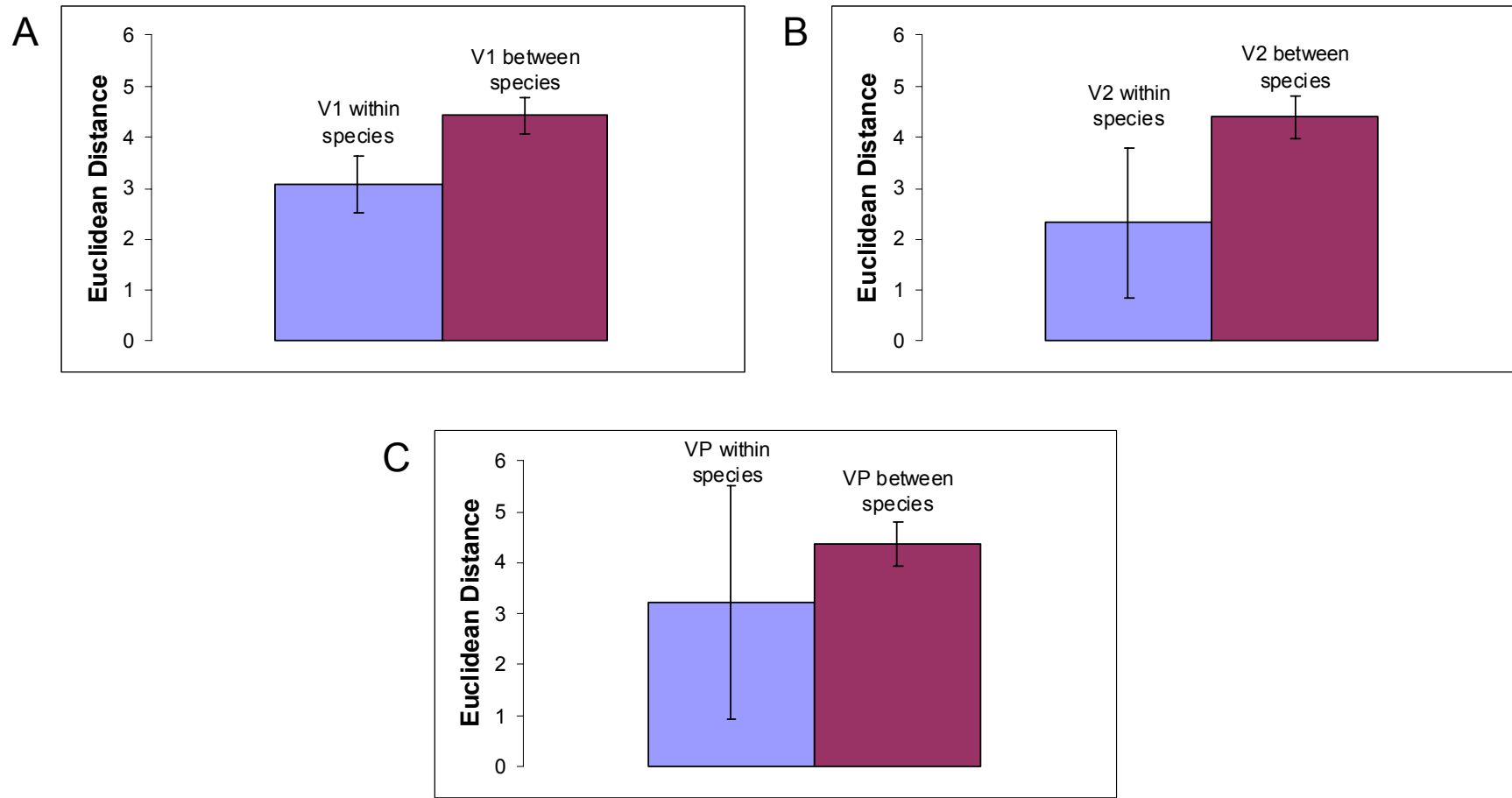
Fig. 4.15 Plot of Euclidean distances of GLI profile feature vectors among and within species (mean and 95% CI) for V1 (A), V2 (B), and VP (C)
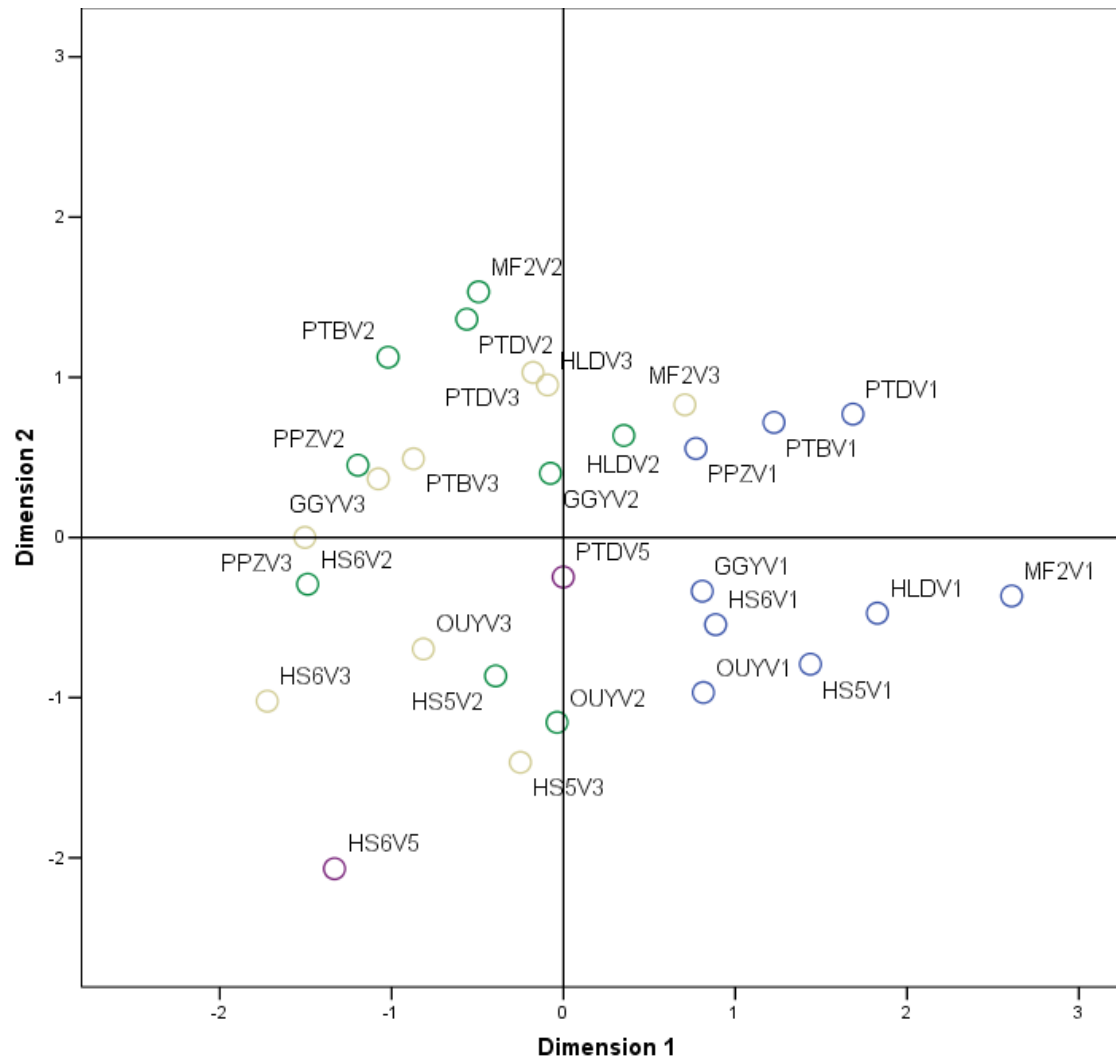
Fig. 4.16 Euclidean distance plot of individual specimen GLI profiles based on a multidimensional scaling procedure
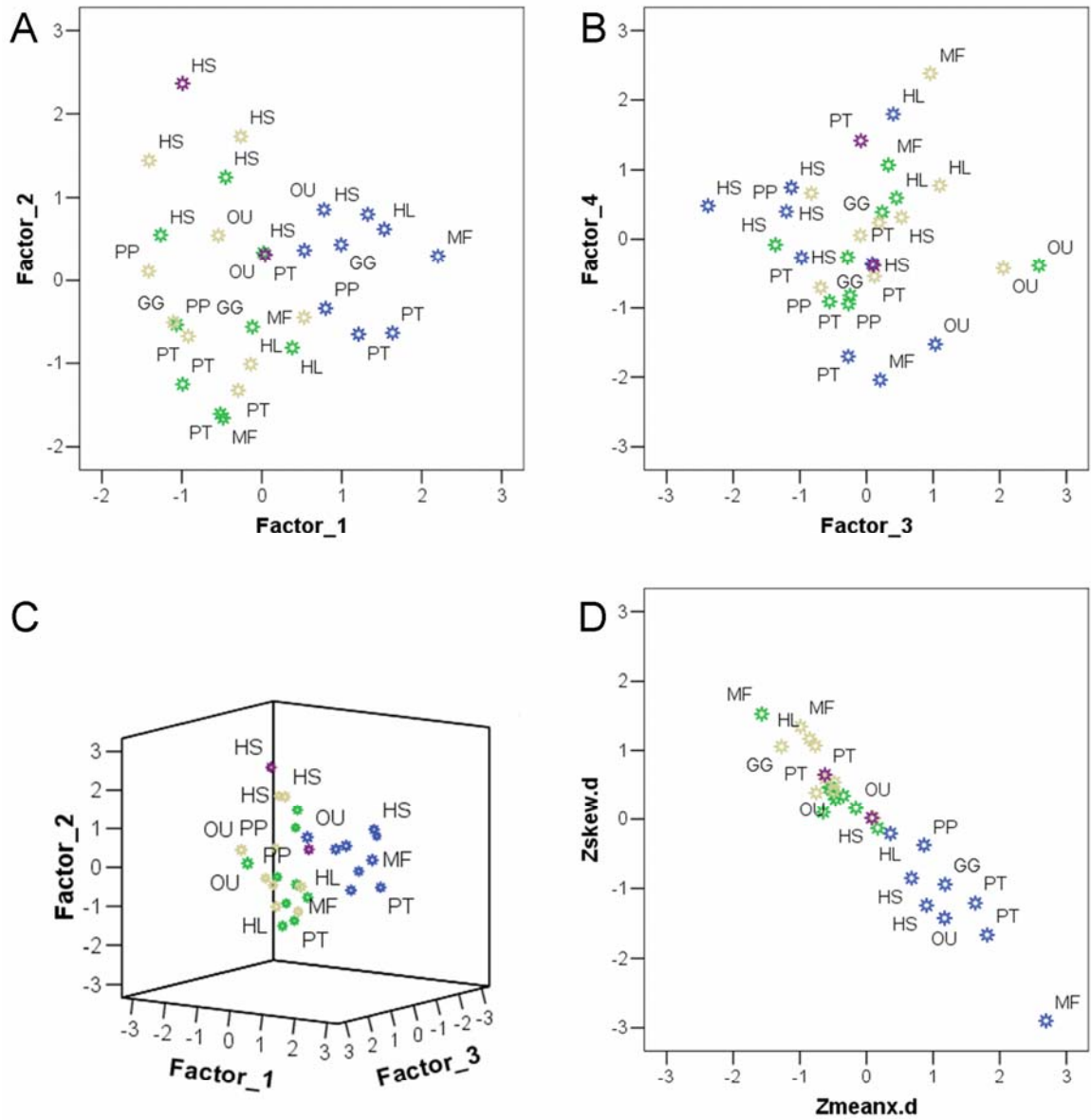
Fig. 4.17 Principle components plots summarizing GLI individual profile data. See Results for details.

Chapter 5. Hominoid Visual Brain Structure Volumes and the Position of the Lunate Sulcus

5.1 Introduction

Can brain size alone explain unique aspects of human behavior, or are there major differences between humans and great apes in the organization of the cerebral cortex that cannot be explained by scaling alone? Gross anatomical landmarks, potentially visible on fossil endocasts, have been used to infer brain reorganization – for example, a decrease in the size of the primary visual area (V1) – in the human evolutionary lineage. Human brain evolution, as indicated by species differences in the volume of V1, is explored here using three approaches.

The human primary visual cortex (VI) has been found to be smaller than predicted for a primate of similar brain size (Filimonoff IN, 1933; Frahm HD *et al.*, 1984; Holloway RL, 1997). It has been suggested that this does not reflect a reduction in visual information processing, but rather, the development of additional brain tissue allocated to higher order functions (Holloway RL, 1997). In fact, the V1 volume of humans is absolutely larger than in any other primate species for which it has been measured (Bush EC and JM Allman, 2004; Frahm HD *et al.*, 1984). Behavioral evidence demonstrates similar visual acuity in humans and macaques (De Valois RL *et al.*, 1974), and in terms

of the size of other visual system structures such as the cross sectional area of the optic nerve, LGN volume, and retinal area, humans are close to what would be expected for a primate of similar body size (Stephan H *et al.*, 1984). The absolute increase in human V1 volume, then, may in part be due to an overall expansion in the size of the neocortex, and yet it does not keep pace with the three-fold expansion of human neocortex over that of great apes.

In fossil hominins, evidence for changes in V1 volume, have been drawn from the position of the lunate sulcus, a gross anatomical landmark for the lateral-anterior limit of V1 in apes and in some monkey species (von Bonin G and P Bailey, 1947; Figure 5.1). A posteriorly-positioned lunate sulcus – such as the one Dart (1925) observed in the Taung *Au. africanus* endocast – is thought to indicate an enlarged posterior parietal association cortex at the expense of V1. More generally, this indicates that a functional reconfiguration may have enabled small-brained hominins to engage in humanlike behaviors. The hypothesis that brain reorganization occurred early in the hominin lineage has been expanded in detail by Holloway (1966; 1975). Although Dart's interpretation of the lunate sulcus in Taung has been questioned (Falk D, 1980), another endocast, Stw 505, has provided clearer evidence for a posteriorly-positioned lunate sulcus in *Au. africanus* (Holloway RL, RJ Clarke *et al.*, 2004).

There are two potential problems with relying on the lunate sulcus as an indication of brain organization. First, although sulci are often used as landmarks for determining the size or cortical regions in hominoids, they are not reliable delimiters of cytoarchitectonic areas (Amunts K, A Schleicher *et al.*, 2007). It has not been demonstrated that the histologically defined V1 volume corresponds to the extent of the

lunate sulcus. The current evidence indicates that the position of the lunate sulcus is a reliable indicator of the extent of the lateral part of V1 in chimpanzees, including two specimens with unusually posterior lunate sulci. (Holloway RL, DC Broadfield, MS Yuan *et al.*, 2003). In fact, Smith (1903) and Black (1915) considered a relationship to striate cortex to be a requirement for lunate sulcus identification in human, based on the observation that the lunate sulcus (also called the Affenspalte or simian sulcus) is a delimiting sulcus of V1 in the species in which it occurs (Brodmann K, 1906; Ingalls NW, 1914). However, it is possible that the lunate sulcus is only an indication of the lateral-anterior limit of V1, and does not correlate with total V1 volume in closely related hominoid species. In the case of V1, it has generally been observed that in humans (which normally lack a lunate sulcus, see Allen JS *et al.*, 2006 for a review) the sulcus best associated with the extent of V1 is the calcarine sulcus. However, Gilissen *et al.* (1995) found that in a sample of 23 human brains, the length of the calcarine sulcus varied considerably in its depth, and therefore speculated that the length of the calcarine would not be a sufficient indicator of the volume of V1 (although this was not directly compared to V1 volumes).

Second, it is possible that the reduced relative V1 volume and posterior lunate sulcus position of humans can be attributed to brain size increase in the hominin lineage, and, therefore, these changes are not in themselves evidence of reorganization. It has been suggested that the position of the lunate sulcus is directly related to brain size – in bigger brained species, the extent of V1 is shifted from a more medial to a more lateral position -- and therefore, the lunate sulcus cannot occur in a posterior position on a small-brained hominoid (Jerison HJ, 1975). Similarly, in primates V1 size scales with negative

allometry to brain size (Bush EC and JM Allman, 2004; Frahm HD *et al.*, 1984), therefore it is possible that reduction in relative V1 volume in the human lineage is an extension of this pattern.

Several hypotheses have been proposed to explain observations about the negative allometric scaling of V1 volume to overall brain volume. Kaas (2000) hypothesized that as cortical areas increase in surface area, it becomes more difficult to maintain connections between them, and as a result the number of cortical areas increases. This is supported by the finding that across mammals the number of neocortical areas (and the number of areas to which each is connected) scale to the 1/3 power of the volume of the cerebral cortex (Changizi MA and S Shimojo, 2005). Thus, in general, larger brains have more visual areas. The role of the primary cortical area in information processing is expected to decrease as its specific functions are delegated to an increasing number of higher order cortical areas. Therefore, the relatively large V1 of macaques is expected to be more functionally generalized than the relatively small V1 of humans. Although such physiological differences have not yet been demonstrated, it is known that histological differences between human and macaque V1 do exist (Preuss TM and GQ Coleman, 2002; Preuss TM *et al.*, 1999).

Bush and Allman (2004) suggested that the geometric requirements of the connection between V1 and the extrastriate areas could explain the negative allometric scaling relationship. Stevens (2001) showed that as LGN neuron number increases, V1 neuron number increases faster – presumably because the LGN is the most important subcortical source of input to V1 – with a scaling coefficient of 3/2. This is because LGN neuron number is approximately equal to retinal neuron number (Schein SJ and FM de

Monasterio, 1987), which scales to the ½ power of overall size, and three (3) types of spatially dependent information – right-left location; up-down location; and line orientation; require that V1 neuron number scale to the 3/2 of LGN neuron number. Following this reasoning, it is anticipated that extrastriate areas, which receive inputs from V1, should increase in neuron number (and thus, volume) at a faster rate than V1 does (Bush EC and JM Allman, 2004). Therefore, as brains grow, so does the proportion of brain tissue allocated to extrastriate areas – and V1 becomes proportionately smaller.

Here, volumes of the primary visual cortex and other brain structures were measured in hominoids and macaque monkeys to study the evolution of the volume of V1, and images of brains were three-dimensionally reconstructed such that these volumes could be compared to the position of an anatomical landmark, the lunate sulcus. In particular, this study sets out to examine whether previous findings that humans have significantly reduced V1 and LGN volumes are confirmed for a larger comparative sample of hominoid brains, and whether the lunate sulcus is a reliable predictor of V1 volume in nonhuman hominoid species. Finally, it has been indicated that humans differ from nonhuman hominoid species in the relative size of specific brain regions, but that these differences are small compared to differences in visual system structures (Holloway RL, 1997; 2002), and that hypothesis is tested here.

5.2 Materials and methods

5.2.1 Specimens and tissue preparation

Measurements were taken on histological sections from a total of 29 brains representing seven hominoid species, plus one cercopithecoid. Included were sections from the left hemispheres of adult specimens. The age and sex distribution is shown [Table 5.1]. In order to accumulate a large and diverse sample, specimens in the study come from several different collections: the Zilles, Bidmon and Stephan comparative neuroanatomy collections at C&O Vogt Institute of Brain Research in Düsseldorf, Germany, the Yakovlev-Haleem and Welker collections at the Armed Forces Institute of Pathology in Washington, D.C., and the Sherwood-Hof collection at The George Washington University, Washington, D.C.

The human and nonhuman hominoid brains from the Zilles collection were immersion fixed with either 4% formaldehyde or Bodian's solution within a few hours after death, embedded in paraffin and serially-sectioned along the coronal plane at a thickness of 20μm (except for one chimpanzee brain, which was horizontally sectioned at a thickness of 15 μm), and stained for Nissl substance (cell bodies) based on Gallyas' procedure (Gallyas F, 1971), using silver (Ag) according to the technique described by Merker (1983). The *Macaca fascicularis* brain from Bidmon's collection was perfusion fixed with 4% formaldehyde in phosphate buffer, embedded in paraffin and serially-sectioned along a coronal plane at 20 microns, and Merker stained for Nissl. The *Gorilla gorilla* brain from the Stephan collection was perfused in situ with Bouin's fluid through the carotid arteries after the blood was washed out with physiological saline, embedded in paraffin and serially-sectioned along the coronal plane at a thickness of 20μm, and stained for Nissl substance using cresyl violet. The *Pan troglodytes* brains from the Yakovlev-Haleem collection were sagittally sectioned at a thickness of 35 microns. The

161

Pan troglodytes brain from the Welker collection was coronally sectioned at a thickness of 50 microns and Nissl stained using thionin. The hominoid brains from the Sherwood-Hof collection were immersion fixed in 10% neutral buffered formalin for no more than 14 days. Left occipital lobe and parieto-occipital lobe blocks were cryoprotected by immersion with increasing concentrations of sucrose solutions up to 30%, frozen on dry ice and serially-sectioned on a microtome at a thickness 40 microns, and sections were stained for Nissl substance with cresyl violet.

5.2.2 Magnetic resonance image acquisition and distance measures

Magnetic resonance images were available for a subsample of the specimens from the Zilles collection (n=5), and were used to make 3D brain reconstructions from which gross anatomical landmarks could be identified, and the distances between them measured and compared to volumetric data.

To improve visualization of the cerebral cortex, on the 2D scans the brainstem and cerebellum were segmented from the brain, and the left and right hemispheres were segmented from each other in HMV software (developed by Hartmut Mohlberg, Jülich Research Center Institute of Medicine, Germany). Three dimensional surface reconstructions which could be manipulated in virtual space were created using the marching squares algorithm in Amira–Advanced 3D Visualization and Volume Modeling Package (Indeed, Visual Concepts GmbH, Berlin, Germany). Three landmarks were identified on the surfaces of the hemispheres, following the description of Holloway (1984; 1988) and Holloway et al. (2004). The hemisphere was aligned such that horizontal length of the brain was maximized, and two points in a plane to the horizontal

162

were identified: the occipital pole (OP), and the frontal pole (FP). The lunate sulcus (LS) landmark refers to the point at the intersection of an imaginary arc running over the surface of the brain between the OP and the FP, and a perpendicular line drawn from the most anterior part of the lunate sulcus to this line, very close to the medial fissure. The three dimensional coordinates (x, y and z) of landmarks were localized in HMV and used to calculate chord distances using the formula for the distance between two points, (x_1, y_1, z_1) and (x_2, y_2, z_2).

$$\text{distance} = \sqrt{[(x_1-x_2)^2+(y_1-y_2)^2+(z_1-z_2)^2]}$$

5.2.3 Estimation of volumes

Manual outlining in Image J (Rasband WS, 1997-2007) was used to calculate area measurements from 600-2400 DPI scans of the histological sections. Using these areas, left V1 (cortex only), left LGN (entire structure) and whole brain (entire structure) volumes were estimated using the Cavalieri principle. Using the same method, neocortex volumes (cortex plus white matter) were obtained by Carol MacLeod. For V1, only grey matter volumes were measured because although V1 cortex can be clearly parcellated from the surrounding cortical areas on the basis of the presence of Gennari's stripe, there is no similar criterion to parcellate V1 white matter from the surrounding white matter on Nissl stained histological sections.

Volume = sum of areas x section thickness x number between sections

Shrinkage was corrected using a shrinkage correction factor for each brain **(C_{ind})**, obtained by comparing the fresh brain volume to the brain volume determined from microscope slides.

$$C_{ind} = \text{volume of fresh brain} \div \text{serial section volume}$$

The postmortem brain volume was estimated from the brain weight given the average specific gravity of brain tissue (1.036 g/cm3; Stephan H, 1960). Thus

$$\textbf{fresh brain volume (cm}^3\textbf{)} = \textbf{fresh brain mass (g)} \div \textbf{1.036}$$

In general, only Nissl stained sections were used for making measurements, although rarely adjacent myelin serial sections, or MR sections, were referred to when Nissl sections were missing or inadequate. There are two exceptions: for one specimen (ptc1 brain, V1 and LGN) measurements were taken on myelin sections only, and one volume (ppm LGN) was measured solely on high power (7T) magnetic resonance scans taken on the brain before processing, and thus did not require correction for shrinkage.

5.2.4 Statistical analyses

5.2.4.1 Visual brain structure volumes

All statistical analyses were assessed with an alpha of .05. Ordinary least squares (OLS) regression analyses were performed to determine whether human V1 and LGN volumes could be accurately predicted from nonhuman scaling relationships. In addition, reduced major axis (RMA) regression analyses were performed to compare the slopes of

different taxonomic groups, and to determine intraspecific scaling patterns within the *H. sapiens* and *Pan troglodytes* samples. In all regression analyses, the volumes of V1 and LGN were dependent variables regressed against the independent variable brain volume, and V1 volume was the dependant variable in a regression against independent variable LGN volume.

The main purpose of this study is to determine whether the human brain is organized differently from the brains of closely-related species. The nonhuman hominoids were considered *a priori* to be the appropriate taxonomic level for this study, as reflected by the sampling strategy. However, since previous studies (Bush EC and JM Allman, 2004; Frahm HD *et al.*, 1984; Holloway RL, 1997) have drawn regressions of V1 against brain size variables for higher-level taxonomic groups (e.g., "primates"), the difference between human observed and predicted values were estimated for several taxonomic levels. Comparisons of human predictions drawn from different reference samples, in addition, provide an estimate of reliability and sensitivity of the regression equation to idiosyncrasies of the sampling design (Holloway RL and D Post, 1982).

To make comparisons at higher taxonomic levels, the *Macaca fascicularis* specimen was included along with other previously published non-hominoid primate volumetric data for LGN (Stephan H *et al.*, 1984) and V1 (Frahm HD *et al.*, 1984); and brain weight data (Stephan H *et al.*, 1988). In all statistical analyses, left V1 and left LGN volumes were doubled to estimate the total (left plus right hemisphere) volumes of V1 and LGN for each specimen because the volumes of V1 (Amunts K, E Armstrong *et al.*, 2007) and LGN (H. Frahm, personal comm.) are not known to exhibit asymmetries. Because autocorrelation is a potential source of error in cases where a part of a structure

165

is regressed against a whole (Deacon T, 1990), the value of the part was subtracted from the value of the whole. Data were then log transformed (base 10). Regression equations were calculated from species mean values, and human values were excluded. Human mean values and individual values were then plotted as points on graphs for visualization of intraspecific variation.

Regressions used to predict human values were compared to phylogenetic independent contrasts (PIC) ordinary least squares regressions. The phylogenetic independent contrasts method uses information about phylogenetic relationships (topology and branch length) to draw regressions of contrasts, which are calculated from pairs of monophyletic groups (species and clades) joined at nodes (Felsenstein J, 1985). In this way, PIC controls differences in scaling relationships between phylogenetic groups. Contrasts were calculated in the PDAP:PDTREE module version 1.07 (Midford PE et al., 2005) of Mesquite software version 2.0 (Maddison WP and DR Maddison, 2006) to create OLS slopes while controlling for phylogenetic relatedness. The primate phylogeny and branch lengths were taken from (Purvis A, 1995), and all polytomies were treated as soft polytomies for determining degrees of freedom (Garland T, Jr. and R Diaz-Uriarte, 1999; Purvis A and T Garland, Jr., 1993). PIC regressions were forced through the origin so it was necessary to map the values for the intercept back onto the original data space, using y-intercept values calculated in PDAP (Garland T et al., 1992; Garland T and AR Ives, 2000). Two types of OLS phylogenetic independent contrast (PIC) regressions were calculated: generic (G-PIC) regressions and *Homo*-specific (H-PIC) regressions (Garland T and AR Ives, 2000; Ross CF et al., 2004). Methodologically, these differ only in the position of the root node; this results in a different y-intercept but

does not alter the slope. For the G-PIC regressions, the primate phylogeny shown here (Fig. 5.2) was used (with the omission of *H. sapiens*) and the root node is that which links the strepsirrhine and haplorrhine primates; these regressions are best suited for comparison of scaling coefficients to the standard OLS regressions. For the H-IC regression, the root was moved to the branch leading to *H. sapiens*, and then *H. sapiens* was pruned from the tree as described by Garland and Ives (2000), for predicting the values of the unmeasured species. The H-PIC procedure displaces the intercept of the regressions towards the new root of the tree, that is, towards the position that would be occupied by *H. sapiens*.

The percent difference between observed (O) and predicted (P) human values (O/P % difference) were calculated from the nonhuman regression equations for V1 as functions of brain minus V1 volume, LGN as functions of brain minus LGN volume, and V1 as a function of LGN volume (Holloway RL, 1997; Holloway RL, 2002). In the regression equation

$$y = mx + c$$

y = predicted $\log_{10}$(dependant variable)

m = slope of regression line

$x = \log_{10}$(independent variable)

c = y intersect of regression line

Therefore the predicted dependant value is:

$$P = 10^{(mx+c)}$$

The difference between the observed minus the predicted value of the dependant variable, as a proportion of the observed value, is:

$$(O-P)/O$$

5.2.4.2 Comparison of lunate sulcus position to relative V1 volume

Nonparametric Spearman's rank correlations were investigated for the volume ratios of V1/brain, V1/neocortex and OP-LS/OP-FP chord ratios. Although multiple correlations were investigated, this was not corrected for because this was an exploratory analysis of slight deviations on the same comparison.

5.2.4.3 Multisystem structure volumes

To explore how changes in the volume of visual system structures compare to other aspects of human brain evolution, for an overlapping sample of hominoid brains, O/P percent differences were calculated and compared for the volumes of non-visual structures: four cortical areas and six brain nuclei. The study was limited to volumetric data for a selection of cortical areas and brain nuclei, because, 1) the LGN and V1 are a brain nucleus and a cortical area and 2) such cytoarchitectonically-defined regions are thought to be more physiologically specific than gross brain structures 3) data for these structures were available for a large sample of hominoids. The cortical areas were prefrontal area 10 (Semendeferi K, 1994; Semendeferi K *et al.*, 2001), limbic frontal area 13 (Semendeferi K, 1994; Semendeferi K *et al.*, 1998), and two components of Broca's language area, areas 44 and 45 (Schenker NM, 2007). Also included were the three

nuclei of the basolateral division of the amygdaloid complex – lateral, basal, and accessory basal, (Barger N et al., 2007) – and three orofacial motor brainstem nuclei -- trigeminal motor (Vmo), facial (VII), and hypoglossal (XII) (Sherwood CC, PR Hof *et al.*, 2005). Nonhuman hominoid differences between observed and expected values were calculated from OLS regressions of the all hominoid species data, using the same formula described above. An effort was made to standardize the data taken from the same individuals. Therefore, where necessary individual values were recalculated to ensure that the same correction factors and estimated brain volumes were used for all brain structures derived from a single brain.

5.3 Results

5.3.1 Absolute visual structure volumes

Fig. 5.1 shows V1 and LGN volumes, as well as several ratios. Specimen values, species mean values, and 95% confidence intervals are shown. The only absolute value or ratio in which *Pan* species are more closely aligned with *Homo* than they are with the other great apes is the V1/LGN volume ratio.

Absolute left V1 volume is greatest in humans, and lowest in the hylobatids, which are phylogenetically most distant from humans. The range of V1 volumes in a species is quite large (*Homo sapiens* CV = 0.23; *Pan troglodytes* CV = 0.2; compare to hominoid CV = 0.41; great ape CV = 0.24). The mean and inter-individual variability in the human sample reported here (n = 10; mean = 7.6238 cm^3; CV = .23) is similar to that reported in a previous study (n = 9; mean = 7.9145 cm3; CV =.19; Gilissen E and K

Zilles, 1995). Note that in adult humans significant intraspecific variation in absolute V1 volume has been attributed to sex (Amunts K, E Armstrong *et al.*, 2007) and to population (Klekamp J et al., 1994), but sex and population-level differences were not examined here.

The largest nonhuman V1 volume is that of a bonobo, near the human mean. A nonparametric test for two independent samples found that the *H. sapiens* sample (n=10) was significantly different from the *Pan troglodytes* sample (n=7) (p<0.001; Mann-Whitney U = .000). No significant difference was found between humans and bonobos, or between chimpanzees and bonobos, but this may be due to small sample size.

Absolute left LGN volume followed a pattern similar to V1 volume, with humans having the largest mean value and gibbons having the lowest mean value. However, there was more intraspecific variability and interspecific overlap in the ranges of individual values than for V1, and a nonparametric test for greater than two samples (Kruskal-Wallis) did not find significant differences between species.

5.3.2 Visual structure volume ratios

Ratios were calculated to explore potential isometric relationships between V1 and LGN volumes to each other, and the relationship of V1 and LGN volumes to brain size. The ratio of V1 to LGN volume is, like absolute V1 volume and absolute LGN volume, greatest in humans and lowest in hylobatids. However, the largest absolute value belongs to a chimpanzee. Also note that although humans have the largest ranges of individual values for both V1 and LGN volumes, for the V1/LGN ratio chimpanzees have the largest range. A Mann-Whitney U test did not find *H. sapiens* to be

170

significantly different from *P. troglodytes* in V1/LGN ratio. However, the *Homo-Pan* clade was found to be significantly different from all other hominoids treated as a single paraphyletic group (p = 0.001; Mann-Whitney U = 15).

The ratio of V1 to neocortex volume follows an inverse trend: it is lowest in humans and highest in *Hylobates*. All great ape ranges overlap with each other in the range of values and confidence interval, but not with the humans and hylobatids. The ratio of V1 to brain volume is similar to that of V1 volume per neocortex volume. Notably, the bonobo ratios cover a large range, with one specimen falling within range of the other ape values, and overlapping in its 95% confidence interval with the hylobatids. although the *P. paniscus* V1/neocortex volume ratio is not. Orangutans have the lowest ape V1/brain ratio and also have large confidence intervals, but do not overlap with the human values, which are rather tightly packed around the mean. It should be noted that the V1/neocortex comparisons included fewer specimens than the V1/brain volume specimens because neocortex volumes were not available for all specimens. The ratio of LGN to brain volume is highest in *Hylobates* and lowest in *Homo*. All great ape species overlap with each other in the range of values, but not with the humans and hylobatids.

5.3.3 Visual structure volume regressions

OLS regressions were created to determine whether human V1 and LGN volumes could be accurately predicted from the nonhuman trend, or whether the human values were exceptional. To examine the effect of phylogenetic bias in the data on scaling relationships, G-PIC regressions were compared with the TIP regressions 95%

171

confidence intervals. Also, RMA regressions were calculated to compare the slopes of different taxonomic levels and groups.

5.3.3.1 Taxonomic levels

To examine the effects of different taxonomic levels (excluding humans), statistically significant (p<.05) regressions are shown for nonhuman hominoids, nonhuman catarrhines, and nonhuman primates (Figs. 5.4-5.6). For these regressions, slopes, y-intercepts, R^2, significance, and the percent differences between observed and predicted human values (O/P % differences) are shown (Table 5.3). OLS regressions were calculated for both for tip data (TIP) and for phylogenetic independent contrasts (PIC). For the TIP data, it was found that the smallest monophyletic group (minus humans) from which it is possible to draw a statistically significant regression was "nonhuman hominoids". For all PIC scaling relationships, it was only possible to draw a significant regression for hominoids for LGN/brain-LGN; note that PIC regressions were drawn from fewer (n-1) data points.

Because the G-PIC regressions tended to fall within the 95% confidence intervals of the TIP regressions (but see below), and because in some cases PIC regressions were not significant whereas TIP were, for the most part only the more traditional TIP data is referred to. Given the TIP data, a typical primate brain of human size would be expected to have a V1 volume 116% larger than the actual average human V1, but an ape V1 would be expected to be only 28% larger. These values are higher when comparing LGN volume to brain volume. A typical primate brain of human size would be expected to have an LGN that is 171% larger and a typical ape LGN would be 33% larger.

172

5.3.3.2 Percent difference between observed and expected human values

The percent difference between human observed and predicted values were calculated for V1 volumes scaled to LGN volumes to indicate whether humans have an unusual pattern of relationship between major cortical and subcortical visual structures. The difference between observed and predicted human values were relatively low regardless of taxonomic level of comparison ranging from humans having a V1 volume that is 33% larger than expected than a primate of similar LGN size to humans having a V1 volume that is 18% larger than expected for a nonhuman hominoid with the same LGN volume. Therefore, although the volume of V1 is greater in humans than expected given the amount of LGN input, the magnitude of the percent difference in observed and predicted values does not indicate that human V1 volume is particularly large relative to that of a nonhuman primate or nonhuman hominoid of similar LGN size.

The H-PIC percent difference between observed and predicted human values were calculated to determine whether phylogenetically-informed predictions for humans produced values that are more closely approximated to observed data. However, surprisingly, the H-PIC % difference O/P *Homo sapiens* values were in some cases actually higher than the TIP % difference O/P *Homo sapiens*: This was the case for LGN volume predicted for a nonhuman hominoid of similar brain size, and V1 and LGN from brain size predictions based on the catarrhine regressions.

5.3.3.3 Differences between hominoid and cercopithecoid regressions

173

The G-PIC OLS regressions predicting V1 and LGN volume from brain volume

for catarrhines did not fall with the 95% confidence interval of the TIP OLS regression

equations, and yielded very different percent differences between observed and predicted

human values (Table 5.3). To further explore the taxonomic differences in scaling, RMA

regressions were calculated for the hominoids and their sister taxon, the cercopithecoids,

and then compared to higher taxonomic levels (Table 5.4). The RMA equations for V1

as a function of brain minus V1, and of LGN as a function of brain minus LGN, show a

decrease in slope from higher to lower taxonomic level from primates to anthropoids to

catarrhines to hominoids. However, for both RMA regressions, the cercopithecoid slope

is steeper than that of any other group, indicating that both visual brain structure volumes

increase rapidly as a function of brain size (Fig. 5.7). The RMA equation for V1 as a

function of LGN volume increases from higher to lower taxonomic level, from primates

to anthropoids to catarrhines to hominoids. However, for this RMA regression, the

cercopithecoid slope is flatter than that of any other group, indicating that V1 increases

slowly as a function of LGN size in this group. Using a resampling test in SMATR

(Warton DI *et al.*, 2006), cercopithecoids and hominoids were found to be significantly

different in the RMA slopes for V1 as a function of brain minus V1 ($t = 5.956$, $p = 0.011$); for LGN as a function of brain minus LGN ($t = 8.590$, $p = 0.007$), and for V1 as

a function of LGN ($t = 4.035$, $p = 0.030$).

5.3.3.4 Dispersal of hominoid individual values over hominoid regressions (including

humans)

In Figs. 5.8-5.10 individual hominoid specimen values were plotted on the hominoid OLS and RMA regressions which were calculated from the hominoid species mean data (including humans) to demonstrate the spread of these values across the regression line and the OLS 95% prediction intervals. In Fig. 5.8, V1 volume as a function of brain minus V1 volume is shown for hominoids. All hominoid mean values, including the human mean value, are bounded by the 95% prediction intervals. Most human values fall between the regression and the lower prediction interval. Bonobo values are very high, and one actually falls above the prediction interval; the bonobo mean is near the upper prediction interval. Other ape values accumulate around the regression.

In Fig. 5.9, LGN volume as a function of brain minus LGN volume is shown for hominoids. All hominoid mean values, including the human mean value, are bounded by the 95% prediction intervals. Most human values fall between the regression line and the lower 95% prediction interval, although one value lies just below the upper prediction interval, and two values lie below the lower prediction interval. A similar spread of values was found for *Pan troglodytes*, for which half lie above or on the upper prediction interval, and half lie below the lower prediction interval. Similarly, the orangutan values showed variation, with one below the lower prediction interval. The bonobos do not have especially large LGN volumes, in contrast to their especially large V1 volumes. All bonobo, gorilla, and gibbon specimen values fell within the prediction interval brackets.

In Fig. 5.10, V1 volume as a function of LGN volume is shown for hominoids. All species mean values are bounded by the 95% prediction intervals. Most values fall

175

within the prediction intervals, with the exception of one human and two chimpanzee

values which fall above the upper 95% prediction interval.

5.3.3.5 Intraspecific regressions: humans and chimpanzees

Finally, RMA regressions for the human and chimpanzee samples are shown to

compare intraspecific trends (Table 5.4). Note that for both species, the intraspecific

slopes for V1 and LGN as a function of brain size are very steep, and the slope for V1 as

function if LGN size is very shallow; in contrast to the interspecific slope. This indicates

that V1 and LGN size increase more rapidly than brain size within species; and that V1

size increases more slowly than LGN size within species. In all cases, the human and

chimpanzee regressions were not found to be significantly different in their slopes, but

were significantly different in their intercepts, as indicated by pair-wise Wald tests for

shifts in elevation: V1 as a function of brain minus V1 (Wald statistic $= 21.466$, p $<.001$),

LGN as a function of brain minus LGN (Wald statistic 67.707, p $<.001$), V1 as a function

of LGN (Wald statistic$=6.638$, p$=.01$).

5.3.4 Lunate sulcus position in relation to V1 volume

V1 volume ratios and lunate sulcus chord ratios are shown in Table5.5. A

nonparametric test found correlations between each of the chord ratios paired with each

of the volume ratios (in all cases, Spearman's rho r $= .9$, p$=.037$). This indicates that ape

brains with more anteriorly-positioned lunate sulci also have larger relative V1 volumes.

However, because the correlation is not perfect, this indicates that some variability in V1

volume is not indicated by the linear distances between the landmarks LS and OP and FP,

and must be attributed to differences in the proportion of V1 on the medial surface and/or in sulci, and/or differences in the shape of the hemispheres and the shape of the lunate sulcus.

5.3.5 Multisystem structure volumes

To provide a context for interpreting the percent differences between observed and predicted values, values from other brain system structures were computed for an overlapping hominoid sample, mostly from the Zilles collection. Species mean volumes are shown in Table 5.6 and data about the regressions and O/P percent differences are shown in Table 5.7. For four of the structures investigated (Vmo, XII, area 13, area 44 and area 45) it was not possible to obtain a statistically significant regression. Note that in original publications regressions were derived, but this seems to be because these specimen values were treated as individual data points, or non-hominoid primates were included. The human O/P percent difference of greatest magnitude is -333.36% for the facial motor (VII) nucleus. The human O/P percent difference of the lowest magnitude is 2.78% for the accessory basal nucleus. According to these data, the human area 10 is 17.56% *smaller* than expected for a nonhuman hominoid; Holloway (2002) calculated that humans have an area 10 that is 6% *larger* than nonhuman hominoids based on a regression of Semendeferi *et al.* (2001). The only differences in the two data sets are the human and chimpanzee brain volume estimates and the correction factors used (see supplementary data, Table 5B), thus indicating that a O/P difference of 24% can be attributed to inter-researcher error. Indeed, Holloway (2002) has suggested that differences of 25-50% might be attributable to experimental error. Given these

guidelines, the only structure listed here that has been shown to undergo a change in relative human value based on the nonhuman hominoid trend is the facial motor nucleus. Further, note that although the human facial motor nucleus is small given the size of the human brain, the facial motor nucleus is not particularly small compared to medulla volume (Sherwood CC, PR Hof *et al.*, 2005). All brain components were scaled to brain volume, but certainly the volumes of functionally specific brain nuclei and cortical areas may be better predicted by the size of the regions in which they are contained than by overall brain volume.

5.4 Discussion

5.4.1 Human predictions

The main purpose of this study was to determine whether brain reorganization in *H. sapiens* is manifest in an unusually small V1 volume for its brain size. The choice of "nonhuman hominoids" as the appropriate group from which to drawn the regression was supported *a posteriori* since it was found to be the lowest taxonomic level (minus humans) for which a regression equation with statistically significant correlations could be drawn. Because the LGN is the primary source of inputs to V1, the relationship of LGN size to brain size, and V1 size to LGN size, were also considered to provide a wider scope. The mean human V1 volume was found to be 28% smaller than was predicted for a nonhuman hominoid of similar brain size based on an OLS regression of TIP data. A reduction of this magnitude has uncertain significance, given the variation that exists within the hominoids, for example, *Pan paniscus* has V1 that is 27% larger than a

178

hominoid of its brain size. Also, a value of this magnitude could be attributed to error

from tissue processing. The data here support the findings of previous studies conducted

which found that humans have smaller V1 and LGN volumes than are expected for a

primate of similar brain volume and (e.g., Frahm HD *et al.*, 1984; e.g., Holloway RL,

1997). However, Conroy and Smith (2007) calculated that the observed human visual

cortex (grey plus white matter) volume was just 18% less than predicted using the same

primate dataset, based on an independent contrasts regression, but note that their data also

differed from the present PIC regressions in that humans were included in the regression,

slopes were drawn from natural logs rather than $\log_{10}$, and different parameters were used

to calculate the independent contrasts. The present study differs from the Stephan (1981)

data set in having a better representation of hominoid species, which were derived from

larger-sized samples, plus one additional catarrhine species. Yet, for humans the H-PIC

prediction indicates that the volume of V1 is 95% smaller than predicted for a nonhuman

primate of similar brain volume, indicating that even after accounting for phylogenetic

trends within primates, human do have a significantly reduced V1 volume.

5.4.2 Multisystem brain structure variability

Although the relative size of visual system structures have been central to many

discussions of brain organization and encephalization, the range of O/P percent

differences calculated from non-visual nuclei and cortical areas indicate that human

visual system O/P percent differences are not unique. It seems this is in contrast to

previous results primarily because 1) they have relied only on the structures reported in

the Stephan data set, which, with the exceptions of V1 and LGN, none are actually nuclei

or cortical areas, 2) here trends were examined only within the hominoids. It has been suggested that visual specialization is the driving force behind encephalization in primates (Barton RA, 1998). However, in the absence of large primate datasets for uni-modal non-visual brain structures, it is not possible to test whether this effect is specific to the visual system. Further, the variability of the regressions here according to taxonomic level, or correction for phylogeny, indicate that within the primates, the visual system may have a larger role in encephalization in some species than in others. Specifically, it is known that a cercopithecoid species, *Macaca mulatta*, has a cerebral cortex of which 55% is mostly or entirely visual in function (Felleman DJ and DC Van Essen, 1991), and within the cercopithecoids visual system structures increase more rapidly with increasing brain size than in hominoids, or in any higher taxonomic level of primates. The enormous amount of encephalization that has taken place in the hominoid (and hominin) lineages does not seem to be due to overall visual specialization.

5.4.3 Hominoid diversity

In contrast to previous studies in which all species were poorly sampled, the current study attempted to evaluate the degree of intraspecific variability by including more hominoid individuals, particularly more individuals of *Pan troglodytes* and *H. sapiens*. In addition, volumetric data from three new hominoid species – *Pan paniscus*, *Pongo pygmaeus*, and *Symphalangus syndactylus,* as well as a *Macaca fascicularis* were compared. These new data demonstrate that hominoid values are more variable than previously appreciated. Given this range, humans overlapped with nonhuman hominoids in the absolute volumes of V1 and LGN. Also, it was found that *Pan paniscus* V1

volumes were particularly large, both absolutely and when compared to brain and LGN volumes.

5.4.4 Cercopithecoid – hominoid differences

A few remarks are made here about the level of taxonomic comparison. This topic has been discussed previously (Clutton-Brock TH and PH Harvey, 1979; Pagel MD and PH Harvey, 1988, 1989; Stephan H *et al.*, 1988). In regressions of brain size as a function of body weight, it has been shown that the lower taxonomic level of the group, the less steep the slope (Stephan H *et al.*, 1988); this trend is seen in the present RMA regressions of V1 as a function of brain-V1 and LGN as a function of brain-LGN. The taxon-level effect has been ascribed evolutionary significance, such as differential selection acting in body size versus brain size in closely related species (Gould SJ, 1966; Lande R, 1979). It has also been suggested that the steeper slopes of higher taxa result from linking the graded shallower slopes of lower taxa, and that the grade-level differences are due to the particular ecological conditions of that group (Pagel MD and PH Harvey, 1989). It seems that V1 and LGN size vary less than brain size. However, there are two deviations from what at first appears to be a "taxon-level effect" in the scaling of V1 and LGN volume to brain volume. First, the steepest slopes were found for the interspecific comparisons. This means that within species, V1 volume and LGN volume increase more rapidly than does brain size. It is speculated that the intraspecific variability in V1 volume and LGN volume is related to variability in size of the retina; unfortunately, this cannot be tested as these data are not available.

Second, it is noteworthy that the sister group of the hominoids, the cercopithecoids, diverges from the taxon-level effect-like trend and in fact has unusually steep slopes for both V1 size/brain size and LGN size/brain size, and consequently, the catarrhine IC slopes are also much steeper than expected. Thus, in the cercopithecoids, visual system brain structures LGN and V1 increase rapidly in volume with increasing brain volume, as compared to other primate groups. This is in contrast to the hominoid trend, and could indicate a cercopithecoid-specific organizational pattern of the visual system. Generally, the visual system of the two major families of catarrhines, cercopithecoids and hominoids, are similar, sharing primate synapomorphies such as stereoscopy, and a notable catarrhine synapomorphy is routine trichromatic vision (Deegan JF and GH Jacobs, 2001; Jacobs GH and JF Deegan, 1999). However, it is becoming increasingly apparent that cercopithecoids and hominoids differ in aspects of visual system neuroanatomy, such as lamination of V1 (Preuss TM *et al.*, 1999) and the percentages of GABAergic interneurons in V1 and V2 (Sherwood CC, MA Raghanti *et al.*, 2007). The different patterns of scaling of visual system brain structures to brain size in cercopithecoids and hominoids indicates that these two taxonomic groups have differences in brain organization.

5.4.5 Developmental considerations

Recent findings about the developmental basis of V1 and surrounding extrastriate areas provide support for Dart's (1925) hypotheses that reduction in V1 size could be directly related to the expansion of adjacent parieto-occipito-temporal areas.

Arealization is the developmental process responsible for breaking up the cortical sheet into functionally distinct cortical areas, and is due to a combination of genetic and extrinsic developmental factors. During neurogenesis, patterning centers in the ventricular zones of telencephalic vesicles generate signaling molecules such as fibroblast growth factors 8 (Fgf8) and 17 (Fgf17) from the anterior neural ridge, the vertebrate ortholog of *Drosophila* wingless (Wnts) and bone morphogenetic proteins (Bmps) from the cortical hem, and sonic hedgehog (Shh) from the medial ganglionic eminence. Signaling molecules regulate the expression of transcription factors (TFs) such as *Emx2*, *Sp8*, *Pax6*, and *Coup-TFI*. The graded expression of TFs across the telencephalon regulates cell survival, proliferation, migration, and differentiation, resulting in the observed regional differences of cerebral cortical areas (Dehay C and H Kennedy, 2007; O'Leary DD et al., 2007). The sizes of cortical territories are directly impacted by the presence of signaling molecules and the expression of TFs. For example, the size and nature of the frontal cortex in mice and zebra fish depends on the dosage of Fgf8, and it is predicted that in humans reduced frontal lobe volume is due to Fgf8 irregularities (Sur M and JL Rubenstein, 2005).

Changes in the expression of the TFs as well as differences in neuronal inputs alter the relative sizes of adjacent neocortical areas. In *Emx2* mutant neonatal mice, the border between visual areas and somatosensory areas is shifted caudally (Bishop KM et al., 2000; Bishop KM et al., 2002). It is also clear that the formation of cortical area depends on thalamic inputs (Dehay C *et al.*, 1996; Dehay C and H Kennedy, 2007). Evidence for this includes an experiment in which developing rat V1 tissue was transplanted into the somatosensory cortex, and took on properties of its host region

(Schlaggar BL and DD O'Leary, 1991). Also, the cortical territory of V1 can be manipulated by altering LGN inputs. In macaques which were enucleated as fetuses, the lack of geniculostriate inputs results in a greatly reduced extent of cortex exhibiting the V1 cytoarchitectural pattern. Instead, much of the cortical territory in the opercular region, and (less so) within the calcarine sulcus that had been destined to become V1 instead exhibits V2-like cytoarchitecture (Dehay C *et al.*, 1996), or perhaps "hybrid" V1-V2 cytoarchitecture (Rakic P *et al.*, 1991). This has lead Dehay and others (1996) to conclude that, without LGN inputs, cortex on the occipital pole by default follows a developmental program that results in the V2 cytoarchitectural pattern. Based on these findings, it is speculated that subtle genetic, epigenetic and developmental differences could alter the relative proportions of V1 and nearby cortical areas in closely related species.

5.4.6 Variability in panin V1 organization

Bonobo V1 volumes stand out as being absolutely large for great apes, and relatively large for hominoids. The degree to which the human V1 volume deviates from the nonhuman hominoid prediction is similar to the degree from which the bonobo V1 volume deviates from the hominoid prediction, but in a different direction. In terms of absolute V1 volume, bonobos overlap with the human range. Bonobos have LGN volumes within the human range, and the ratio of V1 volume to LGN volume is similar in humans and bonobos. In Chapter 4, it was demonstrated that bonobos are closest to humans in having a low volume fraction neuronal tissue as indicated by the grey level index (GLI). This indicates that the increase in V1 volume in humans and bonobos is

accompanied by increased space for interneuronal connections. In summary, bonobos could be described as having humanlike aspects of V1 and LGN organization, but in a much smaller brain, and in this respect they differ from their sister taxon, the chimpanzees. Parsimony suggests that the most recent common ancestor of the panins and hominins also had an enlarged V1 volume with more space for connections, but that this was not matched by an enlargement in LGN volume. The panin-hominin ancestor would also be expected to have a brain volume similar to that of modern panins, based on fossil evidence for endocranial volumes of early hominins. In such a scenario, chimpanzees might have derived a reduced number of V1 interneuronal connections, resulting in a loss of V1 volume relative to brain and LGN volume, and a higher GLI. In the hominin lineage, V1 volume would have maintained constant in spite of overall increase in brain volume.

In terms of V1 volume relative to brain size, chimpanzees are more similar to humans than are bonobos. If aspects of overall brain organization including parietal lobe expansion can be predicted from V1 volume, it is interesting to consider the function of parietal expansion in chimpanzees versus bonobos. Both chimpanzees (Goodall J, 1986; McGrew WC, 1992; Nishida T, 1986) and bonobos (Kano T, 1982, 1992) use tools in the wild. However, chimpanzees are the great apes which use tools most frequently in the wild, and tool use is rare in wild bonobos. Also, whereas chimpanzees tend to use tools for foraging, bonobos are more likely to use objects in social situations (Ingmanson EJ, 1996). Therefore, the increase in tool use in the hominin and chimpanzee lineages could be directly related to the reduction of V1 volume in these species, but not bonobos.

Perhaps the chimpanzee V1 best represents that of the panin-hominin ancestor, whereas the bonobo V1 is an example of neoteny. In humans, V1 volume is largest at the 300th day after conception and begins to decrease during the first decade (Sauer B, 1983). It has been suggested that bonobos show aspects of cranial morphology (Shea BT, 1983) and behavior (Dahl JF, 1986; Kuroda S, 1980) consistent with the hypothesis that they resemble predictions for neoteny in chimpanzees. Therefore, the large V1, and small brain, of bonobos could be exhibiting this trend. However, note that the neuronal density of the human V1 decreases after the 190th day after conception, and that in this respect the V1 of *Pan troglodytes* may be the more paedomorphic since it has a much higher GLI value than *Pan paniscus*.

5.4.7 Lunate sulcus position as an indicator of reorganization

Paleoneurological studies equate lunate sulcus position with the relative volume of the visual cortex, but this assumption had not been tested. The results here are preliminary in that they only incorporate chord measurements and were conducted on a small sample, but they indicate that there is an overall relationship between relative visual system volume and lunate sulcus position. This is supported by developmental evidence suggesting that the relationship between the V1/V2 border and the lunate sulcus position is not entirely arbitrary. In spite of the reduction in V1 area in the enucleated macaques in the study described above, the V1/V2 border still usually occurred near a sulcus, and when it did not, a small "kink" within V2 occurred near the V1/V2 border (Dehay C *et al.*, 1996).

Because the preliminary data do indicate that lunate sulcus position is an indication of V1 volume, then if the lunate sulcus is correctly identified as being in a posterior position on early, small-brained hominins, the would indicate that V1 volume is smaller in some hominins than it is in great apes of similar brain size. This chapter presents evidence of intraspecific variability in relative V1 volume which, along with intraspecific variability in chimpanzee lunate sulcus position (Holloway RL, DC Broadfield, MS Yuan *et al.*, 2003), indicates that to some fossil specimens like ST 505 could be at one end of the distribution. However, the differences observed here between chimpanzees and bonobos in absolute V1 volume, and in microanatomical organization, indicate that species-level variability in brain organization irrespective of brain size was likely to have had existed among early hominin species. It had been proposed by Dart (1925) that the expansion of parietal-temporal-occipital association areas without a change in brain volume led to a proportional reduction in primary visual cortex volume in Taung. Holloway (1966; 1968) associates the expansion of posterior parietal association areas inferred from early hominin endocasts to functions such as advanced communication, tool use and tool-making, social complexity, and long term memory. However, the expansion in volume or number of any part of the brain could lead to a reduction in V1 volume relative to brain volume. For example, the bonobo specimen shown here to have the largest V1 volume was found in a previous study to have a particularly small volume of area 10, a region of the orbitofrontal cortex involved in higher-order cognitive tasks such as future planning and undertaking initiatives (Semendeferi K *et al.*, 2001).

5.5 Conclusions

The data described in this chapter provide evidence for gross-level brain reorganization within the hominoids and within the catarrhines. Within and between hominoid species, V1 volumes are quite variable. Bonobos have absolutely large V1 volumes, and large V1 volumes relative to brain size and relative to LGN size. The evidence here support earlier findings that in the hominin lineage, V1 volume is smaller than expected for a primate of similar brain size. Cercopithecoids and hominoids differ in the scaling relationships of V1 volume and LGN volume as a function of brain size. V1 volume seems to be predictable from lunate sulcus position, therefore evidence of posteriorly-positioned lunate sulci in early fossil hominins suggest that V1 reduction began early in hominin evolution. Decreases in V1 volume may correspond to increases in the volumes of adjacent visual areas.

The multisystem comparisons were intended to assess the degree to which humans diverge from other hominoid species across a larger range of cortical area volumes and brain nuclei. The difference between observed and predicted volumes in humans was greater for some non-visual system structures than for V1 and the LGN. This indicates that there remains much to be studied about the differences in brain organization among humans and closely related species.

This research can be elaborated by using arc measurements, which incorporate more information about brain shape, and an expanded sample. Nonetheless, the current findings do suggest that some evidence of gross-level hominin brain organization can be extrapolated from fossil endocasts. This gives rise to questions for further research: Can

a scaling relationship between lunate sulcus position and V1 volume be used to make quantitative predictions about V1 volume in fossil hominin specimens? Does lunate sulcus position correlate with the volumes of higher-order parietal association areas that show differential activity in tool-making activities, such as Brodmann's area 7? Is the lunate sulcus unique among sulci in indicating a cytoarchitectonic border?

Table 5.1 Specimens and volumes

species	code	sex	age	collection	plane of section	body mass (kg)	brain mass (g)	CF	brain vol. (cm³)	left V1 vol. (cm³)	left LGN vol. (cm³)	neocortex vol. (cm³)[a]
Homo sapiens	hs14	m	37	Zilles	coronal		1437	2.01	1387.07	9.39	0.19	1116.80
Homo sapiens	hs16	m	54	Zilles	coronal		1757	2.44	1695.95	10.40	0.27	
Homo sapiens	hs18	m	56	Zilles	coronal		1270	2.19	1225.87	7.49	0.17	
Homo sapiens	hs20	m	75	Zilles	coronal		1349	2.14	1302.12	8.50	0.17	
Homo sapiens	hs28	m	69	Zilles	coronal		1360	2.12	1312.74	9.18	0.17	
Homo sapiens	hs29	f	85	Zilles	coronal		1046	1.66	1009.65	5.28	0.10	
Homo sapiens	hs38	f	59	Zilles	coronal		1142	2.05	1102.32	6.00	0.14	865.20
Homo sapiens	hs5	f	79	Zilles	coronal		1350	1.92	1303.09	7.59	0.19	
Homo sapiens	hs56	f	72	Zilles	coronal		1216	1.81	1173.75	5.40	0.13	
Homo sapiens	hs6	f	79	Zilles	coronal		1110	1.46	1071.43	7.01	0.16	
Pan troglodytes	ptd	NA	NA	Zilles	coronal	NA	NA	2.05	264.99	2.80	0.09	198.30
Pan troglodytes	ptb	f	24	Zilles	coronal	80	359.5	2.00	347.01	4.70	0.17	262.80
Pan troglodytes	pt1	f	22	Zilles	coronal	50	440	1.99	424.71	4.78	0.17	297.40
Pan troglodytes	pty	m	22	Zilles	horizontal	53	420	2.24	405.41	5.18	0.17	300.10
Pan troglodytes	ptc1	f	NA	Yakovlev-Haleem	sagittal	6.8	NA	2.05	261.11	3.96	0.07	
Pan troglodytes	ptc3	m	6 or 7	Yakovlev-Haleem	sagittal	20.41	NA	2.05	276.81	3.78	0.08	
Pan troglodytes	ptw1	NA	NA	Welker	coronal	NA	NA	2.05	257.66	3.73		
Pan paniscus	ppy	f	2	Zilles	coronal	10.4	392	2.60	378.38	7.34	0.15	279.00
Pan paniscus	ppz	f	A	Zilles	coronal	NA	324	1.63	312.74	5.69	0.13	214.40
Pan paniscus	ppm	f	25	Sherwood-Hof	coronal		337	2.74	325.29	4.39	0.13	
Gorilla gorilla	ggy	f	20	Zilles	coronal	84.7	376	2.04	362.93	4.04	0.15	254.30
Gorilla gorilla	gga	m	JUV	Stephan	coronal	22	450	1.87	434.36	5.09	0.16	313.10
Pongo pygmaeus	ouh	m	37	Zilles	coronal	114	440	2.28	424.71	4.15	0.14	298.90
Pongo pygmaeus	ouy	m	16.5	Zilles	coronal	58	369	2.08	356.18	3.50	0.09	268.50
Pongo pygmaeus	oub	m	34	Zilles	coronal	140	345	2.15	333.01	4.69	0.16	240.30
Hylobates lar	hly	f	A	Zilles	coronal	4	92	2.09	88.80	1.79	0.08	59.60
Hylobates lar	hld	f	22	Zilles	coronal	NA	120	2.16	115.83	2.29	0.09	77.00
Syndactylus symphalangus	ss1	m	33	Sherwood-Hof	coronal		138.7	2.91	133.88	2.73		
Macaca fascicularis	mf2	m	3	Zilles	coronal	2.9	57.6	1.90	55.60	1.36	0.05	

Notes:

a. Neocortex volume includes grey matter and underlying white matter

Table 5.2 Species average volumes and ratios

SPECIES	Brain vol.	Left V1 vol.	Left LGN vol.	Neocortex vol.	V1/BRAIN	LGN/BRAIN	V1/LGN	V1/NEOCORTEX
Homo sapiens	1258.398	7.6237506	0.16751096	991	0.006017	0.0001315	46	8.02259E-05
SD	195.5856	1.745644	0.04443556	177.9080661	0.00075	1.675E-05	5.0158	5.18857E-06
number	10	10	10	2	10	10	10	2
confidence	121.223	1.0819415	0.02754094	246.5634693	0.000465	1.038E-05	3.1088	7.19086E-06
Pan trogldytes	319.6707	4.1341516	0.12536925	264.65	0.013068	0.0003677	36.851	0.000270936
SD	72.1486	0.8089794	0.0511637	47.38146614	0.001669	8.528E-05	11.872	4.76123E-05
number	7	7	6	4	7	6	6	4
confidence	53.44745	0.5992893	0.04093874	46.43298358	0.001236	6.824E-05	9.4998	4.66592E-05
Pan paniscus	338.8031	5.8032322	0.13757006	246.7	0.017019	0.0004063	41.83	0.000291529
SD	34.84275	1.4783842	0.01330556	45.67909806	0.003119	9.681E-06	7.2084	0.000114391
number	3	3	3	2	3	3	3	2
confidence	39.42756	1.6729185	0.01505638	63.3068367	0.00353	1.095E-05	8.1569	0.000158536
Gorilla gorilla	398.6486	4.5645107	0.15426238	283.7	0.011425	0.0003891	29.519	0.000280267
SD	50.50763	0.7366515	0.00593992	41.57787873	0.0004	3.44E-05	3.6387	1.32874E-05
number	2	2	2	2	2	2	2	2
confidence	69.99871	1.0209282	0.00823216	57.62294115	0.000555	4.768E-05	5.0428	1.8415E-05
Pongo pygmaeus	371.2999	4.1168553	0.12956055	269.2333333	0.011237	0.0003534	32.591	0.000224736
SD	47.68314	0.5948496	0.0343214	29.30688201	0.002471	0.0001133	4.7534	7.49148E-05
number	3	3	3	3	3	3	3	3
confidence	53.95756	0.6731233	0.03883761	33.1632496	0.002796	0.0001282	5.3788	8.47725E-05
Hylobates lar	102.3166	2.0433307	0.08311943	68.3	0.019998	0.0008182	24.499	0.000577554
SD	19.11099	0.3522313	0.00926616	12.30365799	0.000293	6.226E-05	1.5065	5.41255E-05
number	2	2	2	2	2	2	2	2
confidence	26.486	0.4881587	0.012842	17.05168667	0.000406	8.629E-05	2.0879	7.50128E-05

Table 5.3 TIP and PIC regression equations and percent (%) difference between observed (O) and predicted (P) human values

V1 as a function of brain-V1	no.	p	R^2	slope	Generic y-intercept	Generic O/P % diff	Homo Specific y-intercept	Homo Specific O/P % diff
TIP nonhuman primates	43	0.00	0.952	0.809	-0.994	-115.95%	NA	NA
IC nonhuman primates	43	0.00	0.868	0.786	-0.957	-95.60%	-1.001	-76.95%
TIP nonhuman catarrhines	14	0.00	0.843	0.586	-0.492	-37.44%	NA	NA
IC nonhuman catarrhines	14	0.00	0.809	0.928	-1.257	-170.54%	-1.357	-115.19%
TIP nonhuman hominoids	6	0.01	0.851	0.588	-0.529	-27.85%	NA	NA
IC nonhuman hominoids	6	not significant						

LGN as a function of brain-LGN	no.	p	R^2	slope	Generic y-intercept	Generic O/P % diff	Homo Specific y-intercept	Homo Specific O/P % diff
TIP nonhuman primates	42	0.00	0.953	0.707	-2.233	-171.38%	NA	NA
IC nonhuman primates	42	0.00	0.880	0.715	-2.234	-187.56%	-2.370	-109.86%
TIP nonhuman catarrhines	13	0.00	0.779	0.472	-1.725	-63.09%	NA	NA
IC nonhuman catarrhines	13	0.00	0.826	0.779	-2.404	-206.91%	-2.532	-128.60%
TIP nonhuman hominoids	5	0.01	0.940	0.403	-1.593	-35.67%	NA	NA
IC nonhuman hominoids	5	0.03	0.825	0.428	-1.653	-40.22%	-1.651	-41.06%

V1 as a function of LGN	no.	p	R^2	slope	Generic y-intercept	Generic O/P % diff	Homo Specific y-intercept	Homo Specific O/P % diff
TIP nonhuman primates	42	0.00	0.983	1.145	1.550	33.45%	NA	NA
IC nonhuman primates	42	0.00	0.944	1.085	1.456	42.80%	1.585	23.06%
TIP nonhuman catarrhines	13	0.00	0.905	1.153	1.574	30.26%	NA	NA
IC nonhuman catarrhines	13	0.00	0.887	1.133	1.545	33.31%	1.613	22.07%
TIP nonhuman hominoids	5	0.03	0.851	1.53	1.824	18.03%	NA	NA
IC nonhuman hominoids	5	not significant						

Table 5.4 RMA regressions for comparisons at different taxonomic levels

V1 as a function of Brain-V1

Group	n	r^2	p	Slope	Lower 95% CI	Upper 95% CI	Intercept	Lower 95% CI	Upper 95% CI
Primates	44	0.95	0.000	0.802	0.747	0.860	-0.983	-1.074	-0.893
Anthropoids	27	0.95	0.000	0.706	0.641	0.776	-0.773	-0.900	-0.646
Catarrhines	15	0.87	0.000	0.573	0.461	0.712	-0.473	-0.747	-0.199
Hominoids	7	0.89	0.001	0.533	0.367	0.775	-0.409	-0.918	0.100
Cercopithecoids	8	0.89	0.000	0.978	0.703	1.362	-1.199	-1.818	-0.581
Homo sapiens	10	0.74	0.001	1.588	1.059	2.381	-3.733	-5.776	-1.691
Pan troglodytes	7	0.64	0.031	0.947	0.498	1.803	-1.443	-3.065	0.178

LGN as a function of Brain-LGN

Group	n	r^2	p	Slope	Lower 95% CI	Upper 95% CI	Intercept	Lower 95% CI	Upper 95% CI
Primates	43	0.94	0.000	0.691	0.639	0.747	-2.219	-2.307	-2.132
Anthropoids	26	0.91	0.000	0.619	0.547	0.700	-2.072	-2.216	-1.927
Catarrhines	14	0.75	0.000	0.449	0.330	0.611	-1.691	-2.001	-1.381
Hominoids	6	0.85	0.009	0.306	0.183	0.511	-1.367	-1.787	-0.946
Cercopithecoids	8	0.86	0.001	0.925	0.638	1.340	-2.559	-3.225	-1.893
Homo sapiens	10	0.85	0.000	1.716	1.259	2.338	-5.799	-7.470	-4.127
Pan troglodytes	6	0.91	0.004	1.975	1.303	2.994	-5.590	-7.713	-3.467

V1 as a function of LGN

Group	n	r^2	p	Slope	Lower 95% CI	Upper 95% CI	Intercept	Lower 95% CI	Upper 95% CI
Primates	43	0.98	0.000	1.170	1.121	1.221	1.584	1.520	1.648
Anthropoids	26	0.97	0.000	1.154	1.077	1.236	1.585	1.504	1.666
Catarrhines	14	0.90	0.000	1.295	1.066	1.574	1.687	1.500	1.874
Hominoids	6	0.88	0.005	1.810	1.143	2.867	2.002	1.491	2.512
Cercopithecoids	8	0.90	0.000	1.062	0.782	1.443	1.488	1.215	1.762
Homo sapiens	10	0.82	0.000	0.922	0.656	1.295	1.622	1.463	1.781
Pan troglodytes	6	0.58	0.078	0.517	0.231	1.161	1.244	0.939	1.548

Table 5.5 Ratios between chord distances between external brain landmarks for comparison with volume ratios

| | CHORD RATIOS | VOLUME RATIOS | |
	OP-LS / OP-FP	V1/BRAIN	V1/NEOCORTEX
Hylobates lar	42.92%	3.96%	5.95%
Pongo pygmaeus	28.39%	2.82%	3.91%
Pongo pygmaeus	21.36%	1.96%	2.78%
Pan paniscus	40.52%	3.64%	5.30%
Pan troglodytes	34.36%	2.71%	3.58%

Notes:

For all correlations between chord ratios and volume ratios, Spearman's rho r = .9 p<.05

"OP" occipital pole, "LS" lunate sulcus, "FP" frontal pole

Table 5.6. Species mean volumes of cortical areas and brain nuclei[a]

Species	Brain[b]	Vmo	VII	XII	area 13	area 10	lateral	basal	accessory basal	area 44	area 45
Homo sapiens	1264586.01	15.48	25.90	28.78	825.62	32052.66	1146.00	881.00	396.40	3445.99	3891.40
Pan troglodytes	342159.50	10.17	24.65	15.69	510.47	4234.68	252.50	424.50	144.35	543.00	572.58
Pan paniscus	338803.09	5.78	14.99	8.19	233.67	5933.86	292.00	426.50	134.95	1061.53	1606.35
Gorilla gorilla	403932.43	18.97	26.53	20.39	556.56	4122.06	200.00	485.00	181.30	370.81	649.00
Pongo pygmaeus	371299.87	15.54	30.70	16.28	659.99	3358.55	229.00	295.00	107.15	714.81	847.15
Hylobates lar	98046.64	3.91	4.12	4.87	102.22	404.29	100.50	150.00	52.60	383.59	237.65

Notes:

a. The data are derived from previous studies which have included hominoid brain specimens from the Zilles collection.

b. All volumes are in mm^3.

Table 5.7. OLS regressions of nonhuman hominoid cortical area and brain nuclei volumes as functions of brain (minus dependent variable) volume and percent (%) difference between observed and predicted human values.

	no.	p	r^2	slope	y-intercept	residual
V1	6	0.01	0.851	0.5878	-0.5291	-27.85%
LGN	5	0.01	0.940	0.4034	-1.5929	-35.67%
Vmo	5	not significant				
VII	5	0.008	0.928	1.358	-6.191	-333.36%
XII	5	not significant				
area 13	5	not significant				
area 10	5	0.002	0.974	1.705	-5.832	-17.26%
lateral	5	0.021	0.869	0.677	-1.384	50.32%
basal	5	0.02	0.872	0.791	-1.787	-27.20%
accessory basal	5	0.021	0.868	0.785	-2.214	2.78%
area 44	5	not significant				
area 45	5	not significant				

Suppl. Table 5.1. Percent (%) difference between obeserved (O) and predicted (O) mean values for hominoid species based on TIP OLS regressions of hominoid mean data (including humans).

V1 as a function of brain-V1	no.	p	r²	slope	intercept	human	chimp	bonobo	gorilla	orangutan	gibbon	siamang
hominoids	7	0.001	0.889	0.503	-0.334	-9.45%	-0.61%	26.52%	-1.98%	-9.14%	-13.95%	2.57%
humans	10	0.001	0.739	1.365	-3.045	1.05%	72.42%	78.98%	66.10%	65.85%	88.45%	87.56%
chimps	7	0.031	0.641	0.758	-0.974	-54.68%	0.17%	26.16%	-7.15%	-12.63%	15.80%	22.91%

LGN as a function of brain-LGN	no.	p	r²	slope	intercept	human	chimp	bonobo	gorilla	orangutan	gibbon
hominoids	6	0.009	0.852	0.282	-1.306	-10.71%	-0.43%	6.96%	13.13%	-1.38%	-9.77%
humans	10	0.000	0.851	1.583	-5.387	1.35%	84.95%	84.96%	82.65%	81.54%	96.26%
chimps	6	0.004	0.905	1.879	-5.348	-791.97%	9.28%	7.80%	-11.63%	-16.31%	83.93%

V1 as a function of LGN	no.	p	r²	slope	intercept	human	chimp	bonobo	gorilla	orangutan	gibbon
hominoids	6	0.005	0.882	1.700	1.937	11.53%	0.32%	16.84%	-28.45%	-5.86%	-0.28%
humans	10	0.000	0.819	0.834	1.580	-0.04%	-44.87%	-11.52%	-55.99%	-49.53%	-108.03%
chimps	6	0.078	0.580	0.394	1.165	37.61%	-2.64%	24.16%	-0.88%	-4.41%	-76.62%

Suppl. Table 5.2. Comparison of adjusted values to published data of Semendeferi et al. (1998, 2002)

Species	code	code	Semendeferi et al. 1998; 2002				Current study			
			CF	brain vol.	area 13 vol.	area 10 vol.	CF	brain vol.	area 13 vol.	area 10 vol.
human	hs20	SN-20784	1.9	1158.3	366.2	14217.7	2.1	1302.1	412.8	16026.3
chimp	pt1	Schimp 1	2.1	393.0	269.9	2239.2	2.0	424.7	255.2	2117.3
bonobo	ppy	YN 86-137	2.5	378.4	110.5	2804.9	2.6	378.4	116.8	2966.9
gorilla	ggy	YN82-140	2.0	362.9	273.2	1942.5	2.0	362.9	278.3	2061.0
orang	ouy	YN 85-38	2.0	356.9	316.6	1611.1	2.1	356.2	330.0	1679.3
gibbon	hly	YN 81-146	2.1	88.8	51.5	203.5	2.1	88.8	51.1	202.1

* the brain volume differs because Semendeferi calculated it from the fixed weight (1200g), whereas I calculated it from the fresh weight (1349g)

** the fresh weight for this specimen is 440g
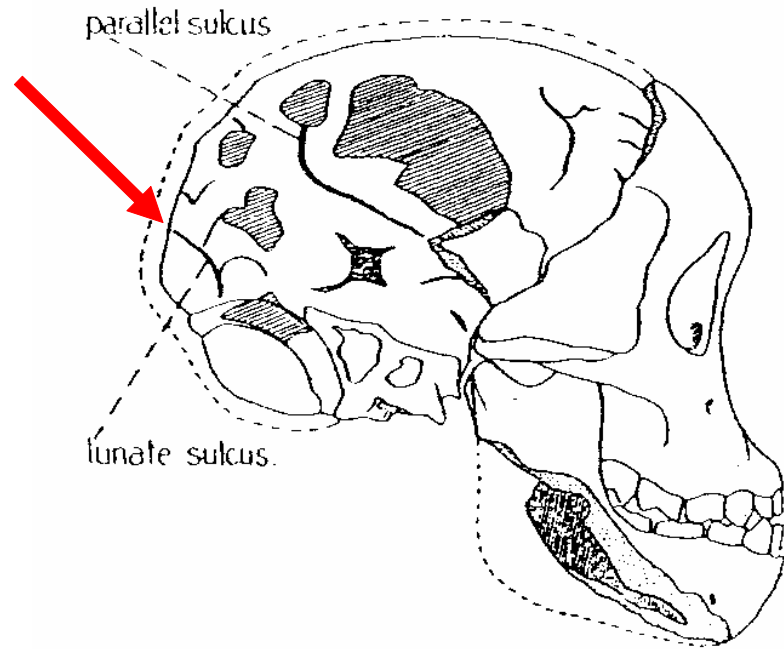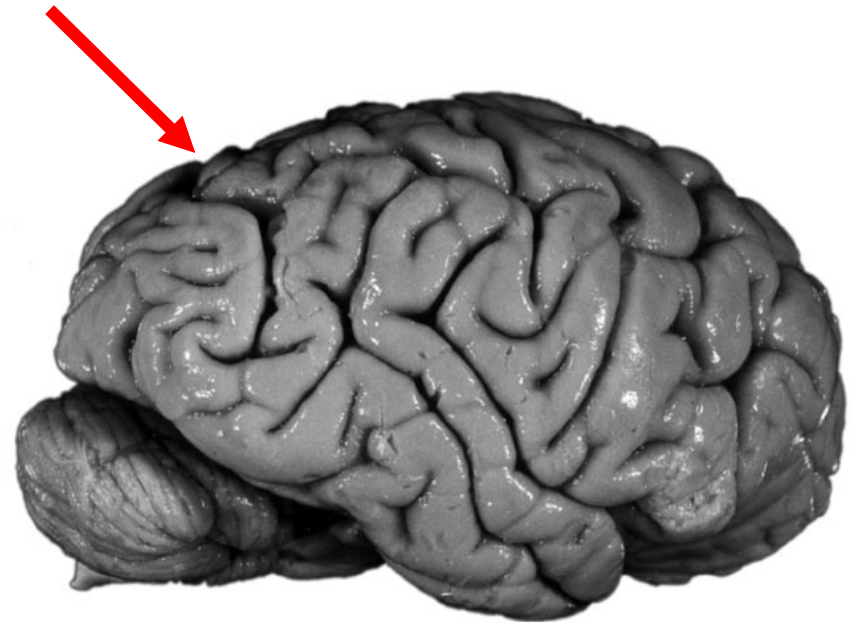
Fig. 5.1. Left lateral view of the position of the lunate sulcus, which has been interpreted as being in a posterior position in the Taung juvenile *Au. afarensis* endocast (A; from Dart, 1925), whereas it is in an anterior position in a typical orangutan brain (B).

(A) Reprinted by permission from Macmillan Publishers Ltd: *Nature* 115, 195-199 © 1925
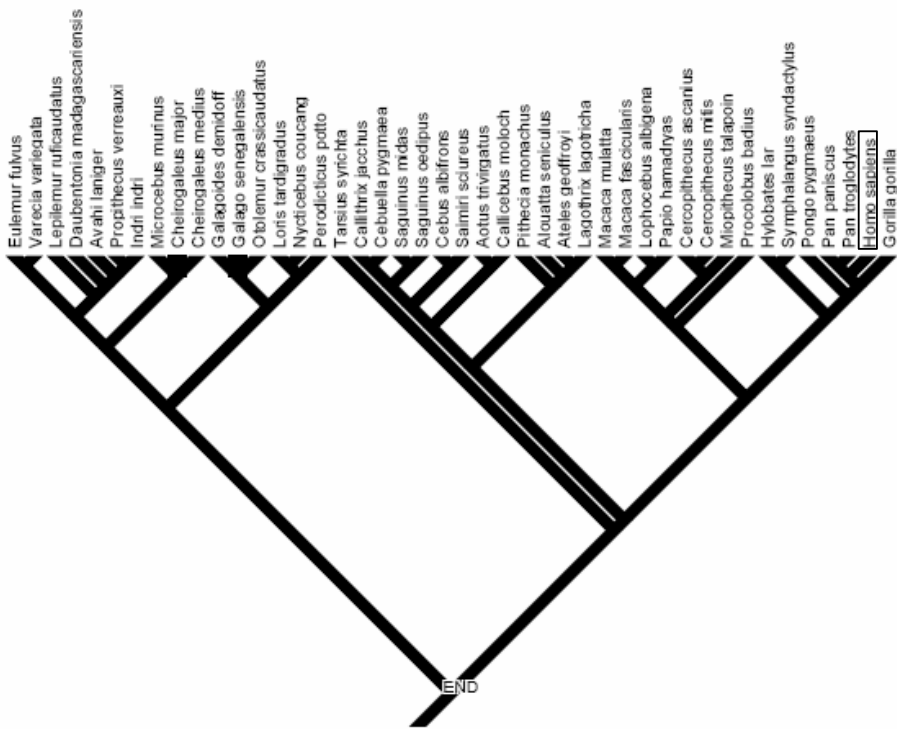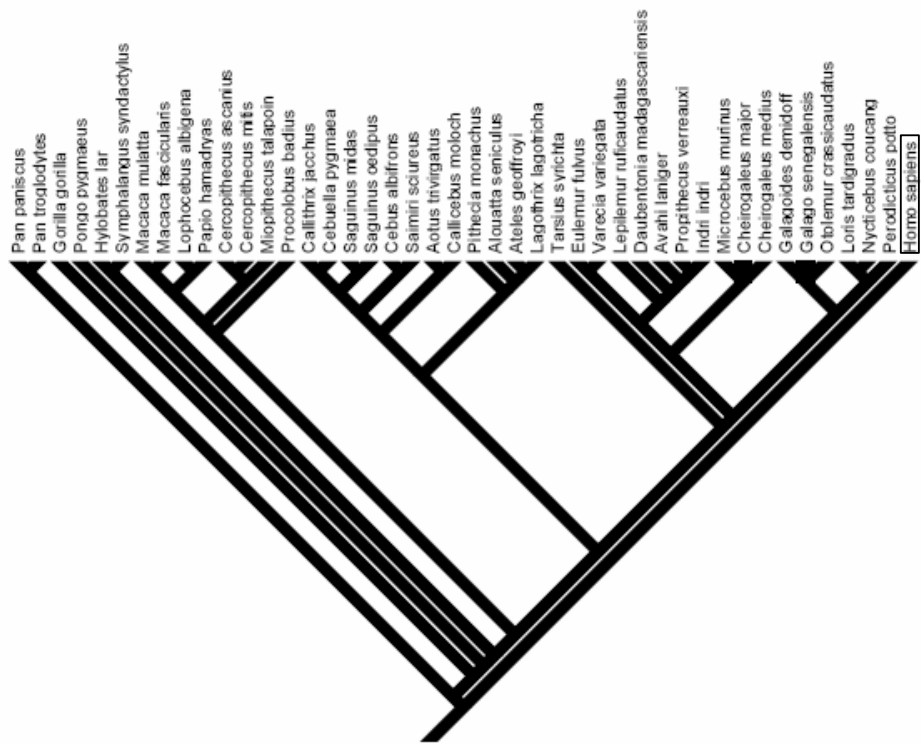
Fig. 5.2 Rooting of primate phylogenetic tree for predicting human values from G-PIC OLS regression (A) and H-PIC OLS regression (B)
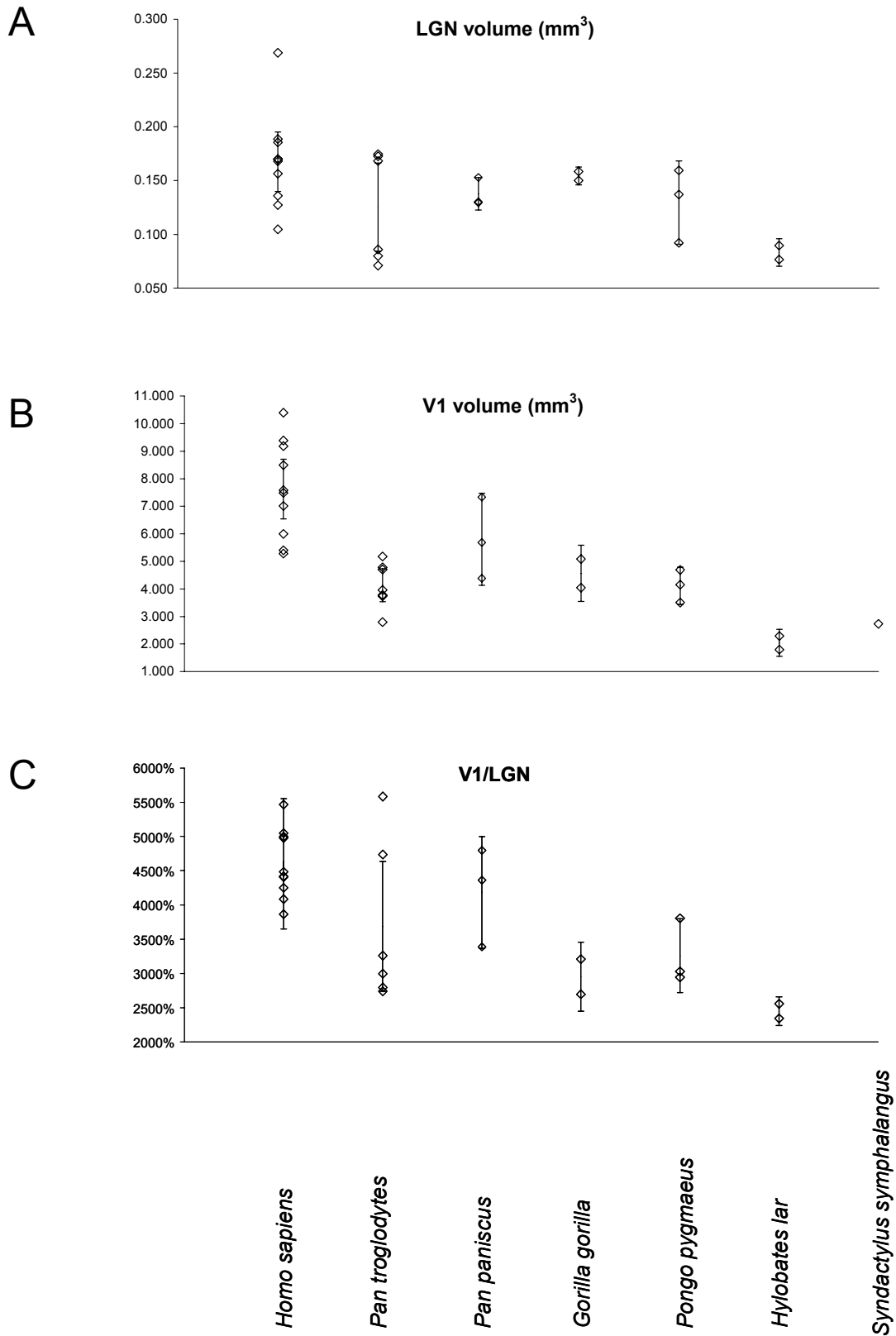
Figure 5.3. Species mean V1 volumes (A), LGN volumes (B), V1/LGN volume ratios (C), LGN/brain volume ratios (D), V1/neocortex volume ratios (E), and V1/brain volume ratios (F).
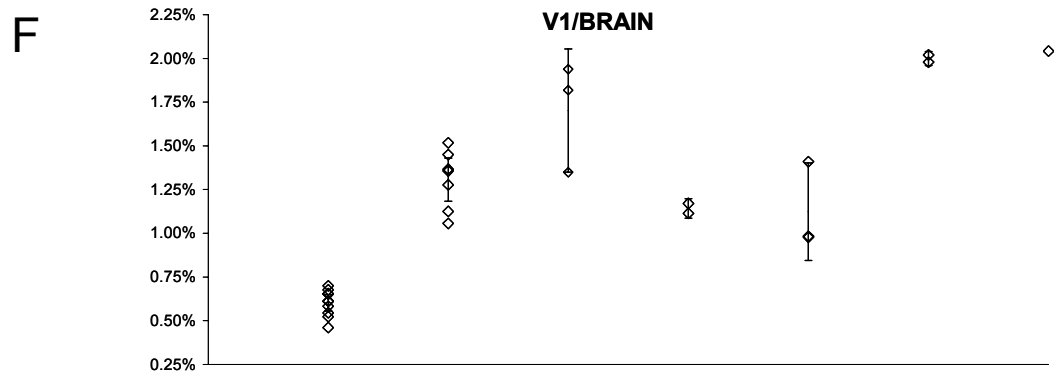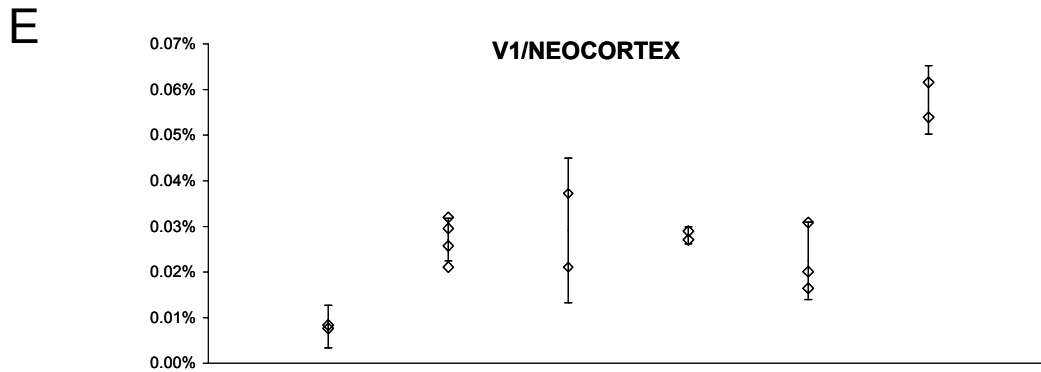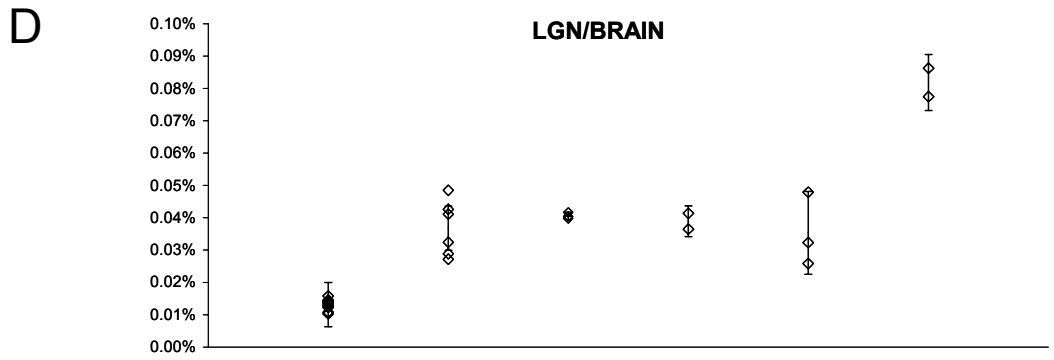
201

Notes:
a.   Only V1 volume and V1/brain volume ratio data are available for *Syndactylus symphalangus*.
b.   Vertical bars indicate 95% confidence intervals.
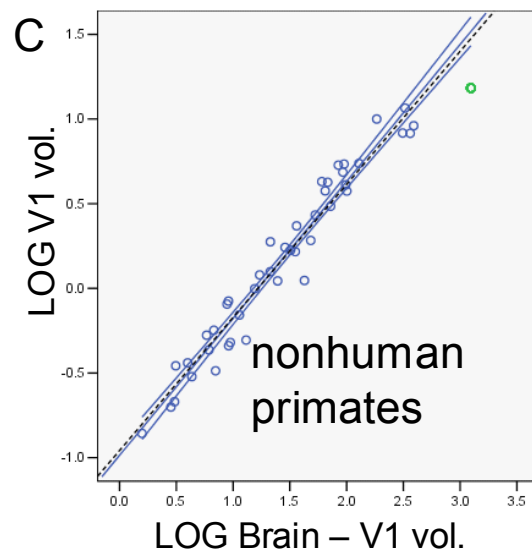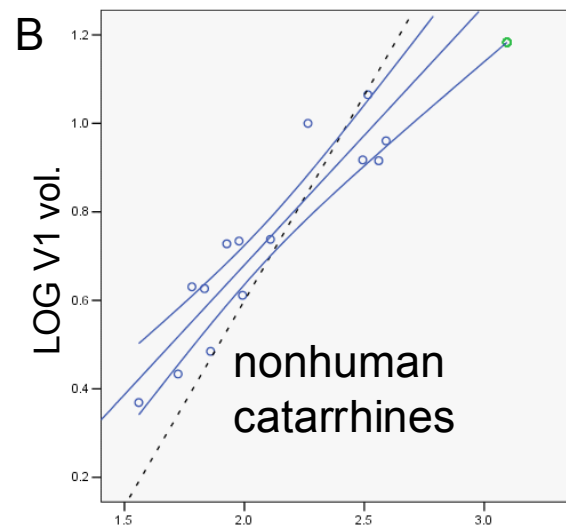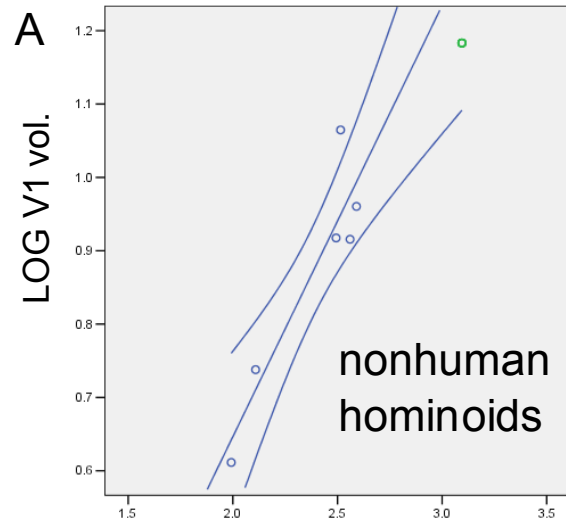
Fig 5.4 V1 as a function of brain-V1: nonhuman hominoid ($y = 0.588x - 0.5291$, p = 0.009, $r^2 = 0.851$) (**A**), nonhuman catarrhine ($y = 0.586x - 0.492$, p <.001, $r^2 = 0.843$) (**B**), and nonhuman primate ($y = 0.809x - 0.994$, p <.001, $r^2 = 0.952$) (**C**) TIP OLS regression lines and 95% confidence intervals (solid line) for predicting human values. Where significant, G-PIC OLS regressions are shown (dotted line). Human values are plotted in green.
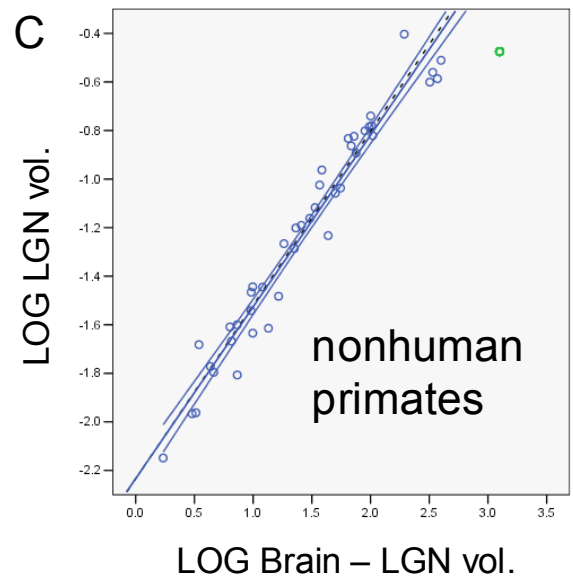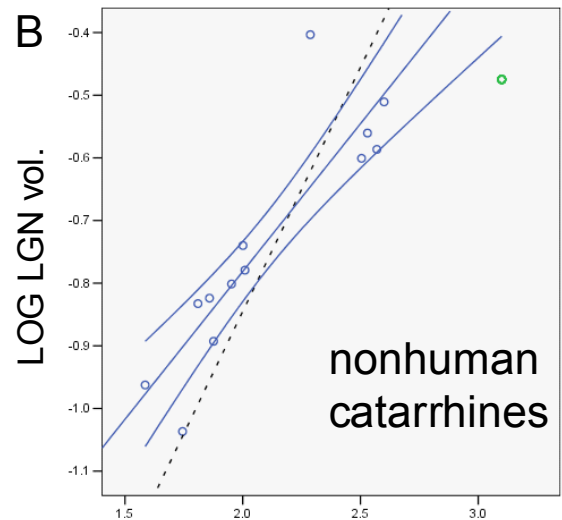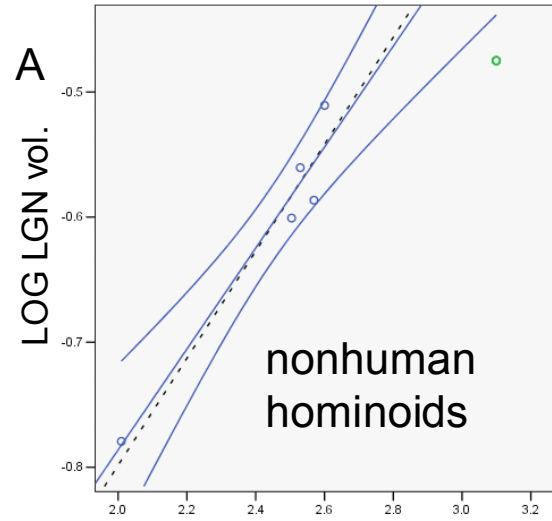
Fig. 5.5 LGN as a function of brain-LGN: nonhuman hominoid ($y = 0.403x - 1.593$, p = 0.006, $r^2 = 0.940$) (**A**), nonhuman catarrhine ($y = 0.472x - 1.725$, p < 0.001, $r^2 = 0.779$) (**B**), and nonhuman primate ($y = 0.707x - 2.233$, p < 0.001, $r^2 = 0.953$) (**C**) TIP LS regression lines and 95% confidence intervals (solid line) for predicting human values. Where significant, G-PIC LS regressions are shown (dotted line). Human values are plotted in green.
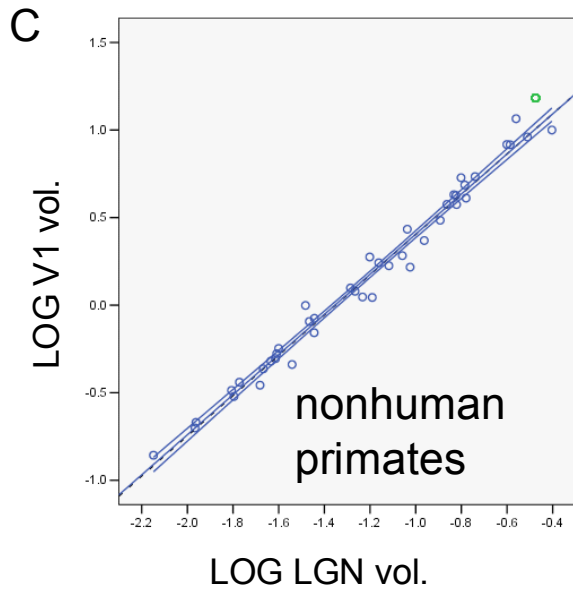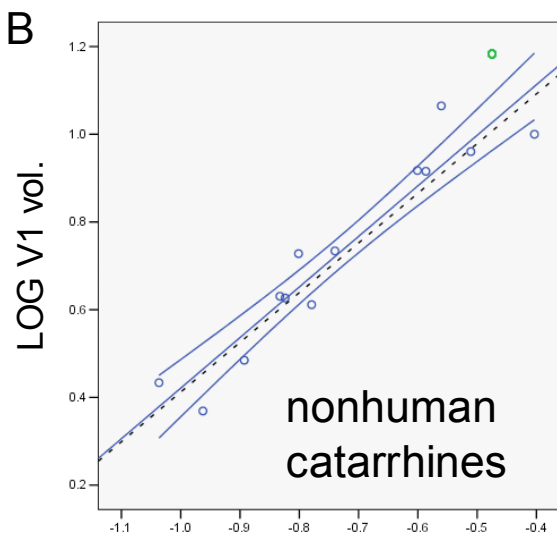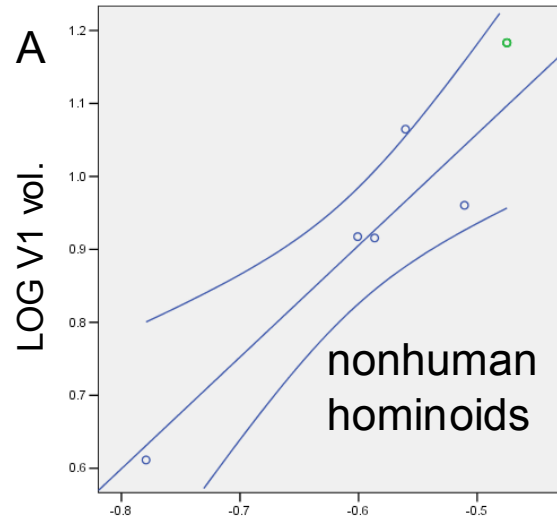
Fig. 5.6 V1 as a function of LGN: nonhuman hominoid ($y = 1.530x + 1.824$, p = 0.026, $r^2 = 0.851$) (**A**), nonhuman catarrhine ($y = 1.153x + 1.574$, p < 0.001, $r^2 = 0.905$) (**B**), and nonhuman primate ($y = 1.145x + 1.550$, p < 0.001, $r^2 = 0.983$) (**C**) TIP LS regression lines and 95% confidence intervals (solid line) for predicting human values. Where significant, G-PIC LS regressions are shown (dotted line). Human values are plotted in green.

Fig 5.7. Comparison of cercopithecoid and hominoid RMA regressions of TIP data of V1 as a function of brain-V1 (cercopithecoids: $y = 0.978x - 1.199$, $r^2 = 0.886$, $p < 0.001$, hominoids: $y = 0.533x - 0.409$, $r^2 = 0.889$, $p = 0.001$) (**A**) and LGN as a function of brain-LGN (cercopithecoids: $y = 0.925x - 2.559$, $r^2 = 0.856$, $p = 0.001$, hominoids: $y = 0.306x - 1.367$, $r^2 = 0.852$, $p = .009$) (**B**)
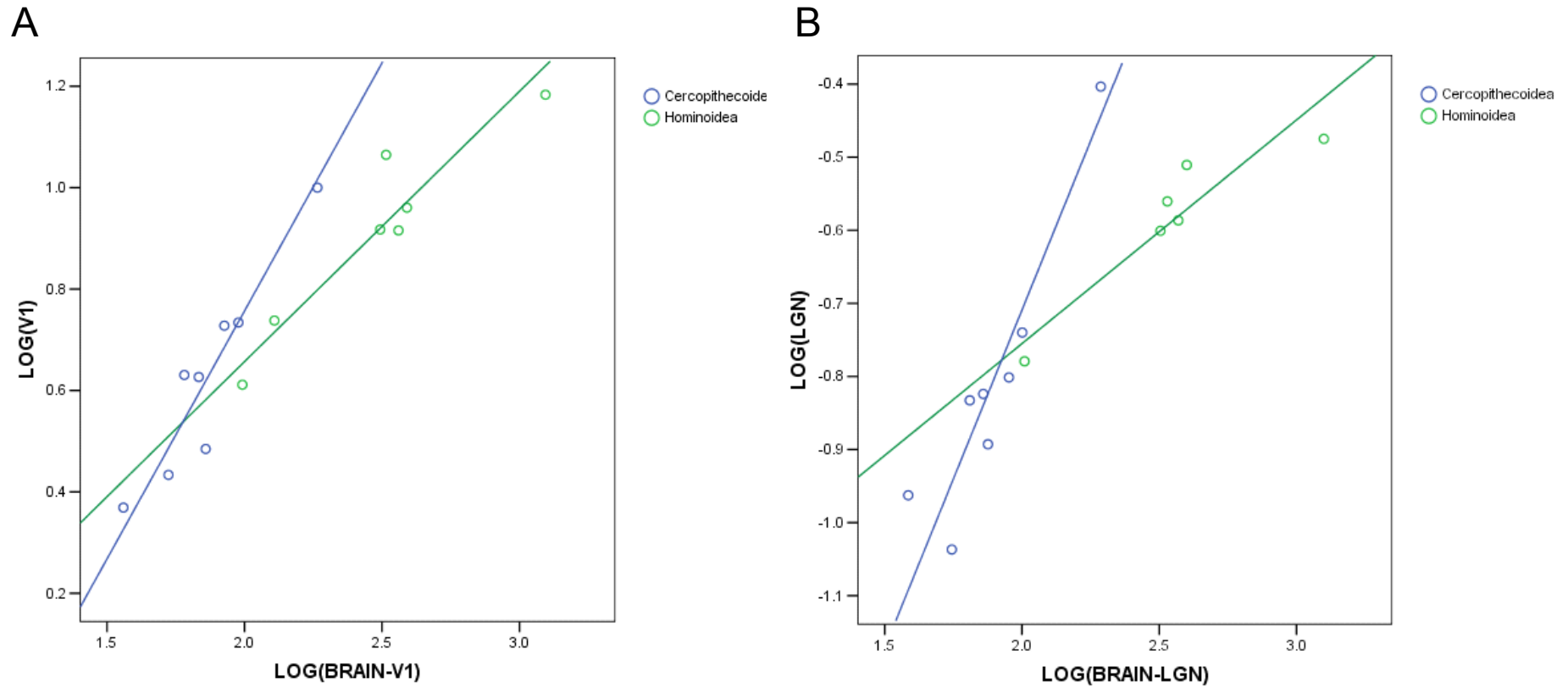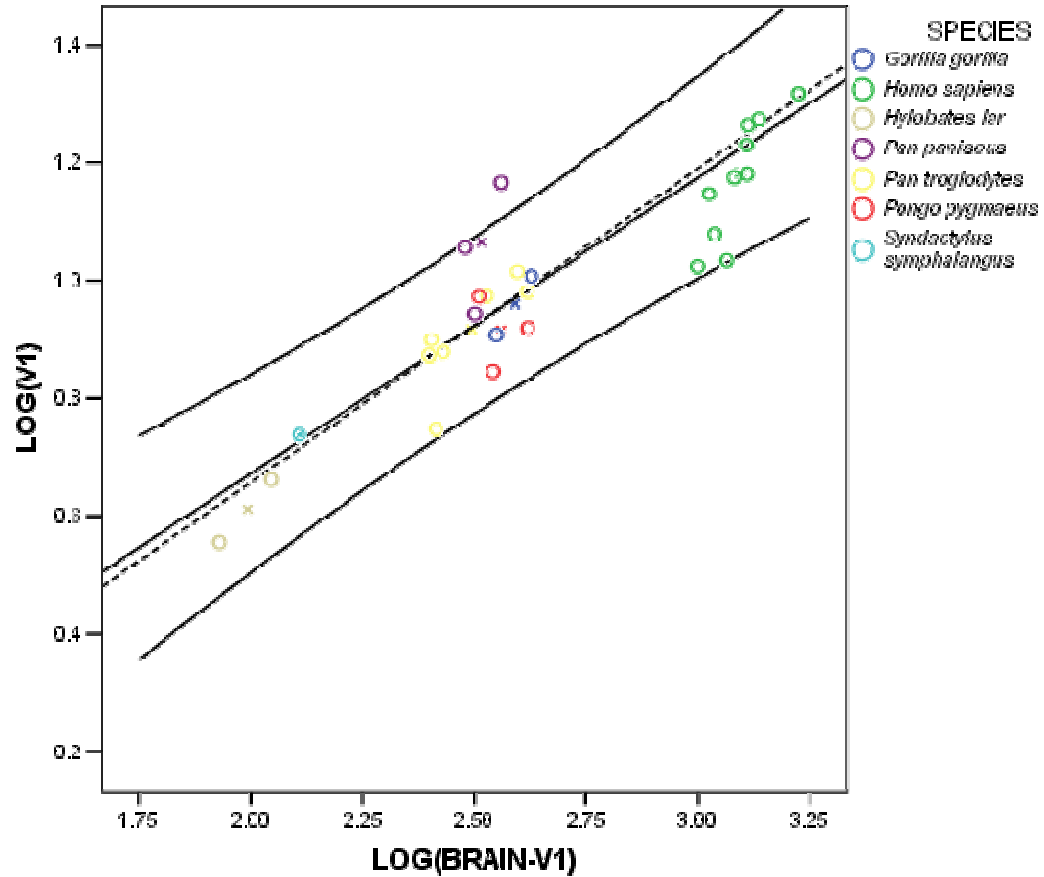
Fig. 5.8 Hominoid regressions of TIP data of V1 vol. as a function of brain-V1.vol.
The solid lines are the OLS regression, with upper and lower 95% prediction intervals. The dashed line is the RMA regression.
The human mean was included in the calculation of the regression equations.
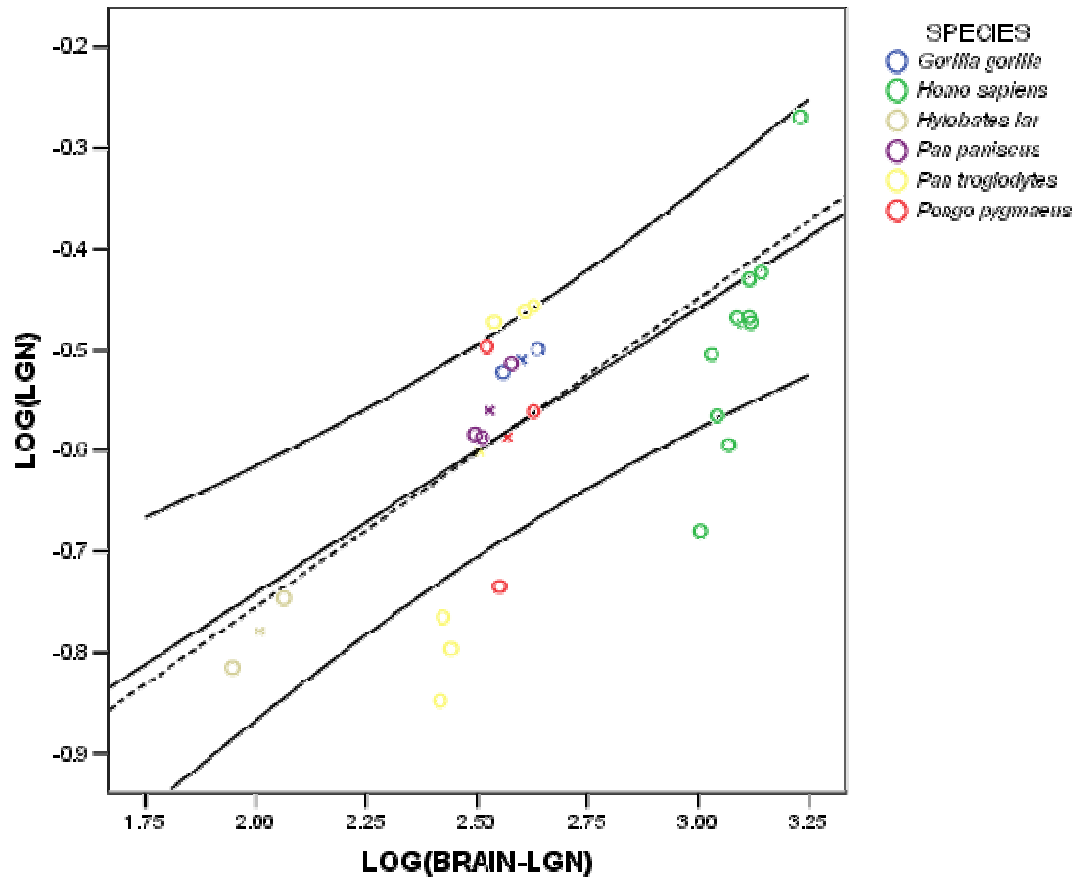
Fig. 5.9 Hominoid regression of TIP data of LGN vol. as a function of brain-LGN vol.
The solid lines are the OLS regression, with upper and lower 95% prediction intervals. The dashed line is the RMA regression.
The human mean was included in the calculation of the regression equations.
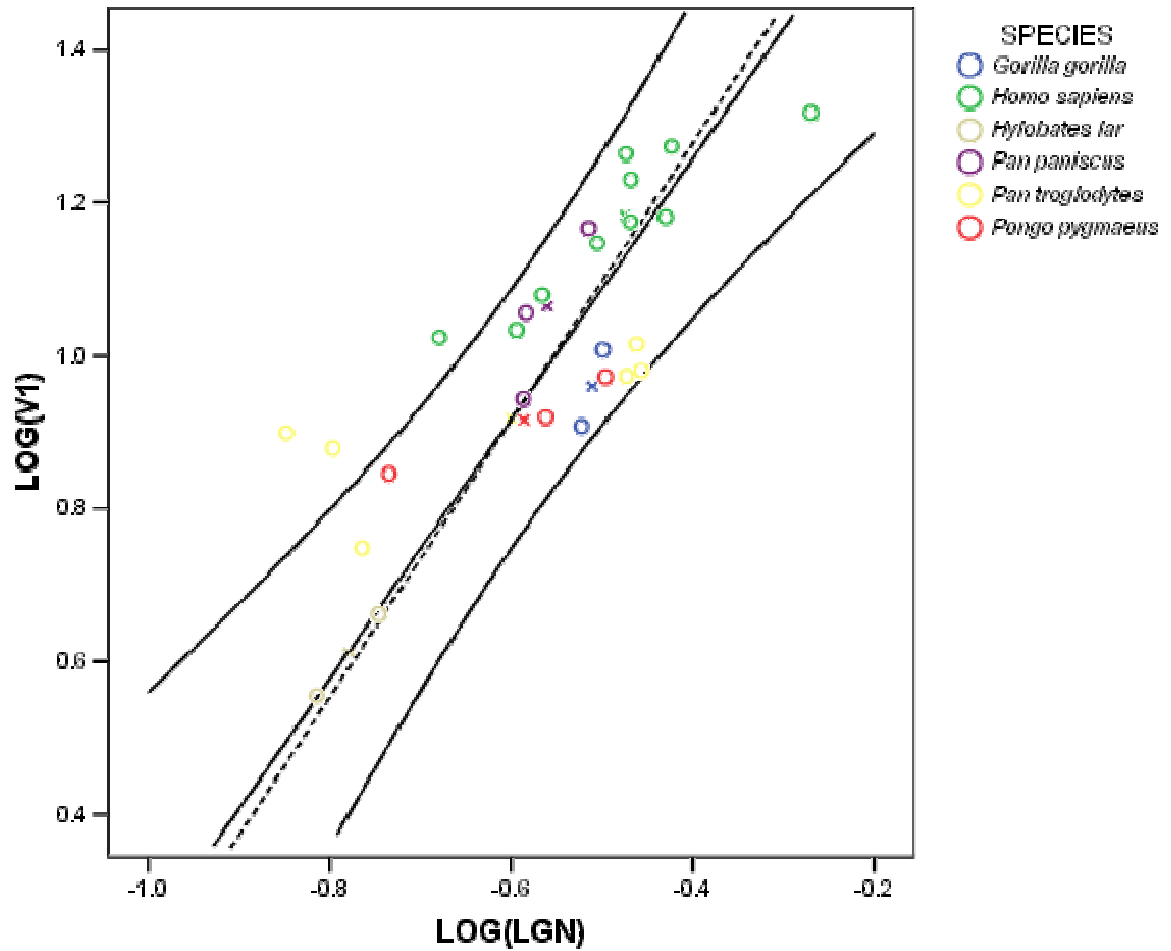
Fig. 5.10 Hominoid regressions of TIP data of V1 vol. as a function of LGN vol.
The solid lines are the OLS regression, with upper and lower 95% prediction intervals. The dashed line is the RMA regression.
The human mean was included in the calculation of the regression equations.

Chapter 6. Lamination of the Lateral Geniculate Nucleus in Catarrhines

6.1 Introduction

The morphology of the dorsal lateral geniculate nucleus (LGN) of the thalamus varies between primate groups (Kaas JH and MF Huerta, 1988; Kaas JH *et al.*, 1978). In addition, there have been some reports of variation in LGN laminar pattern within hominoids (Armstrong E, 1979; Chacko L, 1955; Kanagasuntheram R et al., 1969; Tigges J and M Tigges, 1987). Little is known about how these variations in LGN lamination may related to species-specific adaptations. Although the LGNs of humans and macaques have been well studied, the laminar pattern of other catarrhines requires further documentation. The LGN lamination patterns have not been well documented for the Colobinae, most hylobatid species, orangutans, and bonobos. The aim of this study was to determine the number of LGN parvocellular leaflets in catarrhine species for which the number is unknown, so as to better understand the evolution of the LGN within hominoids. These data are used to explore the possible evolutionary origins of different LGN laminar patterns in the catarrhines. In particular, an evolutionary approach is used to help determine whether the laminar patterns found in humans and macaques are in fact

homologous, and whether deviations from the human-macaque pattern might reflect species-specific adaptations.

The current study examined the dorsal part of the LGN, which is laminated, and which is most often just called the LGN, but is also known as the dLGN (dorsal lateral geniculate nucleus), LGBd (dorsal lateral geniculate body), or CGLd (corpus geniculatus lateralis dorsalis). Therefore, this study excludes the unlaminated anterior LGN, known as LGNv (ventral LGN) or PG (pregeniculate nucleus) (Fig. 6.1).

Generally, the LGN of macaques and humans is said to be comprised of six principle layers (Fig. 6.2), numbered from the most ventral to the most dorsal. The two most ventral layers (layers 1 and 2) are magnocellular, being comprised of large, darkly stained cells. The next four layers (layers 3-6) are parvocellular and are comprised of medium, more lightly stained cells. Parvocellular (P) and magnocellular (M) layers belong to two different retinogeniculocortical pathways, which process different aspects of visual input. The M pathway carries high-contrast visual information, including information about motion. The P pathway carries information about color and fine structure. Each pathway is comprised of a distinct group of nerve fibers originating from retinal ganglion cells and terminating in the lateral geniculate nucleus (LGN) of the thalamus. The M pathway originates in the large, sensitive parasol ganglion cells of the retina, which primarily get inputs from rods, and which synapse in the magnocellular (i.e., large-celled) layers of the LGN, and then project to layer 4Cα of cortical area V1. The P pathway originates in the small, numerous midget ganglion cells of the retina, which primarily get inputs from cones (see below), and which synapse on the

parvocellular (i.e. small-celled) layers of the LGN, which then project to layer 4Cβ of V1 (Leventhal AG *et al.*, 1981; Rodiek RW, 1988).

The nomenclature used here was introduced by Kaas et al. (1978) and is based on cell type and location, with the intention of recognizing homologous layers across species. According to this numbering scheme, the LGNs of all primates have two magnocellular layers (ME – magnocellular external and MI - magnocellular internal) and two parvocellular layers (PE – parvocellular external and PI – parvocellular internal). Further subdivisions of the parvocellular layers are called "leaflets". Therefore, parvocellular layers 3-6 are better described as two parvocellular layers that are divided into four leaflets, as the leaflet pairs are fused rostrally (Kaas JH *et al.*, 1978). Sometimes the leaflets are further subdivided into divisions called subleaflets.

In addition to parvocellular and magnocellular layers, it should be noted that there exist layers superficial to the magnocellular layers, called S layers. These are small layers with more poorly known functions and are not examined in detail here, but they should be acknowledged so as to avoid confusion with adjacent magnocellular layers (e.g., Balado M and E Franke, 1937; Kanagasuntheram R *et al.*, 1969).

In a primate LGN with two parvocellular layers, one layer receives retinal input from the ipsilateral eye, and the other receives retinal input from the contralateral eye. When the parvocellular layers are further subdivided into leaflets, the leaflets are interdigitated such that a leaflet receiving retinal input from the ipsilateral eye is adjacent to a leaflet receiving inputs from the contralateral eye. Therefore, the distinction Kaas et al. (1978) make between "layers" and "leaflets" is important because although in two dimensional cross-sections macaques appear to have a total of 6 layers, of which 4 are P

layers and 2 are M layers, three-dimensional modeling of the LGN shows that pairs of P

layers receiving input from the ipsilateral eye are actually continuous with each other

(Erwin E et al., 1999).

6.2 Materials and methods

Coronal and sagittal sections from adult specimens of humans (*Homo sapiens*),

four great ape species (*Pan troglodytes, Pan paniscus, Gorilla gorilla*, and *Pongo*

pygmaeus), three lesser ape species (*Hylobates lar, Hylobates muelleri, Symphalangus*

syndactylus) six cercopithecine species (*Cercopithecus kandti, Cercopithecus mitis,*

Miopithecus talapoin, Erythrocebus patas, Macaca mulatta, Macaca fascicularis) and

four colobine species (*Nasalis larvatus, Pygathrix nemaeus, Procolobus badius, and*

Colobus angolensis) were investigated for LGN lamination pattern. For each specimen,

sections stained for Nissl substance with either silver or cresyl violet were examined. A

minimum of one left hemisphere was investigated per species, although both right and

left hemispheres were investigated for most specimens (the exact number of specimens

per species is indicated in table 2).

Because the number of layers or leaflets is not constant throughout the anterior-

posterior extent of the LGN, the entire span of the LGN was investigated in each

specimen to determine the maximum number of distinct parvocellular leaflets in a

coronal section. Leaflets were considered distinct if they were separated by a sharp,

soma-poor gap. Such interlaminar zones could be distinguished from the LGN

representation of the optic disc, which is also a type of gap but its orientation does not

follow the laminar pattern. Often, there is no interlaminar space between magnocellular and parvocellular layers, but these two categories of layers were easily distinguished on the basis of location, staining intensity, and cell size. Note that potential "hidden layers" may exist (see discussion), however, because these are not known to exist in catarrhines, and are not visible in the available Nissl stained material, they could not be accounted for in the present study.

These results are interpreted in an evolutionary context as plotted on a catarrhine phylogenetic tree including the key monophyletic groups discussed here, based on several morphological and molecular phylogenies (Purvis A, 1995; Roos C and T Geissmann, 2001, 2001; Ruvolo M, 1997; Ruvolo M et al., 1991; Sterner KN et al., 2006; Takacs Z et al., 2005; Tosi AJ et al., 2003; Xing J et al., 2005). The character plotted is "parvocellular laminar pattern", and the character states in which it occurs are "four parvocellular leaflets" or "two parvocellular layers". The polarity of the character was not determined *a priori* because it is not clear which, of either of these, best represents the ancestral catarrhine state. The maximum parsimony method was used to estimate tree topology.

6.3 Results

A summary of the results of previous studies are shown in Table 6.1, and the results of the current investigation are shown in Table 6.2. Most of the current results are consistent with earlier observations about LGN lamination. However, the current study presents some clarifications and new data, which are discussed below.

In the current sample, the presence of leafleting was not found to vary polymorphically within species. However, in those species in which leafleting occurred, it was found that some but not individuals had further divisions of the parvocellular layers into subsidiary layers. Therefore, all catarrhine parvocellular laminar patterns fall into either the "four parvocellular leaflets" or "two parvocellular layers" categories.

In Fig. 6.3, two equally parsimonious phylogenetic trees are displayed on which species are color-coded to indicate the dispersal of two main parvocellular LGN patterns within the catarrhines. The two trees differ in character polarity, that is, one assumes that the catarrhine ancestral condition is "four parvocellular leaflets", whereas the other assumes that it is "two parvocellular layers". Catarrhine parvocellular patterns are summarized here per monophyletic group. In the hominoid superfamily, both patterns were observed. All four African hominoid species sampled (humans, chimpanzees, bonobos, and gorillas) had four parvocellular leaflets. Two groups had only two parvocellular layers: the orangutans and the hylobatid clade (gibbons and siamangs). Also within the cercopithecoid superfamily, both patterns were observed. All cercopithecine species had four parvocellular leaflets. The colobines were variable: in the presbytin clade, the proboscis monkey (*Nasalis larvatus*) had four parvocellular leaflets, although the red-shanked douc (*Pygathrix nemaeus*) had two parvocellular layers; in the colobin clade, the Angolan colobus monkey (*Colobus angolensis*) had four parvocellular leaflets, whereas the red colobus monkeys (*Procolobus badius*) had two parvocellular layers

It should be noted that the observations made here on orangutans and siamangs are in conflict with some earlier reports: in the current study, both species were found to

have two undivided parvocellular layers. Because studies of LGN lamination have been controversial or entirely nonexistent for orangutans, bonobos, siamangs, and colobines, specimens belonging to each of these groups are illustrated here (Figs 6.4-6.8). For *Hylobates lar*, tracings of the lamina are labeled using both the traditional nomenclature and that of Kaas and Huerta (1978; Fig 6.9). In addition, examples of images from other species investigated are shown for comparative purposes.

6.4 Discussion and conclusions

This study is the first to document and compare the morphology of the LGN in all living hominoid species, and representatives of all catarrhine subfamilies. In the current study, it was found that two main patterns of LGN parvocellular lamination occur within the Catarrhini: two parvocellular layers in some species, and four parvocellular leaflets (with occasional subleaflets) in other species. The phylogenetic distribution of these two conditions on the catarrhine consensus phylogeny indicates that there is some homoplasy.

Because macaques are the usual primate model in neuroscience studies, neuroanatomical studies rarely venture further than comparisons between macaques and humans. As a result, any similarities found between macaques and humans are by default treated as homologous characters. The lamination of the LGN is a good example of the diversity that exists within the catarrhine clade.

6.4.1 Comparison to previous studies of catarrhine LGN lamination

In previous studies, several catarrhine species have been demonstrated to have an LGN lamination pattern of two parvocellular layers further divided into four leaflets.

These include humans (Balado M and E Franke, 1937), chimpanzees (Chacko L, 1955; Tigges J *et al.*, 1977), gorillas (Nakagawa S et al., 1998), and several cercopithecine monkeys (Kaas JH *et al.*, 1978).

Prior to the current study, the only hominoids documented to have an LGN laminar pattern of two undivided parvocellular layers were the lar gibbons (*Hylobates lar*), and the silvery gibbons (Hylobates moloch; Tigges J and M Tigges, 1987). In addition, one other catarrhine species, *Procolobus badius*, was documented as having two undivided parvocellular LGN layers in Schulz (1967), but this rather obscure report has been overlooked and the laminar pattern of the cercopithecines has been generalized to all Old World monkeys (Kaas JH and MF Huerta, 1988; e.g., Kaas JH *et al.*, 1978).

There has been some confusion about the laminar pattern of orangutans and siamangs. The orangutan LGN has been previously described as displaying a pattern of four parvocellular leaflets and two magnocellular layers (Armstrong E and GT Frost, 1988; Balado M and E Franke, 1937; but see Tigges J and M Tigges, 1987). Also, it was suggested that siamangs (*Symphalangus syndactylus*) have four magnocellular leaflets and two parvocellular layers (Kaas JH and MF Huerta, 1988; but see Kaas JH *et al.*, 1978; Kanagasuntheram R *et al.*, 1969). The discrepancy in these older data and the current observations of only two parvocellular layers seems to be due to differences in the identification of layer types (e.g., S layers probably identified as magnocellular layers) and examination of the full rostrocaudal extent of the LGN.

In some species, there are reports of individual specimens in which LGN parvocellular layers are comprised of six fully developed subleaflets, or in some cases, less developed partial subsidiary lamination. Species for which there have been reports

217

of subleaflets or other subsidiary lamination of the parvocellular layers of the LGN include *Homo sapiens* (Hickey TL and RW Guillery, 1979), *Pan troglodytes* (Tigges J *et al.*, 1977), *Macaca mulatta* (Le Gros Clark WE and GG Penman, 1934), *Macaca fascicularis* (O'Brien BJ et al., 1997)*, Papio ursinus* (Campos-Ortega JA and WR Hayhow, 1970), *Mandrillus sphinx* (Kaas JH and MF Huerta, 1988), and *Cercopithecus aethiops* (Kanagasuntheram R *et al.*, 1969). For some species, so few individuals have been examined that it is possible that the subleafleting is actually the predominant condition for the species. In fact, the high incidence of cases of subleafleting in humans has been indicated as a potential specialization, perhaps due to a general pattern of increased variability that follows an increase in brain size; or due to relaxation of selection pressures which in other species constrain LGN morphology (Hickey TL and RW Guillery, 1979).

Although Nissl-stained sections are usually sufficient for demonstrating the lamination pattern of the LGN in primates, the possibility of "hidden layers" can only be ruled out by tracing retinal inputs. Adjacent parvocellular layers receive opposite retinal inputs, as demonstrated by tracing studies. Although in most primate species parvocellular laminae are well separated by inter-laminar space, there are exceptions in the New World monkeys. Retinal projection tracing studies in squirrel and saki monkeys revealed four hidden parvocellular leaflets, despite the fact that these species exhibit a large parvocellular mass that cannot be clearly divided into layers in Nissl stained sections (Kaas JH *et al.*, 1978). Also, owl monkeys and marmosets appear to have two undivided parvocellular layers, but a small degree of hidden leafleting has been exposed in tracing studies (Kaas JH *et al.*, 1978). Although in all other primate species, retinal

tracing studies have confirmed observations about parvocellular lamination made on Nissl sections, it is possible the degree of lamination is underestimated when based only on cytoarchitectural examination.

Within the catarrhines, observations about LGN lamination patterns have been confirmed using retinal tracers in a variety of cercopithecines (Kaas JH and MF Huerta, 1988; Kaas JH *et al.*, 1978 and refs therein). Studies of retinal inputs to the LGN are rare in hominoids because such investigations require invasive procedures, but two individuals have been studied: one chimpanzee (Tigges J *et al.*, 1977), and one gibbon (Hylobates lar; Tigges J and M Tigges, 1987). There is currently no evidence of hidden parvocellular leaflets occurring within the catarrhine primates. However, the existence of hidden layering in the catarrhine outgroup, the platyrrhines, indicates it as a potential catarrhine ancestral state, and it may in fact occur as a primitive retention in some of the species for which tracing studies have not been done.

6.4.2 Phylogenetic implications

The current study has detailed the LGN lamination pattern among crown catarrhine primate species. However, it is difficult to analyze the evolution of the LGN in catarrhines, because the outgroup, the platyrrhines, have lamination patterns that are hard to fit into characters states comparable to those of the catarrhines (see Kaas JH *et al.*, 1978). For example, consider *Hylobates lar*, *Macaca mulatta*, and *Saimiri sciureus*, taxa for which retinal inputs to the LGN have been investigated. *Saimiri sciureus*, have a large, continuous parvocellular mass comprised of four "hidden" parvocellular leaflets. Although the presence of four parvocellular leaflets *in Saimiri sciureus*, resembles the

number of layers with alternating inputs in *Macaca mulatta*, the fact that the leaflets of squirrel monkeys are not all separated by interlaminar space, although those of *Hylobates lar* and *Macaca mulatta* are, makes it difficult to discern meaningful character states at this level. Further research is necessary in order to accurately identify homologous characters. For the purpose of the current study, only lamination patterns of catarrhines evident in cytoarchitecture are considered.

Kaas et al. (1978) speculated that the last common ancestor of anthropoid primates had an LGN lamination pattern that included two undivided parvocellular layers. They suggested that the occurrence of leaflets which are separated by interlaminar space is a primitive catarrhine characteristic, and that the lack of leafleting in hylobatids is most likely an autapomorphy because it is more parsimonious for leafleting to have been lost once than to have developed independently in hominoids and cercopithecoids (Kaas JH *et al.*, 1978).

However, they also point out that hylobatids (and, based on the present study, colobines and orangutans as well) have the simplest and most primitive-looking LGN lamination pattern (Kaas JH *et al.*, 1978). In fact, the only other primates with a similarly simple LGN lamination pattern are the tarsiers. The strepsirrhine primates (galagos, lorises and lemurs) also have only two parvocellular layers and two magnocellular layers, but they exhibit two dominant koniocellular layers visible on Nissl stained material as well.

In light of the new data presented here, it is equally parsimonious to explain the LGN laminar pattern of hylobatids as a retention of the primitive catarrhine pattern, or as the ancestral condition of the hominoid clade, retained in hylobatids and orangutans but

lost in the African hominoids (Fig. 6.3). This finding is not insignificant. Macaques are

used in translational research as a model to better understand the human LGN. The fact

that the laminar patterns of these two taxa might not be derived from a common ancestor

means that extrapolations from macaques to humans of LGN laminar function should be

made with caution.

6.4.3 Functional implications

It is possible that hylobatids, orangutans, and some colobines possess the

primitive LGN lamination pattern and that African apes, cercopithecines, and other

colobines independently evolved greater parvocellular interdigitation. This is also the

simplest explanation in terms of functional and adaptive significance. The alternative

hypothesis, that LGN parvocellular lamination was reduced in these species, would have

to be explained by relaxation of selective pressures that might have lead to a loss of

parvocellular inputs related to color vision. If an LGN with two undivided parvocellular

layers is the primitive condition, why would a pattern of four parvocellular leaflets

develop in the African ape and human clade, the cercopithecine clade, and in some

colobine species? While the functional significance of leafleting is not very well

understood (Campos-Ortega JA and WR Hayhow, 1970; Kaas JH and MF Huerta, 1988;

Kaas JH *et al.*, 1978), available evidence suggests that layering and leafleting might be

related to the thickening of the parvocellular mass (Kaas JH et al., 1972). Because

leaflets alternate with regard to retinal input, Kaas et al. (1978) have suggested that they

probably exist to facilitate inter-ocular interactions. A reduction in the thickness of

parvocellular layers is achieved by splitting each thick parvocellular layer into two

thinner leaflets. This would shorten the distance between neurons receiving inputs from different eyes, and thus facilitate inter-ocular interactions (Kaas *et al.* 1978). Thus, in species with relatively increased parvocellular mass related to enhanced processing capacities for color vision, increased leafleting might be a mechanism to retain optimal inter-ocular interaction.

The amount of LGN tissue delegated to parvocellular and magnocellular inputs varies within primate species, and is related to activity pattern and ecology. Diurnal primates have a proportionally larger parvocellular part of the LGN than do nocturnal primates (Hassler R, 1966), presumably because diurnal species rely more on information of the parvocellular pathway, such as color vision. Similarly, it has been hypothesized that increased lamination through leafleting may be related to improved color vision (Tigges J and M Tigges, 1987).

Physiological studies of lamination in macaques have indicated that leaflets are functionally specific. In rhesus macaques, blue-sensitive cells are found primarily in the ventral-most parvocellular leaflets, PI(LI) and PE(LI) (Schiller PH and JG Malpeli, 1978). The ventral-most pair of parvocellular leaflets also have cells that respond mostly off-center, where as the dorsal parvocellular leaflets PE(LE) and PI(LE) respond mostly on-center (Schiller PH and JG Malpeli, 1978). Interestingly, the pairing of function is patterned by location, and not retinal projection, and therefore functional groups cross parvocellular layers, such that the internal leaflets of PE and PI group together, and the external leaflets of PE and PI group together. Central vision is represented in the segment of the LGN having four parvocellular leaflets in macaques, whereas peripheral vision is represented in the part with just the two undivided layers (Malpeli JG and FH

Baker, 1975), therefore the additional layers may reflect an increased dedication to central vision.

Prior to the present study, it had only been demonstrated that hylobatids (and potentially orangutans) depart from the typical catarrhine LGN lamination pattern, so this taxon has been contrasted from other catarrhine species in this regard. In fact, because it remains the only catarrhine species for which tracing studies confirm two undivided parvocellular layers, it remains possible that the hylobatid laminar pattern is unique among catarrhines. Tigges and Tigges (1987) relate the lamination of gibbons to several aspects of behavior and physiology. It has also been suggested that gibbons are missing the two ventral parvocellular layers, which are important in color vision due to the predominance of blue sensitive cells (Schiller PH and JG Malpeli, 1978). In support of this hypothesis, there is evidence of poor blue discrimination in gibbons (Tigges J, 1963) and a higher rod to cone ratio in gibbons than in rhesus macaques (Polyak S, 1957; Rohen J, 1962).

Also, it has been suggested that the relatively decreased lamination of the gibbon LGN probably does not have a negative effect on other visual functions such as motion detection (Tigges J and M Tigges, 1987). Gibbons require especially highly developed neural substrates of motion detection because they are they are arboreal brachiators which move quickly in a complex three-dimensional environment. Changes in the parvocellular layers are not expected to have a negative effect on motion detection, particularly because it is the magnocellular layers that are the primary conduit of this category of visual information.

Finally, it is interesting to consider how the difference in LGN lamination may relate to the behavioral differences among species of cercopithecoid monkeys. The parvocellular layers of the LGN are involved in color vision. It has been hypothesized that trichromatic color vision, which occurs on all catarrhine species, evolved in catarrhines as a result of either frugivorous (Mollon JD, 1989; Sumner P and JD Mollon, 2000) or folivorous (Dominy NJ and PW Lucas, 2001; Lucas PW *et al.*, 1998) behavior. In fact, the cercopithecoid species with four parvocellular leaflets include both primarily frugivorous cercopithecines and some primarily folivorous colobines. Also, it has been argued recently that *all* catarrhines, including colobines and gibbons (contra Tigges J and M Tigges, 1987) are identical in terms of spectral sensitivity (Deegan JF and GH Jacobs, 2001; Jacobs GH and JF Deegan, 1999). Therefore, any potential difference in color vision would have to be at a post-retinal level.

Traditionally, the LGN is considered a relay nucleus for retinal inputs on their way to the cerebral cortex (Kaas JH *et al.*, 1972). However, recent studies have shown that the human LGN receives inputs from the striate cortex, the thalamic reticular nucleus, and the brainstem; in fact, only 10% of its inputs originate from the retina (Kastner S et al., 2006). Therefore, the LGN is in a strategic position to serve as "gatekeeper" which modulates attention to visual stimuli.

Further, contrary to the previous belief that the LGN only projects to the primary visual area, it has now been demonstrated in two macaque species that the cortical area MT, involved in motion detection, receives a direct LGN input (Sincich LC *et al.*, 2004). These LGN neurons are primarily (70%) located in intercalated layers between the magnocellular and parvocellular layer, with others scattered throughout parvocellular and

magnocellular laminae. Some, but not all, of theses neurons are thought to belong to the koniocellular pathway, inclusion in which is determined by immunostaining for the α subunit of type II Ca^{24}/ calmodulin-dependant protein kinase.

These new findings suggest that the role of the LGN is much more complicated than previously thought. It is interesting to consider that LGN lamination may be related to higher level processing of, for example, parvocellular inputs. In such an example it is possible that 1) the LGN acts as a modulator of parvocellular information, for example, a filter of information related to trichromatic color vision and/or 2) there may be taxonomic differences in the existence of intercalated neuronal populations which may even have direct inputs to higher order, more functionally specific visual cortical areas.

6.4.4 Methodological considerations

The foregoing conclusions should be considered preliminary because of the methodological limitations of this study. Importantly, it was not feasible to reveal the source of retinal input to each LGN layer, and thereby reveal possible "hidden" layers. Because hidden lamination at the level of leaflets or subleaflets hae not been observed in catarrhines thus far, the existence hidden layers in the catarrhines would seem unlikely, but should not be ruled out Therefore, in species for which retinal tracings to the LGN have not been studied the number of leaflets should be taken to be a minimum number. Perhaps the findings here will be confirmed if and when it becomes feasible to use non-invasive methods such as diffusion tensor MRI to study LGN structure and connections in ape species.

Although the samples used in the current study are relatively small, it is important to note that they are significantly improved from previous studies of the LGN in hominoids. Although within-species variation may occur at the level of subsidiary lamination such as subleaflets, at the level of layers and leaflets LGN lamination seems to be standard within species, making it is unlikely that larger samples would have any effect on the general findings made here.

In summary, the increased lamination of parvocellular layers, a parallel occurrence in the African hominoids, cercopithecines, and some colobines, may be functionally relevant. An increased amount of, or better differentiation of parvocellular layers may relate to color vision or to improved perception of central (versus peripheral) vision the more laminated taxa. Alternatively, increased lamination may simply provide more inter-laminar space for neuronal populations which do not participate in the parvocellular and magnocellular geniculocortical pathways, but, rather have direct extrastriate inputs, for example, related to motion detection.

Table 6.1 Summary of previous studies reporting the number of parvocellular leaflets in catarrhine species

Species	number of parvocellular layers and leaflets	publications	retinal projections studied	min no. specimens studied	subleafleting/ subsidiary
HOMINOIDEA					
Homo sapiens	4 leaflets	Balado and Franke 1932;		many	Y
Pan troglodytes	4 leaflets	Tigges et al, 1977	Y	1	Y
Gorilla gorilla	4 leaflets	Nakagawa et al., 1998	N	1	
Pongo pygmaeus	Insufficiently documented/conflicting	Balado and Franke 1937; Armstrong and Frost 1988; Tigges and Tigges 1987	N	1	
Hylobates lar	2 undivided layers	Chacko 1954; Armstrong 1979; Tigges and Tigges, 1987; Kanagasutheram et al. 1969	Y	4	
Hylobates moloch	2 undivided layers	Tigges and Tigges, 1987	N	1	
Hylobates agilis	2 undivided layers	Kanagasutheram et al. 1969	N	2	
Symphalangus syndactylus	Insufficiently documented/conflicting	Kanagasutheram et al. 1969	N	1	
CERCOPITHECOIDEA					
CERCOPITHECINAE					
Cercopithecus ascanius	4 leaflets	Schulz, 1967		1	
Cercopithecus aethiops	4 leaflets plus 2 subleaflets	Kanagasutheram et al. 1969			Y
Macaca rhesus	4 leaflets	Kaas et al., 1978	Y	many	
Macaca fascicularis	4 leaflets				Y
Papio ursinus	4 leaflets plus 2 subleaflets				Y
Mandrillus sphinx	4 leaflets plus 2 subleaflets	Kaas et al., 1972			Y
COLOBINAE					
Procolobus badius	2 undivided layers	Schulz, 1967		1	

Table 6.2 Current sample, in which the number of parvocellular leaflets observed in each specimen is indicated.

| Species	sex	age	number of parvocellular layers and leaflets	subleafleting/ subsidiary
HOMINOIDEA				
Homo sapiens	F	79	4 leaflets	
Homo sapiens	M	75	4 leaflets plus 2 subsidiary leaflets	Y
Pan troglodytes	NA	NA	4 leaflets	
Pan troglodytes	F	22	4 leaflets	
Pan troglodytes	F	24	4 leaflets	
Pan paniscus	F	11	4 leaflets	Y
Pan paniscus	F	2	4 leaflets	
Pan paniscus	F	25	4 leaflets	
Gorilla gorilla	M	JUV	4 leaflets	
Gorilla gorilla	F	20	4 leaflets	
Pongo pygmaeus	M	17	2 undivided layers	
Pongo pygmaeus	M	37	2 undivided layers	
Pongo pygmaeus	M	34	2 undivided layers	
Pongo pygmaeus	F	A	2 undivided layers	
Pongo pygmaeus	M	39	2 undivided layers	
Hylobates lar	F	22	2 undivided layers	
Hylobates lar	F	A	2 undivided layers	
Hylobates muelleri	M	18	2 undivided layers	
Symphalangus syndactylus	M	33	2 undivided layers	
CERCOPITHECOIDEA				
CERCOPITHECINAE				
Cercopithecus kandti	M	A	4 leaflets	
Cercopithecus mitis	M	A	4 leaflets	minor
Miopithecus talepoin	F	A	4 leaflets	
Miopithecus talepoin	M	A	4 leaflets	
Erythrocebus patas	F	A	4 leaflets	minor
Macaca rhesus	NA	A	4 leaflets plus 2 subsidiary leaflets	Y
Macaca fascicularis	M	3	4 leaflets	
COLOBINAE				
Nasalis larvatus	F	A	4 leaflets	
Pygathrix nemaeus	F	A	2 undivided layers	
Procolobus badius	F	A	2 undivided layers	
Procolobus badius	F	A	2 undivided layers	
Colobus angolensis	M	18	4 leaflets	
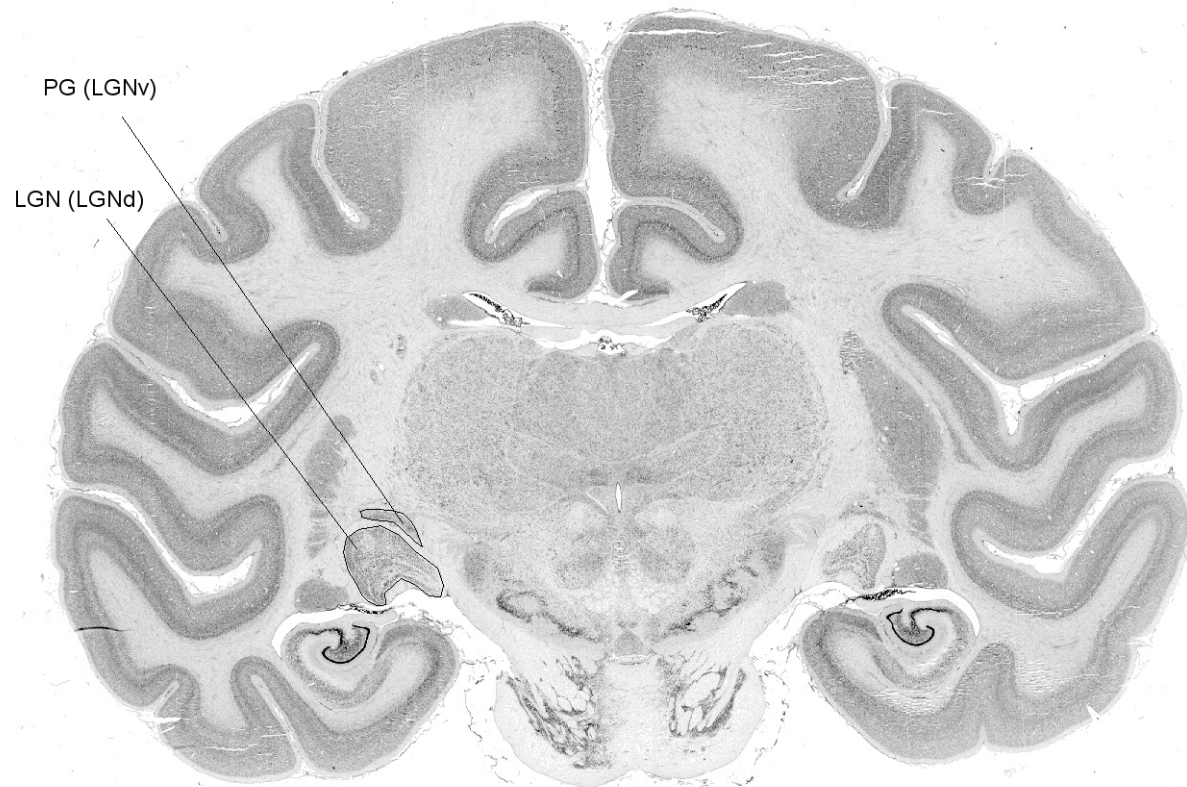
**Fig. 6.1 Coronal section through brain of *Macaca fascicularis* showing location of LGN and PG**
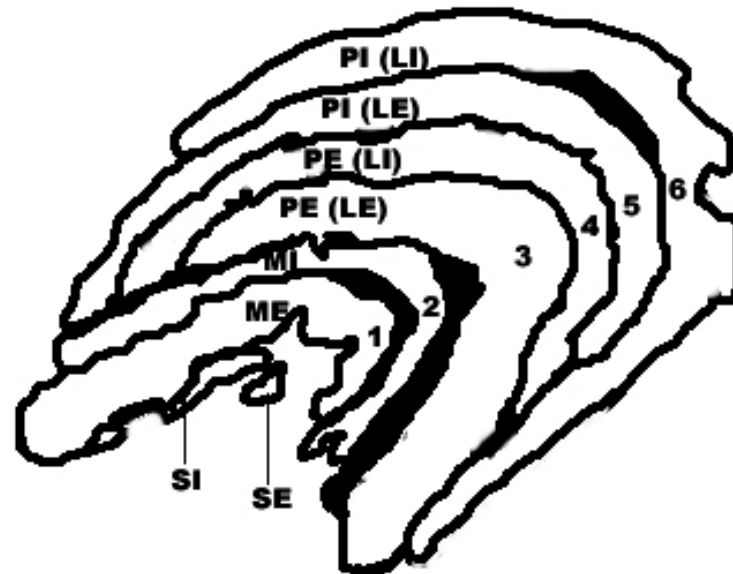
Fig. 6.2. Layers of the LGN in *Macaca fascicularis*.
Traditional (1-6) nomenclature is shown (left) and nomenclature after Kaas and Huerta (1978) is shown (right).
"PI" parvocellular internal; "PE" parvocellular external; "MI" magnocellular internal; "ME" magnocellular external;
"SI" superficial internal ; "SE" superficial external
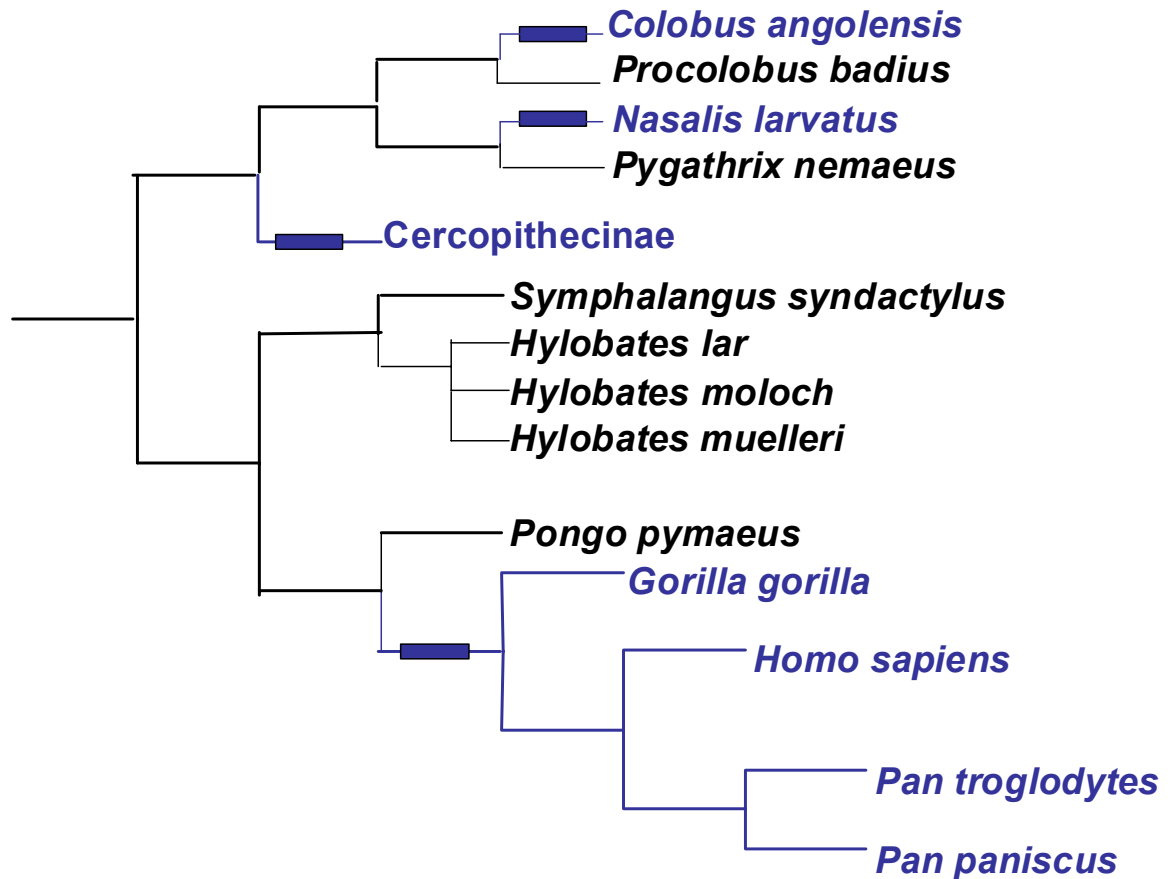
Fig. 6.3 Maximum parsimony analysis of changes in catarrhine LGN laminar pattern.
Changes in the LGN lamination pattern (character state changes) are indicated by bars. Phylogeny based on Ruvolo (1997); Roos and Geissman (2001); Smith and Cheverud (2002); Tosi et al. (2003); Takacs et al (2005); Xing et al. (2005); Sterner et al. (2006) Both the first (**A**) and the second (**B**) hypotheses of character state evolution require an equal number (minimum of 4) character state changes within the catarrhine clade.

B

Colobus angolensis
Procolobus badius
Nasalis larvatus
Pygathrix nemaeus
Cercopithecinae
Symphalangus syndactylus
Hylobates lar
Hylobates moloch
Hylobates muelleri
Pongo pymaeus
Gorilla gorilla
Homo sapiens
Pan troglodytes
Pan paniscus
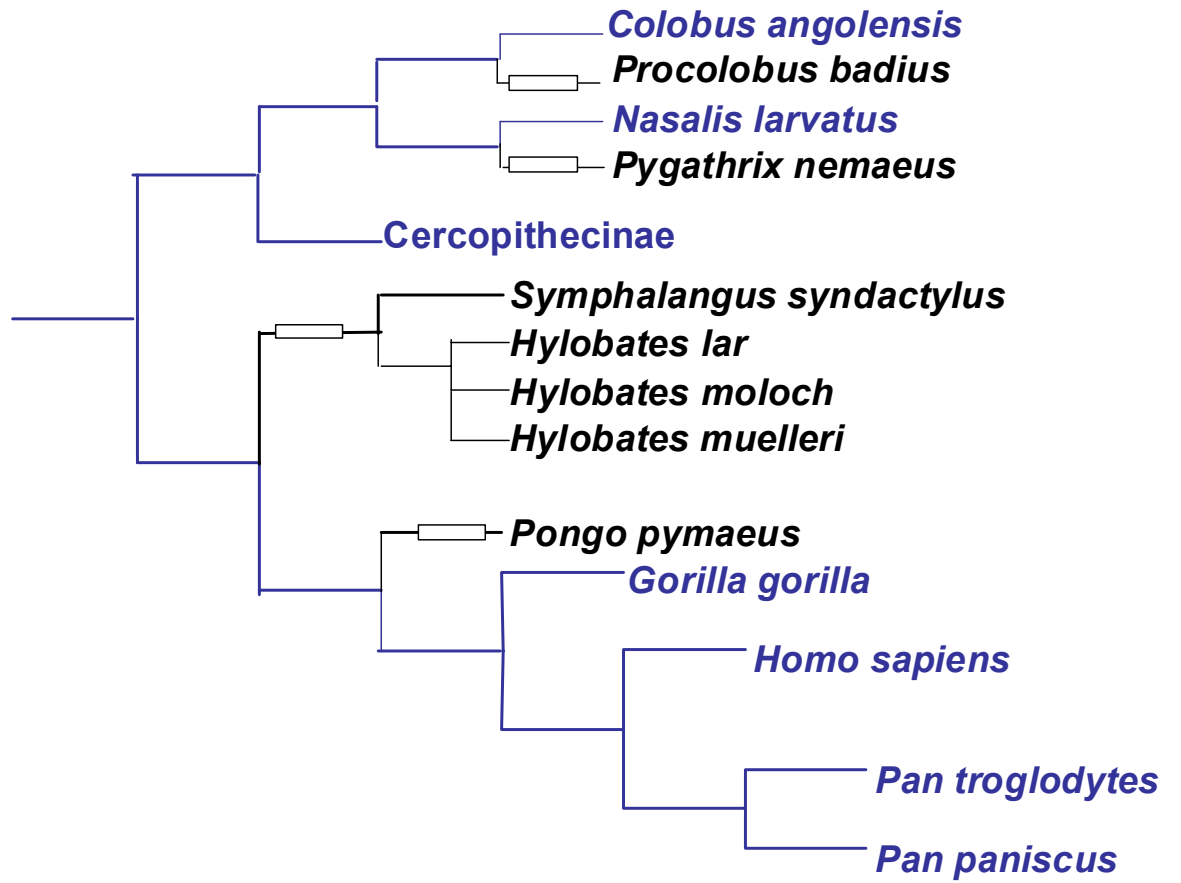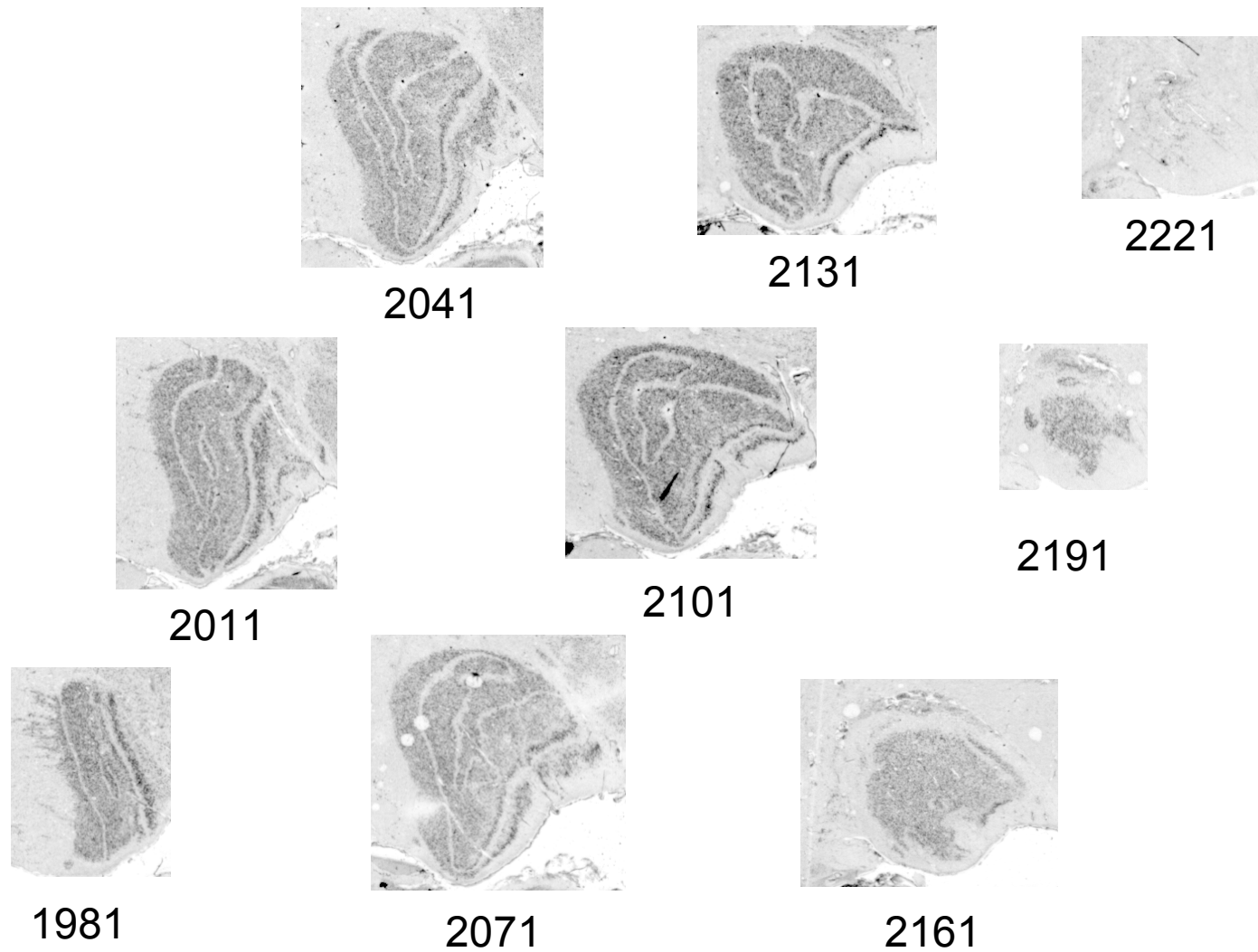
Fig. 6.4. Coronal sections through rostrocaudal extent of LGN in juvenile bonobo, 2 years old.
Section numbers listed below images (thickness = 20 μm).
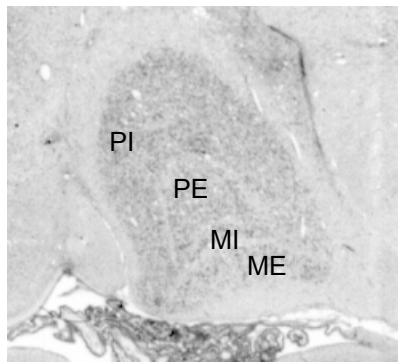
1540

1580

1501
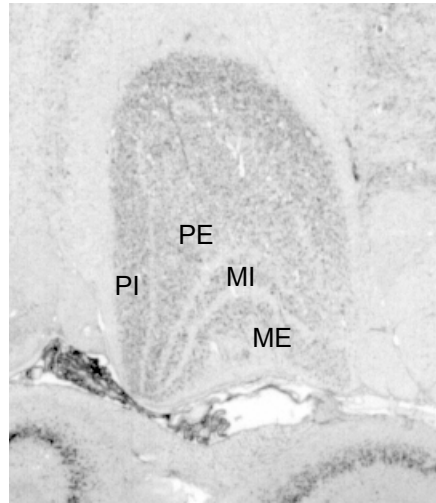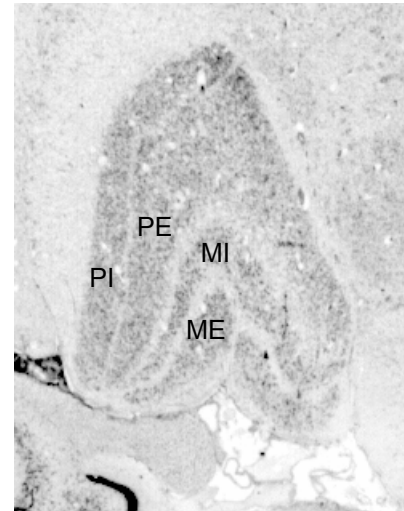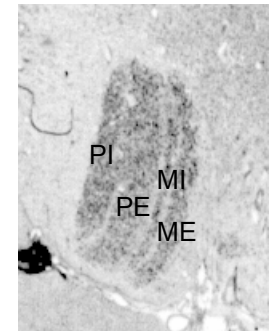
1620

Fig. 6.5. Coronal sections through lateral geniculate nucleus of a red colobus money (*Procolobus badius*). Section numbers listed below images (thickness = 20 μm).
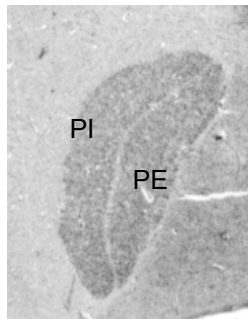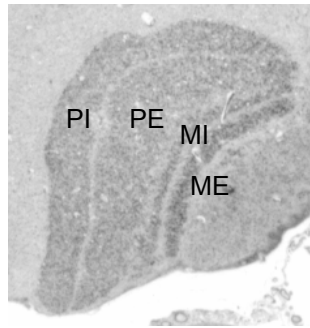
2206

2266

2146
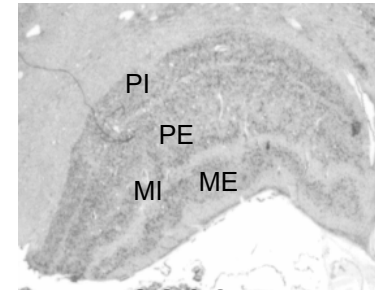
2086
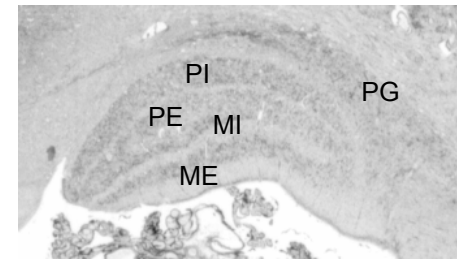
2326

Figure 6.6 Coronal sections through lateral geniculate nucleus of an orangutan (*Pongo pygmaeus*). Section numbers listed below images (thickness = 20 μm).
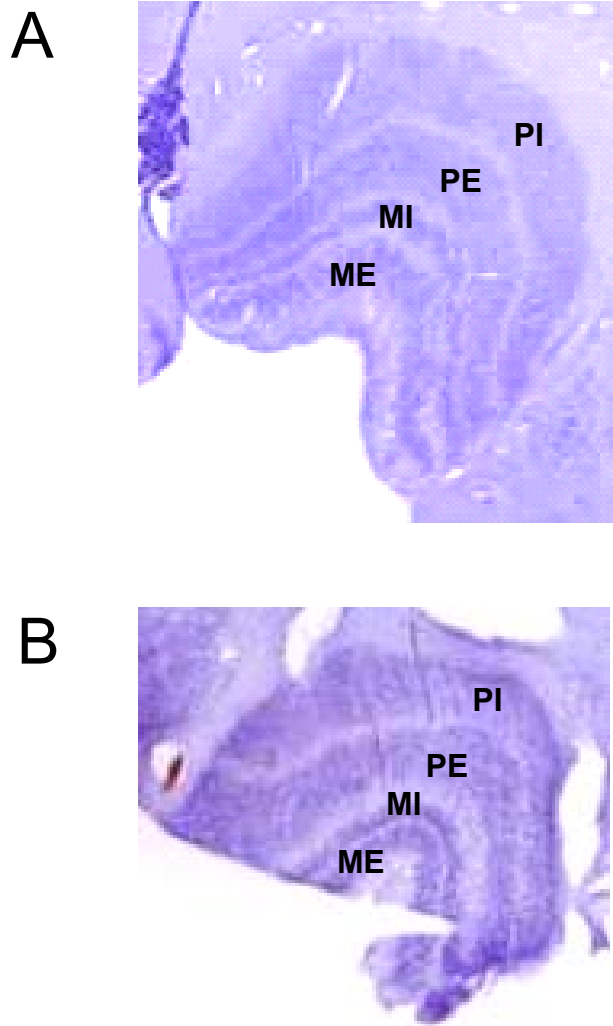
Fig. 6.7. Coronal sections through lateral geniculate nuclei of two different hylobatid species, *Hylobates muelleri* (A) and *Symphalanges syndactyles* (B).
Section thickness is 40 μm.
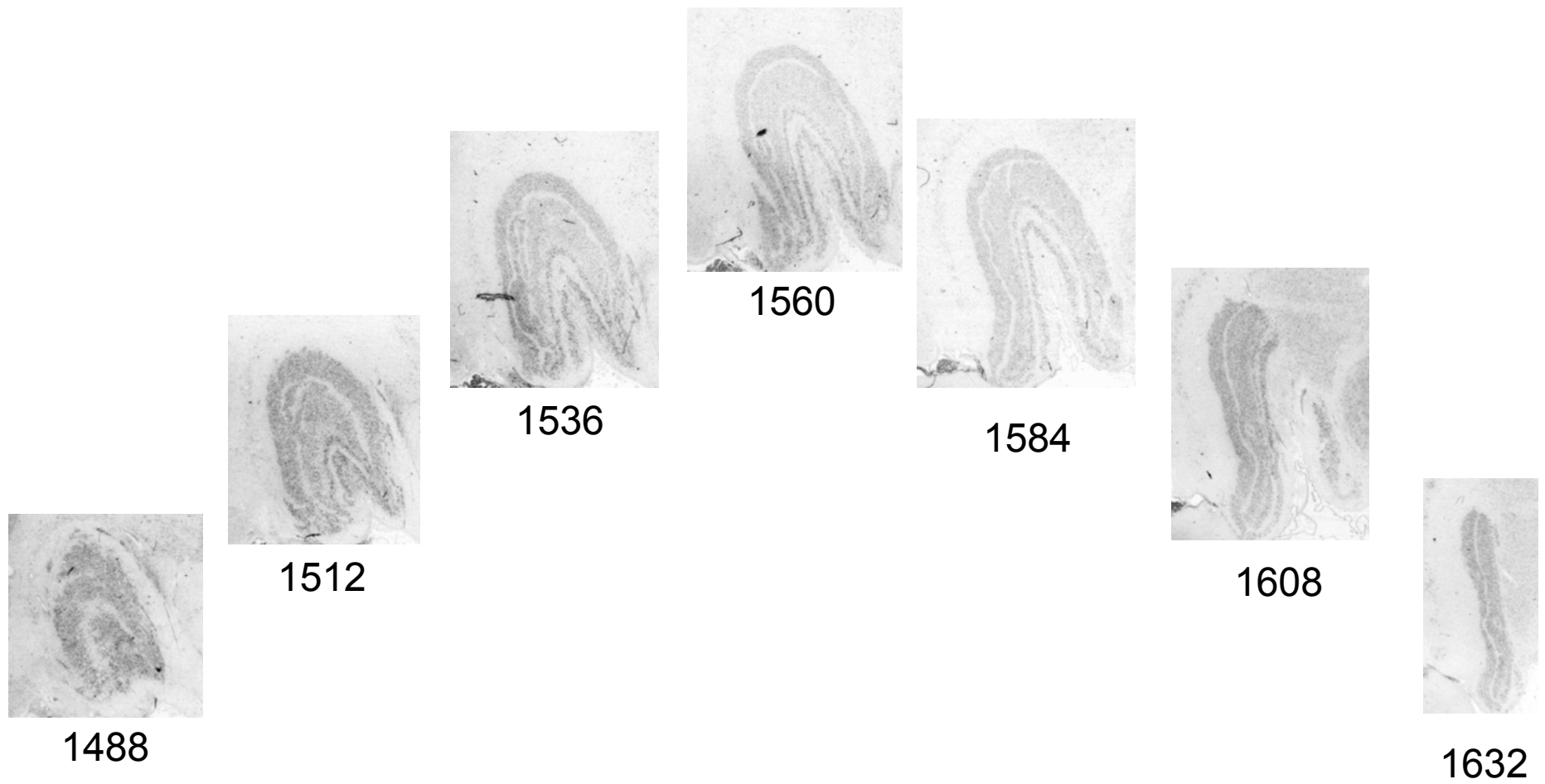
Fig. 6.8. Coronal sections through lateral geniculate nucleus of a proboscis money (*Nasalis larvatus*). Section numbers listed below images (thickness = 20 μm).
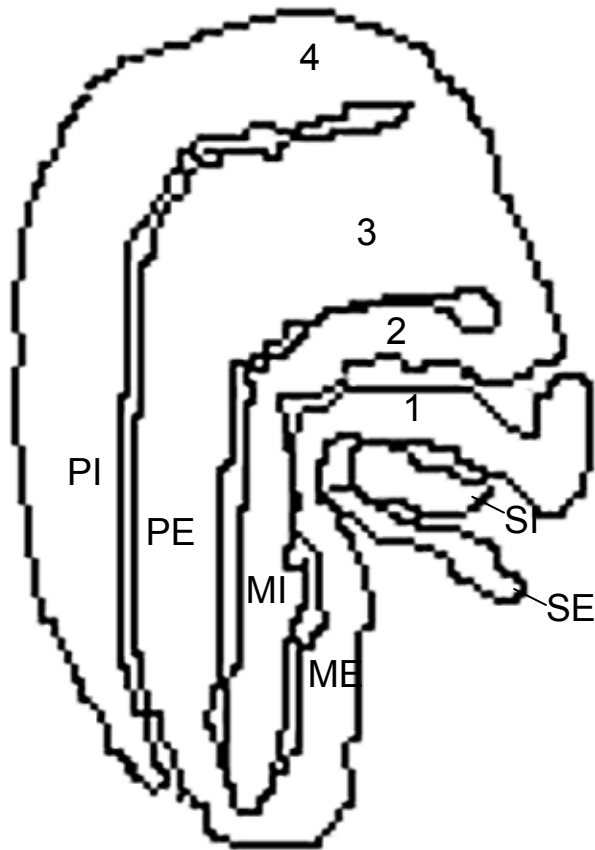
Fig. 6.9 Layers of the LGN in *Hylobates lar.*
Traditional (1-4) nomenclature is shown (left) and
nomenclature after Kaas and Huerta (1978) is shown (right).
"PI" parvocellular internal; "PE" parvocellular external; "MI"
magnocellular internal; "ME" magnocellular external; "SI"
superficial internal ; "SE" superficial external

Chapter 7. Conclusions

7.1 Reorganization in hominin visual brain structures

This dissertation set out to examine whether significant variation exists in the organization of the visual system in hominoid species, in particular whether humans are set apart in any aspect of their visual system. That is, are there differences in the histology, morphology or volumes of hominoid visual brain structures that cannot be explained by brain size scaling, and might indicate species-specific adaptations? As described in Chapter 2, a previous study (Preuss TM *et al.*, 1999) found that a) humans are the only species known to have a unique meshwork arrangement of M pathway fibers in layer IVA of V1, potentially related to improved luminance contrast and motion detection and b) hominoids lack a honeycomb like lamination of V1 layer IVB which is characteristic of cercopithecoids. Similarly, the current dissertation found that quantitative aspects of visual brain structure organization can distinguish humans from other primates, and can distinguish hominoids from cercopithecoids. Further, the visual system characteristics described here exhibited variation within hominoids. Most strikingly, African hominoids on the one hand, and *Pongo pygmaeus* and the hylobatids on the other, differed in the lamination of the LGN, as described in Chapter 7.

It has previously been proposed that human V1 is relatively reduced in comparison to brain size as a result of expansion of higher-order cortical regions of the posterior parietal cortex involved in complex functions such as tool making and language (Holloway RL, 1966; Holloway RL, 1968). That is, it was hypothesized that brain evolution acts on a mosaic of functionally specific units reacting differentially to selection pressures. In the case of humans, it was hypothesized that higher-order areas expanded at an unusually fast pace in humans, while primary areas maintained a slower rate of expansion, resulting in a large brain that is mostly devoted to higher order processing. The data collected in this thesis support the overall notion of mosaic evolution in hominoid brains.

7.2 Reorganization of panin visual brain structures

If the human V1 residual value does reflect a recent reduction in its volume, then the indication of an increase in the volume of V1 in bonobos (albeit based on a much smaller sample) are also worth consideration. First, it is important to consider that although the differences between observed and expected human and bonobo V1 values were of similar magnitude, but in different directions, bonobos overlap with humans in absolute V1 volume, and both species have large V1 volumes relative to their LGN volumes. Also, the low bonobo GLI values in areas V1, V2 and V3 were closer to the human values than were the higher values of other hominoids. Thus, not only is the bonobo V1 volume increased, but this seems to be related to an increase in the amount of space available for interneuronal connections. However, the bonobo GLI values in areas

240

10 and 13 are relatively higher (Semendeferi K *et al.*, 1998, 2001), and thus do not indicate that bonobos have a low volume fraction of cell bodies across all cortical regions. This is the first study of visual cortex to include bonobos, and further studies addressing the number, size and properties of bonobo visual cortex neuron populations will shed light on these differences. Interestingly, in one bonobo individual studied here (Zahlia) a large-for-a-hominoid V1 coexists with a small-for-a-hominoid area 13 (Semendeferi K *et al.*, 1998). Regardless of whether or not the volumes of these structures are directly related, the expansion of V1 and perhaps other visual areas may cause the total size of the visual cortex to dwarf the proportional size of all other brain regions, including area 13.

Organizational changes involving V1 size are thought to be linked to changes in parietal lobe volumes (Holloway RL, 1966). The arealization of the cerebral cortex is affected by both signaling molecule expression and neuronal inputs. Changes in the expression of transcription factors as well as differences in neuronal inputs can cause cortical areas to take on aspects of adjacent cortical regions. For example, fetal enucleation causes cortex normally destined to be V1 to resemble adjacent area V2 instead (Dehay C *et al.*, 1996). In *Emx2* mutant neonatal mice, the border between visual areas and somatosensory areas is shifted caudally (Bishop KM *et al.*, 2000). Similarly, it is speculated that subtle genetic, epigenetic and developmental differences could alter the relative proportions of V1 and nearby cortical areas in closely related species.

These aspects of bonobo brain organization are neither attributed to overall scaling effects, nor to phylogenetic effects. Differences in neural organization between bonobos and chimpanzees are predicted to correspond to observations about behavioral

differences between these species. As discussed in Chapter 5, bonobos have not been

observed to use tools in the wild to the same extant as chimpanzees. This may be related

to the notion that V1 reduction is linked to a proportional increase in the size of posterior

parietal areas activated in tool-making (Stout D and T Chaminade, 2007; Stout D et al.,

2008; Stout D *et al.*, 2000). Also, bonobos have been indicated as showing aspects of

morphological and behavioral neontony, and V1 volume is largest is human juveniles

(Sauer B, 1983).

7.3 System-level brain organization

The results of this dissertation suggest that although gross structure volumes tend

to scale to overall brain size, the microanatomical details of brain organization have more

specific scaling relationships. In Chapter 4, the volume fraction of cortical tissue

occupied by cell bodies in striate and extrastriate visual areas was found not to be

correlated with overall brain size, and yet to scale to the volumes of visual system

structures, particularly V1 volume. This implies that the properties governing the density

of neurons may depend specifically on the size of the visual system, or which ever other

system in which they are found. This suggests that there are local scaling relationships

which predominate versus global scaling constraints on aspects of neuronal connections.

Therefore, caution should be taken in interpreting results produced by pooling brain

tissue across multiple regions, as in the isotropic fractionator method (see for example

Herculano-Houzel S *et al.*, 2007). Previous reports of visual cortex neuron number

scaling to brain weight (e.g. Cragg BG, 1967; Sherwood CC, MA Raghanti *et al.*, 2007)

may actually be demonstrating indirectly that neuron densities scale to visual area volumes, and that these volumes in turn scale to brain weight. In area 9L, neuron density does not scale to brain weight in anthropoids (Sherwood CC *et al.*, 2006). Among hominoids, neither neuron density nor GLI values of areas 10, 13 and 4 scale to brain weight (Sherwood CC and PR Hof, 2007), but this is likely to be due to the low taxonomic level of comparison and/or small sample size. It would be interesting to investigate whether visual area neuron densities and GLI values more specifically scale to the area in which they are located – indicating a standard of total neuron number per cortical area – or whether they systematically scale to early and subcortical structures volumes which are indicative of total neuronal input.

7.4 Differences between hominoids and cercopithecoids in visual system and brain organization

It is becoming increasingly apparent that cercopithecoids and hominoids differ in aspects of visual system neuroanatomy, such as the lack of a dense cytochrome oxidase band and the presence of dark calbindin staining of cell bodies and neuropil in V1 layer 4A (Preuss TM and GQ Coleman, 2002; Preuss TM *et al.*, 1999) and decreased GABAergic interneurons frequencies in hominoid V1 and V2 (Sherwood CC, MA Raghanti *et al.*, 2007). In the present study, it was found that in cercopithecoids increases in V1 and LGN volumes accompanying encephalization scale at a steeper slope than in hominoids. In addition, some other hominoid neurological characteristics that set them apart from cercopithecoids include: the existence of Von Economo neurons in layer Vb

243

of the anterior cingulate cortex (Nimchinsky EA *et al.*, 1999) and the frontoinsular cortex (Hakeem A et al., 2004), the presence of calretinin immunoreactive pyramidal neurons in layer Vb of the anterior cingulate cortex and paracingulate cortex (Hof PR *et al.*, 2001), the presence of calretinin immunoreactive pyramidal neurons in primary motor cortex layer V (Sherwood CC, RL Holloway, JM Erwin, A Schleicher *et al.*, 2004), increased frequencies of parvalbumin immunoreactive pyramidal neurons in primary motor cortex layer V (Sherwood CC, RL Holloway, JM Erwin, A Schleicher *et al.*, 2004), and an expanded neocerebellum (MacLeod CE et al., 2003). A number of differences exist between the visual systems of humans and macaques (see Chapter 2), and it is possible that these are indicative of hominoid and cercopithecoid superfamily-level difference; it is also possible that they are not. Regardless, they indicate that a human brain is not simply a blown-up macaque brain, and provide excellent starting points for future projects which hope to attach neuroanatomical substrates to the behavioral differences known to exist between humans (or hominoids) and other species.

True, not all differences between human and monkey neuroanatomy indicate superfamily-level differences. For example, great apes differ from cercopithecoids and hylobatids in having Von Economo neurons (Nimchinsky EA *et al.*, 1999), and in having a clustered, coil-like organization of cholinergic, serontergic, and dopaminergic fibers in prefrontal areas 9, 32 and 4 (Raghanti MA et al., 2008; Raghanti et al. in prep, 2008), and many studies have not included hylobatids (e.g. Hof PR *et al.*, 2001; e.g. Preuss TM *et al.*, 1999). Further, apparent similarities between human and macaques may conceal the actual diversity of catarrhine phenotypes, as is the case with LGN lamination pattern, in which humans and macaques share four parvocellular leaflets. Although this similarity

facilitates equating macaque LGN layers with human LGN layers, the diversity found here (although it does not fall neatly along taxonomic limes) could indicate that the leafleting of macaques and humans is homoplastic and misleading. Such a finding takes on significance when one considers that most of our understanding of visual brain physiology is based on macaque research. Further research is planned to explore the details of catarrhine lamination pattern, by examining specimens in which histological markers are used to reveal populations of neurons and koniocellular layers not examined in Nissl stained material.

7.5 Variability in the organization of fossil hominin brains

Predictions about the neural organization of fossil species based on brain size alone have lead to the conclusion that observations of a posterior lunate sulcus on small-brained early hominins *must* have been misinterpretations (Armstrong E et al., 1991; Jerison HJ, 1975). But, as discussed in Chapter 3, hominin encephalization and reorganization is not a unilinear process, and other examples of fossil hominin species diverging from a linear evolutionary model from the *Pan-Homo* common ancestor to modern humans have been recognized.

Differences in hominoid visual brain structures point to issues in understanding the variation that exists in the hominin fossil record. The fossil record indicates that hominin species vary in brain shape, brain mass, and cognitive abilities (see Chapter 3). In general, the species with the largest, most human-looking brains are associated with the most sophisticated technology, but exceptions exist. Primate scaling relationships

have been used to predict the size of brain components, including V1, in fossil hominin species (Conroy GC and RJ Smith, 2007), based on assumption that all brain component volumes are closely related to brain size due to developmental constraints (Finlay BL *et al.*, 2001). However, it has also been indicated that brains evolve as a mosaic of systems, in which brain component volumes are better predicted by the size of functionally related brain structures than by overall brain size (Barton RA and PH Harvey, 2000). Chimpanzees and bonobos provide an example that closely related species with similarly sized brains can differ in V1 volume, V1 and extrastriate volume density, and perhaps, other aspects of brain organization. One recent paleoanthropological puzzle is how *Homo floresiensis,* with its chimp-sized brain, became associated with sophisticated stone tools. Notably, *Homo floresiensis* has a posteriorly-positioned lunate sulcus, which may be indicative of the increased size of posterior parietal cortical areas involved in tool-making as compared to chimpanzees. *Australopithecus africanus* also has a similarly-sized brain and a posteriorly positioned lunate sulcus, but lacks the association with stone tools. The degree to which fossil species like *Australopithecus africanus* and *Homo floresiensis* differ in brain organization will never be known, because endocasts only provide information about gross morphology. However, more details about the behavior and phylogenetic relationships of these species will broaden the context for comparing these species. Also, it is encouraging that some information about brain organization can be derived from the fossil endocasts: Of the great apes, the bonobo specimen has the most anteriorly-positioned lunate sulcus. And there is a correlation between lunate sulcus position and V1 volume across apes.

246

7.6 Implications for future studies

Visual aspects of human behaviors such as tool making, art, symbolic activity, language, and social complexity are predicted to have a species-specific neuroanatomical basis. However, such complex functions are extremely difficult to relate to specific neuroanatomical variables. There remains much to explore in human and nonhuman hominoid brain evolution. In fact, the meshwork arrangement of V1 layer 4A is the only qualitative neuroanatomical characteristic of any brain system specific to humans. Although the visual system is the most studied sensory system, many aspects of visual system organization, function, and morphology are still coming to light. For example, in recent years much is being revealed about the koniocellular pathway and other lesser known visual pathways. Comparative neuroimaging is a new field implicating that the human and macaque extrastriate cortices are not functionally identical (Orban GA *et al.*, 2004).

The relationship of the lunate sulcus to V1 volume will be further addressed in a follow up study in which the samples will be expanded, and lunate sulcus arc distances will be compared as well. Eventually, this approach can be expanded to investigate post-lunate surface area measurements, and to indicate the reliability of other cerebral surface landmarks for determining cortical area volumes in ape species. If robust relationships are found between external landmarks and functional regions, these data can be used to test predictions made about the sizes of V1 and other brain components in fossil taxa (Conroy GC and RJ Smith, 2007).

A relative reduction in V1 volume is thought to be directly related to an expansion of posterior parietal cortical areas (Holloway RL, RJ Clarke *et al.*, 2004). In humans, Brodmann's area 7, a superior parietal association area involved in somatosensory and visuomotor integration as well as visuospatial attention and memory, shows differential activation during tool-making by skilled tool-makers (Stout D *et al.*, 2000). Although area 7 and its subdivisions have recently been mapped in humans using the observer independent method (Scheperjans F *et al.*, 2008), little is known about the organization of the posterior parietal lobe in great ape species. Mapping of posterior parietal cytoarchitectonic areas in apes would indicate whether V1 volume reduction is directly related to the volumetric or numerical expansion of functionally distinct posterior parietal areas. This would also allow for comparative studies of aspects of occipital and parietal lobe microanatomical organization, including tests of overall neuron volume and numerical density scaling relationships, and examination of specific neuron populations within theses areas. Further details about the anatomy and function of visual pathways in hominoid brains will contribute to, and create, questions about human evolution.

Bibliography

Aboitiz F, Garcia R (1997) The anatomy of language revisited. Biol Res 30: 171-183.

Albright TD, Desimone R, Gross CG (1984) Columnar organization of directionally selective cells in visual area MT of the macaque. J Neurophysiol 51: 16-31.

Allen JS, Bruss J, Damasio H (2006) Looking for the lunate sulcus: A magnetic resonance imaging study in modern humans. Anat Rec A Discov Mol Cell Evol Biol 288: 867-876.

Allman JM (2000) Evolving Brains. New York: Scientific American Library.

Amunts K, Armstrong E, Malikovic A, Homke L, Mohlberg H, Schleicher A, Zilles K (2007) Gender-specific left-right asymmetries in human visual cortex. J Neurosci 27: 1356-1364.

Amunts K, Malikovic A, Mohlberg H, Schormann T, Zilles K (2000) Brodmann's areas 17 and 18 brought into stereotaxic space-where and how variable? Neuroimage 11: 66-84.

Amunts K, Schleicher A, Burgel U, Mohlberg H, Uylings HB, Zilles K (1999) Broca's region revisited: cytoarchitecture and intersubject variability. J Comp Neurol 412: 319-341.

Amunts K, Schleicher A, Zilles K (2007) Cytoarchitecture of the cerebral cortex--More than localization. Neuroimage 37: 1061.

Amunts K, Schmidt-Passos F, Schleicher A, Zilles K (1997) Postnatal development of interhemispheric asymmetry in the cytoarchitecture of human area 4. Anat Embryol (Berl) 196: 393-402.

Ankney C (1992) Sex differences in relative brain size: The mismeasure of woman, too? Intelligence 16: 329–336.

Armstrong E (1979) Quantitative comparison of the hominoid thalamus. I. Specific sensory relay nuclei. Am J Phys Anthropol 51: 365-382.

Armstrong E, Frost GT (1988) The Diencephalon: A comparative review. In: Orang-Utan Biology (Schwartz JH, ed.). Oxford: Oxford University Press.

Armstrong E, Zilles K, Curtis M, Schleicher A (1991) Cortical folding, the lunate sulcus and the evolution of the human brain. J Hum Evol 20: 341.

Armstrong E, Zilles K, Schlaug G, Schleicher A (1986) Comparative Aspects of the Primate Posterior Cingulate Cortex. J Comp Neurol 253: 539-548.

Bailey P, Von Bonin G (1951) The Isocortex of Man. Urbana: University of Illinois Press.

Bailey P, von Bonin G, McCulloch WS (1950) The Isocortex of Chimpanzee. Urbana: University of Illinois Press.

Balado M, Franke E (1937) Das Corpus Geniculatum Externum.

Barger N, Stefanacci L, Semendeferi K (2007) A comparative volumetric analysis of the amygdaloid complex and basolateral division in the human and ape brain. Am J Phys Anthropol 134: 392-403.

Barton RA (1998) Visual specialization and brain evolution in primates. Proc Biol Sci 265: 1933-1937.

Barton RA, Harvey PH (2000) Mosaic evolution of brain structure in mammals. Nature 405: 1055-1058.

Bauchot R, Stephan H (1967) Encéphales et moulages endocrâniens des quelques insectivores et des primates actuels. In: Problèmes actuels de paléontologie, évolution des vertébrés, pp 575-587. Paris: Éditions du Centre national de la recherche scientifique.

Bauchot R, Stephan H (1969) Encéphalisation et niveau évolutif chez les simiens. Mammalia 33: 225–275.

Beevor CE, Horsley V (1890) A Record of the Results Obtained by Electrical Excitation of the So-Called Motor Cortex and Internal Capsule in an Orang-Outang (*Simia satyrus*). Philos Trans R Soc Lond B Biol Sci 181: 129-158.

Bishop KM, Goudreau G, O'Leary DD (2000) Regulation of area identity in the mammalian neocortex by Emx2 and Pax6. Science 288: 344-349.

Bishop KM, Rubenstein JL, O'Leary DD (2002) Distinct actions of Emx1, Emx2, and Pax6 in regulating the specification of areas in the developing neocortex. J Neurosci 22: 7627-7638.

Black D (1915) A note on the sulcus lunatus in man. J Comp Neurol 25: 129-134.

Bolk L (1910) Beitrage zur Affenanatomie: Das Gehirn von Gorilla. Z f Morph u Anthropol 12A: 141-242.

Bookstein F, Schafer K, Prossinger H, Seidler H, Fieder M, Stringer C, Weber GW, Arsuaga JL, Slice DE, Rohlf FJ, Recheis W, Mariam AJ, Marcus LF (1999) Comparing frontal cranial profiles in archaic and modern homo by morphometric analysis. Anat Rec 257: 217-224.

Borden GJ, Harris KS (1984) Speech science primer. Baltimore: Williams and Wilkins.

Bowmaker JK, Astell S, Hunt DM, Mollon JD (1991) Photosensitive and photostable

    pigments in the retinae of Old World monkeys. J Exp Biol 156: 1-19.

Braak H (1977) The pigment architecture of the human occipital lobe. Anat Embryol

    (Berl) 150: 229-250.

Bridge H, Clare S, Jenkinson M, Jezzard P, Parker AJ, Matthews PM (2005) Independent

    anatomical and functional measures of the V1/V2 boundary in human visual

    cortex. J Vis 5: 93-102.

Broadfield DC, Holloway RL, Mowbray K, Silvers A, Yuan MS, Marquez S (2001)

    Endocast of Sambungmacan 3 (Sm 3): a new *Homo erectus* from Indonesia. Anat

    Rec 262: 369-379.

Brodmann K (1906) Beiträge zur histologischen Lokalisation der Grosshirnrinde. 5.

    Mitteilung: über die allgemeinen Bauplan des Cortex palii bei den Mammalieren

    und zwei homologe Rindenfelder im besonderem. Zugleich ein Beitrag zur

    Furchenlehre. J Psychol Neurol 6: 275-400.

Brodmann K (1909) Vergleichende Lokalisationslehre der Grosshirnrinde in ihren

    Prinzipien dargestellt auf Grund des Zellenbaues. Leipzig: Barth.

Brodmann K (1925) Vergleiehende Lokalisationslehre der Grosshirnrinde. Leipzig.: J. A.

    Barth.

Brown P, Sutikna T, Morwood MJ, Soejono RP, Jatmiko, Saptomo EW, Due RA (2004)

    A new small-bodied hominin from the Late Pleistocene of Flores, Indonesia.

    Nature 431: 1055-1061.

Bruner E (2004) Geometric morphometrics and paleoneurology: brain shape evolution in

    the genus *Homo*. J Hum Evol 47: 279-303.

Bruner E, Manzi G, Arsuaga JL (2003) Encephalization and allometric trajectories in the genus Homo: evidence from the Neandertal and modern lineages. Proc Natl Acad Sci U S A 100: 15335-15340.

Bush EC, Allman JM (2004) Three-dimensional structure and evolution of primate primary visual cortex. Anat Rec 281A: 1088-1094.

Butler AB, Hodos W (1996) Comparative Vertebrate Neuroanatomy: Evolution and Adaptation. New York: Wiley-Liss.

Caceres M, Lachuer J, Zapala MA, Redmond JC, Kudo L, Geschwind DH, Lockhart DJ, Preuss TM, Barlow C (2003) Elevated gene expression levels distinguish human from non-human primate brains. Proc Natl Acad Sci U S A 100: 13030-13035.

Campbell EJM (1968) The respiratory muscles. Ann N Y Acad Sci 155: 135–140.

Campbell EJM (1974) Muscular activity in normal and abnormal ventilation. In: Ventilatory and phonatory control systems. (Wyke B, ed.), pp 3–11. London: Oxford University Press.

Campbell MJ, Morrison JH (1989) Monoclonal antibody to neurofilament protein (SMI-32) labels a subpopulation of pyramidal neurons in the human and monkey neocortex. J Comp Neurol 282: 191-205.

Campos-Ortega JA, Hayhow WR (1970) A new lamination pattern in the lateral geniculate nucleus of primates. Brain Res 20: 335-339.

Cantalupo C, Hopkins WD (2001) Asymmetric Broca's area in great apes. Nature 414: 505.

Casagrande VA, Yazar F, Jones KD, Ding Y (2007) The morphology of the koniocellular axon pathway in the macaque monkey. Cereb Cortex 17: 2334-2345.

Chacko L (1948) The laminar pattern of the lateral geniculate body in the primate. J
Neurol Neurosurg Psychiatry 11: 211–224.

Chacko L (1954) The lateral geniculate body in the New World monkeys. J Anat Soc
India 3: 62–74.

Chacko L (1955) The lateral geniculate body in gibbon (Hylobates hoolock). J Anat Soc
India 4: 69-81.

Chacko L (1955) The lateral geniculate body of the chimpanzee. J Anat Soc India 4: 10–
13.

Chacko LW (1949) A preliminary study of the distribution of cell size in the lateral
geniculate body. J Anat 83: 254-266 253.

Changizi MA (2001) Principles underlying mammalian neocortical scaling. Biol Cybern
84: 207-215.

Changizi MA (2003) Relationship between number of muscles, behavioral repertoire
size, and encephalization in mammals. J Theor Biol 220: 157-168.

Changizi MA, Shimojo S (2005) Parcellation and area-area connectivity as a function of
neocortex size. Brain Behav Evol 66: 88-98.

Clarke S, Miklossy J (1990) Occipital cortex in man: organization of callosal
connections, related myelo- and cytoarchitecture, and putative boundaries of
functional visual areas. J Comp Neurol 298: 188-214.

Clutton-Brock TH, Harvey PH (1979) Comparison and adaptation. Proc R Soc Lond B
Biol Sci 205: 547-565.

Connolly CJ (1933) The brain of a mountain gorilla, Okero (G. beringei). Am J Phys
Anthropol 17: 291-307.

Connolly CJ (1950) External morphology of the primate brain. Springfield, Ill.: C. C. Thomas.

Connor CE (2001) Visual perception: sunny side up. Curr Biol 11: R776-778.

Conroy GC, Falk D, Guyer J, Weber GW, Seidler H, Recheis W (2000) Endocranial capacity in Sts 71 (*Australopithecus africanus*) by three-dimensional computed tomography. Anat Rec 258: 391-396.

Conroy GC, Smith RJ (2007) The size of scalable brain components in the human evolutionary lineage: With a comment on the paradox of Homo floresiensis. HOMO J Comp Hum Biol 58: 1-12.

Conroy GC, Vannier M (1985) Endocranial volume determination of matrix-filled fossil skulls using high resolution computer tomography. In, pp 419-426.

Conroy GC, Vannier MW, Tobias PV (1990) Endocranial features of *Australopithecus africanus* revealed by 2- and 3-D computed tomography. Science 247: 838-841.

Conroy GC, Weber GW, Seidler H, Recheis W, Zur Nedden D, Mariam JH (2000) Endocranial capacity of the Bodo cranium determined from three-dimensional computed tomography. Am J Phys Anthropol 113: 111-118.

Conroy GC, Weber GW, Seidler H, Tobias PV, Kane A, Brunsden B (1998) Endocranial capacity in an early hominid cranium from Sterkfontein, South Africa. Science 280: 1730-1731.

Count EW (1947) Brain and body weight in man: their antecendants in growth and evolution - a study in dynamic somatometry. Ann N Y Acad Sci 46: 993–1122.

Cragg BG (1967) The density of synapses and neurones in the motor and visual areas of the cerebral cortex. J Anat 101: 639-654.

Dacey DM, Petersen MR (1992) Dendritic field size and morphology of midget and parasol ganglion cells of the human retina. Proc Natl Acad Sci U S A 89: 9666-9670.

Dacey DM, Peterson BB, Robinson FR, Gamlin PD (2003) Fireworks in the primate retina: in vitro photodynamics reveals diverse LGN-projecting ganglion cell types. Neuron 37: 15-27.

Dahl JF (1986) Cyclic perineal swelling during the intermenstrual intervals of captive female pygmy chimpanzees (Pan paniscus). J Hum Evol 15: 369.

Damasio H, Grabowski TJ, Tranel D, Hichwa RD, Damasio AR (1996) A neural basis for lexical retrieval. Nature 380: 499-505.

Dart RA (1925) *Australopithecus africanus*: the Man-Ape of South Africa. Nature 115: 195-199.

de Miguel C, Henneberg M (2001) Variation in hominid brain size: How much is due to method? Homo 52: 3-58.

de Sousa A, Wood B (2002) Contribution of central nervous system characters to hominoid phylogenetics. Am J Phys Anthropol: 60-61.

De Valois RL, Morgan H, Snodderly DM (1974) Psychophysical studies of monkey vision. 3. Spatial luminance contrast sensitivity tests of macaque and human observers. Vision Res 14: 75-81.

Deacon T (1990) Fallacies of progression in theories of brain-size evolution. Int J Primatol 11: 193.

Deacon T (1990) Problems of ontogeny and phylogeny in brain-size evolution. Int J Primatol 11: 237.

Deacon TW (1997) The Symbolic Species: The Co-evolution of Language and the Brain. New York: W. W. Norton & Company.

Deaner RO, Isler K, Burkart J, van Schaik C (2007) Overall brain size, and not encephalization quotient, best predicts cognitive ability across non-human primates. Brain Behav Evol 70: 115-124.

Deeb SS, Jorgensen AL, Battisti L, Iwasaki L, Motulsky AG (1994) Sequence Divergence of the Red and Green Visual Pigments in Great Apes and Humans. Proc Natl Acad Sci U S A 91: 7262-7266.

Deegan JF, Jacobs GH (2001) Spectral sensitivity of gibbons: Implications for photopigments and color vision. Folia Primatol (Basel) 72: 26-29.

Dehay C, Giroud P, Berland M, Killackey H, Kennedy H (1996) Contribution of thalamic input to the specification of cytoarchitectonic cortical fields in the primate: effects of bilateral enucleation in the fetal monkey on the boundaries, dimensions, and gyrification of striate and extrastriate cortex. J Comp Neurol 367: 70-89.

Dehay C, Kennedy H (2007) Cell-cycle control and cortical development. Nat Rev Neurosci 8: 438-450.

Dekaban AS, Sadowsky D (1978) Changes in brain weights during the span of human life: relation of brain weights to body heights and body weights. Ann Neurol 4: 345-356.

DeYoe EA, Carman GJ, Bandettini P, Glickman S, Wieser J, Cox R, Miller D, Neitz J (1996) Mapping striate and extrastriate visual areas in human cerebral cortex. Proc Natl Acad Sci U S A 93: 2382-2386.

DeYoe EA, Felleman DJ, Van Essen DC, McClendon E (1994) Multiple processing
streams in occipitotemporal visual cortex. Nature 371: 151-154.

Deyoe EA, Hockfield S, Garren H, Van Essen DC (1990) Antibody labeling of functional
subdivisions in visual cortex: Cat-301 immunoreactivity in striate and extrastriate
cortex of the macaque monkey. Vis Neurosci 5: 67-81.

DeYoe EA, Van Essen DC (1988) Concurrent processing streams in monkey visual
cortex. Trends Neurosci 11: 219-226.

Dobkins KR, Thiele A, Albright TD (2000) Comparison of red-green equiluminance
points in humans and macaques: evidence for different L:M cone ratios between
species. J Opt Soc Am A Opt Image Sci Vis 17: 545-556.

Dominy NJ, Lucas PW (2001) Ecological importance of trichromatic vision to primates.
Nature 410: 363-366.

Dorus S, Vallender EJ, Evans PD, Anderson JR, Gilbert SL, Mahowald M, Wyckoff GJ,
Malcom CM, Lahn BT (2004) Accelerated evolution of nervous system genes in
the origin of Homo sapiens. Cell 119: 1027-1040.

Draper MH, Ladefoged P, Whitteridge D (1959) Respiratory muscles in speech. J Speech
Hear Res 2: 16–27.

Du Boulay G (1956) The significance of digital impressions in children's skulls. Acta
Radiol 46: 112-122.

Dubois E (1897) Sur le rapport du poids de l'encéphale avec la grandeur du corps chez
les mammifères. Bull Soc Anthropol 8: 337–376.

Dulai KS, Bowmaker JK, Mollon JD, Hunt DM (1994) Sequence divergence, polymorphism and evolution of the middle-wave and long-wave visual pigment genes of great apes and Old World monkeys. Vision Res 34: 2483-2491.

Elliot Smith G (1903) The so-called "Affenspalte" in the human (Egyptian) brain. Anatomischer Anzeiger 24: 74-83.

Elton S, Bishop LC, Wood BA (2001) Comparative context of Plio-Pleistocene hominin brain evolution. J Hum Evol 41: 1-27.

Enard W, Khaitovich P, Klose J, Zollner S, Heissig F, Giavalisco P, Nieselt-Struwe K, Muchmore E, Varki A, Ravid R, Doxiadis GM, Bontrop RE, Paabo S (2002) Intra- and interspecific variation in primate gene expression patterns. Science 296: 340-343.

Enard W, Przeworski M, Fisher SE, Lai CS, Wiebe V, Kitano T, Monaco AP, Paabo S (2002) Molecular evolution of FOXP2, a gene involved in speech and language. Nature 418: 869-872.

Erwin E, Baker FH, Busen WF, Malpeli JG (1999) Relationship between laminar topology and retinotopy in the rhesus lateral geniculate nucleus: Results from a functional atlas. J Comp Neurol 407: 92-102.

Fagot J, Deruelle C (1997) Processing of global and local visual information and hemispheric specialization in humans (Homo sapiens) and baboons (Papio papio). Journal of Experimental Psychology: Human Perception and Performance 23: 429-442.

Fagot J, Tomonaga M, Deruelle C (2001) Processing of the global and local dimensions of visual hierarchical stimuli by humans (*Homo sapiens*), chimpanzees (*Pan*

troglodytes), and baboons (*Papio papio*). In: Primate Origins of Human Cognition and Behavior (Matsuzawa T, ed.), pp 87-103. New York: Springer.

Falk D (1980) Hominid brain evolution: The approach from paleoneurology. Yearb Phys Anthropol 23: 93-107.

Falk D (1980) A reanalysis of the South African australopithecine natural endocasts. Am J Phys Anthropol 53: 525-539.

Falk D (1987) Hominid Paleoneurology. Annu Rev Anthropol 16: 13-30.

Falk D, Hildebolt C, Smith K, Morwood MJ, Sutikna T, Brown P, Jatmiko, Saptomo EW, Brunsden B, Prior F (2005) The Brain of LB1, *Homo floresiensis*. Science: 1109727.

Falk D, Redmond JC, Jr., Guyer J, Conroy C, Recheis W, Weber GW, Seidler H (2000) Early hominid brain evolution: a new look at old endocasts. J Hum Evol 38: 695-717.

Felleman DJ, Burkhalter A, Van Essen DC (1997) Cortical connections of areas V3 and VP of macaque monkey extrastriate visual cortex. J Comp Neurol 379: 21-47.

Felleman DJ, Van Essen DC (1987) Receptive field properties of neurons in area V3 of macaque monkey extrastriate cortex. Journal of Neurophysiology 57: 889-920.

Felleman DJ, Van Essen DC (1991) Distributed hierarchical processing in the primate cerebral cortex. Cereb Cortex 1: 1-47.

Felsenstein J (1985) Phylogenies and the Comparative Method. Am Nat 125: 1-15.

Ferrera VP, Nealey TA, Maunsell JH (1994) Responses in macaque visual area V4 following inactivation of the parvocellular and magnocellular LGN pathways. J Neurosci 14: 2080-2088.

Filimonoff IN (1933) Über die Variabilität der Großhirnrindenstruktur. Mitteilung III. Regio occipitalis bei der höheren und niederen Affen. J Psychol Neurol 45: 69-137.

Finlay BL, Darlington RB (1995) Linked regularities in the development and evolution of mammalian brains. Science 268: 1578-1584.

Finlay BL, Darlington RB, Nicastro N (2001) Developmental structure in brain evolution. Behav Brain Sci 24: 263-278; discussion 278-308.

Frahm HD, Stephan H, Baron G (1984) Comparison of brain structure volumes in insectivora and primates. V. Area striata (AS). J Hirnforsch 25: 537-557.

Frahm HD, Stephan H, Stephan M (1982) Comparison of brain structure volumes in Insectivora and Primates. I. Neocortex. J Hirnforsch 23: 375-389.

Frahm HD, Zilles K, Schleicher A, Stephan H (1998) The size of the middle temporal area in primates. J Hirnforsch 39: 45-54.

Fukuda K, Saito N, Yamamoto M, Tanaka C (1994) Immunocytochemical localization of the alpha-, beta I-, beta II- and gamma-subspecies of protein kinase C in the monkey visual pathway. Brain Res 658: 155-162.

Gallyas F (1971) A principle for silver staining of tissue elements by physical development. Acta Morphol Acad Sci Hung 19: 57-71.

Garland T, Harvey PH, Ives AR (1992) Procedures For The Analysis Of Comparative Data Using Phylogenetically Independent Contrasts. Syst Biol 41: 18-32.

Garland T, Ives AR (2000) Using the past to predict the present: Confidence intervals for regression equations in phylogenetic comparative methods. Am Nat 155: 346-364.

Garland T, Jr., Diaz-Uriarte R (1999) Polytomies and Phylogenetically Independent Contrasts: Examination of the Bounded Degrees of Freedom Approach. Syst Biol 48: 547-558.

Gattass R, Rosa MG, Sousa AP, Pinon MC, Fiorani Junior M, Neuenschwander S (1990) Cortical streams of visual information processing in primates. Brazilian Journal of Medical and Biological Research 23: 375-393.

Gattass R, Sousa AP, Mishkin M, Ungerleider LG (1997) Cortical projections of area V2 in the macaque. Cereb Cortex 7: 110-129.

Gerhardt E (1940) Die Cytoarchitektonik des Isocortex parietalis beim Menschen. J Psychol Neurol 49: 367–419.

Geyer S, Schleicher A, Schormann T, Mohlberg H, Bodegard A, Roland PE, Zilles K (2001) Integration of microstructural and functional aspects of human somatosensory areas 3a, 3b, and 1 on the basis of a computerized brain atlas. Anat Embryol (Berl) 204: 351-366.

Ghazanfar AA, Santos LR (2004) Primate brains in the wild: the sensory bases for social interactions. Nat Rev Neurosci 5: 603-616.

Gibbs S, Collard M, Wood B (2000) Soft-tissue characters in higher primate phylogenetics. Proc Natl Acad Sci U S A 97: 11130-11132.

Gibbs S, Collard M, Wood B (2002) Soft-tissue anatomy of the extant hominoids: a
review and phylogenetic analysis. J Anat 200: 3-49.

Gil-da-Costa R, Martin A, Lopes MA, Munoz M, Fritz JB, Braun AR (2006) Species-
specific calls activate homologs of Broca's and Wernicke's areas in the macaque.
Nat Neurosci 9: 1064-1070.

Gilissen E, Iba-Zizen MT, Stievenart JL, Lopez A, Trad M, Cabanis EA, Zilles K (1995)
Is the length of the calcarine sulcus associated with the size of the human visual
cortex? A morphometric study with magnetic resonance tomography. J Hirnforsch
36: 451-459.

Gilissen E, Zilles K (1995) The relative volume of the primary visual-cortex and its
intersubject variability among humans - a new morphometric study. Comptes
Rendus de l'Académie des Sciences - Series IIA - Earth and Planetary Science
320: 897-902.

Gingerich PD, Martin RD (1981) Cranial morphology and adaptations in Eocene
Adapinae. II. The Cambridge skulls of *Adapis parisiensis*. Am J Phys Anthropol
56: 235-257.

Goodale MA, Milner AD (1992) Separate visual pathways for perception and action.
Trends Neurosci 15: 20-25.

Goodall J (1986) The Chimpanzees of Gombe: Patterns of Behavior. Boston: Bellknap
Press of the Harvard University Press.

Goodchild AK, Martin PR (1998) The distribution of calcium-binding proteins in the
lateral geniculate nucleus and visual cortex of a New World monkey, the
marmoset, Callithrix jacchus. Vis Neurosci 15: 625-642.

Gould SJ (1966) Allometry and size in ontogeny and phylogeny. Biol Rev Camb Philos Soc 41: 587-640.

Gould SJ (1975) Allometry in Primates, with Emphasis on Scaling and Evolution of Brain. Contributions to Primatology 5: 244-292.

Gould SJ (1975) On Scaling of Tooth Size in Mammals. Am Zool 15: 351-362.

Gould SJ (1978) Morton's ranking of races by cranial capacity. Unconscious manipulation of data may be a scientific norm. Science 200: 503-509.

Gould SJ (1996) The mismeasure of man. New York: Norton.

Gould WJ, Okamura H (1974) Interrelationships between voice and laryngeal mucosal reflexes. In: Ventilatory and Phonatory Control Systems (Wyke B, ed.), pp 347–369. London: Oxford University Press.

Grabowski TJ, Damasio H, Tranel D, Ponto LL, Hichwa RD, Damasio AR (2001) A role for left temporal pole in the retrieval of words for unique entities. Hum Brain Mapp 13: 199-212.

Grafen A (1989) The phylogenetic regression. Philos Trans R Soc Lond B Biol Sci 326: 119-157.

Grether WF (1940) A comparison of human and chimpanzee spectral hue discrimination curves. Journal of Experimental Psychology 26: 394.

Gundersen HJ, Jensen EB (1987) The efficiency of systematic sampling in stereology and its prediction. J Microsc 147 (Pt 3): 229-263.

Hakeem A, Allman J, Tetreault N, Semendeferi K (2004) The spindle neurons of frontoinsular cortex (area FI) are unique to humans and African great apes. Am J Phys Anthropol 38: 106.

Hanazawa A, Komatsu H (2001) Influence of the direction of elemental luminance gradients on the responses of V4 cells to textured surfaces. J Neurosci 21: 4490-4497.

Harvey PH, Krebs JR (1990) Comparing brains. Science 249: 140-146.

Harvey PH, Pagel MD (1991) The Comparative Method in Evolutionary Biology. Oxford: Oxford University Press.

Harwerth RS, Smith EL, 3rd (1985) Rhesus monkey as a model for normal vision of humans. Am J Optom Physiol Opt 62: 633-641.

Hassler R (1966) Comparative anatomy in day and night active primates. In: Evolution of the forebrain (Hassler R, Stephan H, eds.), pp 419-434. Stuttgart: Thieme.

Haug H (1987) Brain sizes, surfaces, and neuronal sizes of the cortex cerebri: a stereological investigation of man and his variability and a comparison with some mammals (primates, whales, marsupials, insectivores, and one elephant). Am J Anat 180: 126-142.

Hebb DO (1949) The Organization of Behavior: A Neuropsychological Theory. New York: Wiley.

Hendry SH, Reid RC (2000) The koniocellular pathway in primate vision. Annu Rev Neurosci 23: 127-153.

Hendry SH, Yoshioka T (1994) A neurochemically distinct third channel in the macaque dorsal lateral geniculate nucleus. Science 264: 575-577.

Herculano-Houzel S, Collins CE, Wong PY, Kaas JH (2007) Cellular scaling rules for primate brains. Proc Natl Acad Sci U S A 104: 3562-3567.

Herndon JG, Tigges J, Anderson DC, Klumpp SA, McClure HM (1999) Brain weight throughout the life span of the chimpanzee. J Comp Neurol 409: 567-572.

Hickey TL, Guillery RW (1979) Variability of laminar patterns in the human lateral geniculate nucleus. J Comp Neurol 183: 221-246.

Hixon TJ, Weismer G (1995) Perspectives on the Edinburgh study of speech breathing. J Speech Hear Res 38: 42-60.

Hof PR (2000) Neurochemical and cellular specializations in the Mammalian neocortex reflect Phylogenetic Relationships: Evidence from Primates, Cetaceans, and Artiodactyls. Brain Behav Evol: 300.

Hof PR, Morrison JH (1990) Quantitative analysis of a vulnerable subset of pyramidal neurons in Alzheimer's disease: II. Primary and secondary visual cortex. J Comp Neurol 301: 55-64.

Hof PR, Morrison JH (1995) Neurofilament protein defines regional patterns of cortical organization in the macaque monkey visual system: a quantitative immunohistochemical analysis. J Comp Neurol 352: 161-186.

Hof PR, Nimchinsky EA, Perl DP, Erwin JM (2001) An unusual population of pyramidal neurons in the anterior cingulate cortex of hominids contains the calcium-binding protein calretinin. Neurosci Lett 307: 139-142.

Hof PR, Nimchinsky EA, Young WG, Morrison JH (2000) Numbers of Meynert and layer IVB cells in area V1: A stereologic analysis in young and aged macaque monkeys. J Comp Neurol 420: 113-126.

Hof PR, Ungerleider LG, Webster MJ, Gattass R, Adams MM, Sailstad CA, Morrison JH (1996) Neurofilament protein is differentially distributed in subpopulations of

corticocortical projection neurons in the macaque monkey visual pathways. J Comp Neurol 376: 112-127.

Holloway RL (1966) Cranial Capacity, Neural Reorganization, and Hominid Evolution - Search for More Suitable Parameters. American Anthropologist 68: 103-121.

Holloway RL (1968) The evolution of the primate brain: some aspects of quantitative relations. Brain Res 7: 121-172.

Holloway RL (1972) New australopithecine endocast, SK 1585, from Swartkrans, South Africa. Am J Phys Anthropol 37: 173-185.

Holloway RL (1973) Endocranial Volumes of Early African Hominids, and Role of Brain in Human Mosaic Evolution. J Hum Evol 2: 449-459.

Holloway RL (1975) Early hominid endocasts: Volumes, morphology and significance. In: Primate Functional Morphology and Evolution (Tuttle R, ed.), pp 393-416. The Hague: Mouton.

Holloway RL (1979) Brain size, allometry, and reorganization: toward a synthesis. In: Development and evolution of brain size: behavioral implications (Hahn M, Jensen C, Dudek B, eds.), pp 59-88. New York: Academic Press.

Holloway RL (1983) Human brain evolution: a search for units, models and synthesis. Canadian journal of anthropology 3: 215-232.

Holloway RL (1983) The O.H.7 (Olduvai Gorge, Tanzania) parietal fragments and their reconstruction: A reply to Wolpoff. Am J Phys Anthropol 60: 505-516.

Holloway RL (1984) The Taung endocast and the lunate sulcus: a rejection of the hypothesis of its anterior position. Am J Phys Anthropol 64: 285-287.

Holloway RL (1988) Some additional morphological and metrical observations on *Pan* brain casts and their relevance to the Taung endocast. Am J Phys Anthropol 77: 27-33.

Holloway RL (1992) The Failure of the Gyrification Index (Gi) to Account for Volumetric Reorganization in the Evolution of the Human Brain. J Hum Evol 22: 163-170.

Holloway RL (1996) Evolution of the human brain. In: Handbook of human symbolic evolution (Lock A, Peters CR, eds.), pp 74-116. New York: Clarendon Press.

Holloway RL (1997) Brain Evolution. In: Encyclopedia of Human Biology (Dulbecco R, ed.). New York: Academic Press.

Holloway RL (2002) Brief communication: how much larger is the relative volume of area 10 of the prefrontal cortex in humans? Am J Phys Anthropol 118: 399-401.

Holloway RL, Broadfied DC, Yuan M (2004) The Human Fossil Record, Volume Three: Brain Endocasts -- The Paleoneurological Evidence. Hoboken, N.J.: John Wiley & Sons, Inc.

Holloway RL, Broadfield DC, Yuan MS (2003) Morphology and histology of chimpanzee primary visual striate cortex indicate that brain reorganization predated brain expansion in early hominid evolution. Anat Rec 273A: 594-602.

Holloway RL, Broadfield DC, Yuan MS (2004) Methods and Materials of Endocast Analysis. In: The Human Fossil Record, pp 27-37.

Holloway RL, Broadfield DC, Yuan MS, Tobias PV (2003) The lunate sulcus and early hominid brain evolution: Toward the end of a controversy. Am J Phys Anthropol: 117-117.

Holloway RL, Clarke RJ, Tobias PV (2004) Posterior lunate sulcus in *Australopithecus africanus*: was Dart right? CR Palevol 3: 287-293.

Holloway RL, de Lacoste-Lareymondie MC (1982) Brain endocast asymmetry in pongids and hominids: some preliminary findings on the paleontology of cerebral dominance. Am J Phys Anthropol 58: 101-110.

Holloway RL, Post D (1982) The relativity of relative brain size measures and hominid mosaic evolution. In: Primate Brain Evolution: Methods and Concepts (Armstrong E, Falk D, eds.), pp 57-76. New York: Plenum Press.

Hopkins WD, Marino L (2000) Asymmetries in cerebral width in nonhuman primate brains as revealed by magnetic resonance imaging (MRI). Neuropsychologia 38: 493-499.

Horel JA (1994) Local and global perception examined by reversible suppression of temporal cortex with cold. Behav Brain Res 65: 157-164.

Horel JA, Voytko ML, Salsbury KG (1984) Visual learning suppressed by cooling the temporal pole. Behav Neurosci 98: 310-324.

Horton JC, Stryker MP (1993) Amblyopia induced by anisometropia without shrinkage of ocular dominance columns in human striate cortex. Proc Natl Acad Sci U S A 90: 5494-5498.

Hubel DH, Wiesel TN (1968) Receptive fields and functional architecture of monkey striate cortex. J Physiol 195: 215-243.

Humphrey GK, Goodale MA, Bowen CV, Gati JS, Vilis T, Rutt BK, Menon RS (1997) Differences in perceived shape from shading correlate with activity in early visual areas. Curr Biol 7: 144-147.

Hunt DM, Cowing JA, Patel R, Appukuttan B, Bowmaker JK, Mollon JD (1995) Sequence and evolution of the blue cone pigment gene in Old and New World primates. Genomics 27: 535-538.

Hyvarinen J (1981) Regional distribution of functions in parietal association area 7 of the monkey. Brain Res 206: 287-303.

Ingalls NW (1914) The parietal region in the primate brain. J Comp Neurol 24: 291-341.

Ingmanson EJ (1996) Tool-using behavior in wild Pan paniscus: Social and ecological considerations. In: Reaching into thought: The minds of great apes (Russon AR, Bard KA, Parker ST, eds.), pp 190–210. Cambridge, UK: Cambridge University Press.

Jackson WJ, Reite ML, Buxton DF (1969) The chimpanzee central nervous system: a comparative review. Primates Med 4: 1-51.

Jacobs GH, Deegan JF (1993) Photopigments underlying color vision in ringtail lemurs (*Lemur catta*) and brown lemurs (*Eulemur fulvus*). American Journal of Primatology 30: 243-256.

Jacobs GH, Deegan JF (1999) Uniformity of colour vision in Old World monkeys. P Roy Soc Lond B Bio 266: 2023-2028.

Jacobs GH, Deegan JF, Neitz J, Crognale MA, Neitz M (1993) Photopigments and color vision in the nocturnal monkey, *Aotus*. Vision Res 33: 1773-1783.

Jacobs GH, Deegan KF, Moran JL (1996) ERG measurements of the spectral sensitivity of common chimpanzee (Pan troglodytes). Vision Res 36: 2587-2594.

Jacobs GH, Neitz M, Deegan JF, Neitz J (1996) Trichromatic colour vision in New World monkeys. Nature 382: 156.

Jerison HJ (1955) Brain to body ratios and the evolution of intelligence. Science 121: 447-449.

Jerison HJ (1961) Quantitative analysis of evolution of the brain in mammals. Science 133: 1012-1014.

Jerison HJ (1973) Evolution of the brain and intelligence. New York: Academic Press.

Jerison HJ (1975) Fossil evidence of evolution of the human brain. Annu Rev Anthropol 4: 27-58.

Joffe TH, Dunbar RI (1997) Visual and socio-cognitive information processing in primate brain evolution. Proc Biol Sci 264: 1303-1307.

Johnson JI, Kirsch JA, Reep RL, Switzer RC, 3rd (1994) Phylogeny through brain traits: more characters for the analysis of mammalian evolution. Brain Behav Evol 43: 319-347.

Jones EG, Hendry SH (1989) Differential Calcium Binding Protein Immunoreactivity Distinguishes Classes of Relay Neurons in Monkey Thalamic Nuclei. Eur J Neurosci 1: 222-246.

Jones SE, Buchbinder BR, Aharon I (2000) Three-dimensional mapping of cortical thickness using Laplace's equation. Hum Brain Mapp 11: 12-32.

Kaas JH (1993) The organization of visual cortex in primates: problems, conclusions, and the use of comparative studies in understanding brain evolution. In: Functional Organization of the Human Visual Cortex (Gulyas B, Ottoson D, Roland PE, eds.), pp 1-12. Oxford: Perhamon Press.

Kaas JH (1997) Theories of visual cortex organization in primates. In: Cerebral Cortex (Rockland KS, Peters A, eds.), pp 91-125. NY: Plenum Press.

Kaas JH (2000) Why is Brain Size so Important: Design Problems and Solutions as Neocortex Gets Bigger or Smaller. Brain and Mind 1: 7-23.

Kaas JH, Guillery RW, Allman JM (1972) Some principles of organization in the dorsal lateral geniculate nucleus. Brain Behav Evol 6: 253-299.

Kaas JH, Huerta MF (1988) The Subcortical Visual System of Primates. In: Comparative Primate Biology, Volume 4: Neurosciences (Stelis HD, Erwin J, eds.), pp 327-391. New York: Liss.

Kaas JH, Huerta MF, Weber JT, Harting JK (1978) Patterns of retinal terminations and laminar organization of the lateral geniculate nucleus of primates. J Comp Neurol 182: 517-553.

Kanagasuntheram R, Krishnamurti A, Wong WC (1969) Observations on the lamination of the lateral geniculate body in some primates. Brain Res 14: 623-631.

Kano T (1982) The use of leafy twigs for rain cover by the pygmy chimpanzees at Wamba. Primates 23: 453-457.

Kano T (1992) The Last Ape: Pygmy Chimpanzee Behavior and Ecology. Palo Alto, CA: Stanford University Press.

Kastner S, Schneider KA, Wunderlich K (2006) Beyond a relay nuiclenus: neuroimaging views on the human LGN. Progress in Brain Research 155: 125-143.

Kawamura S (1959) The process of sub-cultural propagation among Japanese macaques. Primates 2: 43–60.

Kirk EC (2006) Visual influences on primate encephalization. J Hum Evol 51: 76.

Klekamp J, Riedel A, Harper C, Kretschmann HJ (1994) Morphometric study on the postnatal growth of the visual cortex of Australian aborigines and Caucasians. J Hirnforsch 35: 541-548.

Kourtzi Z, Tolias AS, Altmann CF, Augath M, Logothetis NK (2003) Integration of local features into global shapes: monkey and human FMRI studies. Neuron 37: 333-346.

Kretschmann HJ, Tafesse U, Herrmann A (1982) Different Volume Changes of Cerebral-Cortex and White Matter during Histological Preparation. Microscopica Acta 86: 13-24.

Krompecher, Lipak (1966) A simple method for determining cerebralization, brain weight and intelligence. J Comp Neurol 93: 37-51.

Krubitzer L (1995) The organization of neocortex in mammals: are species differences really so different? Trends Neurosci 18: 408.

Kuroda S (1980) Social behavior of the pygmy chimpanzees. Primates 21: 181-197.

Kuypers HG, Szwarcbart MK, Mishkin M, Rosvold HE (1965) Occipitotemporal Corticocortical Connections In The Rhesus Monkey. Exp Neurol 11: 245-262.

Lacoste-Royal G, Mathieu M, Nalbantoglu J, Julien JP, Gauthier S, Gauvreau D (1990) Lack of association between two restriction fragment length polymorphisms in the genes for the light and heavy neurofilament proteins and Alzheimer's disease. Can J Neurol Sci 17: 302-305.

Lande R (1979) Quantitative Genetic Analysis of Multivariate Evolution, Applied to Brain: Body Size Allometry. Evolution 33: 402.

Lashley KS, Clark G (1946) The Cytoarchitecture of the Cerebral Cortex of Ateles - a

    Critical Examination of Architectonic Studies. J Comp Neurol 85: 223-305.

Le Gros Clark WE (1927) Description of the Cerebral Hemispheres of the Brain of a

    Gorilla (John Daniels I). J Anat 61: 467-475.

Le Gros Clark WE (1941) The laminar organization and cell content of the lateral

    geniculate body in the monkey. J Anat 75: 419-433.

Le Gros Clark WE (1941) The lateral geniculate body in the platyrrhine monkeys. J Anat

    76: 131-140.

Le Gros Clark WE, Penman GG (1934) The Projection of the Retina in the Lateral

    Geniculate Body. Proc Roy Soc London, s B 114: 291.

Le May M (1976) Morphological cerebral asymmetries of modern man, fossil man and

    nonhuman primates. Ann N Y Acad Sci 280: 349-366.

Le May M, Billig MS, Geschwind N (1982) Asymmetries in the brains and skulls of

    nonhuman primates. In: Primate Brain Evolution: Methods and concepts

    (Armstrong E, Falk D, eds.), pp 263-277. New York: Plenum Press.

Leakey LSB, Tobias PV, Napier JR (1964) A new species of genus Homo from Olduvai

    Gorge. Nature 202: 7-9.

Leuba G, Saini K (1996) Calcium-binding proteins immunoreactivity in the human

    subcortical and cortical visual structures. Vis Neurosci 13: 997-1009.

Leventhal AG, Rodieck RW, Dreher B (1981) Retinal ganglion cell classes in the Old

    World monkey: morphology and central projections. Science 213: 1139-1142.

Leyton ASF, Sherrington CS (1917) Cbservations on the excitable cortex of the

    chimpanzee, orang-utan, and gorilla. Q J Exp Physiol 11: 135-222.

Livingstone M, Hubel D (1988) Segregation of form, color, movement, and depth: anatomy, physiology, and perception. Science 240: 740-749.

Lucas PW, Darvell BW, Lee PK, Yuen TD, Choong MF (1998) Colour cues for leaf food selection by long-tailed macaques (*Macaca fascicularis*) with a new suggestion for the evolution of trichromatic colour vision. Folia Primatol (Basel) 69: 139-152.

Lucas PW, Dominy NJ, Riba-Hernandez P, Stoner KE, Yamashita N, Loria-Calderon E, Petersen-Pereira W, Rojas-Duran Y, Salas-Pena R, Solis-Madrigal S, Osorio D, Darvell BW (2003) Evolution and function of routine trichromatic vision in primates. Evolution Int J Org Evolution 57: 2636-2643.

Lueck CJ, Zeki S, Friston KJ, Deiber MP, Cope P, Cunningham VJ, Lammertsma AA, Kennard C, Frackowiak RS (1989) The colour centre in the cerebral cortex of man. Nature 340: 386-389.

Lund JS (1973) Organization of neurons in the visual cortex, area 17, of the monkey (*Macaca mulatta*). J Comp Neurol 147: 455-496.

Lund JS, Hendrickson AE, Ogren MP, Tobin EA (1981) Anatomical organization of primate visual cortex area VII. J Comp Neurol 202: 19-45.

Lund JS, Yoshioka T (1991) Local circuit neurons of macaque monkey striate cortex: III. Neurons of laminae 4B, 4A, and 3B. J Comp Neurol 311: 234-258.

Lynch JC (1980) The functional organization of posterior parietal association cortex. Behav Brain Sci 3: 485-534.

Lyon DC, Kaas JH (2002) Evidence for a modified V3 with dorsal and ventral halves in macaque monkeys. Neuron 33: 453-461.

MacKinnon IL, Kennedy JA, Davis TV (1956) The estimation of skull capacity from roentgenologic measurements. Am J Roentgenol Radium Ther Nucl Med 76: 303-310.

MacLarnon A (1993) The Vertebral Canal. In: The Nariokotome *Homo erectus* Skeleton (Walker A, Leakey R, eds.), pp 359-446. Cambridge, MA: Harvard University Press.

MacLarnon A (1995) The Distribution of Spinal-Cord Tissues and Locomotor Adaptation in Primates. J Hum Evol 29: 463-482.

MacLarnon AM, Hewitt GP (1999) The evolution of human speech: the role of enhanced breathing control. Am J Phys Anthropol 109: 341-363.

MacLarnon AM, Hewitt GP (2004) Increased breathing control: Another factor in the evolution of human language. Evol Anthropol 13: 181 - 197.

MacLeod CE, Zilles K, Schleicher A, Rilling JK, Gibson KR (2003) Expansion of the neocerebellum in Hominoidea. J Hum Evol 44: 401-429.

Maddison WP, Maddison DR (2006) Mesquite: A modular system for evolutionary analysis. http://mesquiteproject.org. In, 1.1 ed.

Malikovic A, Amunts K, Schleicher A, Mohlberg H, Eickhoff SB, Wilms M, Palomero-Gallagher N, Armstrong E, Zilles K (2007) Cytoarchitectonic analysis of the human extrastriate cortex in the region of V5/MT+: a probabilistic, stereotaxic map of area hOc5. Cereb Cortex 17: 562-574.

Malpeli JG, Baker FH (1975) The representation of the visual field in the lateral geniculate nucleus of *Macaca mulatta*. J Comp Neurol 161: 569-594.

Manouvrier L (1898) Aperçu de céphalométrie anthropologique. L'intermédiare des
Biologistes 1: 470-480, 490-501.

Manouvrier L (1903) Conclusions générales sur l'anthropologie des sexes et applications
sociales. Revue de l'École d'Anthropologie 13: 405–423.

Martin RD (1981) Relative brain size and basal metabolic rate in terrestrial vertebrates.
Nature 293: 57-60.

Martin RD (1990) Primate origins and evolution: a phylogenetic reconstruction.
London/New Jersey: Chapman Hall/Princeton Univ. Press.

Martin RD, Genoud M, Hemelrijk CK (2005) Problems of allometric scaling analysis:
examples from mammalian reproductive biology. J Exp Biol 208: 1731-1747.

Mauss T (1911) Die Faserarchitektonische Gliederung des Cortex Cerebri der
anthropomorphen Affen. J Psychol Neurol 18: 410-467.

Mayhew TM, Olsen DR (1991) Magnetic resonance imaging (MRI) and model-free
estimates of brain volume determined using the Cavalieri principle. J Anat 178:
133-144.

McGrew WC (1992) Chimpanzee material culture. Cambridge, UK: Cambridge
University Press.

McHenry HM (1988) New estimates of body weight in early hominids and their
significance to encephalization and megadontia in "robust " australopithecines. In:
Evolutionary History of the "Robust" Australopithecines (Grine FE, ed.), pp 133-
148. New York: Aldine de Gruyter.

McKeefry DJ, Zeki S (1997) The position and topography of the human colour centre as revealed by functional magnetic resonance imaging. Brain 120 (Pt 12): 2229-2242.

Merker B (1983) Silver staining of cell bodies by means of physical development. J Neurosci Methods 9: 235-241.

Midford PE, Garland T, Jr., Maddison WP (2005) PDAP Package of Mesquite. In, 1.07 ed.

Miller JA (1991) Does brain size variability provide evidence of multiple species in *Homo habilis*? Am J Phys Anthropol 84: 385-398.

Mollon JD (1989) "Tho' she kneel'd in that place where they grew." The uses and origins of primate colour vision. J Exp Biol 146: 21-38.

Morwood MJ, Soejono RP, Roberts RG, Sutikna T, Turney CS, Westaway KE, Rink WJ, Zhao JX, van den Bergh GD, Due RA, Hobbs DR, Moore MW, Bird MI, Fifield LK (2004) Archaeology and age of a new hominin from Flores in eastern Indonesia. Nature 431: 1087-1091.

Munkle MC, Waldvogel HJ, Faull RL (2000) The distribution of calbindin, calretinin and parvalbumin immunoreactivity in the human thalamus. J Chem Neuroanat 19: 155-173.

Nakagawa S, Tigges J, Tigges M (1998) Laminar organization of the lateral geniculate nucleus of the gorilla. Folia Primatol (Basel) 69: 377-380.

Nakamura K, Kubota K (1995) Mnemonic firing of neurons in the monkey temporal pole during a visual recognition memory task. J Neurophysiol 74: 162-178.

Nathans J, Thomas D, Hogness DS (1986) Molecular genetics of human color vision: the genes encoding blue, green, and red pigments. Science 232: 193-202.

Nimchinsky EA, Gilissen E, Allman JM, Perl DP, Erwin JM, Hof PR (1999) A neuronal morphologic type unique to humans and great apes. Proc Natl Acad Sci U S A 96: 5268-5273.

Nishida T (1986) Local tradition and cultural transmission. In: Primate societies (Smuts B, Cheney D, Seyfarth R, Wrangham R, Struhsaker T, eds.), pp 462-474. Chicago: University of Chicago Press.

Nissl F (1898) Nervenzellen und graue Substanz. Muench med Wchnschr 45: 988-992,1023-1029,1060-1062.

Noback CR, Gross L (1959) Brain of a gorilla. I. Surface anatomy and cranial nerve nuclei. J Comp Neurol 111: 321-344.

Nolte J (1998) The Human Brain: An Introduction to Its Functional Anatomy (Paperback). St Louis, Missouri: C. V. Mosby.

O'Brien BJ, Abel PL, Olavarria JF (1997) A morphological anomaly of the dorsal lateral geniculate nucleus in *Macaca fascicularis*. Cell Tissue Res 289: 11-16.

O'Leary DD, Chou SJ, Sahara S (2007) Area patterning of the mammalian cortex. Neuron 56: 252-269.

Olivier G, Tissier H (1975) Determination of cranial capacity in fossil men. Am J Phys Anthropol 43: 353-362.

Orban GA, Van Essen D, Vanduffel W (2004) Comparative mapping of higher visual areas in monkeys and humans. Trends Cogn Sci 8: 315-324.

Pagel MD (1992) A Method for the Analysis of Comparative Data. J Theor Biol 156: 431-442.

Pagel MD, Harvey PH (1988) The Taxon-Level Problem In The Evolution Of Mammalian Brain Size - Facts And Artifacts. Am Nat 132: 344-359.

Pagel MD, Harvey PH (1989) Taxonomic differences in the scaling of brain on body weight among mammals. Science 244: 1589-1593.

Passingham RE (1975) The brain and intelligence. Brain Behav Evol 11: 1-15.

Pasupathy A, Connor CE (2002) Population coding of shape in area V4. Nat Neurosci 5: 1332-1338.

Pearson K (1926) On the reconstruction of cranial capacity from external measurements. Man 26: 46-50.

Perrett DI, Smith PA, Potter DD, Mistlin AJ, Head AS, Milner AD, Jeeves MA (1985) Visual cells in the temporal cortex sensitive to face view and gaze direction. Proc R Soc Lond B Biol Sci 223: 293-317.

Peters A, Sethares C (1991) Layer IVA of rhesus monkey primary visual cortex. Cereb Cortex 1: 445-462.

Peters A, Sethares C (1991) Organization of pyramidal neurons in area 17 of monkey visual cortex. J Comp Neurol 306: 1-23.

Peters M, Jancke L, Staiger JF, Schlaug G, Huang Y, Steinmetz H (1998) Unsolved Problems in Comparing Brain Sizes in Homo Sapiens. Brain and Cognition 37: 254-285.

Peters M, Jancke L, Zilles K (2000) Comparison of overall brain volume and midsagittal corpus callosum surface area as obtained from NMR scans and direct anatomical

measures: a within-subject study on autopsy brains. Neuropsychologia 38: 1375-1381.

Pickering SP (1930) Correlation of brain and head measurements, and relation of brain shape and size to shape and size of the head. Am J Phys Anthropol 15: 2-51.

Pilbeam D (1969) Early Hominidae and Cranial Capacity. Nature 224: 386.

Pitts G, Bullard T (1968) Some interspecific aspects of body composition in mammals. In: Body Composition in Animals and Man, pp 45-70. Washington, DC: National Academy of Science.

Polyak S (1957) The vertebrate visual system. In. Chicago: Univ. of Chicago Press.

Preuss TM, Coleman GQ (2002) Human-specific organization of primary visual cortex: alternating compartments of dense Cat-301 and calbindin immunoreactivity in layer 4A. Cereb Cortex 12: 671-691.

Preuss TM, Qi H, Kaas JH (1999) Distinctive compartmental organization of human primary visual cortex. Proc Natl Acad Sci U S A 96: 11601-11606.

Prothero J (1997) Scaling of cortical neuron density and white matter volume in mammals. J Hirnforsch 38: 513-524.

Purvis A (1995) A Composite Estimate Of Primate Phylogeny. Philos Trans R Soc Lond B Biol Sci 348: 405-421.

Purvis A, Garland T, Jr. (1993) Polytomies in Comparative Analyses of Continuous Characters. Syst Biol 42: 569-575.

Rademacher J, Burgel U, Geyer S, Schormann T, Schleicher A, Freund HJ, Zilles K (2001) Variability and asymmetry in the human precentral motor system. A

cytoarchitectonic and myeloarchitectonic brain mapping study. Brain 124: 2232-
2258.

Radinsky L (1967) Relative brain size: a new measure. Science 155: 836-838.

Radinsky L (1972) Endocasts and studies of primate brain evolution. In: The Functional
and Evolutionary Biology of Primates (Tuttle R, ed.), pp 175-184. Chicago:
Aldine - Atherton Inc.

Raghanti MA, Stimpson CD, Marcinkiewicz JL, Erwin JM, Hof PR, Sherwood CC
(2008) Cholinergic innervation of the frontal cortex: Differences among humans,
chimpanzees, and macaque monkeys. J Comp Neurol 506: 409-424.

Raghanti MA, Stimpson CD, Marcinkiewicz JL, Erwin JM, Hof PR, Sherwood CC
(2008) Differences in cortical serotonergic innervation among humans,
chimpanzees, and macaque monkeys: A comparative study. Cereb Cortex 18:
584-597.

Rakic P, Suner I, Williams RW (1991) A novel cytoarchitectonic area induced
experimentally within the primate visual cortex. Proc Natl Acad Sci U S A 88:
2083-2087.

Rasband WS (1997-2007) ImageJ. In, 1.32 ed. Bethesda, Maryland, USA
http://rsb.info.nih.gov/ij/: National Institutes of Health.

Regan BC, Julliot C, Simmen B, Vienot F, Charles-Dominique P, Mollon JD (2001)
Fruits, foliage and the evolution of primate colour vision. Philos Trans R Soc
Lond B Biol Sci 356: 229-283.

Reno PL, Meindl RS, McCollum MA, Lovejoy CO (2005) The case is unchanged and remains robust: Australopithecus afarensis exhibits only moderate skeletal dimorphism. A reply to Plavcan et al. (2005). J Hum Evol 49: 279-288.

Riegele L (1931) Die Cytoarchitektonik der Felder der Broca'schen Region. J Psychol Neurol 42: 496–514.

Rilling JK, Barks SK, Parr LA, Preuss TM, Faber TL, Pagnoni G, Bremner JD, Votaw JR (2007) A comparison of resting-state brain activity in humans and chimpanzees. Proc Natl Acad Sci U S A 104: 17146-17151.

Rilling JK, Insel TR (1998) Evolution of the cerebellum in primates: differences in relative volume among monkeys, apes and humans. Brain Behav Evol 52: 308-314.

Rilling JK, Insel TR (1999) The primate neocortex in comparative perspective using magnetic resonance imaging. J Hum Evol 37: 191-223.

Rilling JK, Seligman RA (2002) A quantitative morphometric comparative analysis of the primate temporal lobe. J Hum Evol 42: 505-533.

Rockel AJ, Hiorns RW, Powell TP (1980) The basic uniformity in structure of the neocortex. Brain 103: 221-244.

Rodiek RW (1988) The Primate Retina. In: Comparative Primate Biology, Volume 4: Neurosciences (Stelis HD, Erwin J, eds.), pp 203-278. New York: Liss.

Rohen J (1962) Sehorgan. In: Primatologia: Handbuch der Primatenkunde. (Hofer H SA, Starck D, ed.), pp 1–210. Base: S. Karger.

Roos C, Geissmann T (2001) Molecular phylogeny of the major hylobatid divisions. Mol Phylogenet Evol 19: 486-494.

Roos C, Geissmann T (2001) Molecular phylogeny of the major hylobatid divisions. Mol Phylogenet Evol 19: 486-494.

Rosa MG, Tweedale R (2005) Brain maps, great and small: lessons from comparative studies of primate visual cortical organization. Philos Trans R Soc Lond B Biol Sci 360: 665-691.

Ross CF, Henneberg M, Ravosa MJ, Richard S (2004) Curvilinear, geometric and phylogenetic modeling of basicranial flexion: is it adaptive, is it constrained? J Hum Evol 46: 185-213.

Rottschy C, Eickhoff SB, Schleicher A, Mohlberg H, Kujovic M, Zilles K, Amunts K (2007) Ventral visual cortex in humans: Cytoarchitectonic mapping of two extrastriate areas. Hum Brain Mapp.

Ruff CB, Trinkaus E, Holliday TW (1997) Body mass and encephalization in Pleistocene *Homo*. Nature 387: 173-176.

Ruvolo M (1997) Molecular Phylogeny of the Hominoids: Inferences from multiple independent DNA sequence data sets. Mol Biol Evol 14: 248-265.

Ruvolo M, Disotell TR, Allard MW, Brown WM, Honeycutt RL (1991) Resolution of the African hominoid trichotomy by use of a mitochondrial gene sequence. Proc Natl Acad Sci U S A 88: 1570-1574.

Sauer B (1983) Qualitative and quantitative development of the visual cortex in man. J Comp Neurol 214: 441-450.

Schein SJ, de Monasterio FM (1987) Mapping of retinal and geniculate neurons onto striate cortex of macaque. J Neurosci 7: 996-1009.

Schenker NM (2007) Comparative analysis of Broca's area in hominoids. In: Anthropology. San Diego: University of California, San Diego. pp 143.

Schenker NM, Buxhoeveden DP, Amunts K, Zilles K, Semendeferi K (in press) A comparative quantitative analysis of cytoarchitectonics and minicolumnar organization in Broca's area in humans and great apes. J Comp Neurol.

Scheperjans F, Hermann K, Eickhoff SB, Amunts K, Schleicher A, Zilles K (2008) Observer-Independent Cytoarchitectonic Mapping of the Human Superior Parietal Cortex. Cereb Cortex 18: 846-867.

Schiller PH, Malpeli JG (1978) Functional specificity of lateral geniculate nucleus laminae of the rhesus monkey. J Neurophysiol 41: 788-797.

Schlaggar BL, O'Leary DD (1991) Potential of visual cortex to develop an array of functional units unique to somatosensory cortex. Science 252: 1556-1560.

Schleicher A, Amunts K, Geyer S, Kowalski T, Schormann T, Palomero-Gallagher N, Zilles K (2000) A stereological approach to human cortical architecture: identification and delineation of cortical areas. J Chem Neuroanat 20: 31-47.

Schleicher A, Amunts K, Geyer S, Morosan P, Zilles K (1999) Observer-independent method for microstructural parcellation of cerebral cortex: A quantitative approach to cytoarchitectonics. Neuroimage 9: 165-177.

Schoenemann PT (2004) Brain size scaling and body composition in mammals. Brain Behav Evol 63: 47-60.

Schoenemann PT, Sheehan MJ, Glotzer LD (2005) Prefrontal white matter volume is disproportionately larger in humans than in other primates. Nat Neurosci 8: 242-252.

Schulz H-D (1967) Metrische Untersuchungen an den Schichten des Corpus geniculatum

    laterale tag- und nachtaktiver Primaten. In: Hohen Medizinischen Fakultaet.

    Frankfurt a. M., Germany: Johann Wolfgang Goethe-Universitaet Frankfurt a. M.

Semendeferi K (1994) Evolution if the hominoid prefontal cortex: a quantitative and

    image analysis of area 13 and 10. In: University of Iowa.

Semendeferi K, Armstrong E, Schleicher A, Zilles K, Van Hoesen GW (1998) Limbic

    frontal cortex in hominoids: a comparative study of area 13. Am J Phys Anthropol

    106: 129-155.

Semendeferi K, Armstrong E, Schleicher A, Zilles K, Van Hoesen GW (2001) Prefrontal

    cortex in humans and apes: a comparative study of area 10. Am J Phys Anthropol

    114: 224-241.

Semendeferi K, Damasio H (2000) The brain and its main anatomical subdivisions in

    living hominoids using magnetic resonance imaging. J Hum Evol 38: 317-332.

Semendeferi K, Damasio H, Frank R, Van Hoesen GW (1997) The evolution of the

    frontal lobes: a volumetric analysis based on three-dimensional reconstructions of

    magnetic resonance scans of human and ape brains. J Hum Evol 32: 375-388.

Semendeferi K, Lu A, Schenker N, Damasio H (2002) Humans and great apes share a

    large frontal cortex. Nat Neurosci 5: 272-276.

Sereno MI, Dale AM, Reppas JB, Kwong KK, Belliveau JW, Brady TJ, Rosen BR,

    Tootell RB (1995) Borders of multiple visual areas in humans revealed by

    functional magnetic resonance imaging. Science 268: 889-893.

Shariff GA (1953) Cell Counts in the Primate Cerebral Cortex. J Comp Neurol 98: 381-

    400.

Shea BT (1983) Allometry and heterochrony in the African apes. Am J Phys Anthropol 62: 275-289.

Sherwood CC, Broadfield DC, Holloway RL, Gannon PJ, Hof PR (2003) Variability of Broca's area homologue in African great apes: Implications for language evolution. Anat Rec 271A: 276-285.

Sherwood CC, Cranfield MR, Mehlman PT, Lilly AA, Garbe JA, Whittier CA, Nutter FB, Rein TR, Bruner HJ, Holloway RL, Tang CY, Naidich TP, Delman BN, Steklis HD, Erwin JM, Hof PR (2004) Brain structure variation in great apes, with attention to the mountain gorilla (*Gorilla beringei beringei*). Am J Primatol 63: 149-164.

Sherwood CC, Hof PR (2007) The evolution of neuron types and cortical histology in apes and humans. In: Evolution of Nervous Systems, Vol. 4: The Evolution of Primate Nervous Systems (Kaas JH, Preuss TM, eds.), pp 355-378. Oxford: Academic Press.

Sherwood CC, Hof PR, Holloway RL, Semendeferi K, Gannon PJ, Frahm HD, Zilles K (2005) Evolution of the brainstem orofacial motor system in primates: a comparative study of trigeminal, facial, and hypoglossal nuclei. J Hum Evol 48: 45-84.

Sherwood CC, Holloway RL, Erwin JM, Hof PR (2004) Cortical Orofacial Motor Representation in Old World Monkeys, Great Apes, and Humans. II. Stereologic Analysis of Chemoarchitecture. Brain Behav Evol 63: 82-106.

Sherwood CC, Holloway RL, Erwin JM, Schleicher A, Zilles K, Hof PR (2004) Cortical Orofacial Motor Representation in Old World Monkeys, Great Apes, and

Humans. I. Quantitative Analysis of Cytoarchitecture. Brain Behav Evol 63: 61-81.

Sherwood CC, Holloway RL, Semendeferi K, Hof PR (2005) Is prefrontal white matter enlargement a human evolutionary specialization? Nat Neurosci 8: 537-538.

Sherwood CC, Lee PW, Rivara CB, Holloway RL, Gilissen EP, Simmons RM, Hakeem A, Allman JM, Erwin JM, Hof PR (2003) Evolution of specialized pyramidal neurons in primate visual and motor cortex. Brain Behav Evol 61: 28-44.

Sherwood CC, Raghanti MA, Stimpson CD, Bonar CJ, de Sousa AA, Preuss TM, Hof PR (2007) Scaling of inhibitory interneurons in areas V1 and V2 of anthropoid primates as revealed by calcium-binding protein immunohistochemistry. Brain Behav Evol 69: 176-195.

Sherwood CC, Stimpson CD, Raghanti MA, Wildman DE, Uddin M, Grossman LI, Goodman M, Redmond JC, Bonar CJ, Erwin JM, Hof PR (2006) Evolution of increased glia-neuron ratios in the human frontal cortex. Proc Natl Acad Sci U S A 103: 13606-13611.

Sherwood CC, Wahl E, Erwin JM, Hof PR, Hopkins WD (2007) Histological asymmetries of primary motor cortex predict handedness in chimpanzees (Pan troglodytes). J Comp Neurol 503: 525-537.

Shibata T, Ioannides AA (2001) Contribution of the human superior parietal lobule to spatial selection process: an MEG study. Brain Res 897: 164-168.

Simmons K (1942) Capacities by both plastic and water techniques with linear measurements of the Reserve Collection; white and Negro. Hum Biol 14: 473–498.

Simon O, Mangin JF, Cohen L, Le Bihan D, Dehaene S (2002) Topographical layout of hand, eye, calculation, and language-related areas in the human parietal lobe. Neuron 33: 475-487.

Sincich LC, Park KF, Wohlgemuth MJ, Horton JC (2004) Bypassing V1: a direct geniculate input to area MT. Nat Neurosci 7: 1123-1128.

Skinner M, Wood B (2006) The evolution of modern human life history - a paleontological perspective. In: The Evolution of Modern Human Life History (Hawkes K, Paine R, eds.), pp 331-364. Santa Fe: School of American research.

Smith GE (1924) The Evolution of Man. London: Oxford University Press.

Snell O (1891) Die Abhängigkeit des Hirngewichtes von dem Körpergewicht und den geistigen Fähigkeiten. Arch Psychiat Nervenkr 23: 436-446.

Solnitzky O, Harman P (1943) The lateral geniculate complex in the spider monkey, *Ateles ater.* Yale J Biol Med 15: 615–639.

Spence KW, Fulton JF (1936) The effects of occipital lobotomy on vision in chimpanzee. Brain 59: 35-50.

Stephan H (1960) Methodische Studien über den quantitativen Vergleich architektonischer Struktureinheiten des Gehirns. Z wiss Zool 164: 143-172.

Stephan H, Baron G, Frahm HD (1988) Comparative size of brains and brain components. In: Neurosciences (Stelis HD, Erwin J, eds.), pp 138-181. New York: Liss.

Stephan H, Bauchot R, Andy OJ (1970) Data on the size of the brain and of the various brain parts in insectivores and primates. In: The Primate Brain (Noback CR, Montagna W, eds.), pp 289-296. New York: Appleton-Century-Crofts.

Stephan H, Dieterlen F (1982) Relative brain size in Muridae with special reference to *Colomys goslingi*. Z Saugertierk 47: 38-47.

Stephan H, Frahm H, Baron G (1981) New and revised data on volumes of brain structures in insectivores and primates. Folia Primatol (Basel) 35: 1-29.

Stephan H, Frahm HD, Baron G (1984) Comparison of brain structure volume in insectivora and primates IV. Non-cortical visual structures. J Hirnforsch 25: 385-403.

Stephan H, Kuhn HJ (1982) The brain of *Micropotamogale lamottei* Heim De Balsac, 1954. Z Saugertierk 47: 129-142.

Sterner KN, Raaum RL, Zhang YP, Stewart CB, Disotell TR (2006) Mitochondrial data support an odd-nosed colobine clade. Mol Phylogenet Evol 40: 1-7.

Stevens CF (2001) An evolutionary scaling law for the primate visual system and its basis in cortical function. Nature 411: 193-195.

Stout D, Chaminade T (2007) The evolutionary neuroscience of tool making. Neuropsychologia 45: 1091-1100.

Stout D, Toth N, Schick K, Chaminade T (2008) Neural correlates of Early Stone Age toolmaking: technology, language and cognition in human evolution. Philos Trans R Soc Lond B Biol Sci.

Stout D, Toth N, Schick K, Stout J, Hutchins G (2000) Stone tool-making and brain activation: Position emission tomography (PET) studies. J Archaeol Sci 27: 1215-1223.

Sumner P, Mollon JD (2000) Catarrhine photopigments are optimized for detecting targets against a foliage background. J Exp Biol 203: 1963-1986.

Sur M, Rubenstein JL (2005) Patterning and plasticity of the cerebral cortex. Science 310: 805-810.

Symington J (1916) Endocranial casts and brain form: a criticism of some recent speculations. J Anat Physiol 11: 111-130.

Taglialatela JP, Russell JL, Schaeffer JA, Hopkins WD (2008) Communicative Signaling Activates `Broca's' Homolog in Chimpanzees. Curr Biol 18: 343.

Takacs Z, Morales JC, Geissmann T, Melnick DJ (2005) A complete species-level phylogeny of the Hylobatidae based on mitochondrial ND3-ND4 gene sequences. Mol Phylogenet Evol 36: 456-467.

Tigges J (1963) On colour vision in gibbon and orang-utan. Folia Primatol (Basel) 1: 188-198.

Tigges J, Bos J, Tigges M (1977) An autoradiographic investigation of the subcortical visual system in chimpanzee. J Comp Neurol 172: 367-380.

Tigges J, Tigges M (1979) Ocular dominance columns in the striate cortex of chimpanzee (Pan troglodytes). Brain Res 166: 386-390.

Tigges J, Tigges M (1987) Termination of retinofugal fibers and lamination pattern in the lateral geniculate nucleus of the gibbon. Folia Primatol (Basel) 48: 186-194.

Tigges M, Tigges J, Sporborg CD (1981) Will the real Meynert cell please stand up? Soc Neurosci Abstr 7: 831.

Tobias PV (1964) The Olduvai Bed I hominine with special reference to its cranial capacity. Nature 202: 3-4.

Tobias PV (1971) The Brain in Hominid Evolution. New York: Columbia University Press.

Tobias PV (2001) Re-creating ancient hominid virtual endocasts by CT-scanning. Clin Anat 14: 134-141.

Tomonaga M (2001) Investigating visual perception and cognition in chimpanzees (*Pan troglodytes*) through visual search and related tasks: from basic to complex processes. In: Primate Origins of Human Cognition and Behavior (Matsuzawa T, ed.), pp 55-86. New York: Springer.

Tootell RB, Mendola JD, Hadjikhani NK, Ledden PJ, Liu AK, Reppas JB, Sereno MI, Dale AM (1997) Functional analysis of V3A and related areas in human visual cortex. J Neurosci 17: 7060-7078.

Tootell RB, Taylor JB (1995) Anatomical evidence for MT and additional cortical visual areas in humans. Cereb Cortex 5: 39-55.

Tosi AJ, Disotell TR, Morales JC, Melnick DJ (2003) Cercopithecine Y-chromosome data provide a test of competing morphological evolutionary hypotheses. Mol Phylogenet Evol 27: 510-521.

Tower DB (1954) Structural and functional organization of mammalian cerebral cortex; the correlation of neurone density with brain size; cortical neurone density in the fin whale (Balaenoptera physalus L.) with a note on the cortical neurone density in the Indian elephant. J Comp Neurol 101: 19-51.

Uddin M, Goodman M, Erez O, Romero R, Liu G, Islam M, Opazo JC, Sherwood CC, Grossman LI, Wildman DE (2008) Distinct genomic signatures of adaptation in pre- and postnatal environments during human evolution. Proc Natl Acad Sci U S A 105: 3215-3220.

Uddin M, Opazo JC, Wildman DE, Sherwood CC, Hof PR, Goodman M, Grossman LI (2008) Molecular evolution of the cytochrome c oxidase subunit 5A gene in primates. BMC Evol Biol 8: 8.

Ungerleider LG, Mishkin M (1982) Two cortical visual systems. In: Analysis of Visual Behavior (Ingle DJ, Goodale MA, Mansfield RJW, eds.), pp 549-586. Cambridge, MA: MIT Press.

Uspenskii S (1954) A new method for measuring cranial capacity. Am J Phys Anthropol 22: 115-117.

Vaisnys JR, Lieberman D, Pilbeam D (1984) An alternative method of estimating the cranial capacity of Olduvai Hominid 7. Am J Phys Anthropol 65: 71-81.

Valverde F (1978) The organization of area 18 in the monkey. A Golgi study. Anat Embryol (Berl) 154: 305-334.

Van Der Gucht E, Youakim M, Arckens L, Hof PR, Baizer JS (2006) Variations in the structure of the prelunate gyrus in Old World monkeys. Anat Rec A Discov Mol Cell Evol Biol 288: 753-775.

Van Dongen PAM (1998) Brain size in vertebrates. In: The Central Nervous System of Vertebrates (Nieuwenhuys RH, Donkelaar HJt, Nicholson C, eds.), pp 2099–2134. Berlin: Springer.

Van Essen DC (1985) Functional organization of the Primate Visual Cortex. In: Cerebral Cortex (Peters A, Jones EG, eds.), pp 259-329. New York: Plenum Press.

Van Essen DC (2004) Organization of visual areas in macaque and human cerebral cortex. In: The Visual Neurosciences (Chalupa L, Werner J, eds.), pp 507-521. Cambridge, MA: MIT Press.

Van Essen DC, Anderson CH, Felleman DJ (1992) Information processing in the primate visual system: an integrated systems perspective. Science 255: 419-423.

Van Essen DC, Drury HA (1997) Structural and Functional Analyses of Human Cerebral Cortex Using a Surface-Based Atlas. J Neurosci 17: 7079-7102.

Van Essen DC, Newsome WT, Bixby JL (1982) The pattern of interhemispheric connections and its relationship to extrastriate visual areas in the macaque monkey. J Neurosci 2: 265-283.

Van Essen DC, Newsome WT, Maunsell JH, Bixby JL (1986) The projections from striate cortex (V1) to areas V2 and V3 in the macaque monkey: asymmetries, areal boundaries, and patchy connections. J Comp Neurol 244: 451-480.

Van Essen DC, Zeki SM (1978) The topographic organization of rhesus monkey prestriate cortex. J Physiol 277: 193-226.

Vanduffel W, Fize D, Mandeville JB, Nelissen K, Van Hecke P, Rosen BR, Tootell RB, Orban GA (2001) Visual motion processing investigated using contrast agent-enhanced fMRI in awake behaving monkeys. Neuron 32: 565-577.

Vekua A, Lordkipanidze D, Rightmire GP, Agusti J, Ferring R, Maisuradze G, Mouskhelishvili A, Nioradze M, De Leon MP, Tappen M, Tvalchrelidze M, Zollikofer C (2002) A new skull of early Homo from Dmanisi, Georgia. Science 297: 85-89.

Vital-Durand F, Blakemore C (1981) Visual cortex of an anthropoid ape. Nature 291: 588-590.

von Bonin G, Bailey P (1947) The neocortex of Macaca mulatta. Urbana, IL: University of Illinois Press.

von Economo C (1929) The Cytoarchitechtonics of the Human Cortex. Oxford: Oxford
University Press.

Walker AE, Fulton JF (1936) The External Configuration of the Cerebral Hemispheres of
the Chimpanzee. J Anat 71: 105-116 109.

Warton DI, Wright IJ, Falster DS, Westoby M (2006) Bivariate line-fitting methods for
allometry. Biol Rev Camb Philos Soc 81: 259-291.

Weaver AGH (2001) The cerebellum and cognitive evolution in Pliocene and Pleistocene
hominids. In: (Trinkaus E, ed.) Anthropology, Physical (0327); Psychology,
Cognitive (0633). Albuquerque, NM: The University of New Mexico. pp 307.

Weaver AGH (2005) Reciprocal evolution of the cerebellum and neocortex in fossil
humans. Proc Natl Acad Sci U S A.

Welcker H (1885) Die Capacität und die drei Hauptdurchmesser der Schädelkapsel bei
den verschiedenen Nationen. Arch fur Anthrop 16: 1-159.

Wickett JC, Vernon PA, Lee DH (1994) *In vivo* brain size, head perimeter, and
intelligence in a sample of healthy adult females. Personality and Individual
Differences 16: 831-838.

Wolpoff MH (1969) Cranial capacity and taxonomy of Olduvai Hominid-7. Nature 223:
182-183.

Wolpoff MH (1981) Cranial capacity estimates for Olduvai Hominid-7. Am J Phys
Anthropol 56: 297-304.

Woolsey CN, Marshall WH, Bard P (1943) Note on the organization of the tactile
sensory area of the cerebral cortex of the chimpanzee. J Neurophysiol 6: 287-291.

Wree A, Schleicher A, Zilles K (1982) Estimation of volume fractions in nervous tissue with an image analyzer. J Neurosci Methods 6: 29-43.

Xing J, Wang H, Han K, Ray DA, Huang CH, Chemnick LG, Stewart CB, Disotell TR, Ryder OA, Batzer MA (2005) A mobile element based phylogeny of Old World monkeys. Mol Phylogenet Evol 37: 872-880.

Yantis S (2001) Visual Perception: Essential Readings. Phildelphia, PA: Psychology Press Ltd.

Yantis S, Schwarzbach J, Serences JT, Carlson RL, Steinmetz MA, Pekar JJ, Courtney SM (2002) Transient neural activity in human parietal cortex during spatial attention shifts. Nat Neurosci 5: 995-1002.

Yoshioka T, Hendry SH (1995) Compartmental organization of layer IVA in human primary visual cortex. J Comp Neurol 359: 213-220.

Zeki S (2003) Improbable areas in the visual brain. Trends Neurosci 26: 23-26.

Zeki SM (2004) Improbable areas in color vision. In: The Visual Neurosciences (Chalupa LM, Werner JS, eds.), pp 1029-1039. Cambridge, MA: MIT Press.

Zilles K (1972) Biometrische Analyse der Frischvolumina verschiedener prosencephaler Hirnregionen von 78 menschlichen, adulten Gehirnen. Gegenbaurs morphologisches Jahrbuch 118: 234–273.

Zilles K, Armstrong E, Moser KH, Schleicher A, Stephan H (1989) Gyrification in the cerebral cortex of primates. Brain Behav Evol 34: 143-150.

Zilles K, Armstrong E, Schleicher A, Kretschmann HJ (1988) The human pattern of gyrification in the cerebral cortex. Anat Embryol (Berl) 179: 173-179.

Zilles K, Clarke S (1997) Architecture, connectivity, and transmitter receptors of human extrastraite visual cortex: comparisons with nonhuman primates. In: Cerebral Cortex (Rockland KS, Kaas JH, Peters A, eds.): Plenum Press.

Zilles K, Palomero-Gallagher N (2001) Cyto-, myelo-, and receptor architectonics of the human parietal cortex. Neuroimage 14: S8-20.

Zilles K, Rehkämper G (1988) The brain, with special reference to the telencephalon. In: Orang-Utan Biology (Schwartz JH, ed.), pp 157-176. Oxford: Oxford University Press.

Zilles K, Schlaug G, Matelli M, Luppino G, Schleicher A, Qu M, Dabringhaus A, Seitz R, Roland PE (1995) Mapping of human and macaque sensorimotor areas by integrating architectonic, transmitter receptor, MRI and PET data. J Anat 187 (Pt 3): 515-537.

Zilles K, Schleicher A, Palomero-Gallagher N, Amunts K (2002) Quantitative analysis of cyto- and receptor architecture of the human brain. In: Brain Mapping: The Methods (Toga AW, Mazziotta JC, eds.), pp 573-602: Elsevier Science (USA).

Zilles K, Schleicher A, Pehlemann FW (1982) How many sections must be measured in order to reconstruct the volume of a structure using serial sections? Microsc Acta 86: 339-346.

Zollikofer CPE (2002) A Computational Approach to Paleoanthropology. Evol Anthropol Suppl 1: 64-67.

Zollikofer CPE, Ponce de Leon MS, Lieberman DE, Guy F, Pilbeam D, Likius A, Mackaye HT, Vignaud P, Brunet M (2005) Virtual cranial reconstruction of *Sahelanthropus tchadensis*. Nature 434: 755-759.

Zollikofer CPE, Ponce de Léon MS, Martin RD (1998) Computer-assisted

paleoanthropology. Evol Anthropol 6: 41-54.